NUCLEAR STRUCTURE STUDIES AT INTERMEDIATE ENERGIES

DOE/ER/40405--T5

DE92 004109

Summary Progress Report
July 1987 through July 1990

Norton M. Hintz, Principal Investigator
Anil Sethi, Research Associate
Xin-hua Yang, Research Associate[a)]
Michael A. Franey, Research Associate[b)]
Magdy Gazzaly, Research Associate[c)]
Dimitris Mihailidis, Research Assistant
Anthony M. Mack, Research Assistant

Prepared for the U.S. Department of Energy
under Grant Number DE-FG02-88ER40405 A002

July 1990

University of Minnesota
School of Physics and Astronomy
116 Church St. S. E.
Minneapolis, MN 55455

BITNET: FVS6259@UMNACVX
FAX: 612-624-4578

a) Joined group, April 1990
b) Part time
c) Left group, August 1989

Note

The data and calculations presented here represent work in progress and so are preliminary (unless otherwise noted) and should not be quoted without the author's permission.

Table of Contents

I. Introduction and Summary

The period covered in this summary report is roughly from July 1987 through July 1990. This constitutes a final report, to date, for the three-year grant which expires 31 December 1990. The report contains some material from our 1987-88 and 1988-89 reports.

The group at present consists of Norton M. Hintz Prof. of Physics and Principal Investigator; Anil Sethi, Xin-hua Yang, Michael Franey, Research Associates; Dimitris Mihailidis and Anthony Mack, Research Assistants. Most of the experimental work reported here was done at the Los Alamos Meson Physics Facility. Experiment numbers refer to LAMPF experiments unless otherwise noted.

An active collaboration, involving sharing of scientific staff and computer facilities, exists with the Minnesota group under Prof. Dietrich Dehnhard. In addition we have collaborated with nuclear theorists at Minnesota (Bayman, Ellis) and elsewhere (J. Shepard and E. Rost, Univ. of Colorado; W. G. Love, Univ. of Georgia; L. Ray, Univ. of Texas; G. Brown, SUNY; A Lallena, Univ. of Granada).

Somewhat fewer new experiments were run during the past three years than in the previous three years since beam was not available at HRS during 1989. This, however, gave us more time for analysis of data from completed experiments.

Our main activities in the past three years were:

A. Experimental

1. A search for dibaryon resonances using the reaction $\vec{p} + {}^{3}He \rightarrow d + x$ (E973U).
2. A study of the shape transition nuclei ${}^{150}Nd$, ${}^{154}Gd$, ${}^{192}Os$ and

^{194,196}Pt in (p,p') to test the IBA (E903U).

3. A search for low lying high multipole magnetic states in ^{48}Ti (E1047).

4. Search for ($N^{-1}\Delta$) excitations at low q in the (p,^{3}He) reaction (E1030U).

5. Measurement of the spin-averaged slope parameter in p-p elastic scattering (E1027U).

6. Participation in experiments of other groups: Fermilab 581 (coulomb nuclear interference polarimeter), E955 (elastic polarized proton scattering from polarized ^{13}C), E1036 (analyzing power in ^{9}Be ($\vec{p},\pi^{\pm}$) reaction), E1080 (spin response in ^{40}Ca), E1131 (Spin observables for inclusive proton scattering - the first MRS experiment), ^{28}Si(p,p') at various energies to study M(1) excitations (Saturne).

B. Theoretical Analysis

1. Analysis of ^{208}Pb($\pi^{\pm},\pi^{\pm\prime}$) data (E601) using a variety of pion scattering programs.

2. Analysis of elastic and inelastic proton scattering at 650 MeV from ^{206,207,208}Pb to determine neutron-proton density differences and transition matrix elements (E855). An MA thesis has been completed on the first part of this work.

3. Study of relativistic and non-relativistic impluse approximations applied to cross section and spin observable measurements on the stretched states in ^{28}Si(p,p') (E451, 623). A paper has been completed in collaboration with the Rutgers group.

4. Further studies on the effects of meson mass reduction in medium on

proton-nucleus scattering (elastic and inelastic), i.e., nucleon "swelling" effects, in collaboration with G. Brown, SUNY.

5. Studies of the effects of medium modification of the tensor force on the proton excitation of stretched states in ^{208}Pb (E686), in collaboration with A. M. Lallena, Univ. of Granada.
6. Global analysis of ^{28}Si and ^{58}Ni (p,p') data on stretched states (σ, Ay, D_{ij}) at 135 to 800 MeV (IUCF data and E178, 451, 623, 896) using relativistic and non-relativistic scattering theories.
7. Analysis of data from E903-903U on transitional nuclei within the framework of the IBM.

C. Other Activities

1. Participation in installation and development of new Medium Resolution Spectrometer (MRS) at LAMPF.
2. Development (assembly and modification) of Computer Program Library -- mostly relativistic proton and electron programs, and pion programs.
3 Detector (large CsI crystals) development for two-arm ($\vec{p}$,2p) coincidence experiment (E1201) scheduled for preliminary run in Sept. 90.
4. Submission of four new proposals (two accepted) and eight updates (five raised in priority or given more time).
5. One of us (M.F.) served on the D.O.E. committee, "Nuclear Physics Computer Networking" which issued its final report, May 1990 (DOE/ER-0458T).

II. Research Program (July 87 - June 90)

A. E973, Search for Narrow Resonances in the B = 2 Missing Mass Spectrum from p + ^{3}He → d + mm. (Minnesota, Texas, LANL spokesmen; Texas, Udine, Minnesota, LANL, Virginia participants).

This work was stimulated by theoretical controversy[1-3] over the existence of narrow (Γ < 100 MeV) resonances in the B = 2 system, and by suggestive cross section data from Saclay[4] on the ^{3}He(p,d)X reaction in the missing mass (mm) range ~ 1.9 - 2.3 GeV. However, the Saclay group measured cross sections only and the statistics were marginal. In this experiment, which ran in Oct 86 and again briefly in Aug. - Sept. 87, a liquid ^{3}He target was used and both cross sections and analyzing powers (A_y) were measured at $\theta_L = 22^\circ$, 2.0 - 2.2 GeV mm. The data was anlyzed during 1987-88 and a paper published in Phys. Rev. C[5]. The results are shown in Figs. 1 and 2 together with the Saclay data. The energies at which structures were observed in the Saclay cross section data are shown by vertical arrows. The dashed, lines indicate the values of mm predicted by the rotation-like formula of conventional models (for J = ℓ)[3] and by bag models (for ℓ = 0)[1,2]

$$mm = m_0 + m_1 J(J+1). \qquad (1)$$

The values of m_0 and m_1 (m_0 = 2.014 GeV, m_1 = 18.7 MeV, J = 0-2 for the first band and m_0 = 2.155 GeV, m_1 = 18.7 MeV, J = 0, 1 for the second band) were deduced by Tatischeff[4] and are 0.90 and 0.95 of the bag model prediction (valid for first band only). Table I gives the values of m_0 and

m_1, from Eq. (1) experiment and from the bag model (x0.9). No clear evidence for structure was observed in our cross section data, but the A_y show considerable structure with peaks at or near all of the states predicted in the energy range of this experiment.

The LAMPF PAC has approved an additional 150 hours for this experiment and it is scheduled to run in Sept. 90.

References

1. P. J. G. Mulder et al., Phys. Rev. Lett. 40, 1543 (1978) and references therein, M. Rosina and H. J. Pirner, Nucl. Phys. A367, 398 (1981), B. A. Shahbazian et al., Nucl. Phys. A374, 73c (1982) and M. P. Locher et al., Advances in Nuclear Physics. Volume 17, page 47, editors J. W. Negele and E. Vogt (1986).
2. P. J. G. Mulder et al., Phys. Rev. D21, 2653 (1980).
3. M. H. MacGregor, Phys. Rev. Lett. 42, 1724 (1979).
4. B. Tatischeff, Nucl. Phys. A446, 355 (1985); B. Tatischeff et al., Europhysics Lett. 4, 671 (1987); Phys. Rev. C36, 1995 (1987); Z. Phys. A328, 147 (1987) and IPNO-DRE 87.16, Orsay preprint and references therein (1987). See also B. Tatischeff, Phys. Lett. 154B, 107 (1985).
5. L. Santi, et al., Phys. Rev. C38, 2466 (1988).

Table I

Position and FWHM (in GeV) for the structures in A_y as obtained from the fit to our data (see text), compared with SACLAY results[4] and predicted (see text) resonances. Total χ^2 for the fit was 56 for n = 74 degrees of freedom.

Fit results		SACLAY results		Rotational Formula	bag model
peak position	peak FWHM	peak position	peak FWHM	resonance mass	resonance mass x 0.9
2.015±0.005	0.034±0.014			2.015	2.015(ℓ=0,s=0) 2.017(ℓ=1,s=1)
2.054±.004	0.011±.006			2.052	2.098(ℓ=1,s=2) 2.100(ℓ=1,s=0,1,2)
2.125±.003	0.006±.007	2.124±.003	0.025±.002	2.124	2.121(ℓ=0,s=2) 2.129(ℓ=1,s=0,1)
2.152±.004	0.020±.010	2.155 (?)	0.018 (?)	2.155	2.164(ℓ=1,s=1)
2.181±.005	0.020±.008	2.192±.003	0.025±.006	2.192	2.175(ℓ=2,s=0) 2.180(ℓ=1,s=0,1,2) 2.185(ℓ=1,s=1,2)

Figure Captions

Fig. 1. Differential cross section (•) from this work compared with those from SACLAY at 0.75 GeV (x). The vertical dashed lines correspond to masses predicted using Eq. 1. The arrows correspond to the energies at which structure was observed at SACLAY.

Fig. 2. A_y calculated before and after dummy-target subtraction, together with the results of our fit (solid curve). The -- • • -- curve represents a linear "background" term while the -- • -- curve represents the total non resonant background. The vertical lines and arrows have the same meaning as in Fig. 1.

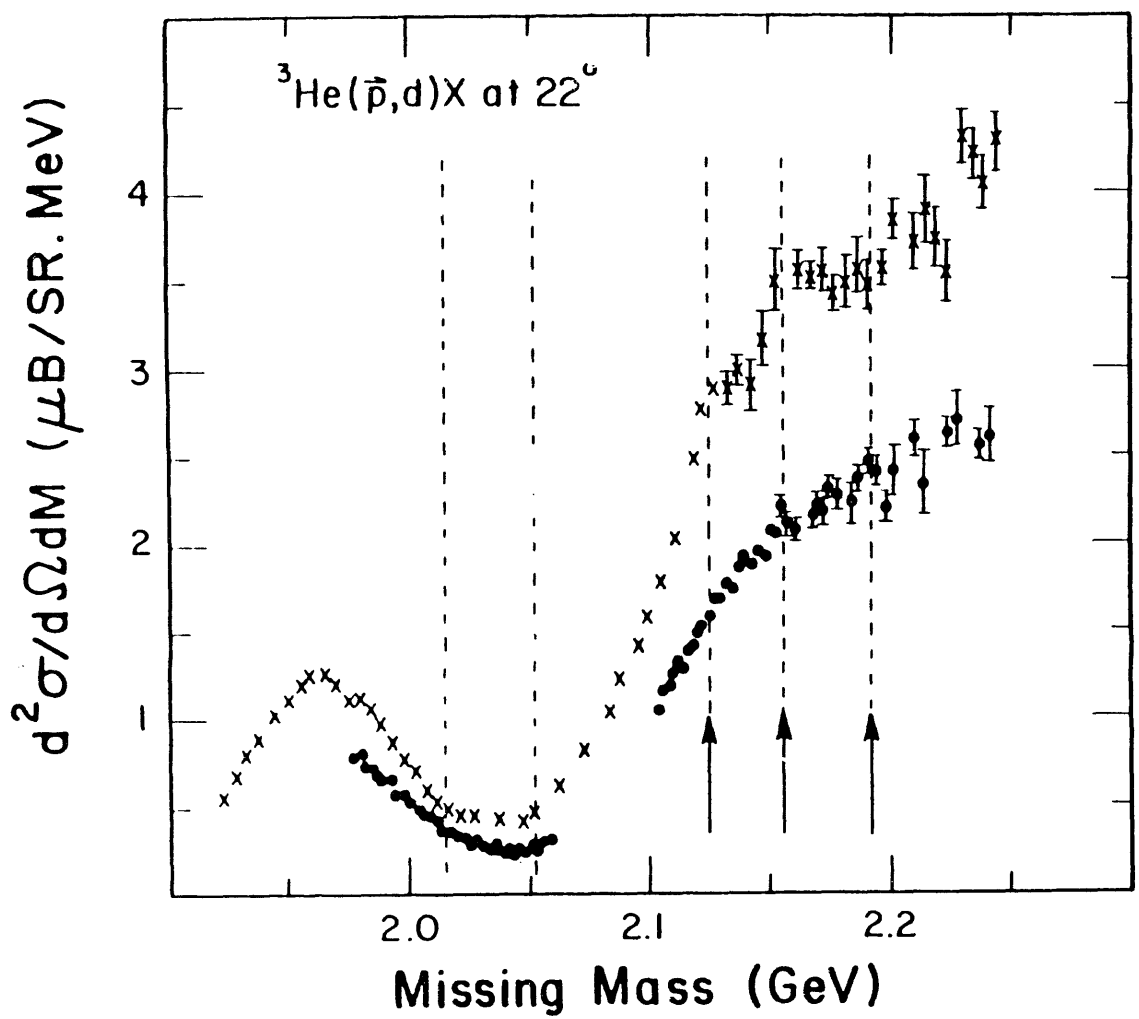

Figure 1

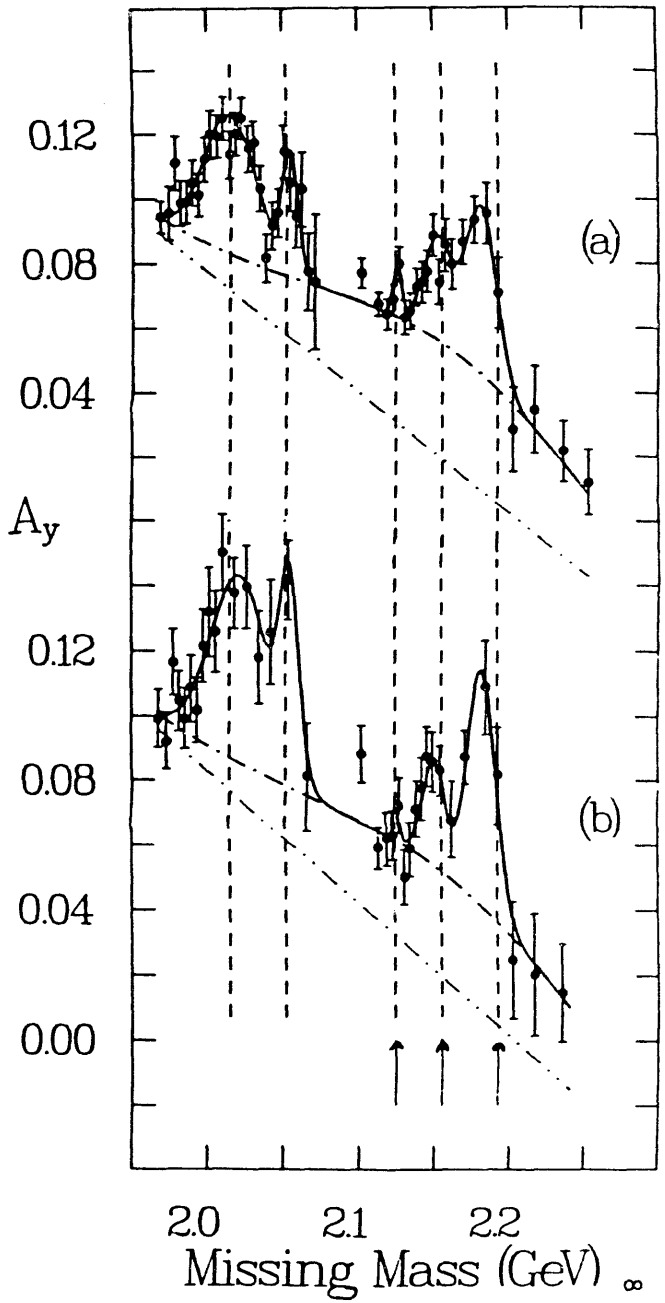

Figure 2

II.B. Analysis of $^{208}Pb(\pi^{\pm},\pi^{\pm\prime})$ Data at T_π = 180 MeV (E601, Minnesota spokesman; LANL, U. Texas participation).

The purpose of E601 was to compare neutron-proton transition matrix element ratios derived from $\pi^{\pm}$ inelastic scattering to collective states in ^{208}Pb with those obtained from a comparison of (p,p') and (e,e')[1,2]. Data was obtained at EPICS for the elastic and inelastic scattering to the 3^-, $5^-_{1,2,3}$, 2^+_1, 4^+_1,6^+_1, and 8^+_1 states over the angular range θ_L = 14 - 60°.

The first calculations were done with the coordinate space program DWPI.[3] The free π-N phase shifts used correspond to an energy of 35 MeV below the actual π-N center of mass energy. A two parameter Fermi (2PF) distribution taken from electron scattering[4] (R = 6.624 fm, a = 0.549 fm) was used for both the neutron and proton ground state density (ρ_o). The results are shown in Fig. 1 for energy shifts of 28 and 35 MeV, the latter being the best choice.

Inelastic calculations were then done, also using DWPI with the vibrating density model. The only free parameters, the deformations β_n and β_p, were varied to get the best simultaneous fits to the π^+ and π^- data which are shown in Figs. 2-5. Neutron and proton transition matrix elements were then calculated from

$$M_i(\lambda) = \int_0^\infty \rho^{tr}_i(r)\, r^{\lambda+2}\, dr \qquad \text{(i: n or p)} \qquad (1)$$

where

$$\rho^{tr}_i = \beta_i R_i \frac{\partial \rho^i_o}{\partial r} \qquad (2)$$

The reduced matrix element ratios were then calculated from

$$\tilde{M}_n/\tilde{M}_p = (Z/N)\ M_n/M_p\ (= \beta_n/\beta_p \text{ in this case}). \qquad (3)$$

These are shown in Table I along with the range of values derived from (ee') - (pp') comparisons above T_p = 500 MeV. The $\pi^{\pm}$ values are generally within ~ ± 10% of the e-p values (except for the 8^+ state for which the simple collective model has less validity). This agreement is within errors due to absolute normalization and peak fitting and the crudeness of the model.

To explore the model-dependence of the results, calculations in momentum space are being performed. The elastic differential cross sections were calculated with the modified computer code PIPIT.[5] It is a first-order optical-model calculation made by solving the Lippmann-Schwinger equation[6]. In the calculation, the collision matrix was calculated using free π-nucleon phase shifts and a separable off-shell extrapolation. The Coulomb distortion effects were included and the nuclear matter distributions were assumed to have a two parameter fermi form. The values of R and a are deduced from the charge distribution[4] with the relation $\langle r^2\rangle_{matter} = \langle r^2\rangle_{charge} - \langle F_p^2\rangle$, where F_p is the proton charge distribution radius in the nucleus. In our calculation, $\langle F_p^2\rangle$ is chosen to be $(1.1\text{fm})^2$ based on the theoretical explanation of the EMC effect.[5] In the first calculation, the R in the two parameter fermi distribution for both neutrons and protons is fixed to that of the charge distribution (R = 6.624fm) and a is calculated from $\langle r^2\rangle_{matter}$ and R. This gives a = 0.462.

The number of partial waves chosen was 19 for good convergence of the nuclear scattering amplitude over the partial wave sum. To get the best fit, the energy shift downward of the π-N center-of-mass energy for the π^+-N t-matrix is 25 MeV and that for π^- is 18 MeV. The difference between the energy shifts of π^+ and π^- might be due to the Coulomb interaction.[7] The resultant fits to the elastic cross sections are shown in Figs. 6 and 7. A second calculation was made constraining R and a to obtain the same central density for the proton matter and charge distribution. This leads to R_p = 6.683 fm and a_p = 0.424 fm. These results are shown in Figs. 8 and 9 and are very similar to those in Figs. 7 and 8 indicating that the pions are mainly sensitive to the r.m.s. radii which are the same for both sets of R and a.

Another more consistant method of choosing the parameters in the two parameter fermi distribution has been investigated. The central densities of the charge and matter in the model are expressed as follows:

$$\rho_{oi} = \frac{3}{4\pi} \frac{1}{R_i^3 + \pi^2 a_i^2 R_i} \cdot f_i \qquad (4)$$

where i indicates charge, proton or neutron, and

$$f_i = \begin{matrix} Z, \text{ for charge and proton} \\ N, \text{ for neutron} \end{matrix}$$

In addition to the relations between charge, proton and neutron rms radii, the central densities provide another constraint on choosing R_i and a_i.

The R_c and a_c are well determined by electron and muon scattering. Assuming $\rho_{op} = \rho_{oc}$ and $\langle r^2 \rangle_{proton} = \langle r^2 \rangle_{charge} - F_p^2$, the R_p and a_p are

determined uniquely. The R_n and a_n are searched for the fit of the experiment data. Then the central density and rms radius of the neutron distribution can be calculated directly. The results show that the central density of matter $\rho_{om}(\rho_{om} = \rho_{op} + \rho_{on})$ is about $0.16/fm^3$ and the difference between the rms radii of the proton and neutron density, $\Delta r(\Delta r = \langle r^2\rangle^{1/2}_{neutron} - \langle r^2\rangle^{1/2}_{proton})$ is about 0.05 fm if F_p is chosen as 1.1 fm. If F_p is taken as 1.3 fm[7] ρ_{om} is almost the same but Δr is about 0.075 fm. These results are consistant with other experiments, and the uncomfortably large value of the central matter density is removed.[7] The fits for $F_p = 1.1$ fm are shown in Figs. (10) and (11). The results for $F_p = 1.3$ fm are shown in Figs. (12) and (13).

The calculations of inelastic angular distributions using momentum space programs are now under way.

Table I

Neutron and Proton deformation parameters[a)]

and reduced matrix element ratios.

E_x (MeV)	J^π	β_n	β_p	$\tilde{M}_n/\tilde{M}_p$ This	Other[b)]
2.61	3^-_1	0.144	0.116	1.24	1.1-1.2
3.20	5^-_1	0.077	0.060	1.28	1.1-1.3
3.71	5^-_2	0.044	0.044	1.00	~ 1.1
3.96	5^-_3	0.022	0.022	1.00	-
4.09	2^+_1	0.065	0.055	1.18	~ 1.3
4.32	4^+_1	0.085	0.075	1.13	1.1-1.2
4.42	6^+_1	0.072	0.072	1.00	0.8-1.1
4.61	8^+_1	0.060	0.060	1.00	1.4-1.9

a) For R = 6.624 fm, a = 0.549 fm for both neutrons and protons.

b) An extensive compilation with original references is given in Ref. 2. These are all from an (e,e') - (p,p') comparison.

References

1. M. M. Gazzaly, et al., Phys. Rev. C25, 408 (1982).
2. N. M. Hintz, et al., Phys. Rev. C37, 692 (1988).
3. R. A. Eisenstein and G. W. Miller, Comput. Phys. Commun. 11, 95 (1976).
4. C. W. de Jager, H. de Vries and C. de Vries, At. Data Nucl. Data Tables 14, 479 (1974).
5. R. A. Eisenstein and F. Tabakin, Comput. Phys. Commun. 12, 237 (1976).
6. A. Kerman, H. McManus and R. Thaler, Ann. Phys. 8, 551 (1959).
7. C. Olmer, et al., Phys. Rev. C21, 254 (1980).

Figure Captions

Fig. 1: Differential elastic cross sections for $^{208}Pb(\pi^-,\pi^-)$ and $^{208}Pb(\pi^+,\pi^+)$ at 180 MeV. The solid curve shows a DWPI calculation at an energy shift of 35 MeV. The dashed curve represents the same calculation at an energy shift of 28 MeV (both downward).

Fig. 2: Differential inelastic cross sections for $^{208}Pb(\pi^-,\pi^-)$ at 180 MeV for 3^- (2.61 MeV), 5_1^- (3.20 MeV), 5_2^- (3.71 MeV), 5_3^- (3.96 MeV) states. The solid curve shows a DWPI calculation at an energy shift of 35 MeV. The dashed curve represents the same calculation at an energy shift of 28 MeV (both downward).

Fig. 3: Differential inelastic cross sections for $^{208}Pb(\pi^+,\pi^+)$ at 180 MeV for 3^- (2.61 MeV), 5_1^- (3.20 MeV), 5_2^- (3.71 MeV), 5_3^- (3.96 MeV) states. The solid curve shows a DWPI calculation at an energy shift of 35 MeV. The dashed curve represents the

same calculation at an energy shift of 28 Mev (both downward).

Fig. 4: Differential inelastic cross sections for $^{208}Pb(\pi^-,\pi^{-\prime})$ at 180 MeV for 2^+(4.09 MeV), 4^+ (4.32 MeV), 6^+ (4.42 MeV), 8^+ (4.61 MeV) states. The solid curve shows a DWPI calculation at an energy shift of 35 MeV. The dashed curve represents the same calculation at an energy shift of 28 Mev (both downward).

Fig. 5: Differential inelastic cross sections for $^{208}Pb(\pi^+,\pi^{+\prime})$ at 180 MeV for 2^+(4.09 MeV), 4^+ (4.32 MeV), 6^+ (4.42 MeV), 8^+ (4.61 MeV) states. The solid curve shows a DWPI calculation at an energy shift of 35 MeV. The dashed curve represents the same calculation at an energy shift of 28 Mev (both downward).

Fig. 6: Differential elastic cross section for $^{208}Pb(\pi^+,\pi^+)$ at 180 MeV. The solid curve shows a PIPIT calculation at an energy shift of 25 MeV downward, using R = 6.624 fm and a = 0.549 fm (n and p).

Fig. 7: Differential elastic cross section for $^{208}Pb(\pi^-,\pi^-)$ at 180 MeV. The solid curve shows a PIPIT calculation at an energy shift of 18 MeV downward, with the same density parameters as in Fig. 6.

Fig. 8: Same as Fig. 6 but for R = 6.683 fm and a = 0.424 fm.

Fig. 9: Same as Fig. 8 but for π^-.

Figs. 10,11: PIPIT predictions for π^+ and π^- elastic scattering from ^{208}Pb using central proton density constraint as discussed in text, for F_p = 1.1 fm.

Figs. 12,13: Same as Figs. 10,11 except for F_p = 1.3 fm.

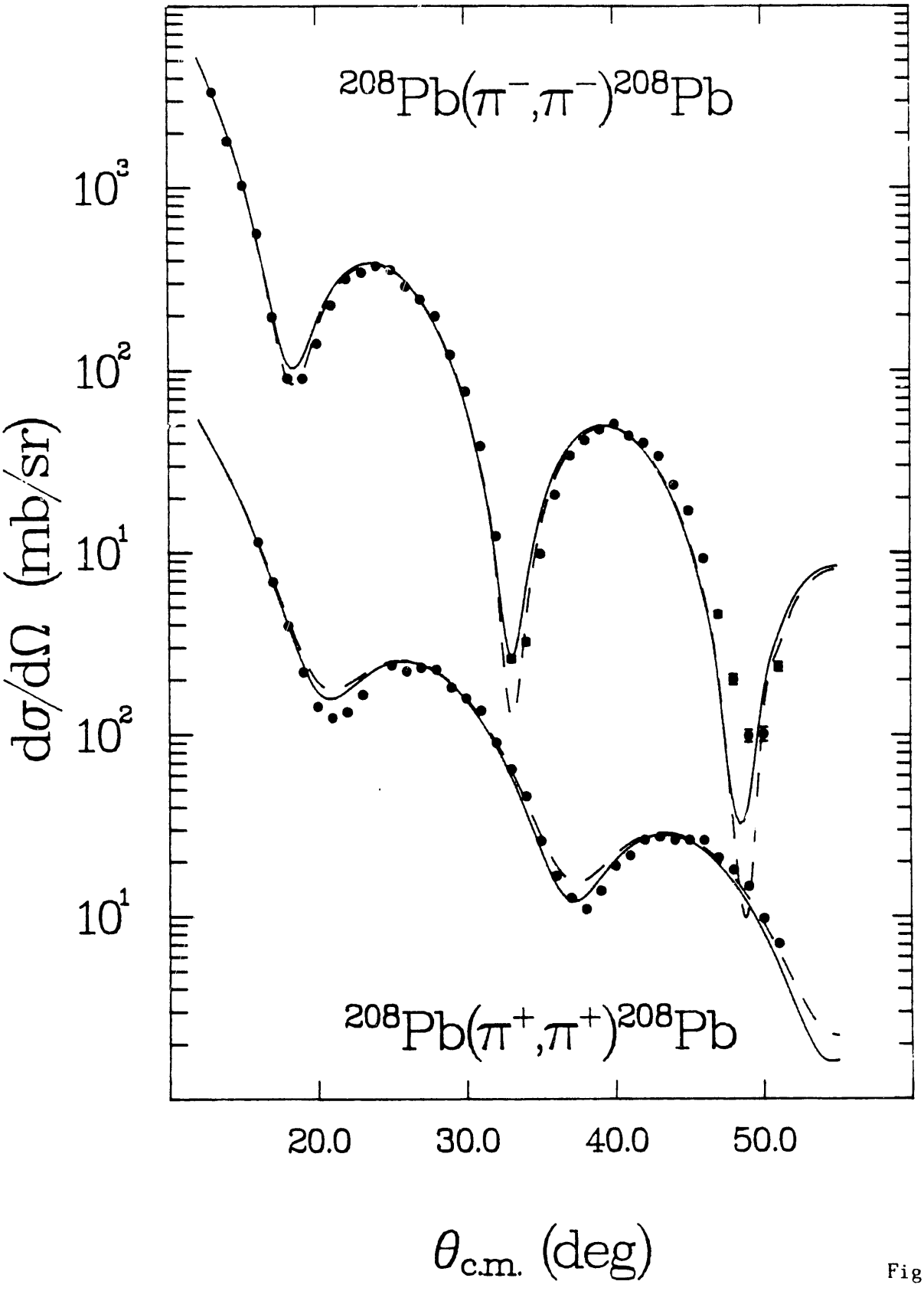
$^{208}Pb(\pi^-,\pi^-)^{208}Pb$
$^{208}Pb(\pi^+,\pi^+)^{208}Pb$
10^3
10^2
10^1
10^2
10^1
$d\sigma/d\Omega$ (mb/sr)
20.0
30.0
40.0
50.0
$\theta_{c.m.}$ (deg)

Figure 1

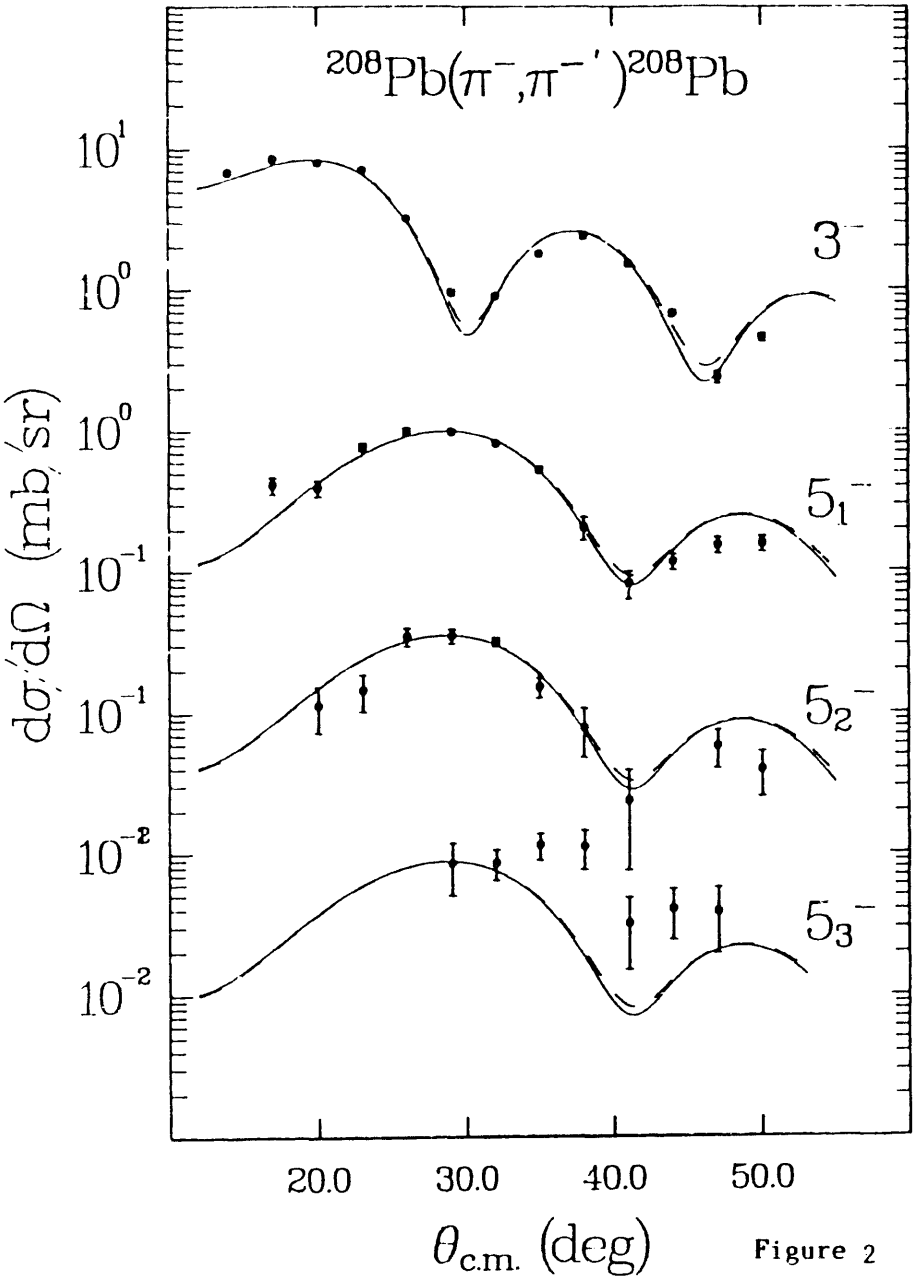

Figure 2

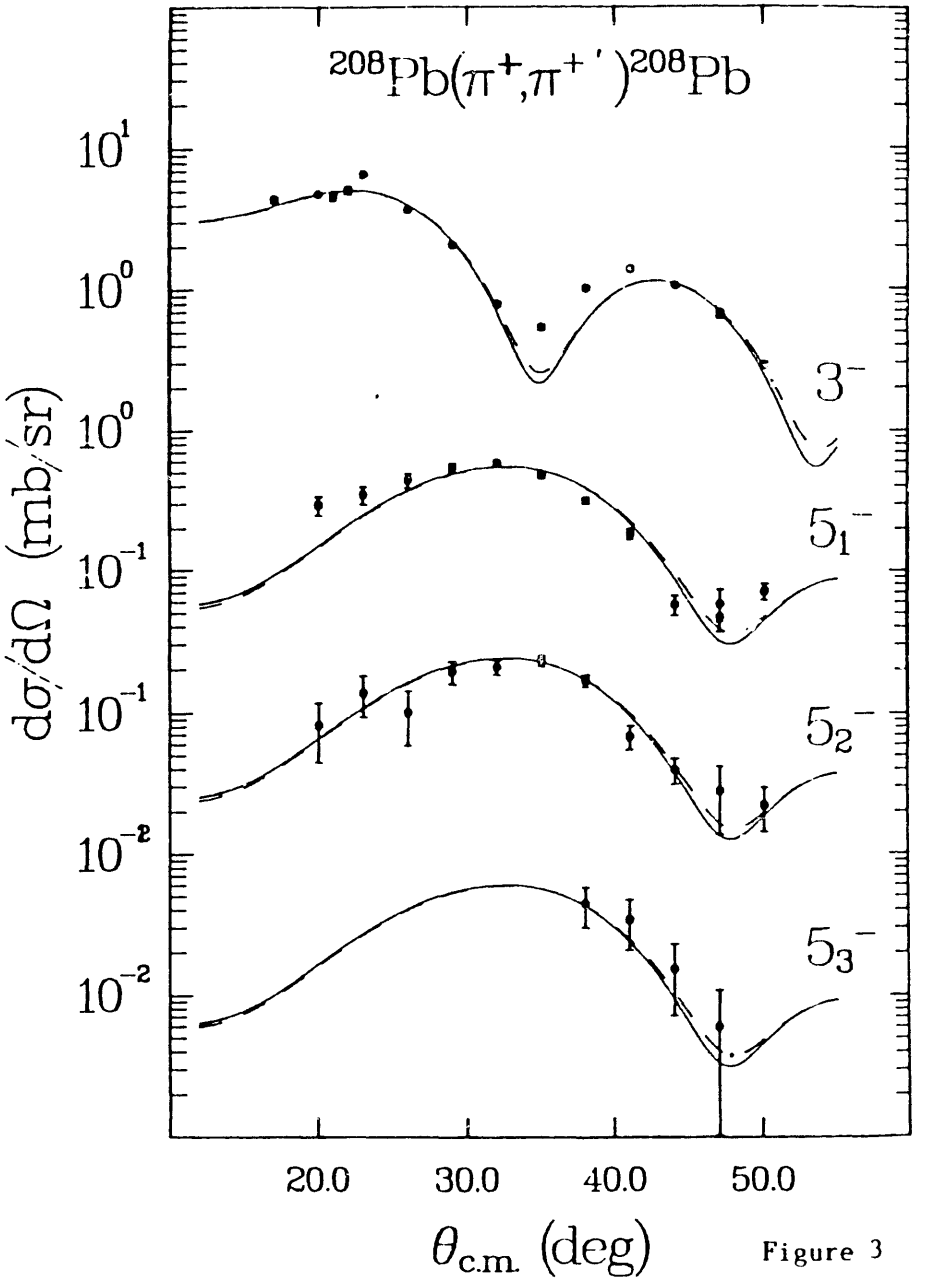

Figure 3

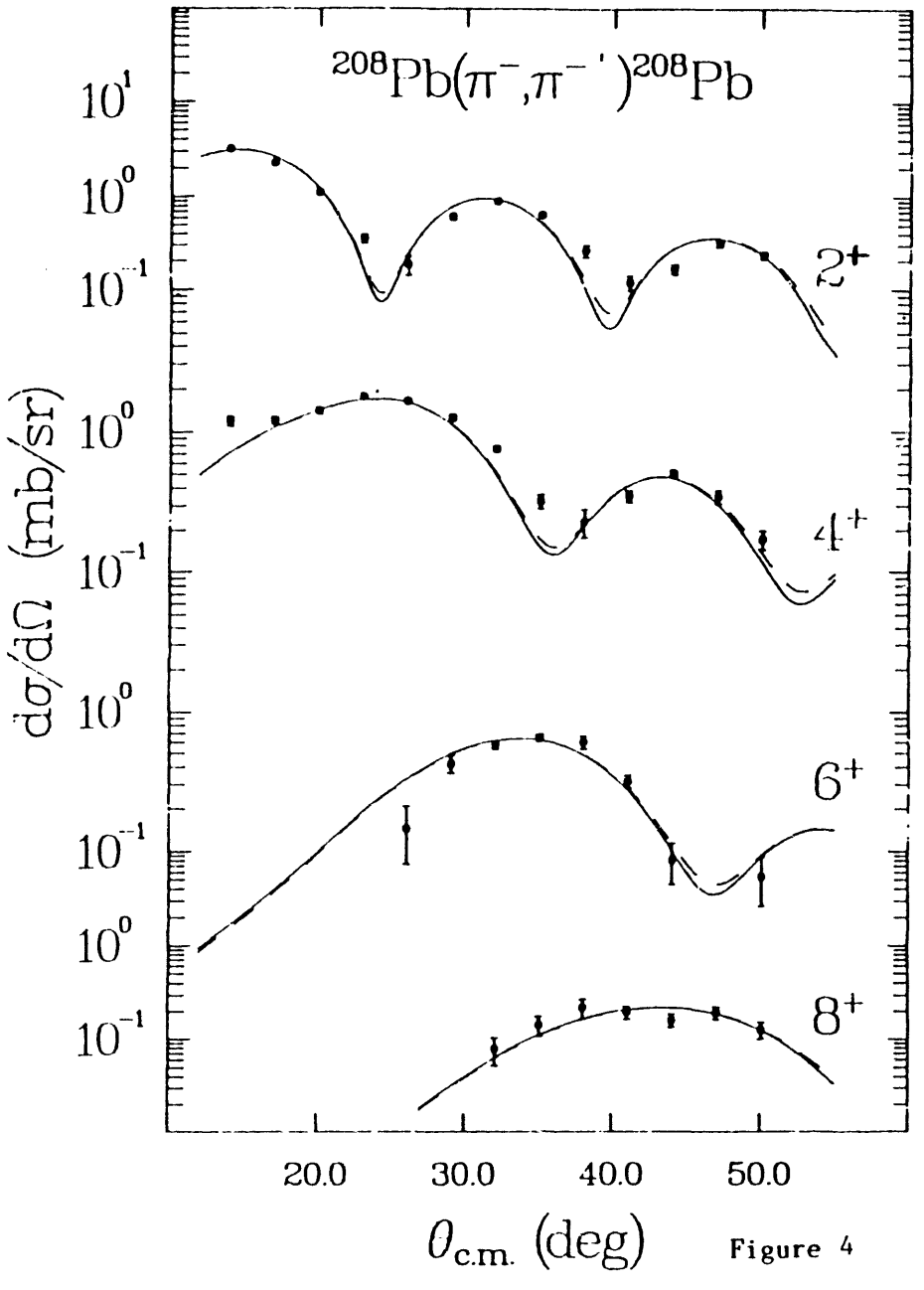

Figure 4

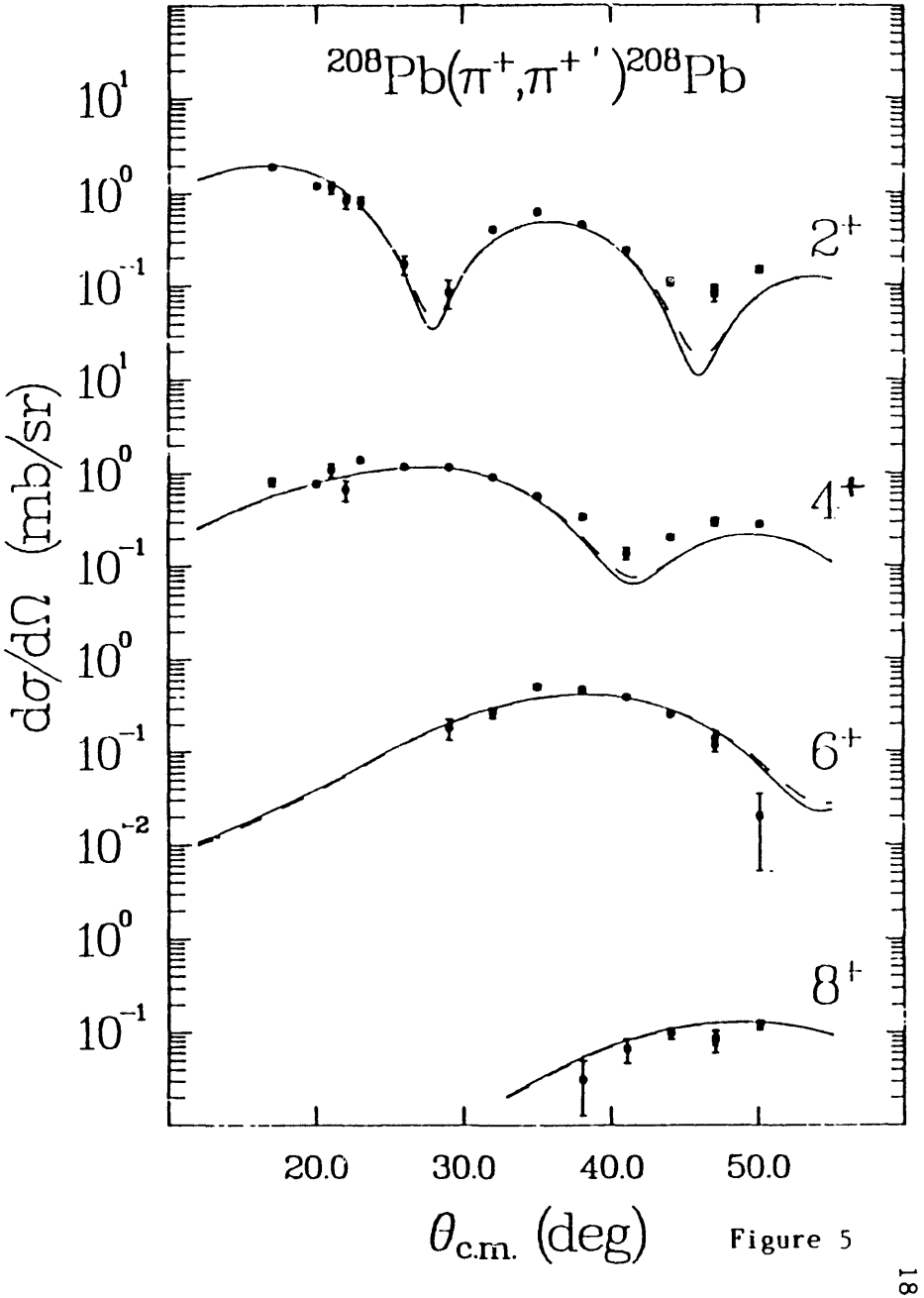

Figure 5

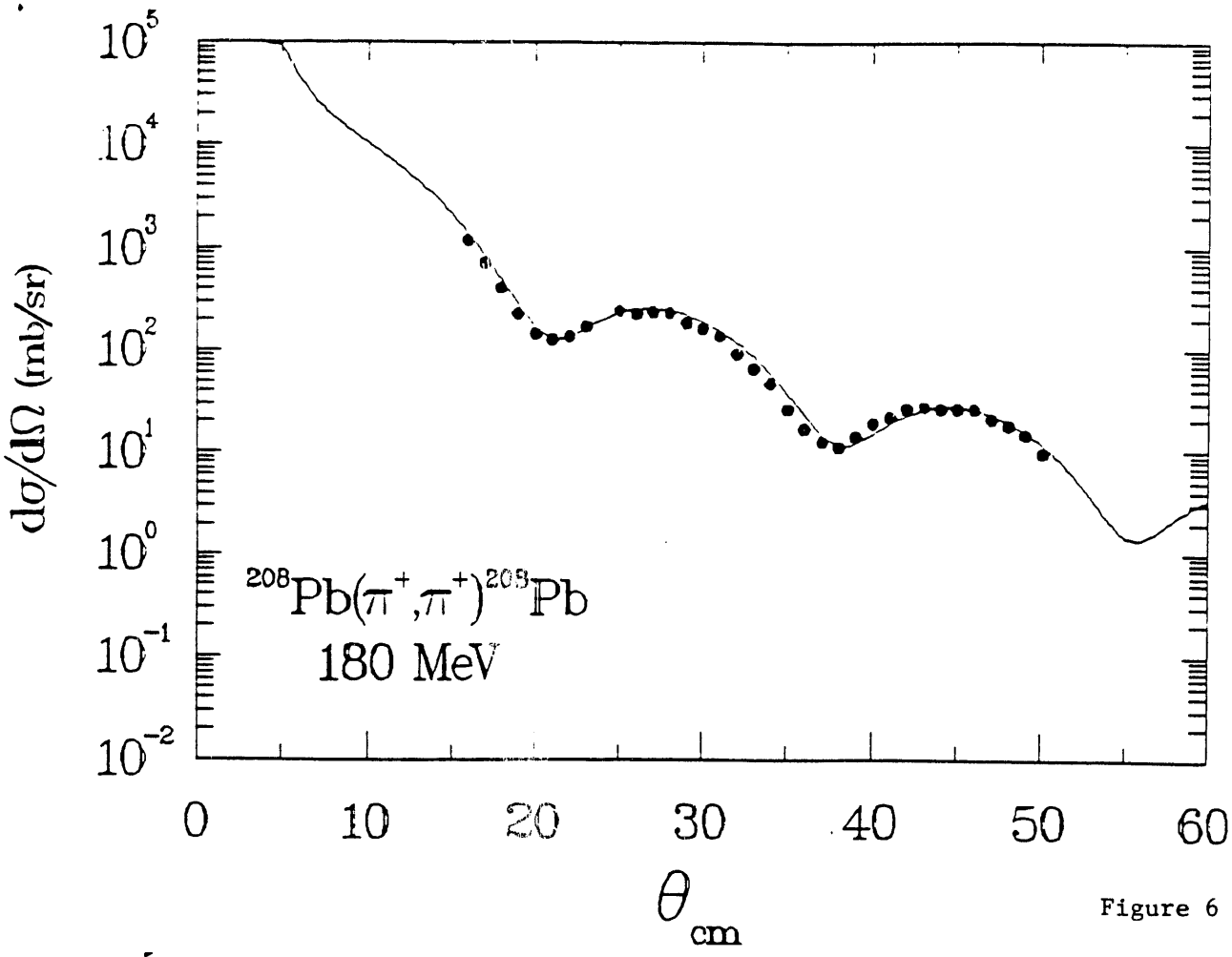

Figure 6

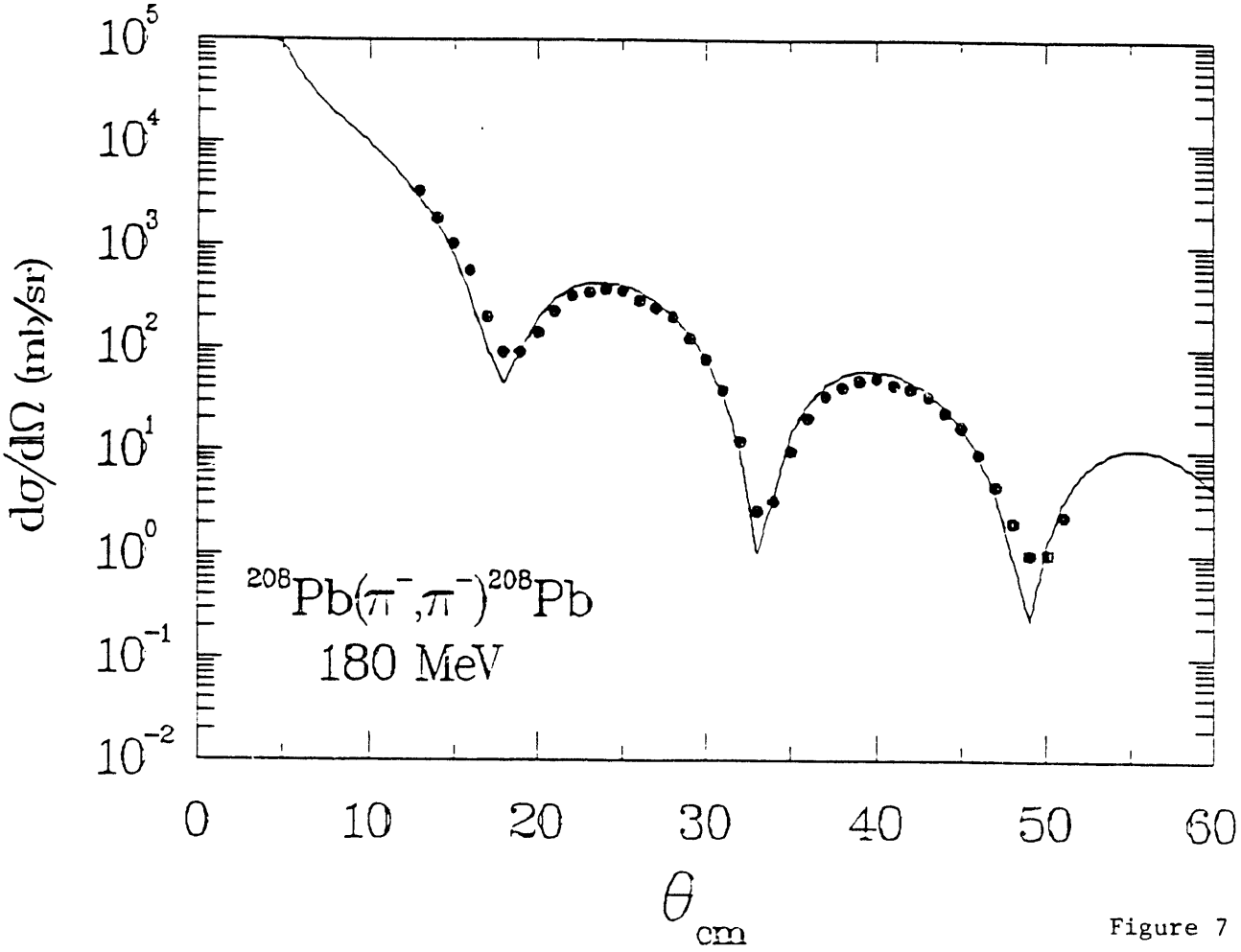

Figure 7

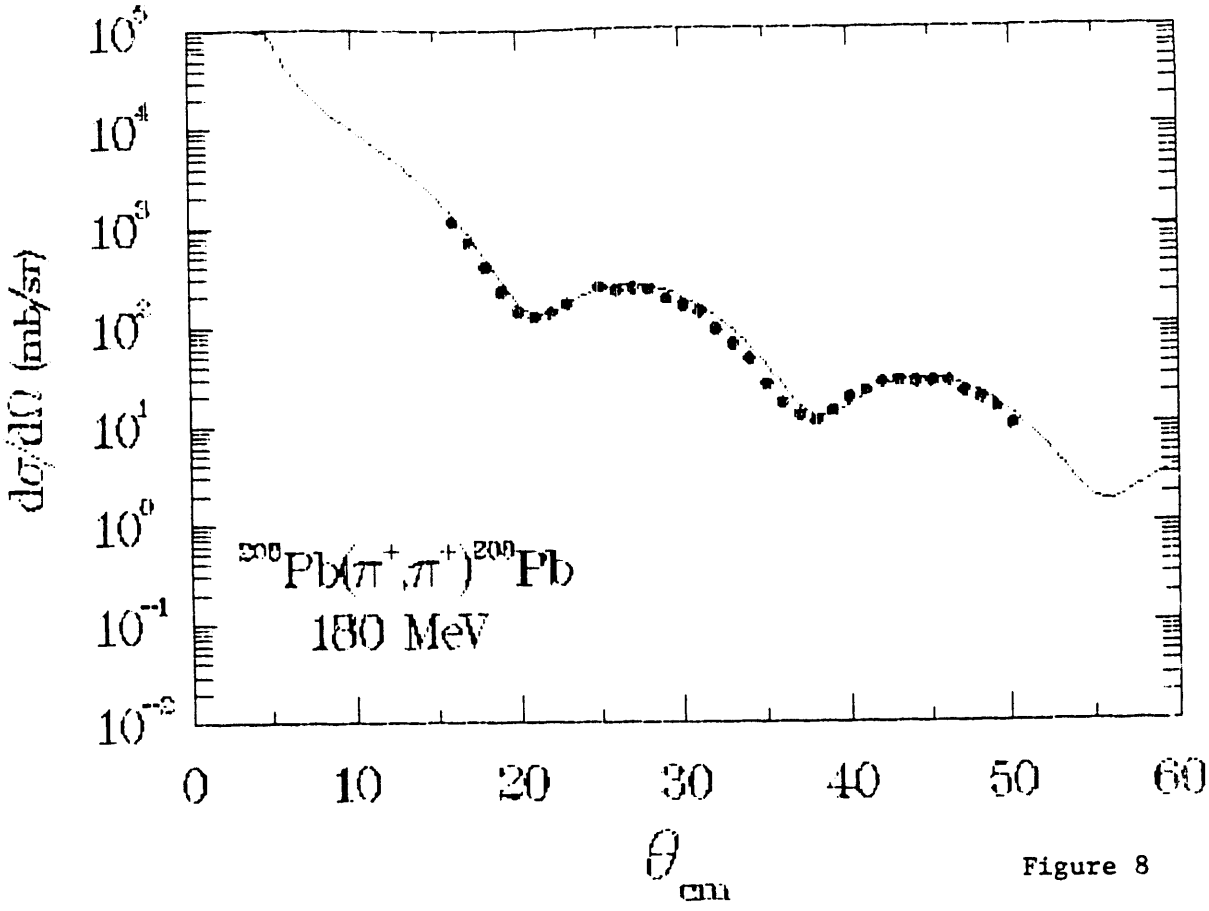

Figure 8

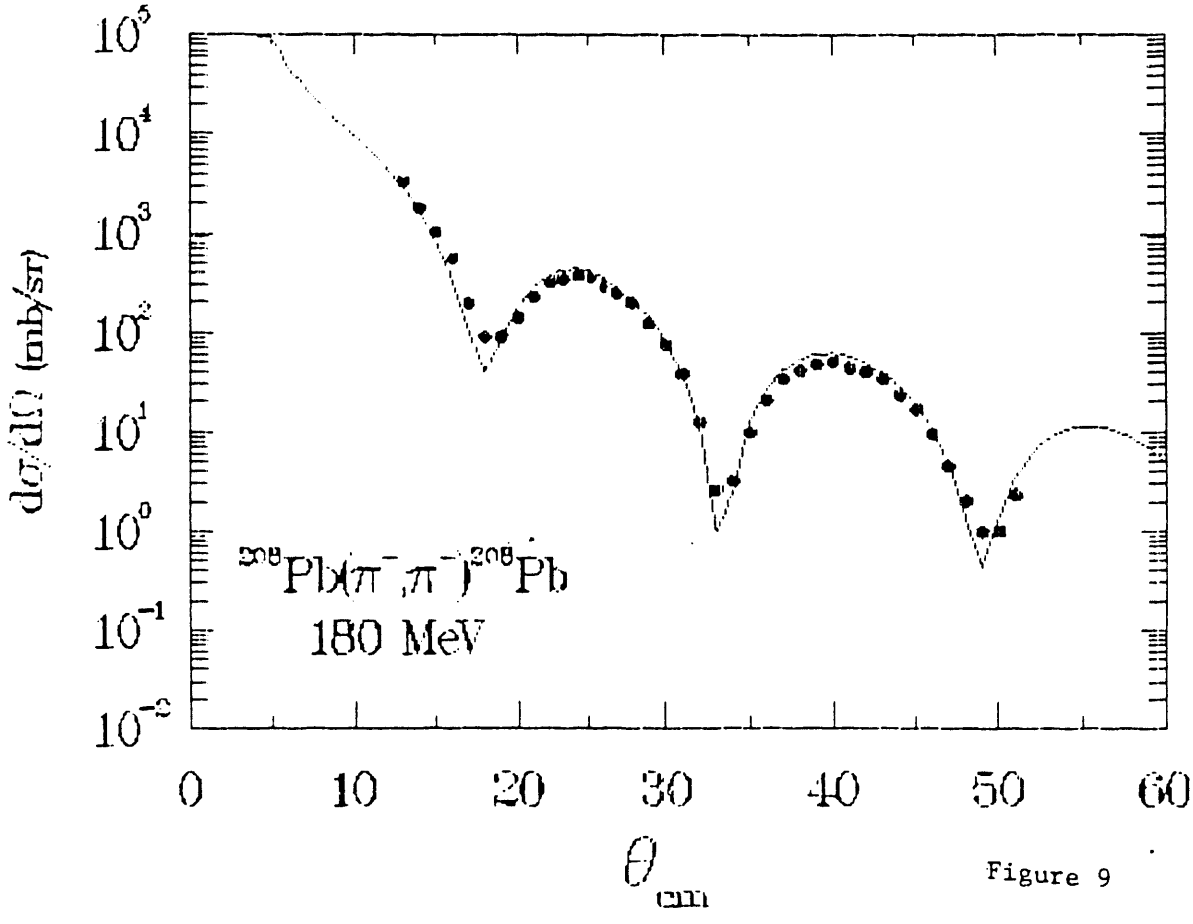

Figure 9

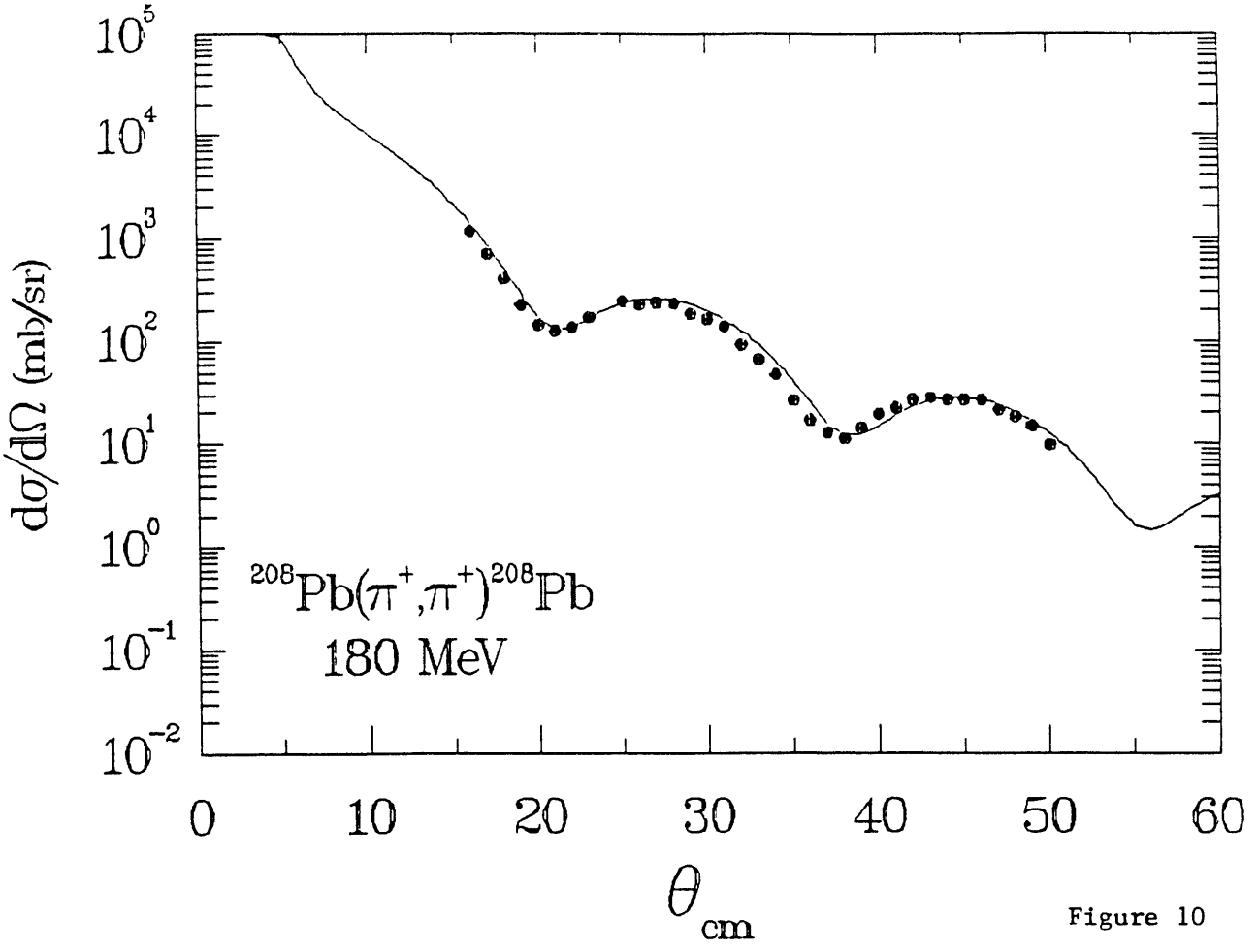

Figure 10

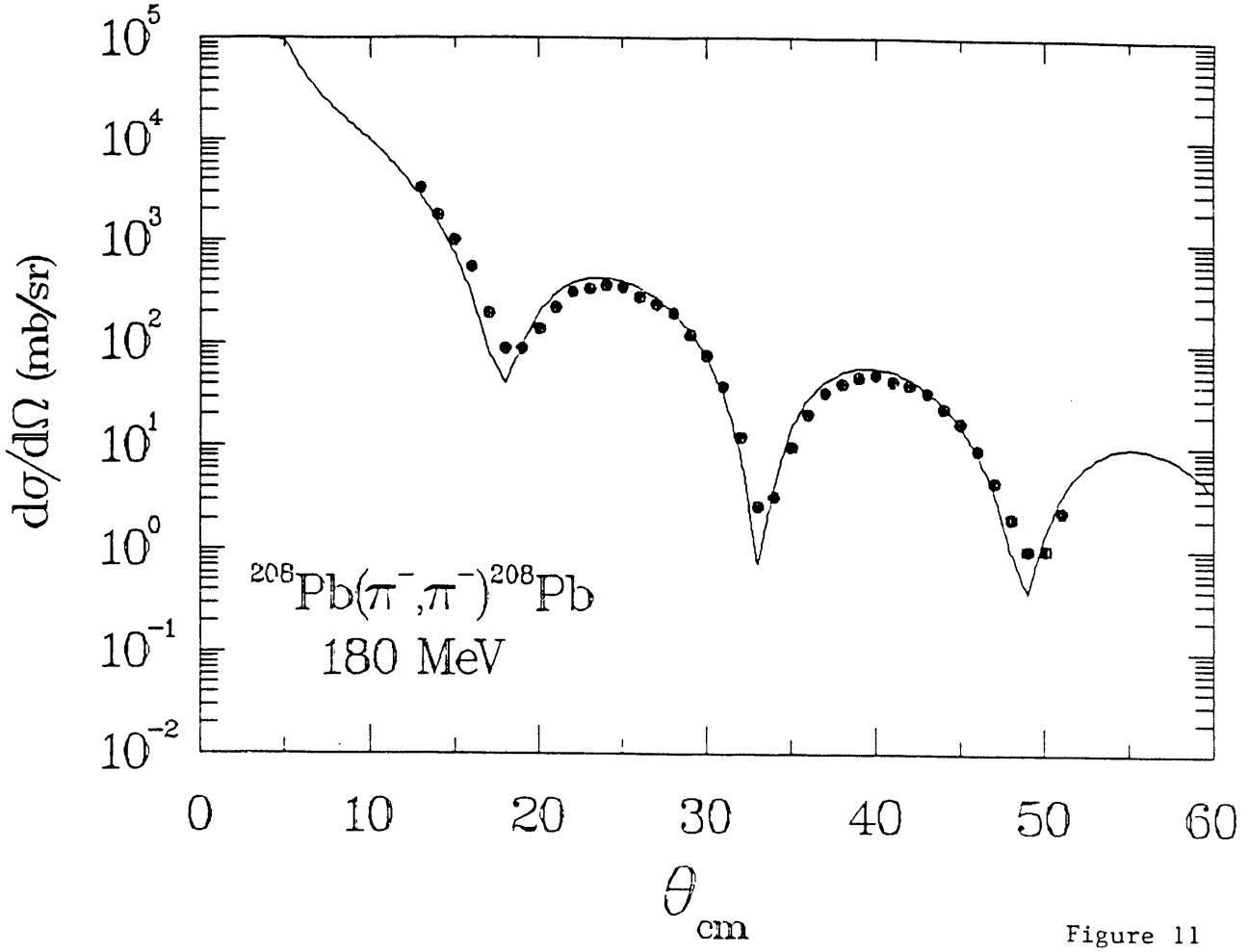

Figure 11

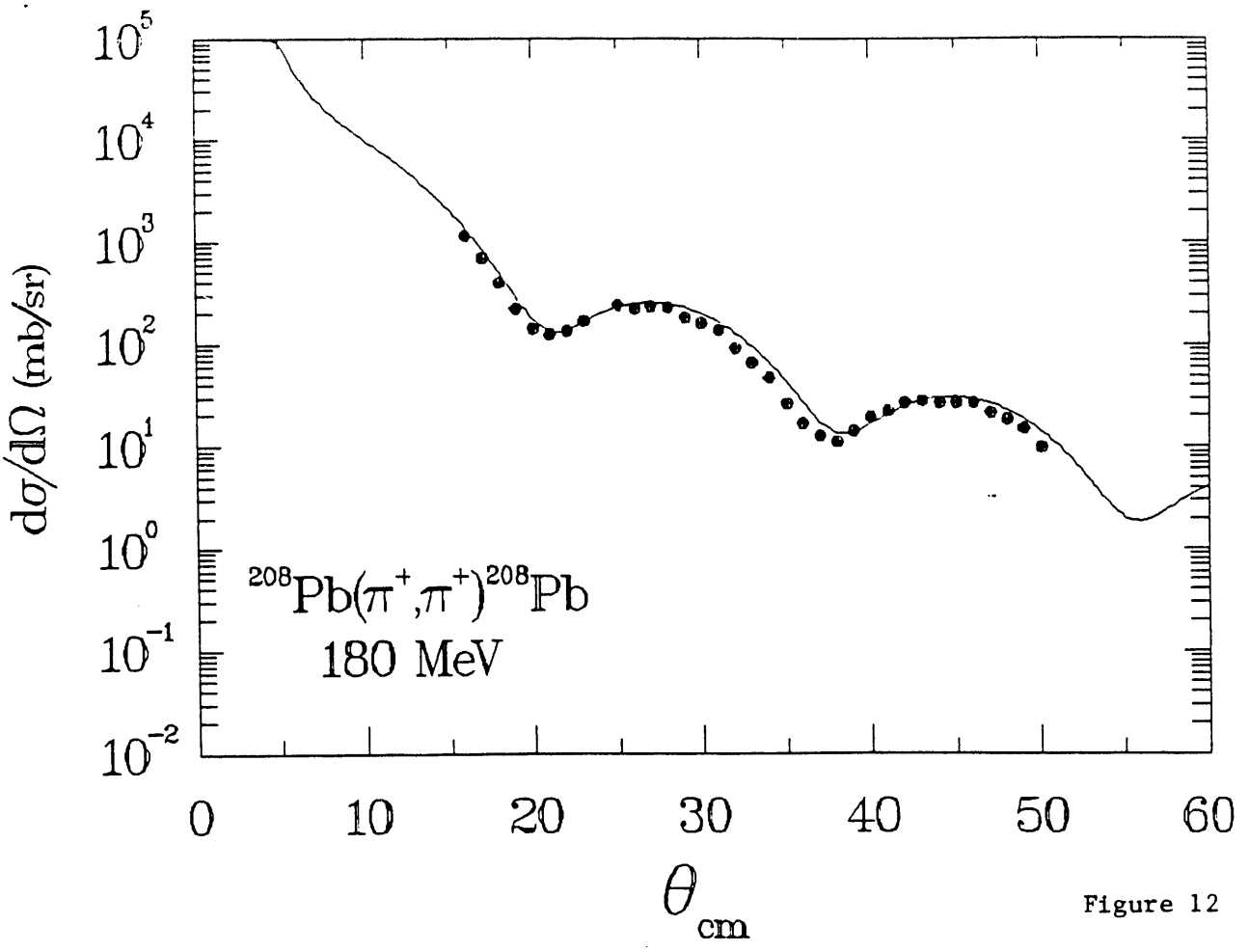

Figure 12

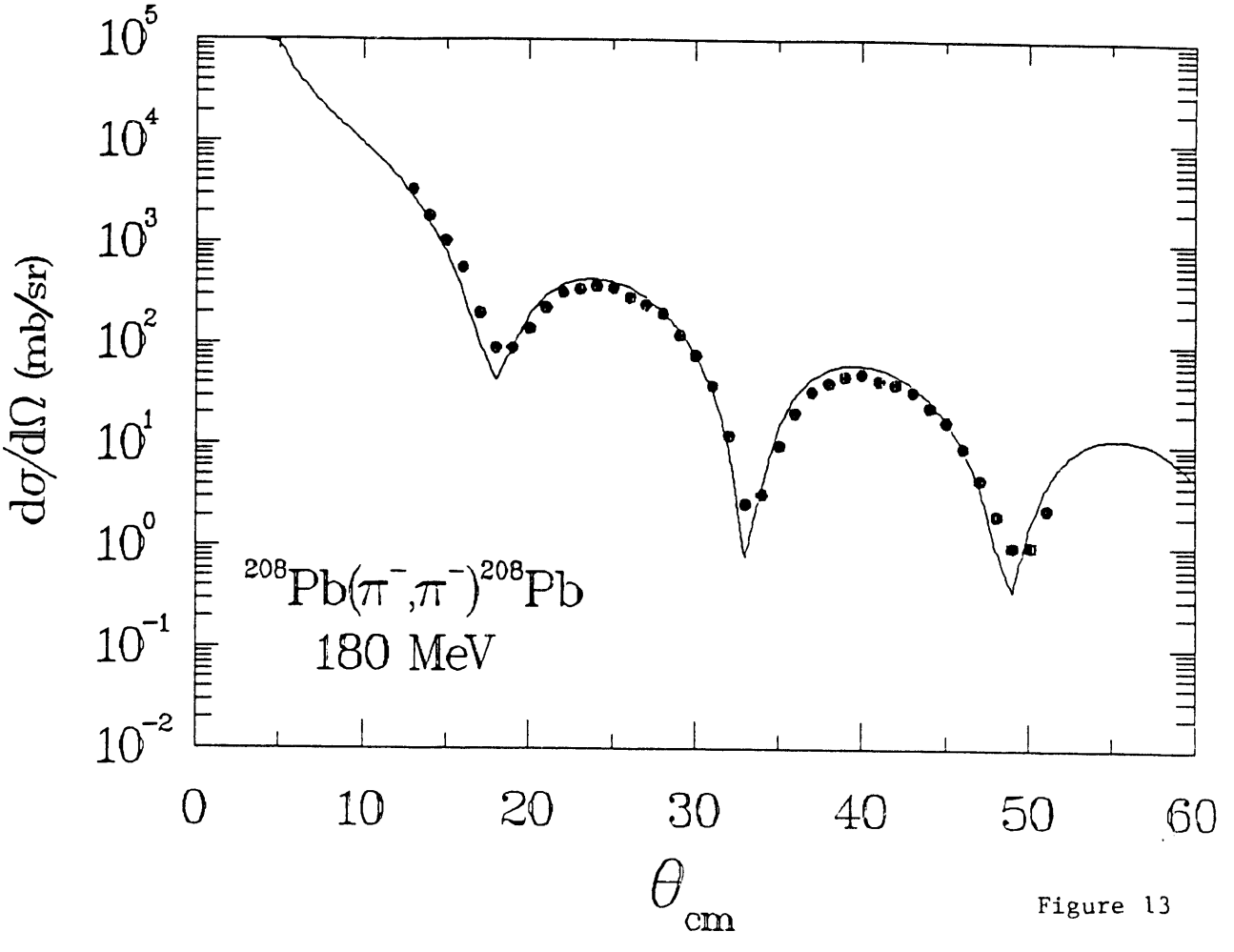

Figure 13

II.C. E855, Measurement of the ^{206,207,208}Pb Neutron Density Differences (Minnesota spokesman, U. Texas, LANL participants).

The purpose of this experiment was to obtain precise elastic proton scattering data, at T_p = 650 MeV for ^{206,207,208}Pb. Cross sections and analyzing powers were measured from $\theta_L \sim 3\text{-}26^\circ$ with a statistical accuracy of $< \pm 1\%$ in σ and $\lesssim 0.005$ for A_y (over most of the angular range). During most of the experiment the energy resolution was $\Delta E \sim 120$ keV, FWHM, limited by target thickness (~ 150 mg/cm^2), but sufficient to resolve a number of low lying states. The ultimate objective is to obtain neutron density differences (static and transition), using electron scattering data to fix proton densities. During the period of this report, final corrections were made to the data and phenomenological optical model (POP) as well as collective form factor (CFF) analyses were completed. In addition we are exploring the use of a modified (for "swelling" effects) non relativistic impulse approximation (see Sect. II.G. below) to extract quantitative information on neutron densities.

Here we report the final results for the optical model and CFF analyses. The optical model analysis was performed with the program RELOM[1], using a ten-parameter optical potential of the form:

$$U_{opt}(r) = V\, f(x_R) + i\, Wf(x_I) - (V_s - iW_s)\, \frac{2}{r} f'(x_s)\vec{\ell}\cdot\vec{\sigma} + V_c(r) \qquad (1)$$

where

$$f(x) = \frac{1}{1+e^x}\ ,\ f'(x) = \frac{d}{dr} f(x),\ \text{and}$$

$$x_R = \frac{r - r_R A^{1/3}}{a_R} \quad , \quad x_I = \frac{r - r_I A^{1/3}}{a_I} \quad , \quad x_s = \frac{r - r_s A^{1/3}}{a_s} \quad .$$

Three solutions for each isotope were found and are listed in Table I and plotted in Fig. 1. The resulting cross section and analyzing powers are compared with experimental data in Figs. 2 and 3.

Also shown in Table I are the r.m.s. radii of the (dominant) imaginary potentials, $\langle r^2 \rangle_W$ for the three potential sets. For comparison are shown the $\langle r^2 \rangle_m$ for the theoretical (HFB) matter densities of Decharge[8]. In a folding model, such as the first order impulse approximation, the potential and matter radii are related by

$$\langle r^2 \rangle_W = \langle r^2 \rangle_m + \langle r^2 \rangle_\tau = \langle r^2 \rangle_m + \text{constant} \qquad (2)$$

where $\langle r^2 \rangle_\tau$ is that of the N-N imaginary t-matrix. It can be seen that whereas the theoretical matter radii increase approximately linearly with A, the phenomenological potential radii show a decrease from ^{207}Pb to ^{208}Pb, indicating possible matter density discrepancies with those of Decharge, at least for ^{207}Pb.

The inelastic states of ^{206}Pb and ^{208}Pb were then fit with the collective vibrational model. The program ECIS was used to obtain values for β_λ and $\delta_\lambda = \beta_\lambda R_I$, the (imaginary) deformation length. Excitation was assumed to take place as a one-step process. Coupling between states was neglected. The β_λ and δ_λ for each solution are given in Table II. The resulting cross sections and analyzing powers are compared with experimental data in Figs. 4-12.

The deformation lengths (which were similar for all three potential sets) were compared with electron scattering data[2], when available, in order to decompose potential deformation lengths into their neutron and proton parts. We assume that the interaction potential can be written.

$$H_{int} = \delta_U \frac{dU_{opt}}{dr} \simeq \delta_n \frac{\partial U_n}{\partial r} + \delta_p \frac{\partial U_p}{dr} \quad , \tag{3}$$

where δ_U is the deformation length as determined above, U_n and U_p are the neutron and proton contributions to the optical potential.

It can be shown[3] that $\delta_n = \frac{\partial \delta_U - (1-\bar{K})\delta_p}{1+\bar{K}}$, where $\bar{K} = .142$ for ^{208}Pb and $\bar{K} = .134$ for ^{206}Pb at $T_p = 650$ MeV. δ_p is related to B(Eλ) by

$$\delta_p = \frac{4\pi\sqrt{B(E\lambda)}}{Z(\lambda+2)\langle r^{\lambda-1}\rangle_q} \qquad \text{(q:charge)} \tag{4}$$

if we assume $\delta_p = \delta_q$. The B(Eλ) have been obtained from electron scattering[2] for many of these states and are listed in Table III. Also, in Table III are the values of δ_p and δ_n obtained from this analysis, and $\frac{\bar{M}_n}{\bar{M}_p}$ for each state, where

$$M_i(\lambda) = \frac{\lambda+2}{4\pi} \langle r^{\lambda-1}\rangle_i \, \delta_i \qquad \text{(i:n, p, or q)} \tag{5}$$

is the reduced matrix element (N or Z factors omitted). The $\langle r^{\lambda-1}\rangle$ for ^{208}Pb were calculated from point densities of Ray, Coker, and Hoffmann[4], Hoffmann et al.,[5] and Ray,[6] and are given in Ref. 3. The values for ^{206}Pb

were scaled by $A^{(\lambda-1)/3}$ from those of ^{208}Pb. The values for the reduced matrix element ratios for ^{208}Pb are close to those obtained previously[7] at 800 MeV except for the 8^+ state for which the model is very rough. They are, however, systematically a bit lower than the 800 MeV values in accord with the trends noted in Ref. 7. The matrix element ratios for ^{206}Pb are new and indicate that the 2^+state, as expected, is neutron dominated, whereas the 4^+ (4.35 MeV) state is strongly proton dominated.

This work formed the M.A. thesis for one of our group (A.M.M.) and a paper is in preparation.

References

1. G. J. Pyle, computer program RAROMP, Univ. of Minnesota, Informal Report COO-1265-64, 1964 (unpublished) modified for relativistic energies.
2. Values for ^{206}Pb were taken from M. P. Webb, Nuclear Data Sheets 26, 145 (1979); values for ^{208}Pb have been compiled in Ref. 3 where original references are given.
3. M. M. Gazzaly, N. M. Hintz, G. S. Kyle, R. K. Owen, G. W. Hoffmann, M. Barlett, and G. S. Blanpied, Phys. Rev. C25, 408 (1982).
4. L. Ray, W. R. Coker and G. W. Hoffmann, Phys. Rev. C18, 2641 (1978).
5. G. Hoffmann, et al., Phys. Rev. C21, 1488 (1980).
6. L. Ray, Phys. Rev. C19, 1855 (1979).
7. N. M. Hintz, D. Cook, M. Gazzaly, M. A. Franey, M. L. Barlett, G. W. Hoffmann, R. Fergerson, J. McGill, G. Pauletta, R. L. Boudrie, J. B. McClelland, and K. W. Jones, Phys. Rev. C37, 692 (1988).
8. J. Decharge, Centre d'Etudies de Bruyeres-le-Chatel report CEA-N-2260 (1982), unpublished.

Table I

Phenomenological optical model parameters at T_p = 650 MeV for Pb isotopes.
The potential is defined in the text (energies in MeV, lengths in fm).

		V	r_R	a_R	W	r_I	a_I	V_{so}	W_{so}	r_{so}	a_{so}	v^2	$\langle r^2 \rangle_W$	$\langle r^2 \rangle_m$ [a]
^{206}Pb	I	-0.74	1.5419	0.4678	-68.06	1.0748	0.6437	-1.22	-0.29	1.0726	0.8616	187	5.468	5.458
^{207}Pb	I	-0.68	1.5395	0.4619	-67.42	1.0764	0.6433	-1.23	-0.27	1.0740	0.8616	169	5.481	5.465
^{208}Pb	I	-0.58	1.5373	0.4388	-68.94	1.0727	0.6472	-1.25	-0.28	1.0696	0.8704	146	5.480	5.474
^{206}Pb	II	57.51	0.6903	0.4304	-71.77	1.0654	0.6648	-1.18	-0.21	1.0854	0.8563	258	5.465	5.458
^{207}Pb	II	50.94	0.6986	0.4346	-70.90	1.0676	0.6626	-1.20	-0.19	1.0837	0.8590	228	5.477	5.465
^{208}Pb	II	55.74	0.6895	0.4667	-72.66	1.0639	0.6647	-1.22	-0.21	1.0800	0.8643	190	5.472	5.474
^{206}Pb	III	1.76	1.1911	0.0018	-61.83	1.0844	0.6478	-1.07	-0.17	1.1058	0.8376	262	5.514	5.458
^{207}Pb	III	1.62	1.1914	0.0029	-61.39	1.0860	0.6459	-1.10	-0.15	1.1032	0.8414	232	5.525	5.465
^{208}Pb	III	1.69	1.1807	0.0869	-64.33	1.0786	0.6537	-1.14	-0.18	1.0958	0.8539	195	5.514	5.474

[a] Theoretical (HFB) densities of Decharge, Ref. 8.

Table II

Deformations (β_λ) and (imaginary) deformation lengths (δ_U) for three potential sets.

Nucleus	λ^π	E_{ex}(MeV)	β_λ I	β_λ II	β_λ III	δ_U(fm) I	δ_U(fm) II	δ_U(fm) III	δ_U(fm) (aver.)
^{206}Pb	2^+	0.80	.047	.048	.046	.298	.302	.295	.298
	4^+	1.68	.028	.028	.028	.178	.176	.179	.178
	4^+	2.00	.015	.016	.016	.095	.101	.102	.099
	7^-	2.20	.025	.028	.026	.159	.176	.167	.167
	3^-	2.65	.122	.125	.125	.774	.787	.801	.787
	2^+	4.11	.066	.067	.066	.419	.422	.423	.421
	4^+	4.35	.078	.080	.081	.495	.503	.519	.506
	6^+	4.39	.080	.081	.080	.508	.510	.512	.510
	8^+	4.59	.057	.059	.057	.362	.371	.365	.366
^{208}Pb	3^-	2.61	.125	.127	.127	.794	.801	.812	.802
	5^-	3.20	.055	.056	.056	.350	.353	.358	.354
	5^-	3.71	.042	.043	.043	.267	.271	.275	.271
	2^+	4.09	.072	.073	.072	.458	.460	.460	.459
	4^+	4.32	.086	.085	.087	.547	.536	.556	.546
	6^+	4.42	.077	.078	.077	.489	.492	.492	.491
	8^+	4.61	.063	.065	.063	.400	.410	.403	.404

Table III

Neutron-proton transition matrix element ratios for several excited states of ^{206}Pb and ^{208}Pb. References for the B(Eλ) are given in Ref. 2 and 3.

Nucleus	λ^{π}	E (MeV)	δ_U (fm)	δ_p (fm)	δ_n (fm)	B(Eλ) (e^2b^λ)	$\tilde{M}_n/\tilde{M}_p$	M_n/M_p
^{206}Pb	2^+	0.80	.298	.248	.336	0.115(6)	1.388	2.099
	3^-	2.65	.787	.818	.763	0.64(6)	0.985	1.490
	2^+	4.11	.421	.351	.474	0.23(2)	1.384	2.093
	4^+	4.35	.506	.660	.388	0.22(2)	0.644	0.974
^{208}Pb	3^-	2.61	.802	.798	.805	0.621(16)	1.065	1.636
	5^-	3.20	.354	.395	.323	0.0447(30)	0.936	1.438
	5^-	3.71	.271	.290	.257	0.0241(18)	1.014	1.558
	2^+	4.09	.459	.409	.497	0.318(16)	1.245	1.913
	4^+	4.32	.546	.546	.546	0.155(10)	1.096	1.684
	6^+	4.42	.491	.635	.383	0.0665(67)	0.726	1.116
	8^+	4.61	.404	.298	.484	0.0054(9)	2.216	3.405

Figure Captions

Fig. 1: Optical model potentials for ^{208}Pb vs. r at T_p = 650 MeV. The solutions for the other isotopes are very similar. Solutions I-III are represented by solid, chain-dashed, and dashed lines respectively in this and subsequent figures.

Fig. 2: Elastic cross sections compared with optical model predictions.

Fig. 3: Elastic analyzing powers compared with optical model predictions. The three curves are as in Fig. 1.

Figs. 4-11: Inelastic cross sections and analyzing powers for states in ^{206,208}Pb compared with predictions of the vibrating potential model ("collective form factors"). The states (labelled J^{π}) are those given in Table II.

Fig. 12: Measured cross sections and analyzing powers for unresolved 4^+(4.35 MeV) - 6^+(4.39 MeV) doublet in ^{206}Pb. The top curve in each figure shows the predictions of the vibrating potential model with potential set I. The lower curves in the lower figure show the separate 4^+ and 6^+ components.

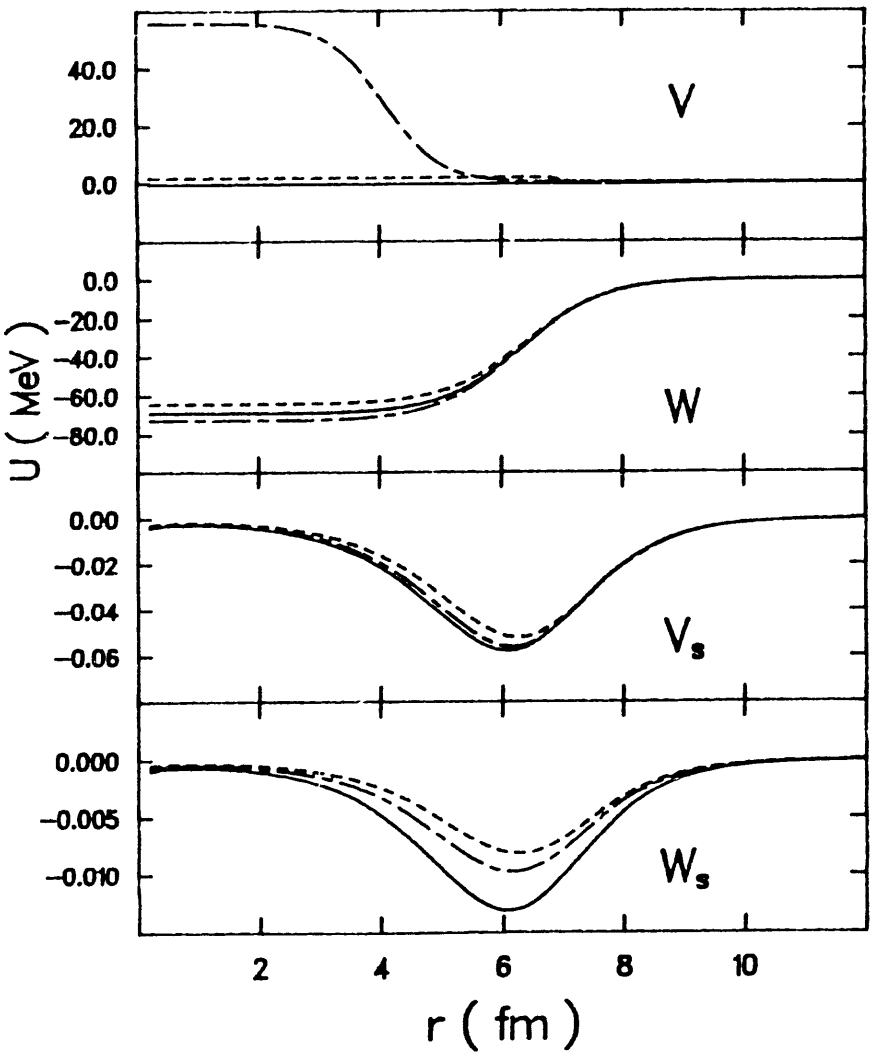

Figure 1

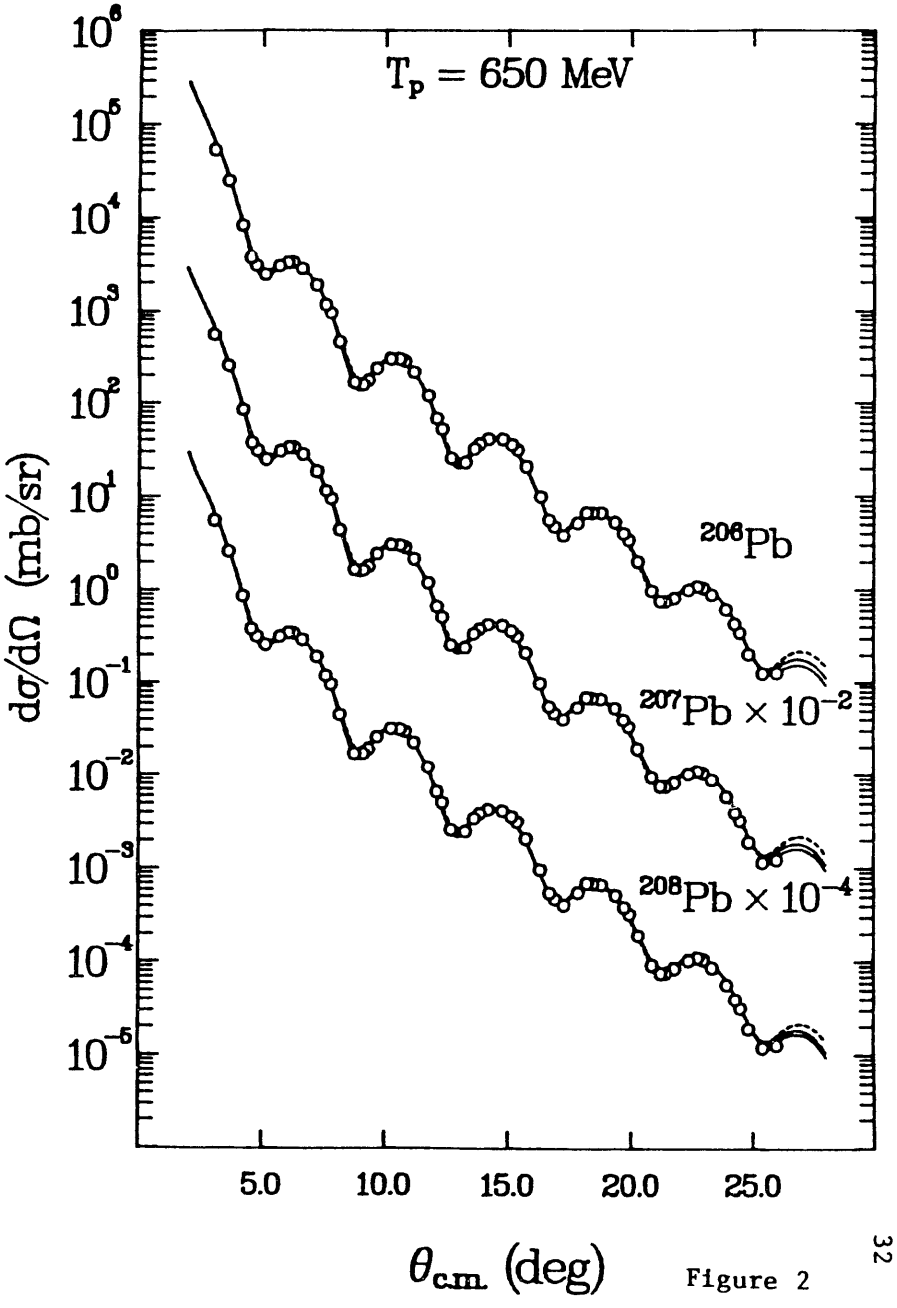

Figure 2

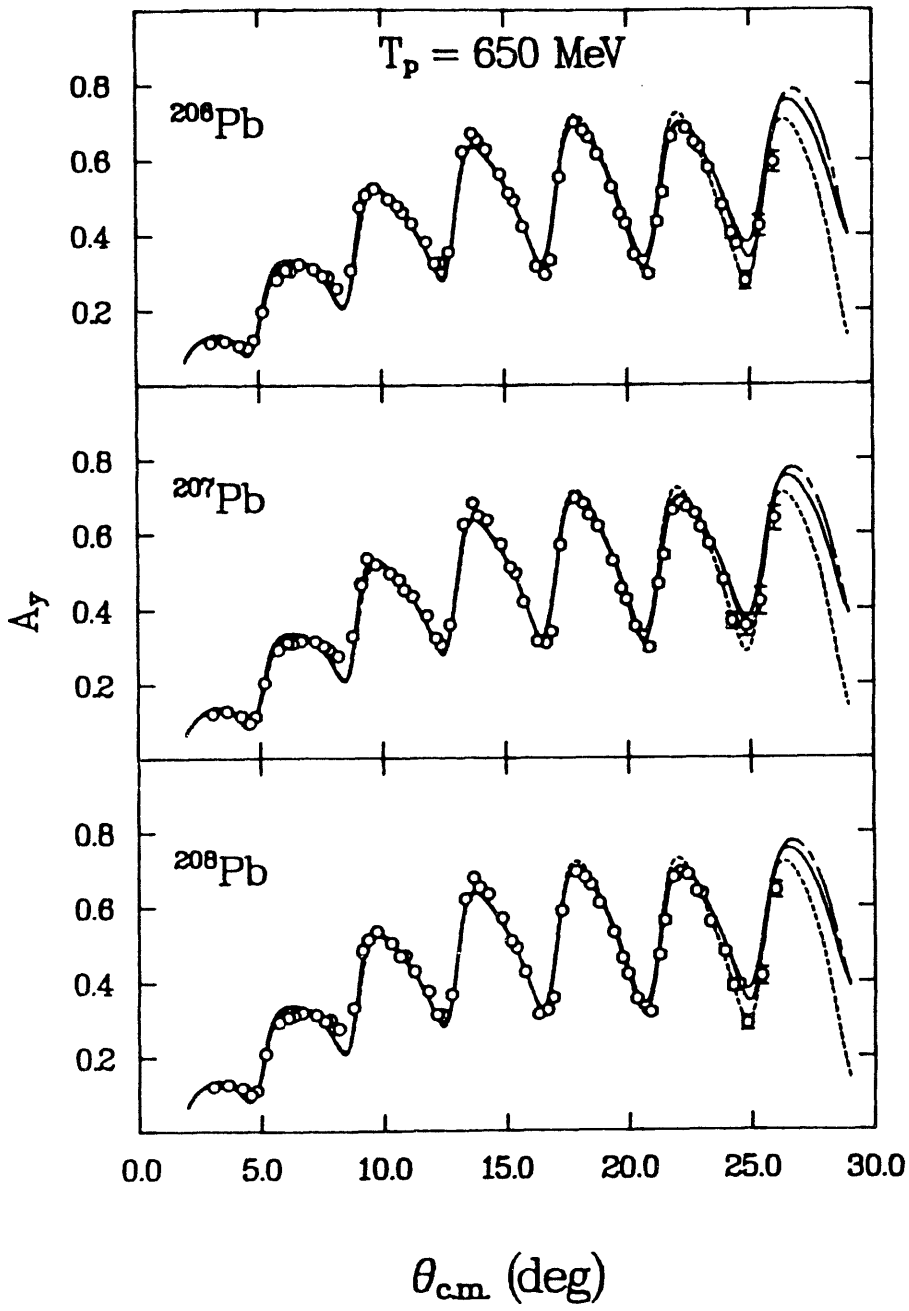

Figure 3

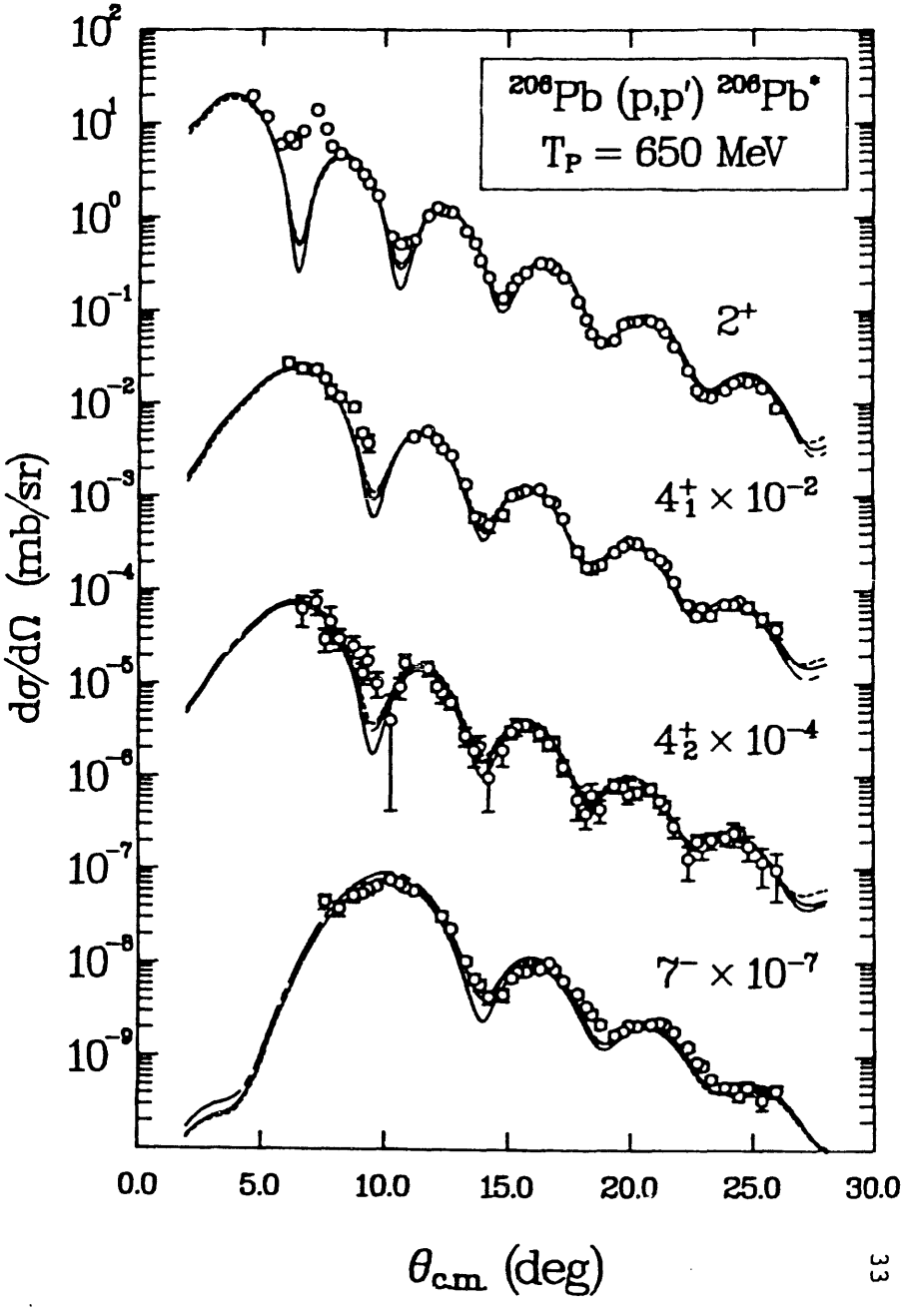

Figure 4

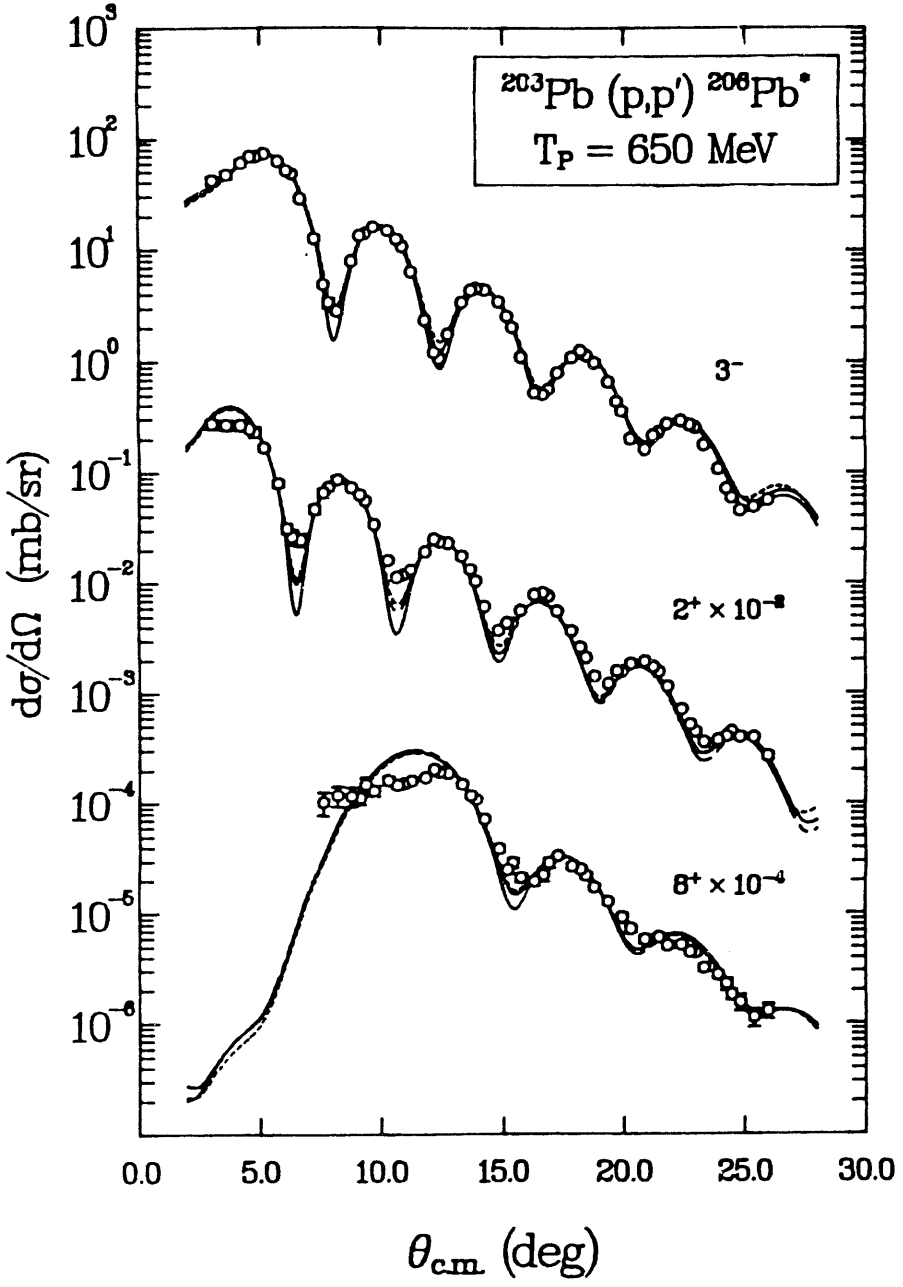

Figure 5

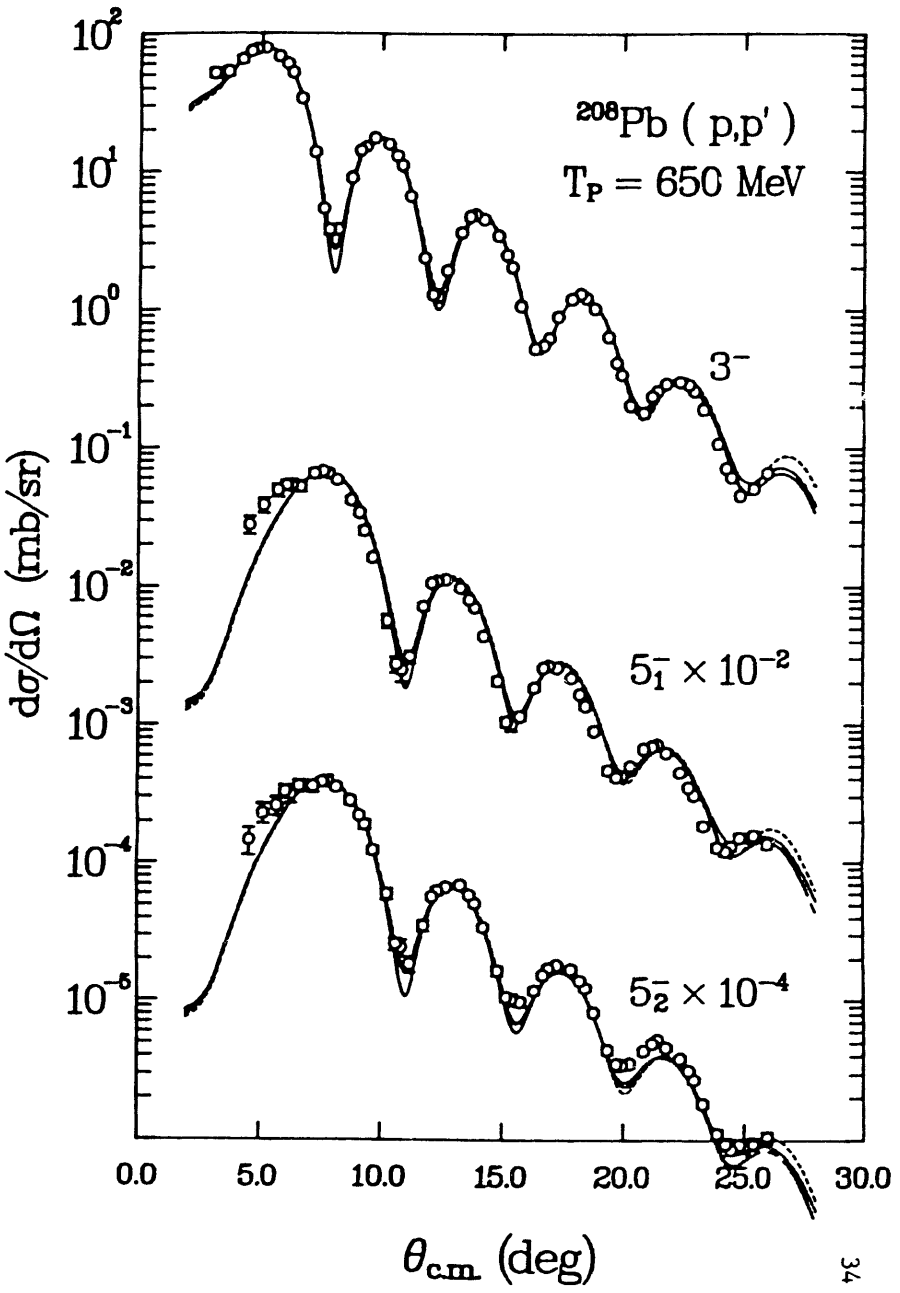

Figure 6

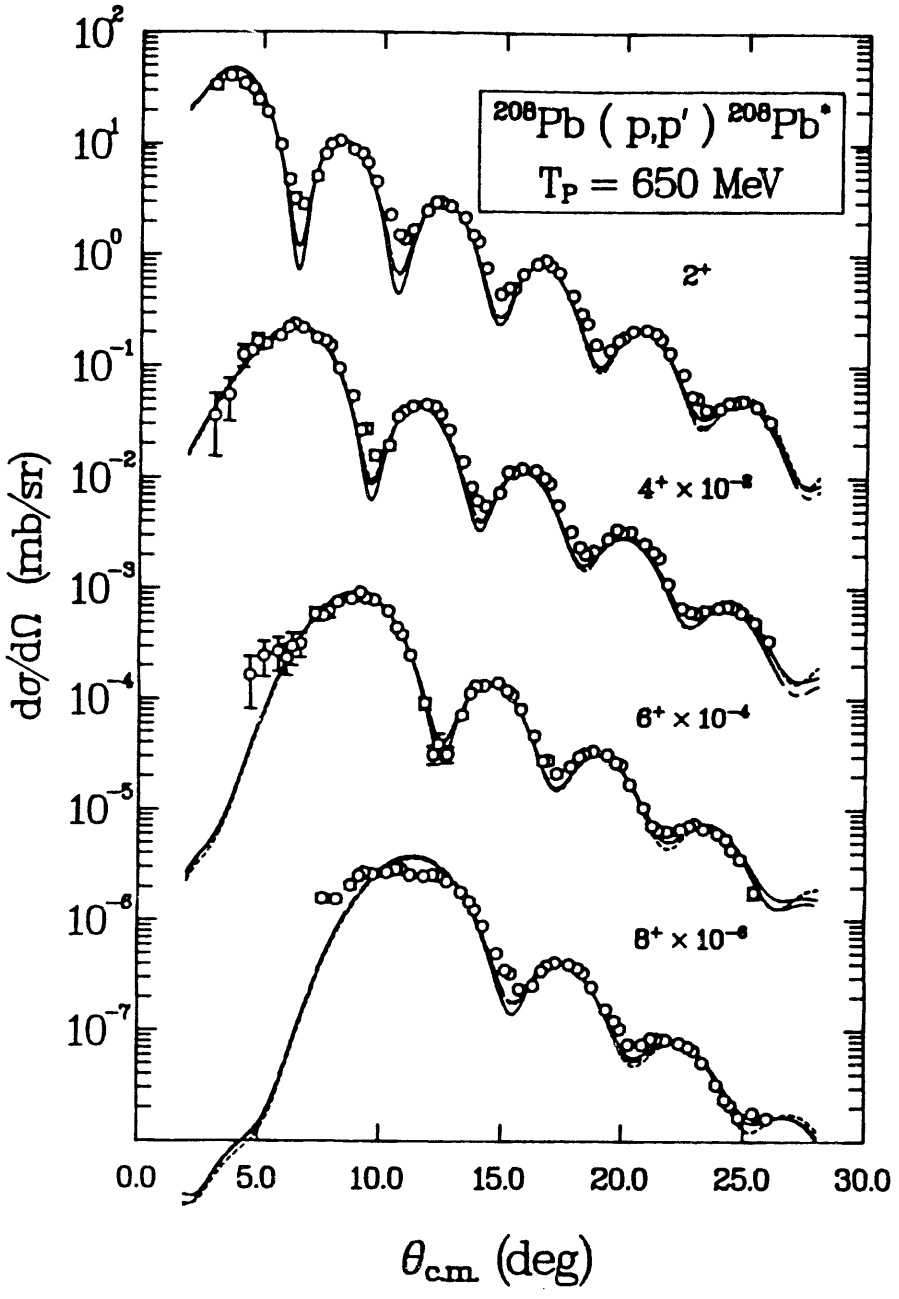

Figure 7

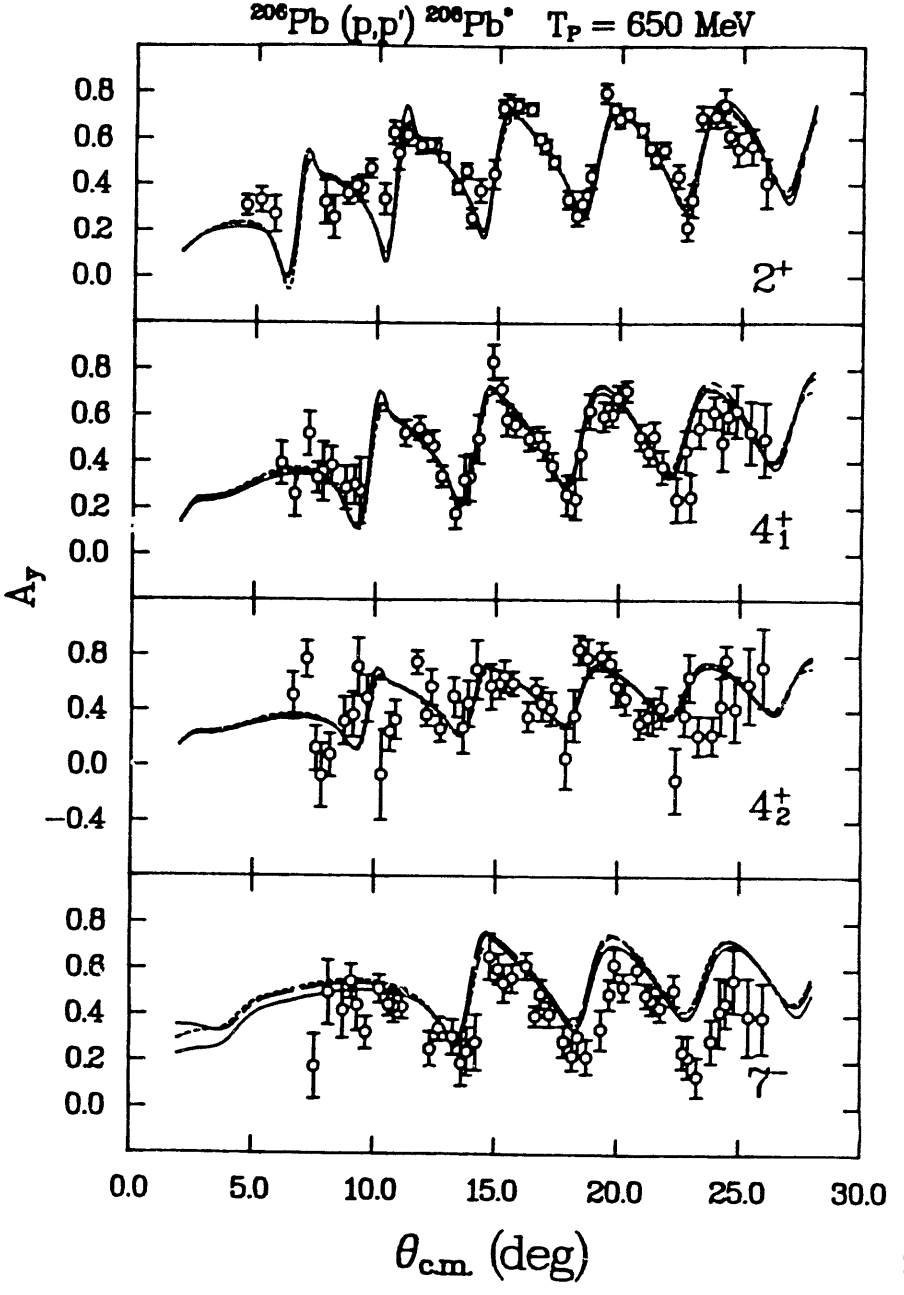

Figure 8

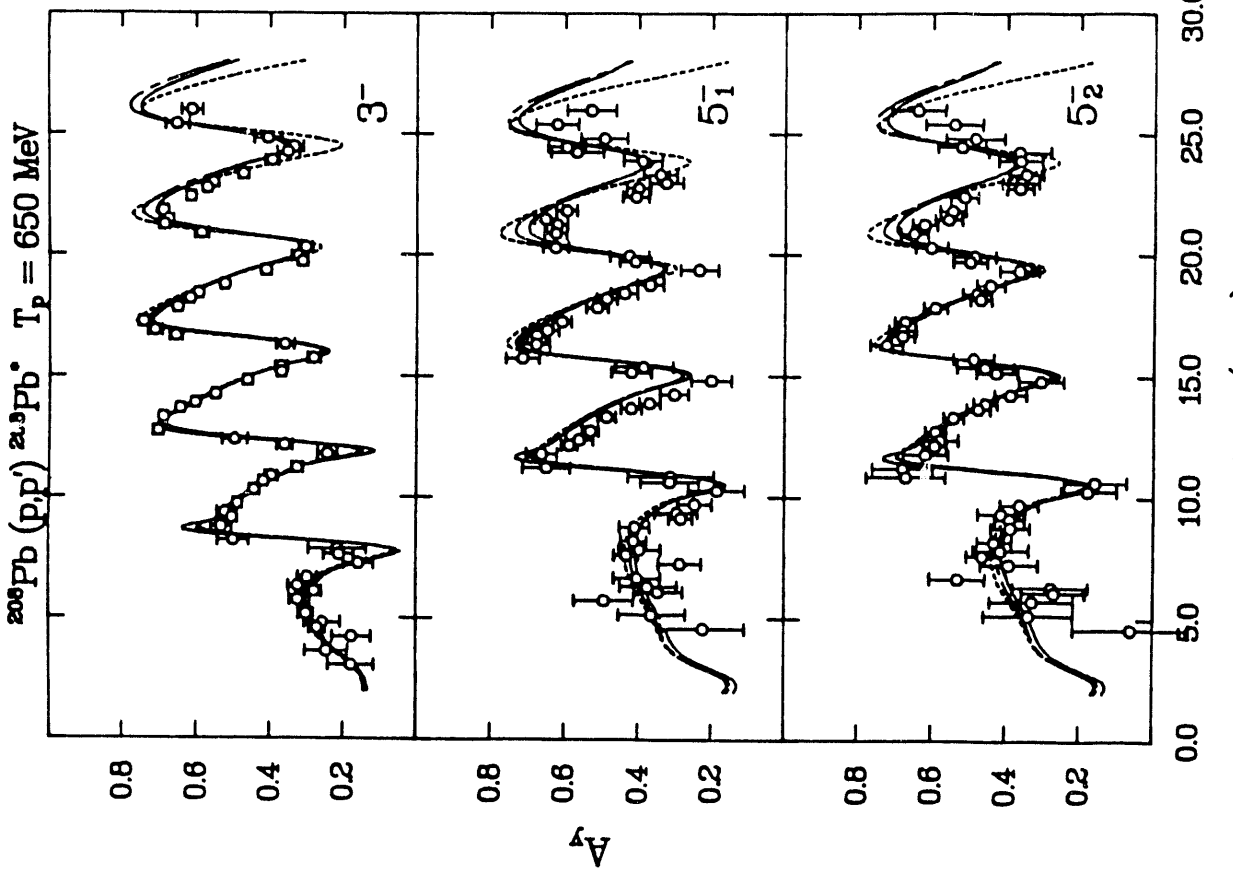

Figure 9

Figure 10

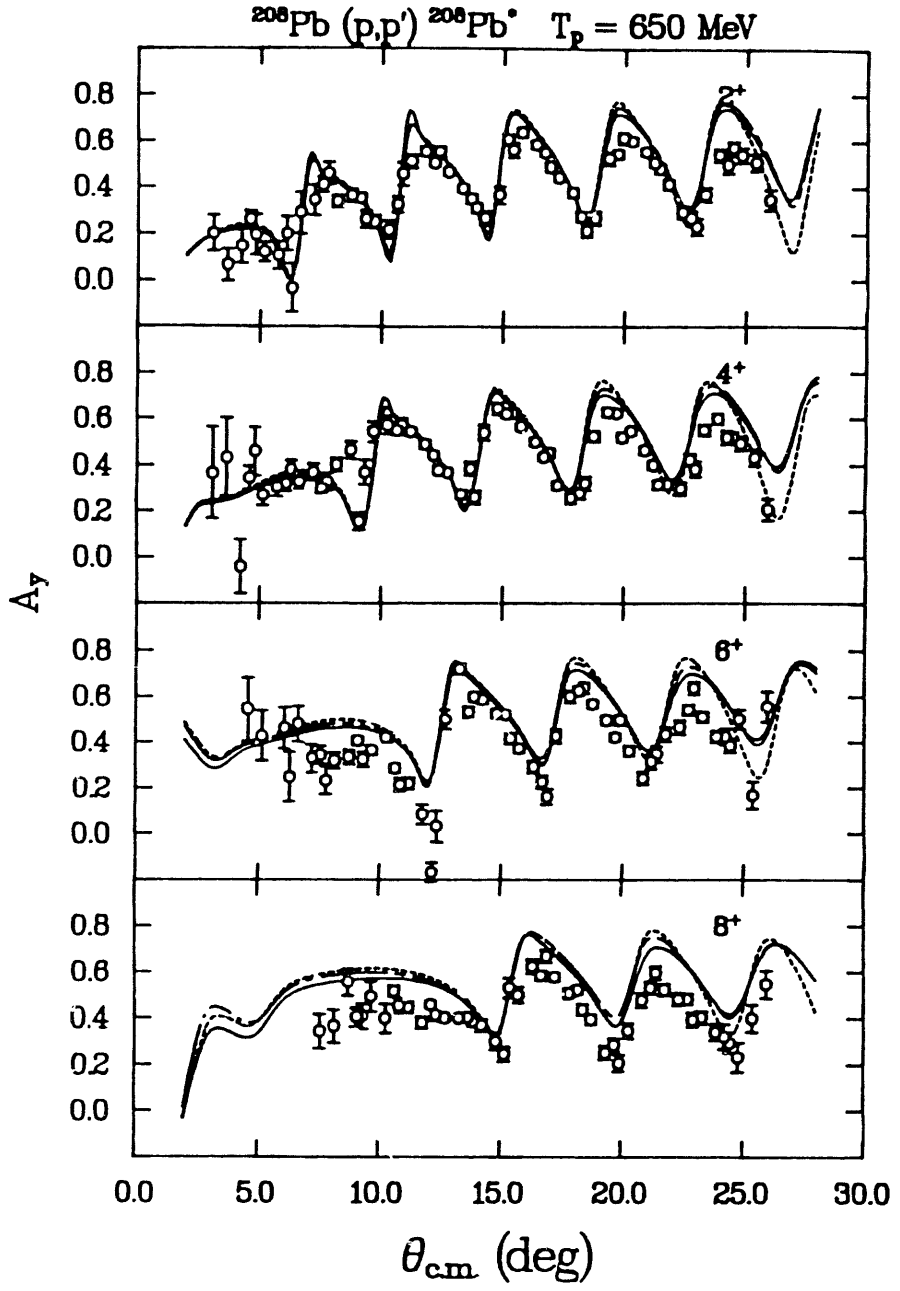

Figure 11

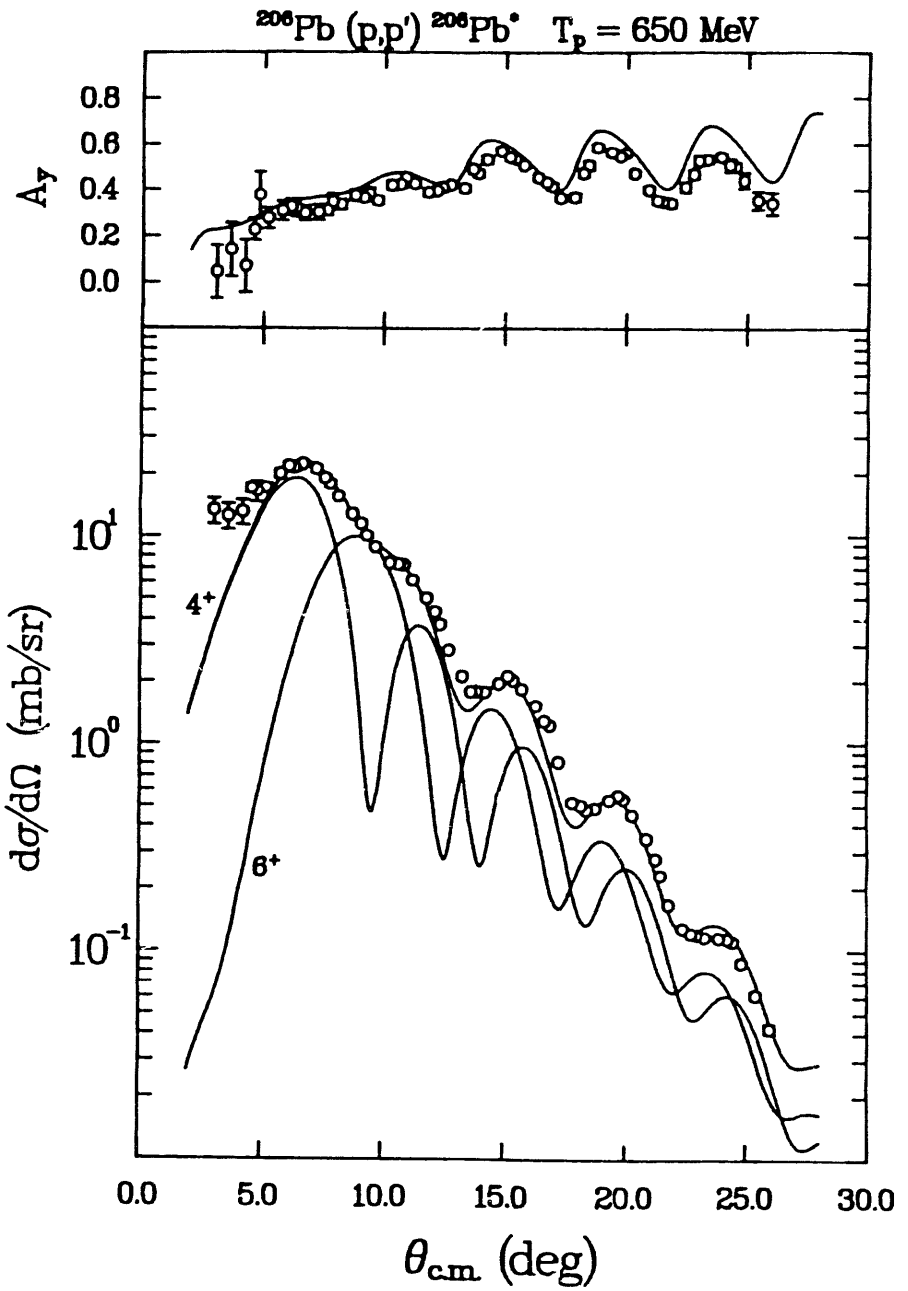

Figure 12

II.D. E903U, Inelastic Scattering of 650 MeV Protons from ^{194,196}Pt (Minnesota Spokesman, U. Texas, INS Tokyo, CEN Saclay participants).

The goal of experiment E903U was to study additional transition nuclei at the end of the rare earth region using inelastic proton scattering. These nuclei are known to undergo complex changes in shape as one goes from one end of the transition region to the other. Hence their study provides an excellent test of the interaction boson model (IBM)[1].

The survey of the transition region began with experiment 903 -- a study of ^{150}Nd, ^{154}Gd and ^{192}Os. Two additional targets ^{194,196}Pt (supplied by CEN Saclay) were included in the subsequent experiment E903U which ran in Sept. 88. We are also awaiting the scheduling of E1133 to study ^{182}W at T_p = 650 MeV at HRS. Experiment E903U was performed using 647 MeV polarized protons. During the experiment data runs were also performed on ^{150}Nd, ^{154}Gd and ^{192}Os to extend the angular range of previous data by taking data at θ = 3°, 5°, 17° and 19°. For ^{194,196}Pt, data were acquired in steps of $\Delta\theta$ = 2° from 3° to 21°. Figures 1 and 2 show the spectra obtained for ^{194}Pt and ^{196}Pt at θ_L = 15° and 17° respectively. Peak stripping of the data was performed with the program LOAF[2]. Angular distributions for the cross sections and analyzing power were calculated for several low lying states (0_1^+, 2_1^+, 2_2^+, 3^-, 4_1^+, 4_2^+, 4_3^+) in both the nuclei. These are shown in Figs. 3-15. Due to target contaminants (oxygen and carbon) the small angle data below ~ 7° are unreliable. These data need to be restripped by suitably subtracting the contributions from the contaminants. Elastic σ and A_y data for ^{150}Nd and ^{154}Gd (including new data from E903U) are shown in Figs. 16, 17 along with optical model fits.

The data analysis was performed as follows. To understand the shape transitions occurring in the nuclei it is important to obtain their deformation parameters. Owing to the strongly coupled nature of the low lying levels, the coupled channels program ECIS[3] was used. The optical potential was assumed to have a Woods Saxon shape and it included both real and imaginary spin orbit terms. To begin with several sets of phenomenological optical potentials were obtained for ^{194,196}Pt using program RELOM[4]. Next, ECIS was used to obtain deformation parameters β_λ for the excited states. All calculations were done by assuming a simple $\frac{dU}{dr}$ form factors for these states. Also, the same deformation, β_λ was assumed for all parts of the potential. The optical potentials are given in Tables I and II and the deformation parameters in Table III. The σ ans A_y predictions from RELOM and ECIS are shown in Figs. 3-13. With these deformation parameters, we have calculated the matrix elements using the relationship

$$M_{0\lambda}^{\lambda} = \frac{3ZeR^{\lambda}}{4\pi} \beta_\lambda \qquad (1)$$

where λ is the multipolarity of the transition, and R is the half value radius. The deduced matrix elements were next compared with the predictions of the IBM as a test of the applicability of the model with reference to the role played by g-bosons.

The nuclei ^{194,196}Pt belong to a very interesting but complex region of the periodic table characterized by shape changes between spherical and deformed. The transition region can be grouped into two parts--light transitional nuclei, e.g., Nd, Sm and Gd undergo a rather abrupt change in shape from spherical to prolate axially symmetric deformed, with the

deformation setting in around N ~ 90. The heavy transitional nuclei ($180 \leq A \leq 200$) in contrast, experience a gradual shape change from prolate through oblate to sperhically symmetric. The light W, Os isotopes display rotational features whereas the heavier Pt isotopes are more of the vibrational type. Due to the complex nature of these transitions, simple rotational and/or vibrational models are inapplicable to these nuclei. In the past, various models have been ussed to describe these nuclei with varying degrees of success[5-7]. The IBM has on the other hand, provided a very elegant description of the Pt-Os region.

The IBM, in its simplest form, describes the low-lying collective states of an even-even nucleus in terms of the s-(L=0) and d-(L=2) bosons. In a further simplification (IBM-1) no distinction is made between neutron and proton bosons. It is quite easy to describe the Os-Pt region in the IBM-1 using the powerful methods of group theory, for e.g., the light Os isotopes are SU(3) like (axially symmetric rotors) whereas ^{196}Pt is known[8] to correspond to O(6) group symmetry ("γ-soft" asymmetric rotor). Thus the Pt isotopes can be treated in terms of small perturbations of the O(6) limit[9] towards the SU(3) limit.

An analysis of our data on ^{194,196}Pt was recently reported[10] and will be submitted for publication, while a related work on ^{194,196}Pt $(\vec{p},p')$ at T_p = 135 MeV is about to be published in Nuclear Physics A[11]. Here we present a brief summary.

An IBM-1 hamiltonian applicable to Pt region is

$$H = a_1 \hat{L}\cdot\hat{L} + a_2 \hat{Q}\cdot\hat{Q} \qquad (2)$$

where $\hat{L} = (d^{+}\tilde{d})^{(1)}$ is an angular momentum operator and

$$\hat{Q} = (d^{+}s + s^{+}\tilde{d})^{(2)} + \chi_{dd}(d^{+}\tilde{d})^{(2)}$$

is the quadrupole operator. s^{+} and s denote L = 0 creation and destruction operators respectively. a_1, a_2 and χ_{dd} are adjusted to fit the B(E2)'s and energy spectra. The transition operators are given by

$$T(E2) = q\hat{Q}$$

$$T(E4) = h(d^{+}\tilde{d})^{(4)} \qquad (3)$$

The parameters a_1 and a_2 affect only the energy spectra and have no effect on the B(E2)s. Thus a single parameter χ_{dd} is able to describe the whole transition region between the O(6) and SU(3) limits:

$\chi_{dd} = 0 \leftrightarrow O(6)$: ^{196}Pt

$= -\frac{7}{2} \leftrightarrow SU(3)$: Light Os isotopes

Thus χ_{dd} which is obtained by fitting experimental B(E2) ratio: $B(E2; 2_2 \rightarrow 0_1)/B(E2; 2_2 \rightarrow 2_1)$ specifies the location of a given nucleus in the Os-Pt region.

The above model has had remarkable success[9] in accurately predicting a number of B(E2) values connecting several states in the Pt isotopes (Tables IV & V), but it fails badly when applied to E4 data (Table VI). Our

calculations were made with $\chi_{dd} = 0.04$ (^{194}Pt), $= 0$ (^{196}Pt); $a_1 = .018$ and $a_2 = -.025$. A comparison of B(Eλ)s shows that whereas the B(E2)s agree quite well, this is not the case for the E4 matrix elements in particular $M^4_{04_2}$ and $M^4_{04_3}$ which are grossly underpredicted[3]. This indicated a need to modify the above simple model which is done by introducing a g-boson in the hamiltonian[12]

$$H = a_1 \hat{L}\cdot\hat{L} + a_2 \hat{Q}\cdot\hat{Q} + \epsilon_g (g^+\tilde{g})^{(0)} \tag{4}$$

where $\hat{L} = (d^+ \tilde{d})^{(1)}$

and $$\hat{Q} = (d^+ s + s^+\tilde{d})^{(2)} + \chi_{dd}(d^+\tilde{d})^{(2)} + \chi_{gd}(g^+\tilde{d} + d^+\tilde{g})^{(2)} + \chi_{gg}(g^+\tilde{g})^{(2)} \tag{4a}$$

where ϵ_g denotes the g-boson energy. The Eλ transition operators then become

$$T(E2) = q\hat{Q}$$

$$T(E4) = h[(g^+ s + s^+\tilde{g})^{(4)} + \eta_{dd}(d^+\tilde{d})^{(4)} + \eta_{gd}(g^+\tilde{d} + d^+\tilde{g})^{(4)} + \eta_{gg}(g^+\tilde{g})^{(4)}] \tag{5}$$

In the above scheme, at most one g-boson is allowed (in addition to the usual s and d bosons). Preliminary calculations indicated that the E2

properties are unaffected by the g boson terms, whose main effect is on the E4 predictions. Therefore, the E2 parameters were kept fixed at their IBM-1 values. ϵ_g was set equal to 1.5 MeV which is approximately the pairing gap in the region. The role of the parameter χ_{gg} is to adjust the g-boson energy levels whereas χ_{gd} determines the mixing of g-boson configurations into the pure sd-boson states. Thus χ_{gd} and χ_{gg} were adjusted to get a good description (correct energy and mixing of sdg bosons) for the $4^+_{2,3}$ states. The values of χ_{gd} and χ_{gg} used were 1.5 and 1.7 respectively. This new model scheme leads to significantly improved E4 predictions while maintaining the good fits to the E2 data (Tables IV-VI).

It is interesting to test the naive assumption in IBM-1 that the proton and neutron bosons are identical. To do this one needs to invoke IBM-2 (p - n), where a simple hamiltonian is usually of the form[13].

$$H = \epsilon(\hat{n}_{d_\pi} + \hat{n}_{d_\nu}) + \kappa(\hat{Q}_\pi \cdot \hat{Q}_\nu) + V_{\pi\pi} + V_{\nu\nu} \tag{6}$$

Here, ϵ is the energy difference between the d- and s-bosons, and the quadrupole operator, Q is

$$\hat{Q} = (s^+_\sigma \tilde{d}_\sigma + d^+_\sigma s_\sigma)^{(2)} + \chi_\sigma (d^+_\sigma \tilde{d})^{(2)} \tag{7}$$

where $\sigma = \pi, \nu$.

$V_{\pi\pi}(V_{\nu\nu})$ represent the d-boson conserving residual p-p (n-n) interactions,

$$V_{\sigma\sigma} = \frac{1}{2} \sum_{L=0,2,4} C_{L\sigma} (d^+_\sigma d^+_\sigma)^{(L)} \cdot (\tilde{d}_\sigma \tilde{d}_\sigma)^{(L)} \tag{8}$$

and these are found to be more important near the closed shell nuclei.

The IBM-2 calcualtions, owing to the size of the basis space, are much more tedious than the IBM-1 calculations. However, a simpler procedure is to map (project) out of IBM-2 space the smaller IBM-1 space. The resulting "projected IBM-2" parameters are then used within IBM-1 model scheme and calculations are performed as described earlier. The results of such a prescription (including a g-boson) are shown in Tables IV-VI and these once again reveal the importance of including the g-boson in the IBM if the E4 properties of a nucleus are to be described satisfactorily.

References

1. A. Arima and F. Iachello, Annals of Phys. 99, 25 (1976); 111, 201 (1978); 123, 468 (1979); 40, 385 (1978) and Phys. Rev. Lett. 40, 468 (1978).
2. L. E. Smith, program LOAF, unpublished (1983).
3. J. Raynal, program ECIS, unpublished (1979).
4. G. J. Pyle, program RAROMP, University of Minnesota Information Report COO-1265-64, 1964 (unpublished), modified for relativistic energies.
5. M. Baranger and K. Kumar, Nuc. Phys. A122, 241 (1968); A122, 273 (1968); A92, 608 (1967).
6. U. Gotz et al., Nuc. Phys. A192, 1 (1972).
7. A. S. Davydov and G. F. Fillipov, Nuc. Phys. 8, 237 (1958).
8. J. A. Cizewski, et al., Phys. Rev. Lett. 40, 167 (1978); R. F. Casten and J. A. Cizewski, Phys. Lett. 185B, 293 (1987).
9. R. F. Casten and J. A. Cizewski, Nuc. Phys. A309, 477 (1978); A425, 653 (1984).

10. A. Sethi, M. Franey, M. Gazzaly, N. Hintz, A. Mack, D. N. Mihailidis, K. Jones, D. Ciskowski, G. Pauletta, L. Santi and D. Goutte, "Symposium in Honor of A. Arima: Nuclear Physics in 1990s", Santa Fe, N. Mexico, May 1-5, 1990, and to be submitted to Phys. Rev. C.

11. A. Sethi,F. Todd Baker, G. T. Emery, W. P. Jones, and M. A. Grimm, Jr., to be published in Nuclear Physics.

12. P. van Isacker, programs PHINT and FBEM unpublished.

13. T. Otsuka et al., Phys. Lett. 76B, 139 (1978); Interacting Bosons in Nuclear Physics, ed. F. Iachello (Plenum Press, New York, 1979).

14. F. T. Baker, et al., Nuc. Phys. A266, 337 1976).

15. C. Baktash, et al., Phys. Rev. C18, 131 1978).

16. K. Stelzer, et al., Phys. Lett. 70B, 297 1977).

17. J. E. Glenn and J. X. Saladin, Phys. Rev. Lett. 20, 1298 (1968).

18. J. A. Cizewski, et al., Nuc. Phys. A323, 349 (1979); H. H. Bolotin et al., Nuc. Phys. A370, 146 (1981).

19. W. T. A. Borghols, et al., Phys. Lett. 182B, 301 (1986).

Table I

Optical Model parameter Sets for $^{194,196}Pt$[a]

(Lengths in fermi and Potentials in MeV)

A	Set	V_v	r_r	a_r	W_v	r_i	a_i	V_s	W_s	r_s	a_s	χ^2_{Total} [b]
194	I	-0.0923	1.7462	0.019	-58.7353	1.0878	0.6147	-1.1403	- .259	1.0824	.8167	5.7
	* II	10.236	1.0871	0.3139	-55.1985	1.0963	0.6112	-1.1529	-.0807	1.0852	.8275	3.8
	III	3.5633	1.1638	0.0019	-59.8025	1.0844	0.6298	-1.1278	-.0907	1.0944	.810	4.3
196	I	2.3909	1.1104	.0015	-64.7817	1.0621	0.640	-1.2872	-.2239	1.047	.8632	6.4
	* II	6.0986	1.1099	.2198	-51.3326	1.0969	0.6024	-1.0180	-.1403	1.0943	.8066	3.8

a) The Optical potential used is

$$U(r) = V_v f(x_r) + iW_v f(x_i) - (V_s + iW_s)\frac{2}{r} f'(x_s)\vec{\ell}\cdot\vec{s} + V_c(r)$$

where

$$f(x) = \frac{1}{1+e^x}\ ;\ f'(x) = \frac{d}{dr} f(x) \text{ and } x_r = \frac{r - r_r A^{1/3}}{a_r}, \text{ etc.}$$

b) $\chi^2_{Total} = \chi^2_r + \chi^2_{Ay}$ $V_c(r)$ = Coulomb potential due to a uniformly charged sphere.

*Optical potential parameter set used in the analysis described in the text

Table II

Optical Model Parameter Sets[a)]

For ^{150}Nd, ^{154}Gd

(Lengths in fermi and potentials in MeV)

Nucleus	V_v	r_r	a_r	W_v	r_i	a_i	v_s	W_s	r_s	a_s	r_c[b)]
^{150}Nd	3.5633	1.1638	.0026	-39.3269	1.0757	.6668	-.3937	-.3899	1.1707	.7106	1.20
^{154}Gd	3.5634	1.1638	.0025	-32.5523	1.142	.6308	-.404	-.1377	1.2292	.6087	1.20

a) The optical potential used has the same form as in Table I.

b) The Coulomb potential used is that due to a uniformly charged sphere of radius $R_c = r_c A^{1/3}$.

Table III

Deformation Parameters, β_λ and deformation lengths $\delta_\lambda = \beta_\lambda R_i$.

	J^π	E_x(MeV)	β_λ	this δ_λ(fm)	previous δ_λ(fm)
^{194}Pt	2_1^+	0.33	-.166	-1.05	-0.9[a]
	2_2^+	0.62	+.012	+0.07	+0.075[a]
	4_1^+	0.81	-.045	-0.29	-0.21[a]
	4_2^+	1.23	±.034	±0.21	±0.12[a]
	4_3^+	1.91	±.060	±0.38	±0.24[a]
^{196}Pt	2_1^+	0.36	-.158	-1.01	-1.05[b]
	4_1^+	0.88	-.041	-0.26	-0.28[b]
	4_2^+	1.29	±.055	±0.35	
	4_3^+	1.89	±.045	±0.29	

a) Ref. 11

b) Ref. 14

Table IV

Experimental B(E2) Values compared with IBM predictions for ^{196}Pt

Units are e^2b^λ

$J_i \rightarrow J_f$	Expt	IBM-1 (sd)	IBM-2 (sdg)	Projected IBM-2(sdg)
$2_1^+ \rightarrow 0_1^+$	0.30±.02[a]	0.35	0.40	0.29
	0.28±.02[b]			
$2_2^+ \rightarrow 0_1^+$	0.0015±.002[a]	0.0014	0.009	0.008
	0.0019±.0002[b]			
$2_2^+ \rightarrow 2_1^+$	0.423±.015[c]	0.442	0.430	0.319
$4_1^+ \rightarrow 2_1^+$	0.449±022[c]	0.46	0.57	
$4_2^+ \rightarrow 2_1^+$	0.01±.005[c]	7×10^{-6}	5×10^{-4}	
$4_2^+ \rightarrow 2_2^+$	0.28±.12[d]	0.26	0.33	
$4_2^+ \rightarrow 4_1^+$	0.87±.43[c]	0.23	0.24	
$6_1^+ \rightarrow 4_1^+$	0.48±.14[c]	0.49	0.65	
$6_2^+ \rightarrow 4_2^+$	0.28±.06[d]	0.31	0.44	
$Q_{2_1^+}$	0.63±.06[e]	0.25	0.61	

a) this expt. b) Ref. 10 c) Ref. 15

d) Ref. 16 e) Ref. 17

Table V

Experimental B(E2)s compared with IBM predictions
For ^{196}Pt

$J_i \rightarrow J_f$	Expt	IBM-1 (sd)	IBM-2 sdg
$2_1^+ \rightarrow 0_1^+$	0.288±02 [a]	0.27	0.31
	0.276±.001 [b]		
$2_2^+ \rightarrow 0_1^+$	3×10^{-6} [b]	0	7.9×10^{-4}
$2_2^+ \rightarrow 2_1^+$	0.318±.023 [b]	0.354	0.406
$0_2^+ \rightarrow 2_1^+$	0.022±01 [b]	0	0.002
$0_2^+ \rightarrow 2_2^+$	0.14±.08 [b]	0.36	0.44
$4_1^+ \rightarrow 2_1^+$	0.38±.03 [b]	0.354	0.44
$4_2^+ \rightarrow 2_1^+$	0.003±001 [b]	0	0.006
$4_2^+ \rightarrow 2_2^+$	0.177±.025 [b]	0.189	0.247
$4_2^+ \rightarrow 3_1^+$	<0.06 [c]	0	0.007
$4_2^+ \rightarrow 4_1^+$	0.193±.097 [b]	0.17	0.204
$6_1^+ \rightarrow 4_1^+$	0.40±0.11 [b]	0.36	0.50

a) this expt. b) Ref. 8, 18 c) Ref. 17

Table VI

A Comparison of E4 Matrix Elements with IBM predictions

^{194}Pt		Expt	IBM-1 (sd)	IBM-2 sdg
	$0_1 \rightarrow 4_1$	-1332 ± 50 [a]	[-1332]	[-1332]
		-1320 ± 32 [b]		
	$0_1 \rightarrow 4_2$	$\pm 996 \pm 250$ [a]	59	-850
		$\pm 658 \pm 105$ [b]		
	$0_1 \rightarrow 4_3$	$\pm 1759 \pm 300$ [a]	0.6	-1710
		$\pm 1593 \pm 37$ [b]		
^{196}Pt				
	$0_1 \rightarrow 4_1$	-1273 ± 100 [a]	[-1273]	[-1270]
		-1550 ± 160 [c]		
	$0_1 \rightarrow 4_2$	$\pm 1707 \pm 390$ [a]	0	-1450
		1410 ± 140 [c]		
	$0_1 \rightarrow 4_3$	$\pm 1390 \pm 110$ [a]	0	-1320
		2100 ± 150 [b]		

a) this expt.

b) Ref. 11

c) Ref. 19

Figure Captions

Fig. 1: Spectrum of inelastically scattered protons from ^{194}Pt at T_p = 647 MeV and $\theta_L = 15^o$.

Fig. 2: Same as Fig. 1 but for ^{196}Pt at $\theta_L = 17^o$.

Fig. 3: Elastic σ and A_y for $\vec{p}$ + ^{194}Pt at T_p = 647 MeV. Predictions using set II in Table I.

Fig. 4: Cross section and analyzing power for the 2_1^+ (.329 MeV) state in ^{194}Pt($\vec{p}$,p') at T_p = 647 MeV. Also shown are the collective form factor fits using dU/dr form factor (first order vibrational model).

Fig. 5: Same as Fig. 4, but for the 2_2^+ (.622) state. The fits are obtained using second order vibrational model and a $0/2_1/2_2$ coupled channels calculation.

Fig. 6: Same as Fig. 5, but for the 4_1^+ (.811) state. The predictions are based on a $0/2_1/4_1$, coupling.

Fig. 7: Same as Fig. 4, but for the 4_2^+ (1.229) state.

Fig. 8: Same as Fig. 4, but for the 4_3^+ (1.911) state.

Fig. 9: Same as Fig. 3, but for $\vec{p}$ + ^{196}Pt. The predictions were obtained with optical potential Set II in Table I.

Fig. 10: Same as Fig. 4, but for the 2_1^+ (.356) state in ^{196}Pt($\vec{p}$,p').

Fig. 11: Same as Fig. 6, but for the 4_1^+ (.877) state in ^{196}Pt($\vec{p}$,p').

Fig. 12: Same as Fig. 4, but for the 4_2^+ (1.293) state in ^{196}Pt($\vec{p}$,p').

Fig. 13: Same as Fig. 4, but for the 4_3^+ (1.888) state in ^{196}Pt($\vec{p}$,p').

Fig. 14: σ and A_y data for 0_2^+ (1.135) state in ^{196}Pt($\vec{p}$,p').

Fig. 15: Same as Fig. 14, but for 3^- (1.447) state.

Fig. 16: Same as Fig. 3, but for $\vec{p}$ + ^{150}Nd at T_p = 647 MeV. Predictions are based on optical potential parameters from Table II.

Fig. 17: Same as Fig. 3 but for $\vec{p}$ + ^{154}Gd at T_p = 647 MeV. Predictions obtained with optical potential given in Table II.

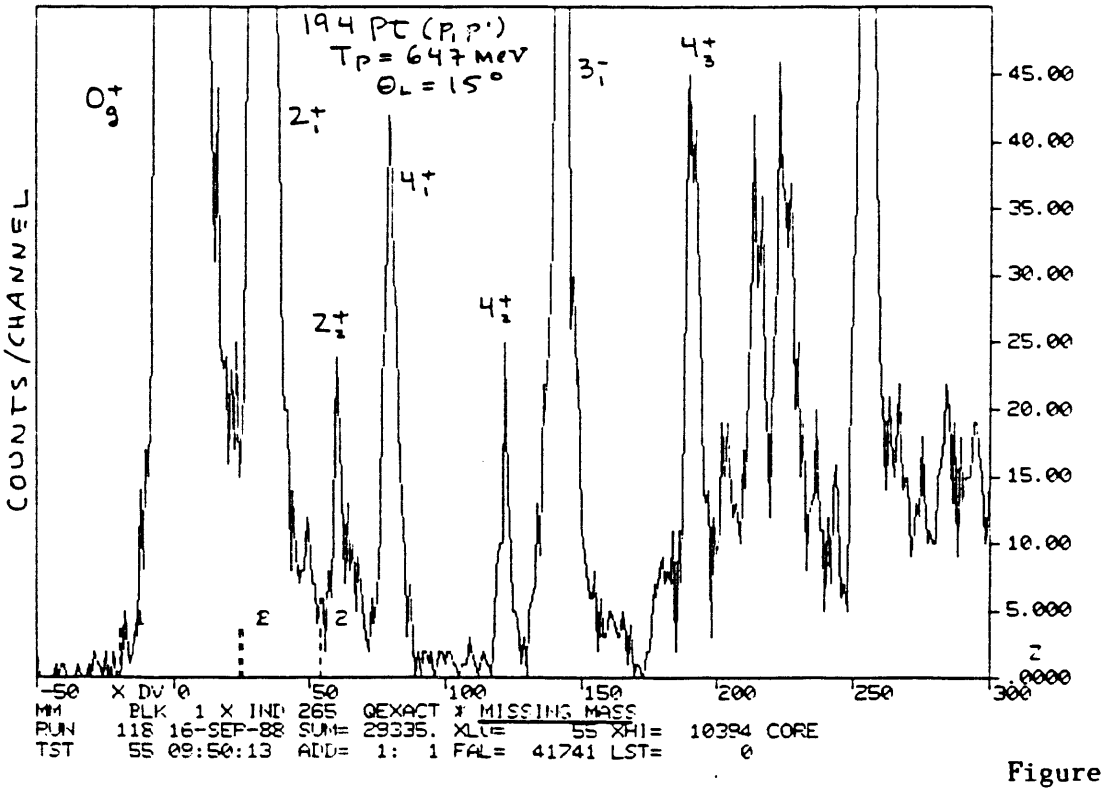

Figure 1

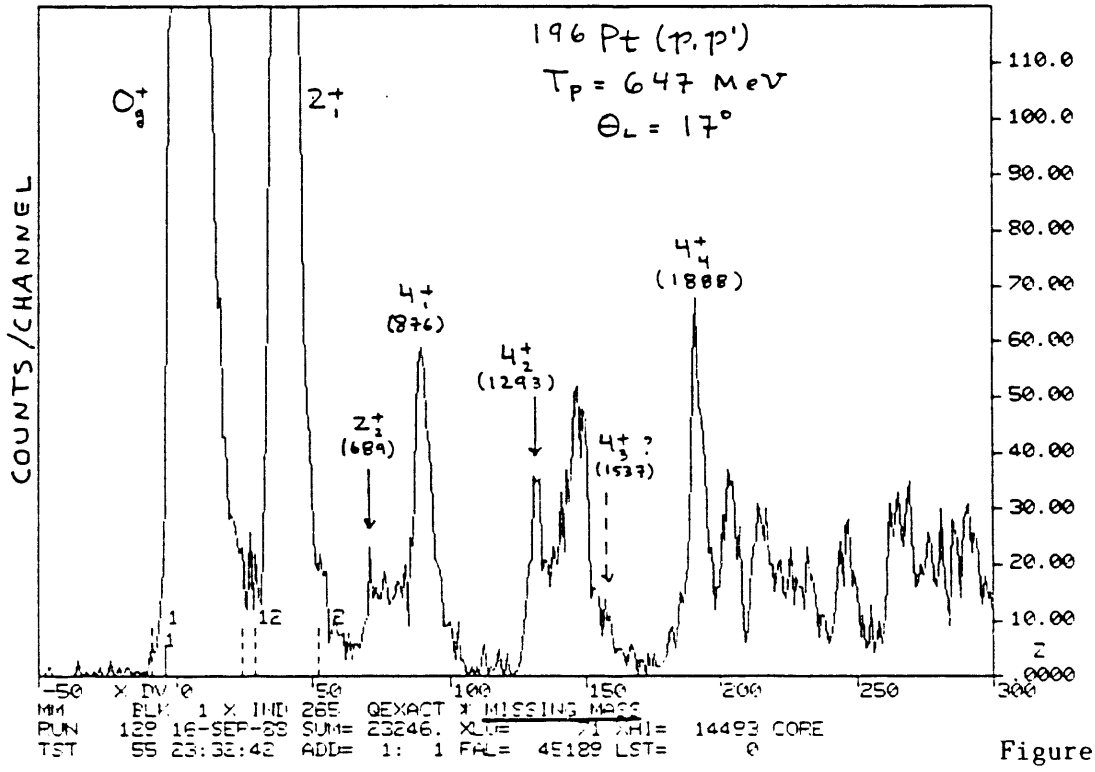

Figure 2

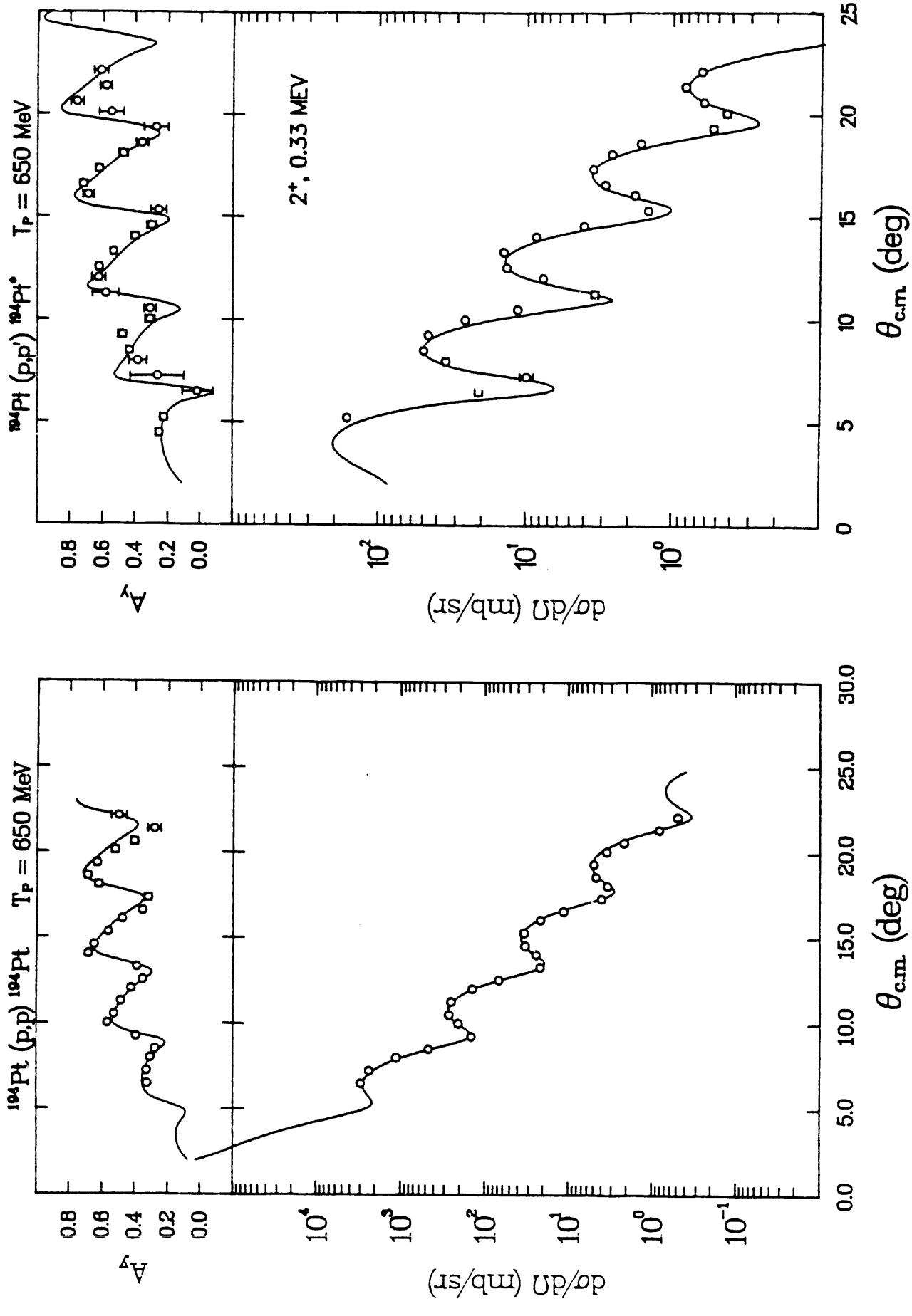

Figure 3

Figure 4

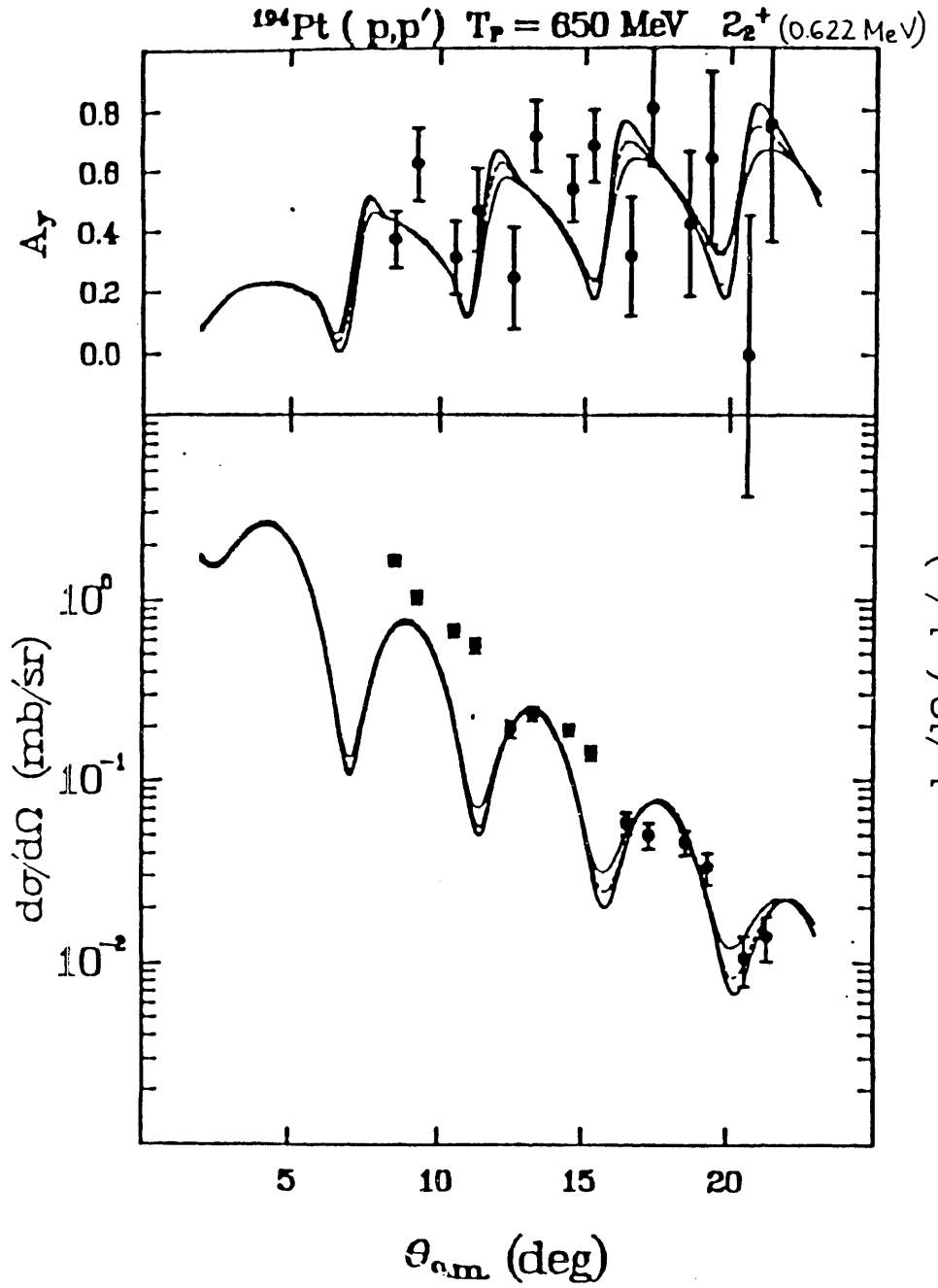
^{194}Pt (p,p′) T_p = 650 MeV 2_2^+ (0.622 MeV)
A_y
0.8
0.6
0.4
0.2
0.0
$d\sigma/d\Omega$ (mb/sr)
10^0
10^{-1}
10^{-2}
5
10
15
20
$\theta_{c.m.}$ (deg)

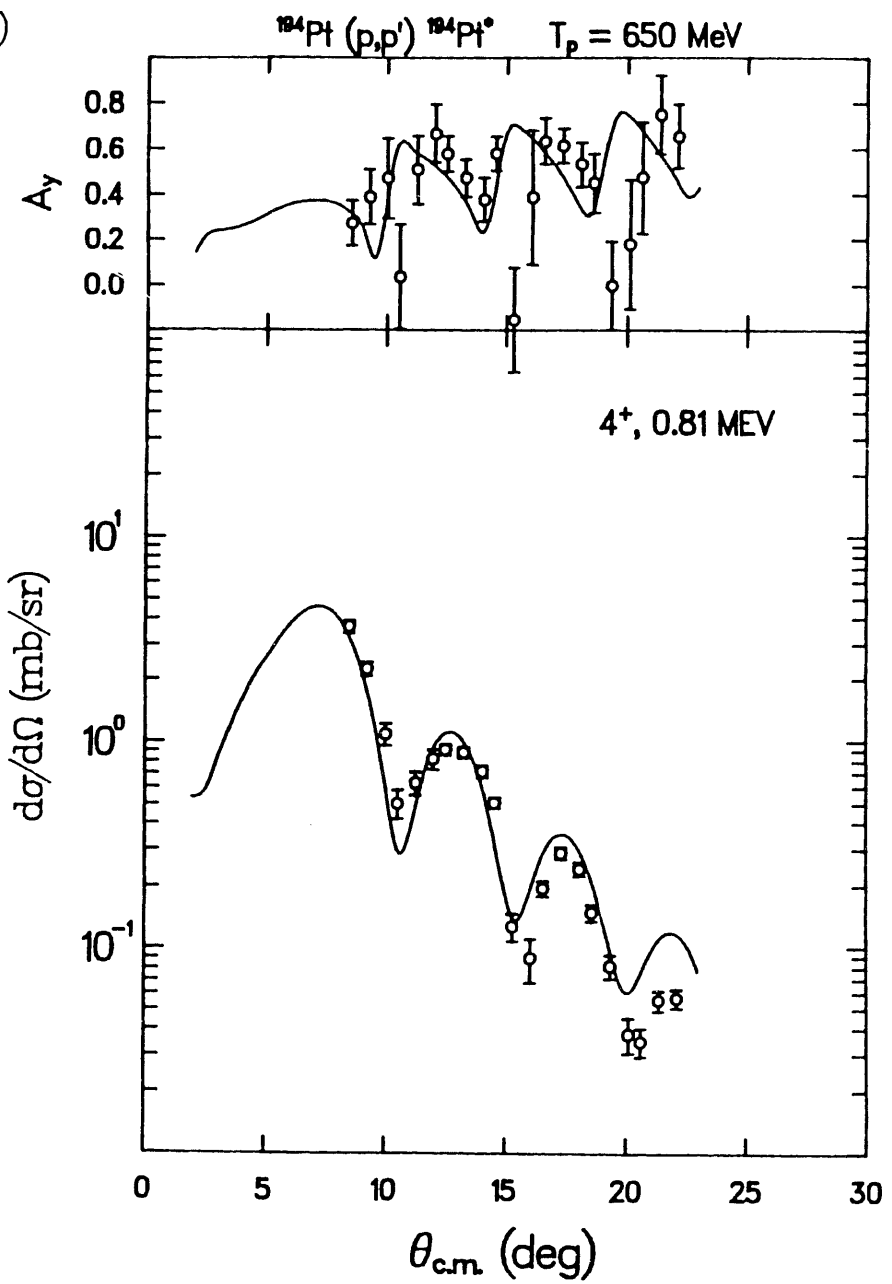
^{194}Pt (p,p') ^{194}Pt* T_p = 650 MeV
A_y
0.8
0.6
0.4
0.2
0.0
4$^+$, 0.81 MEV
$d\sigma/d\Omega$ (mb/sr)
10^1
10^0
10^{-1}
0
5
10
15
20
25
30
$\theta_{c.m.}$ (deg)

Figure 6

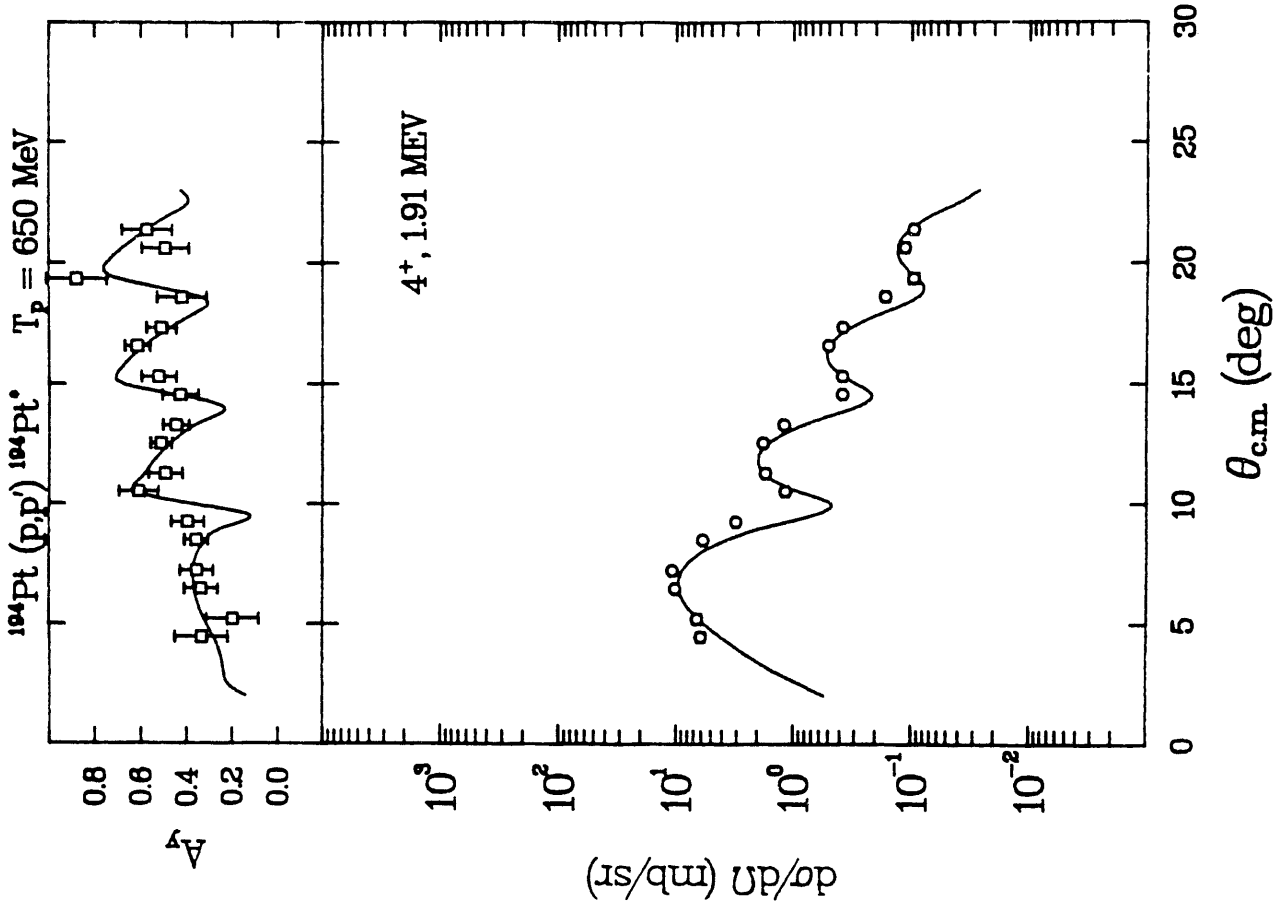

Figure 8

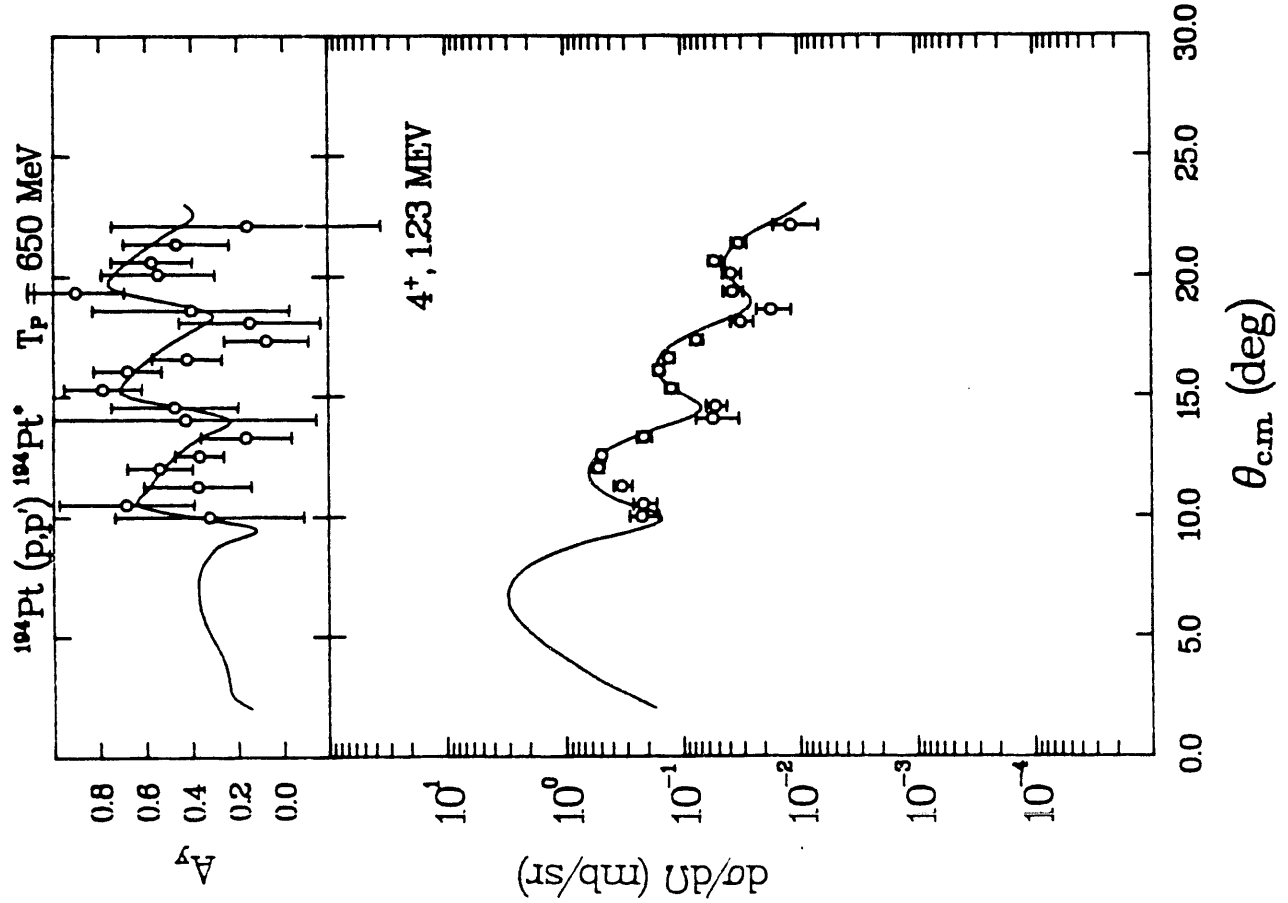

Figure 7

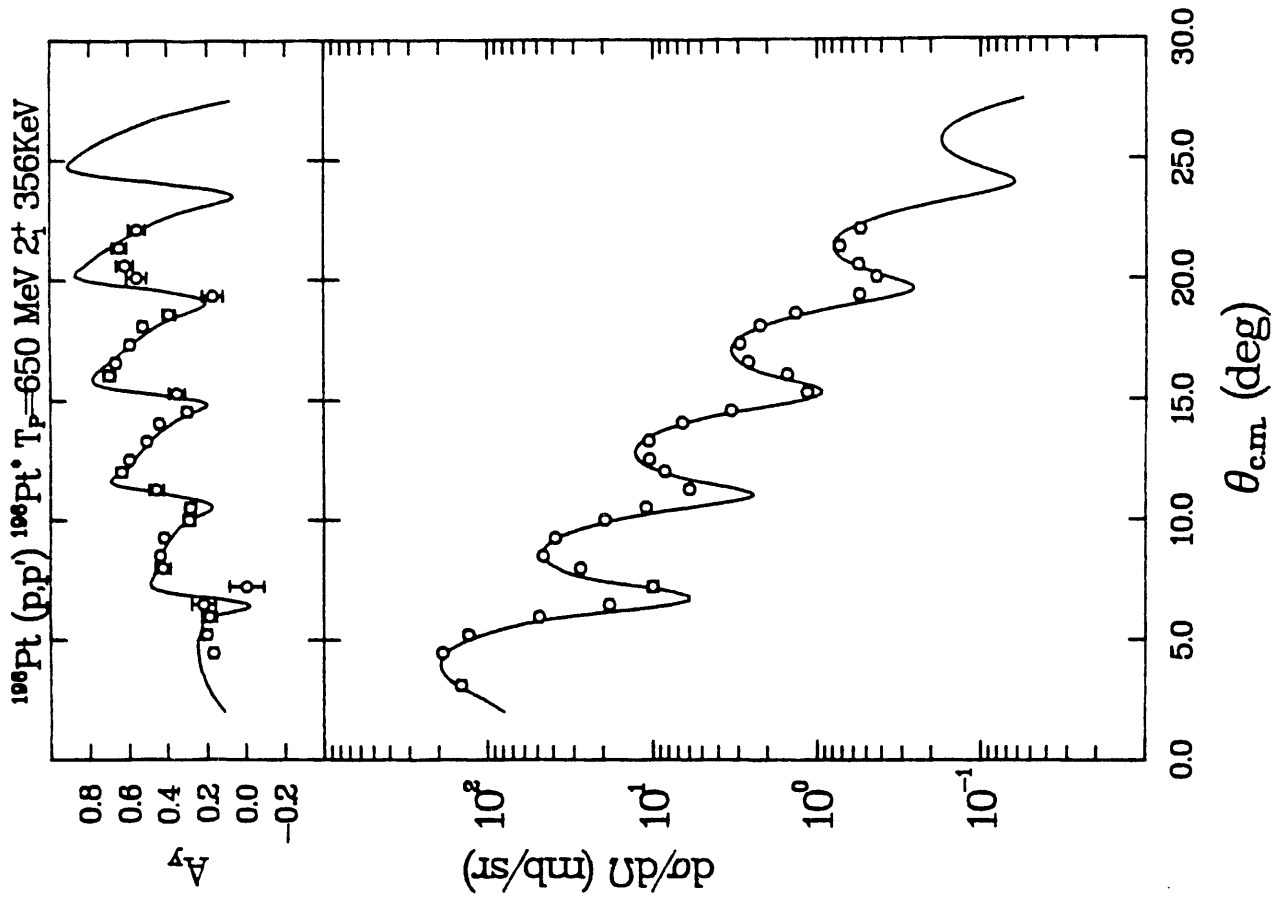

Figure 10

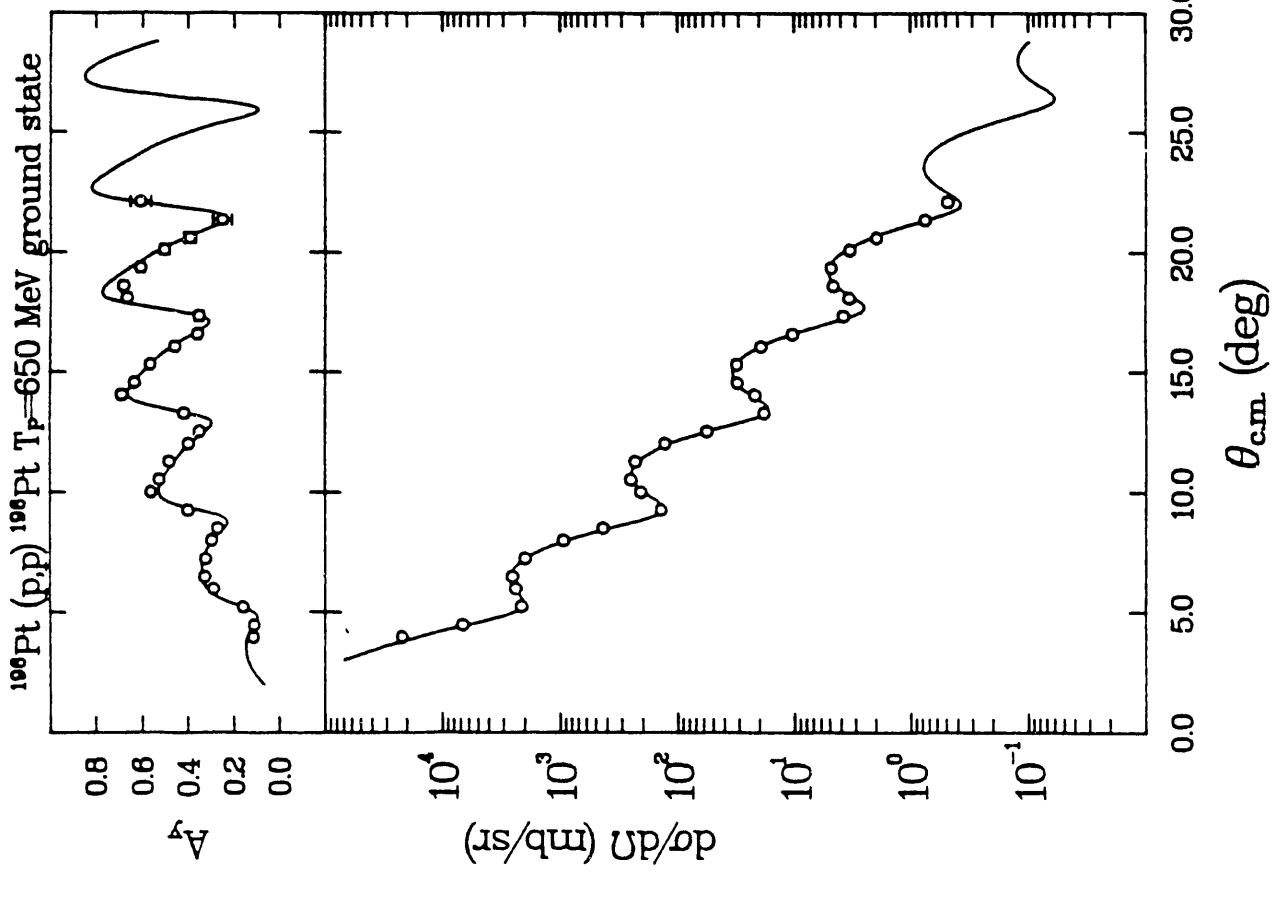

Figure 9

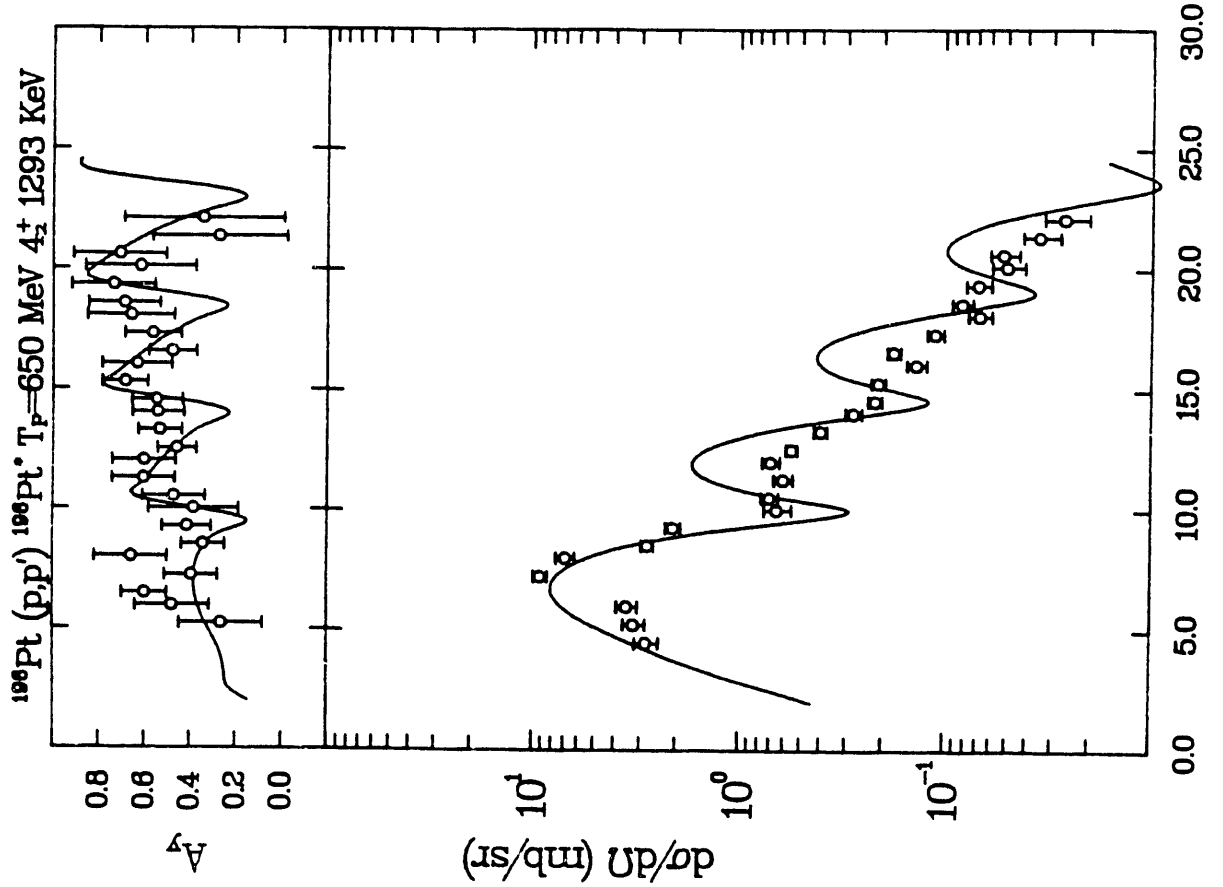

Figure 12

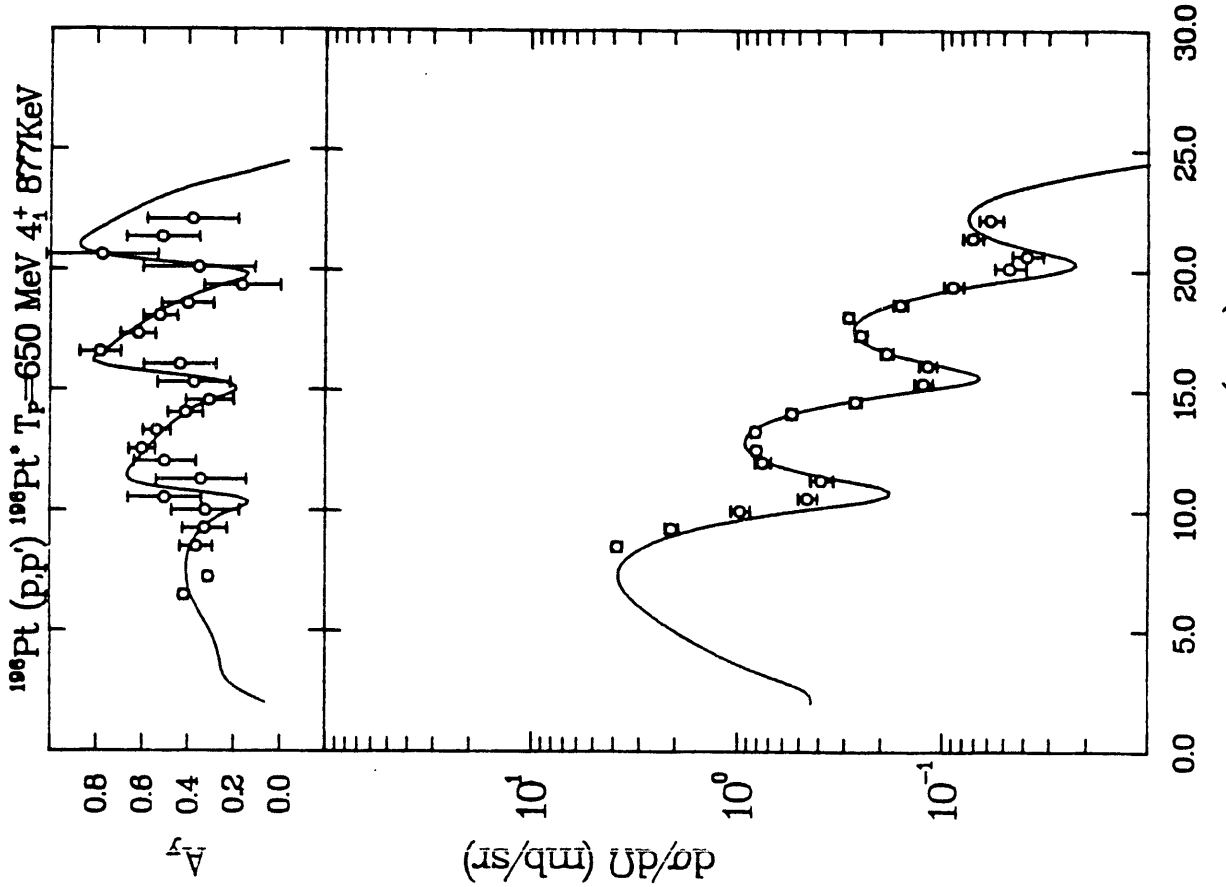

Figure 11

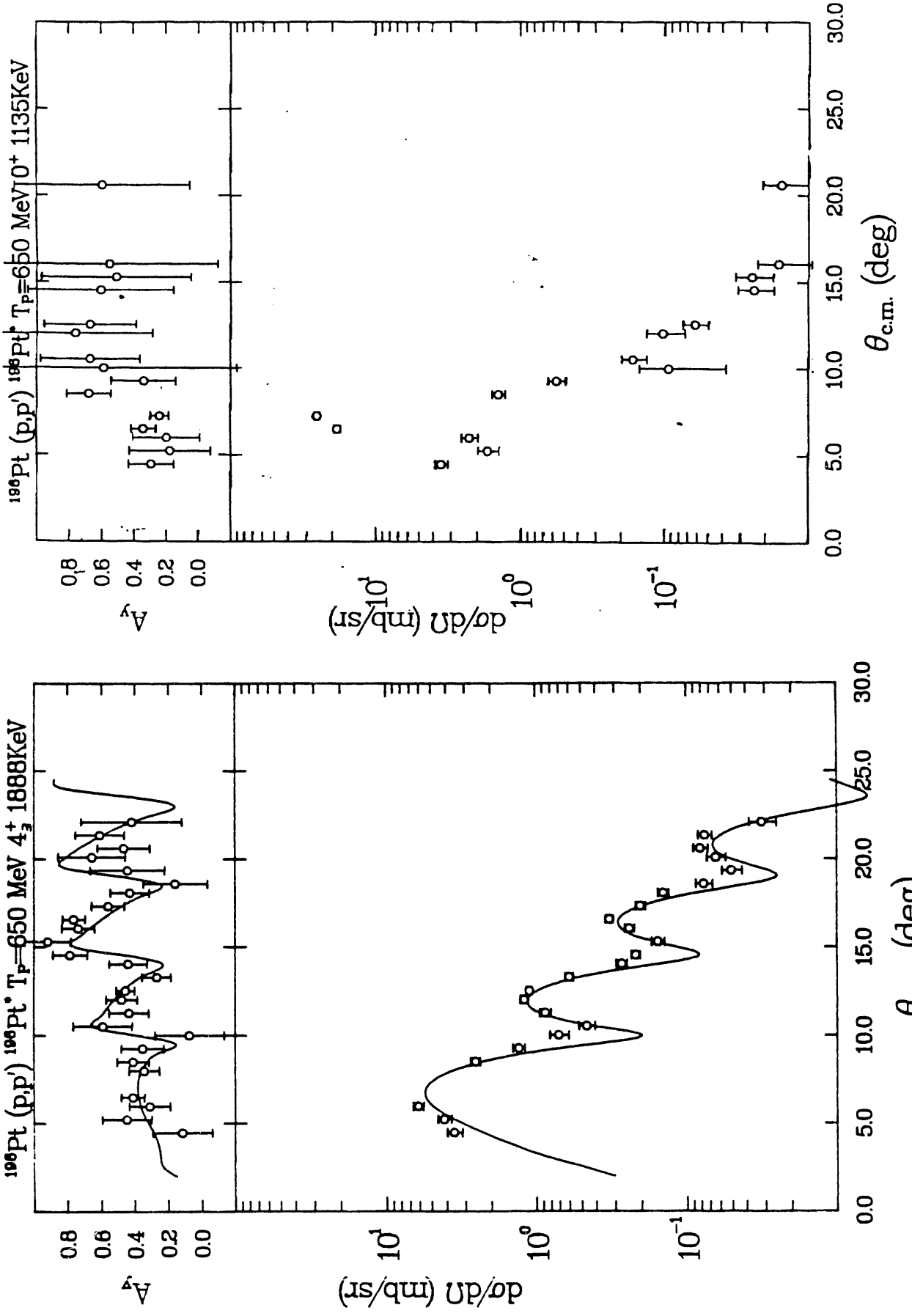

Figure 13

Figure 14

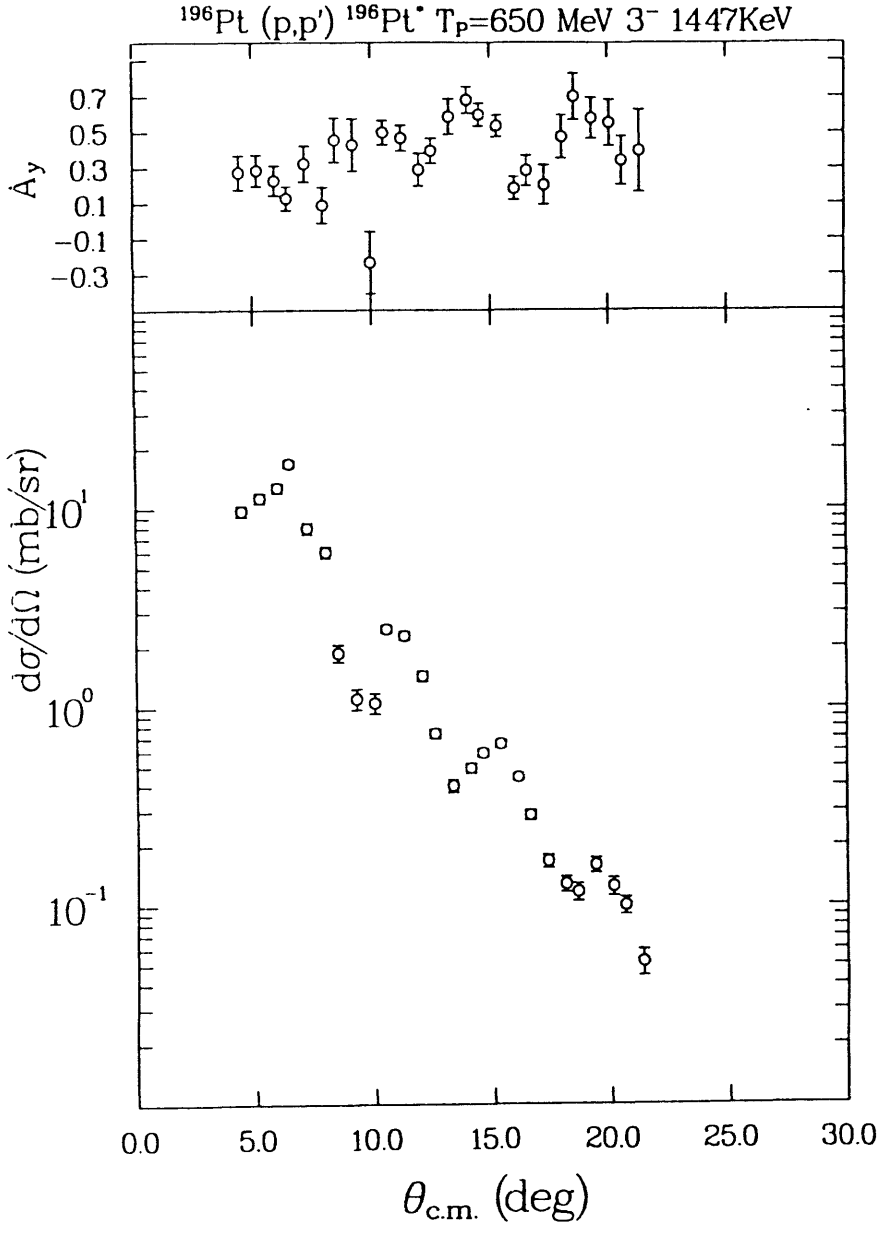

Figure 15

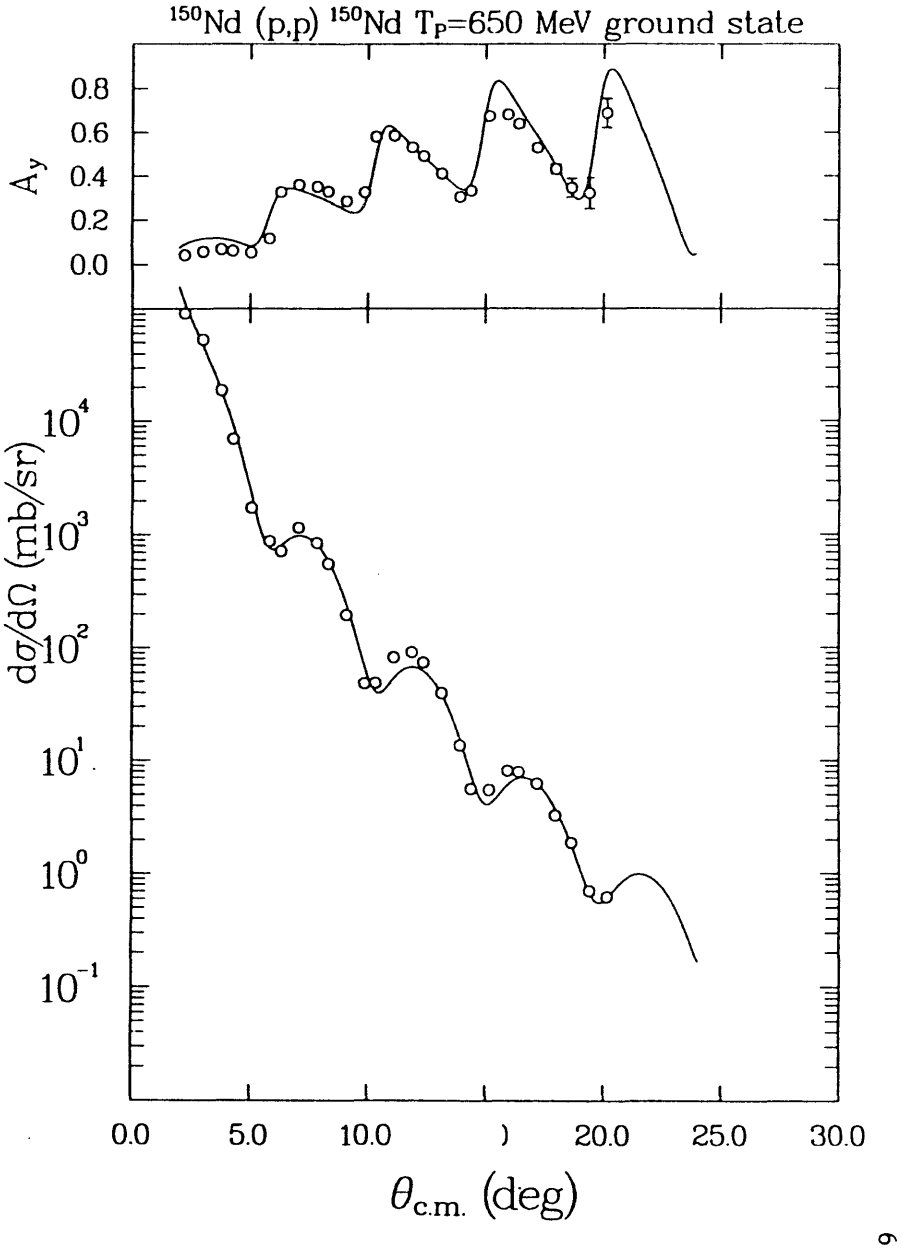

Figure 16

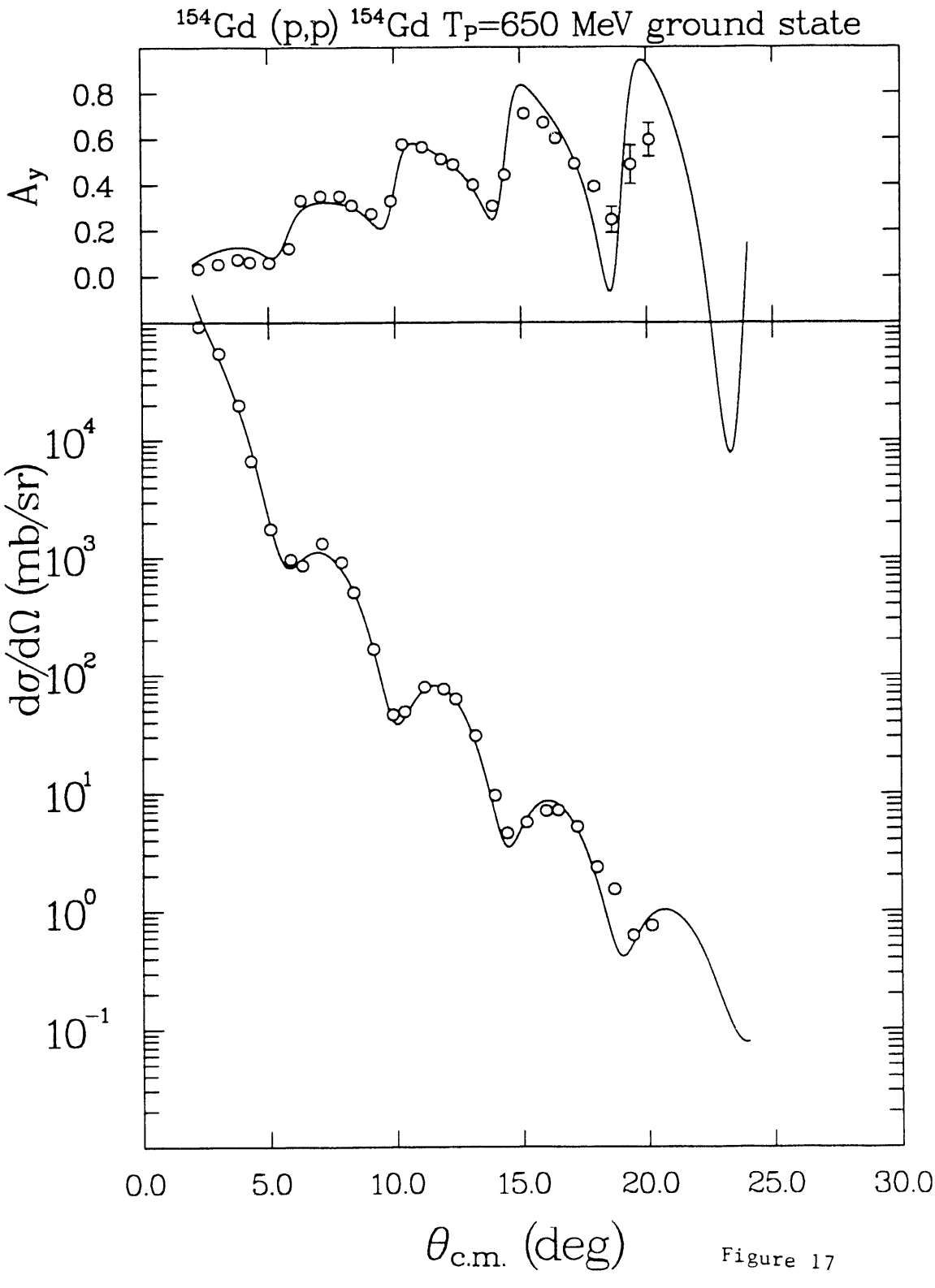
^{154}Gd (p,p) ^{154}Gd T_P=650 MeV ground state
A_y
0.8
0.6
0.4
0.2
0.0
$d\sigma/d\Omega$ (mb/sr)
10^4
10^3
10^2
10^1
10^0
10^{-1}
0.0
5.0
10.0
15.0
20.0
25.0
30.0
$\theta_{c.m.}$ (deg)

Figure 17

II.E. E1030U, Search for Recoil Free Δ Production in the (p,^{3}He) Reaction at 647 MeV. (Minnesota spokesman, U. Texas, LANL participants).

Most experiments to date on the production of the Δ-isobar in nuclei have utilized inelastic scattering or charge exchange reactions. The kinematic region in these experiments is limited to q(momentum transfer) $\geq \omega$ (energy transfer) and thus the Δ recoils with considerable energy. However, in mass pickup reactions, such as (π,p), (p,d), (p,t), (p,^{3}He), -- etc. one can explore kinematic regions near $q = 0$ and $\omega \sim 300$ MeV to search for possible bound, low angular momentum ($N^{-1}\Delta$) states. In the first experiment of this type[1] a relatively narrow ($\Gamma \sim 55$ MeV) peak was seen in the ^{13}C(p,d) reaction at $T_p = 800$ MeV at $\omega = 241$ MeV, when the deuterons were detected in coincidence with back-to-back two proton decay. Since at $T_p = 800$ MeV this value of ω corresponds to $q \sim 0$ and the transfer cross section calculated in the DWBA exhibits a narrow peak (of width ~ 50 MeV) around $q = 0$, we interpret the peak seen in the (p,d) reaction as a "slice" of a broad Δ resonance seen through the narrow (p,d) kinematic window. The energy transfer, ω, near $q = 0$ can be varied by varying the incident proton energy. However, the (p,d) reaction suffers from a large background due to quasi-free deuteron production in the $p + N \rightarrow d + \pi$ reaction, and has the selection rule (for a one-step process) of $\Delta T = \frac{1}{2}$. For this reason we began (E851) a study of the (p,t) reaction, which has a lower quasi-free triton production background, and also allows $\Delta T = 1$ as might be expected for a Δ excitation.

Unfortunately, in both the (p,d) and (p,t) reactions, the elastic protons flood the focal plane around the crucial $q \sim 0$ region and so it is not clear that the peaks seen are not due to a leak through the particle

identification gates. For this reason we began a study of the (p,^{3}He) reaction, since the B-field near q = 0 for ^{3}He is well below that for elastic protons. Our first (p,^{3}He) results at T_p = 497 MeV (E1030) and 647 MeV (E1030U) in Nov. 87 and Sept. 88 were made at HRS where many overlapping runs were necessary. The results were inconclusive (Fig. 1), a broad peak was seen around the value of ω expected for quasi-free ^{3}He production in the p + ^{2}N → ^{3}He + π reaction which obscured most of the q ~ 0 region of Δ production.

Some additional time remains on E1030U (102 hrs) which we intend to use on the more suitable new MRS facility. An additional refinement will be the use of large CsI detectors (currently being developed for our E1201) to gate on the expected two-proton decay of a possible "bound state" Δ-resonance.

References

1. C. L. Morris, et al, Phys. Lett. 123B, 37 (1983).

Figure Captions

Fig. 1: Yield curve for ^{3}He in the 647 MeV bombardment of ^{12}C (solid circles) and ^{208}Pb (crosses) at $\theta_L = 6^o$ vs. energy transfer (ω). Arrows show location of ^{3}He peaks expected for quasi-free production in the p + ^{2}N → ^{3}He + π (QF (π)), for quasi-free Δ-production in the p + ^{2}N → ^{3}He + π (QF (Δ)), and the value of ω for minimum q (q_{min} ~ .5f^{-1}), where recoil free Δ production could occur.

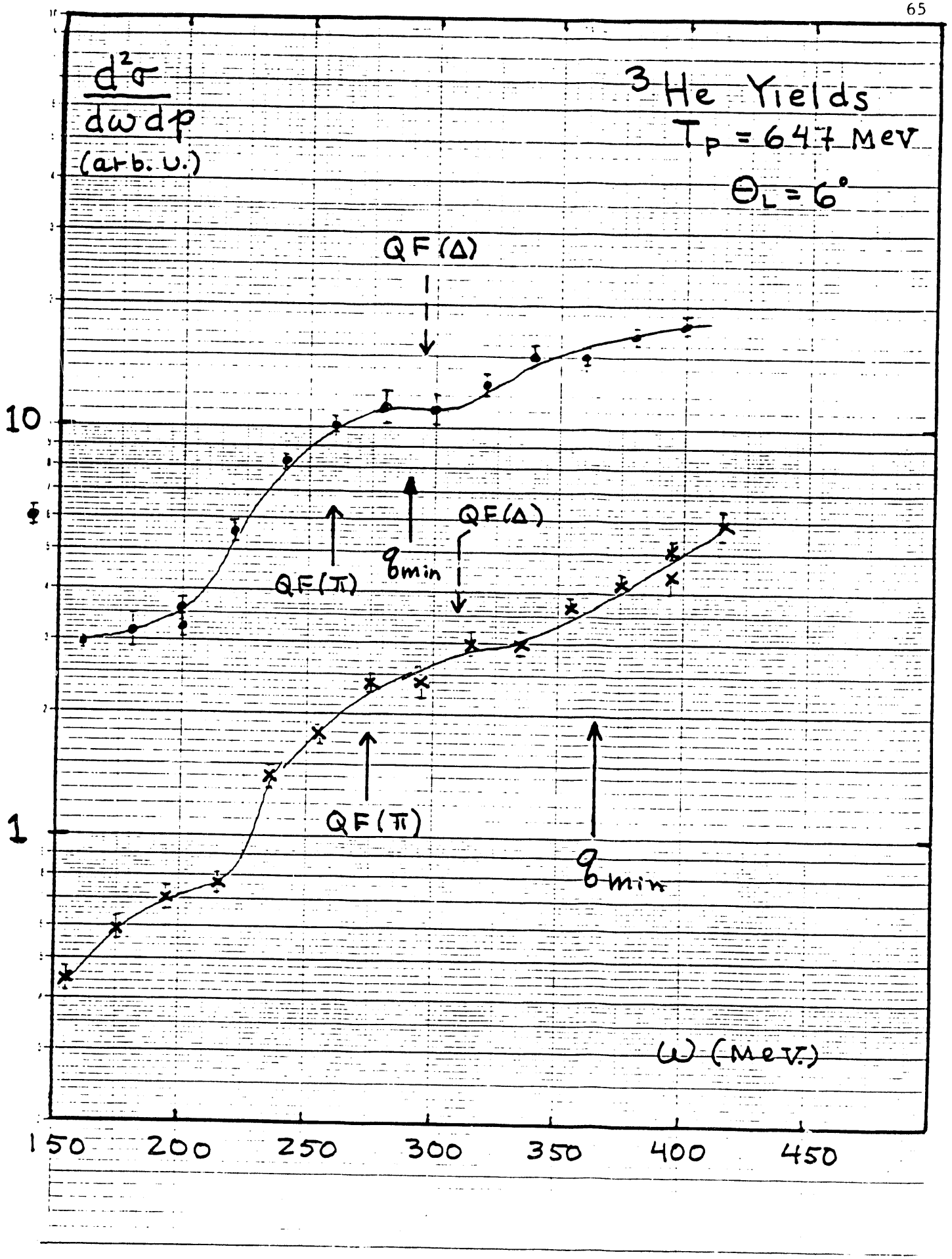
$\frac{d^2\sigma}{d\omega dp}$
(arb. u.)
^{3}He Yields
T_p = 647 MeV
θ_L = 6°
QF(Δ)
QF(π)
q_{min}
QF(Δ)
QF(π)
q_{min}
10
1
150
200
250
300
350
400
450
ω (MeV.)

Figure 1

II. F. E1047, Search for Low-Lying Magnetic States in an $1f_{7/2}$ Shell Nucleus. (Minnesota spokesman; U. Texas, Osaka U., Rutgers participants).

Much effort has been made to study collective M(1) and GT transitions in nuclei but rather little in the search for higher λ magnetic multipole excitations. This experiment was inspired by a paper of L. Zamick[1] in which he discusses λ = 1,3,5 and 7 spin and orbital modes in ^{48}Ti in the context of a pure ($f_{7/2}$) model. In a later work[2] by Liu and Zamick, the shell model basis was expanded to allow one or two nucleons into the upper f-p shell ($1f_{5/2}$, $2p_{1/2,3/2}$). The conclusion was that a large fraction of the total B(Mλ) strength for each multipolarity was to be found in a few states between ~ 5 and 15 MeV.

This experiment was designed to search for these states (they are not expected to have large cross sections in (p,p')) by measuring the spin flip probability, S_{nn}, and the analyzing power, A_y, in narrow energy intervals (~ 50 - 70 keV) from E_x = 0 to 15 MeV. The unnatural parity magnetic states are expected to have large S_{nn} and small A_y, whereas the "background" natural parity states should have the opposite. Thus, for example, the product $S_{nn}(1-A_y)$ should be largest for the magnetic states. The experiment was run at HRS at T_p = 497 MeV in Nov. 1987 and data reduction done in 1988 and 1989. The data reduction was lengthy since ~ 300 runs had to be replayed, each several times because of bin number limitations in the focal plane polarimeter program DNC which calculates the spin depolarization coefficients D_{ij}.

The final results for $S_{nn}(1-A_y)$ in 70 keV bins are shown in Figs. 1-4 at angles θ_L = 4, 10, 13, and 17.4° (maxima of cross sections predicted for

λ = 1,3,5 and 7 respectively). The statistics are somewhat poorer than originally anticipated due to low beam currents during the scheduled run. The results are not dramatic although some suggestion of peaks is seen at or near energies predicted by Liu and Zamick (arrows) for λ = 5 and 7 in Figs. 3 and 4. The states predicted below 9 MeV are all T = 2 (both isoscalar, τ = 0 and isovector, τ = 1 or mixed); those above 9 MeV are T = 3 and so isovector. Arrows are also shown in Fig. 2 at the location of λ = 3 states seen in (e,e') by Richter.[3)]

A request for more time using the new high intensity polarized proton souce at LAMPF was rejected by PAC in Jan. 90. We intend to try again at a later date when the new source is fully operational. A request will be made also to run at a lower energy where the relative strength of magnetic excitations is greater.

References

1. L. Zamick, Phys. Rev. C33, 691 (1986).
2. H. Liu and L. Zamick, Phys. Rev. C36, 2064 (1987).
3. T. Guhr, et al., Institut fur Kernphysik Technische Hochschule Darmstadt report IKDA 90/2, unpublished.

Figure Captions

Fig. 1: Spectrum for $S_{nn}(1-A_y)$ for $^{48}Ti(p,p')$ at $\theta_L = 4^o$ (maximum for λ = 1) at T_p = 497 MeV in 70 keV energy bins. Vertical lines (solid for T = 2, dashed for T = 3) show location of strongest

states predicted in Ref. 2. Arrows show location of 1^+ states seen in (e,e') (Ref. 3).

Fig. 2: Same as Fig. 1 but for $\theta_L = 10^\circ$ (maximum for $\lambda = 3$). Arrows show location of tentative 3^+ states seen in (e,e') (Ref. 3).

Fig. 3: Same as Fig. 1 but for $\theta_L = 13^\circ$ (maximum for $\lambda = 5$).

Fig. 4: Same as Fig 1 but for $\theta_L = 17.4^\circ$ (maximum for $\lambda = 7$).

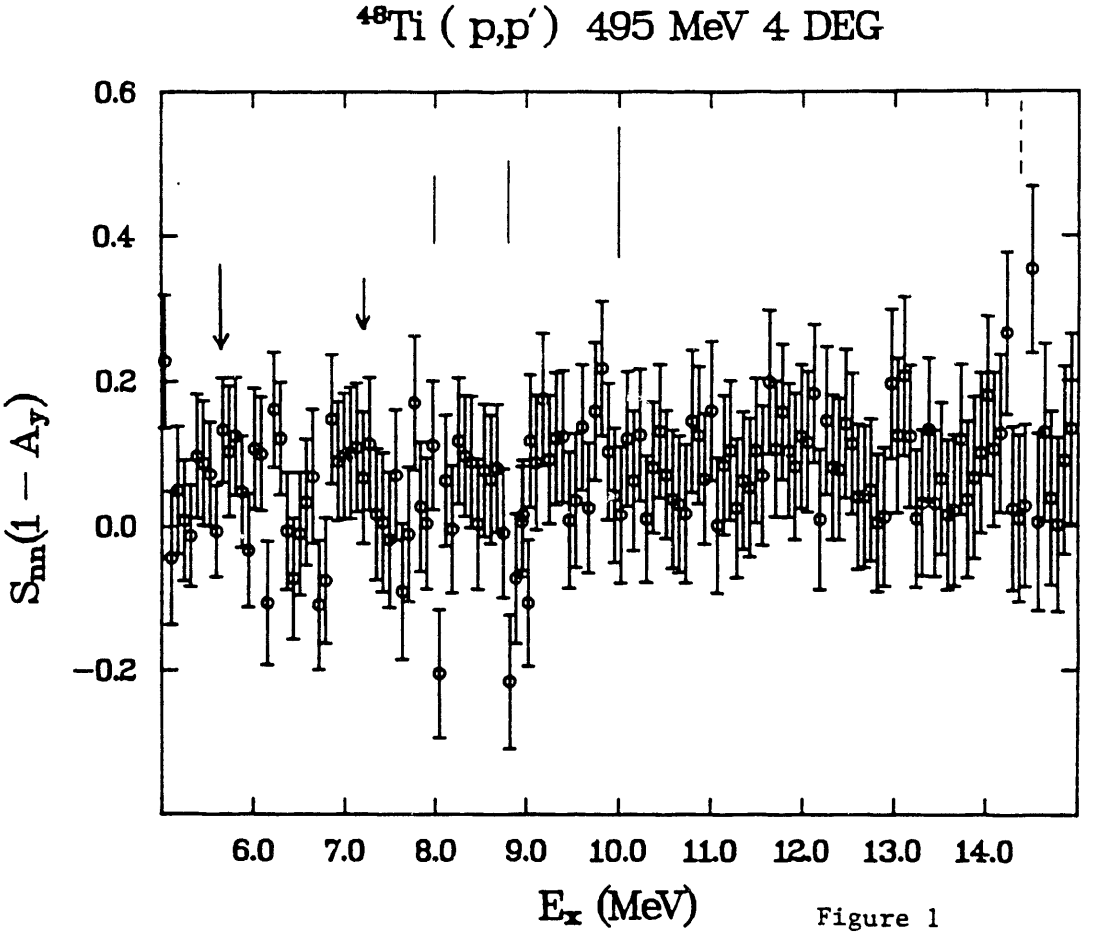

Figure 1

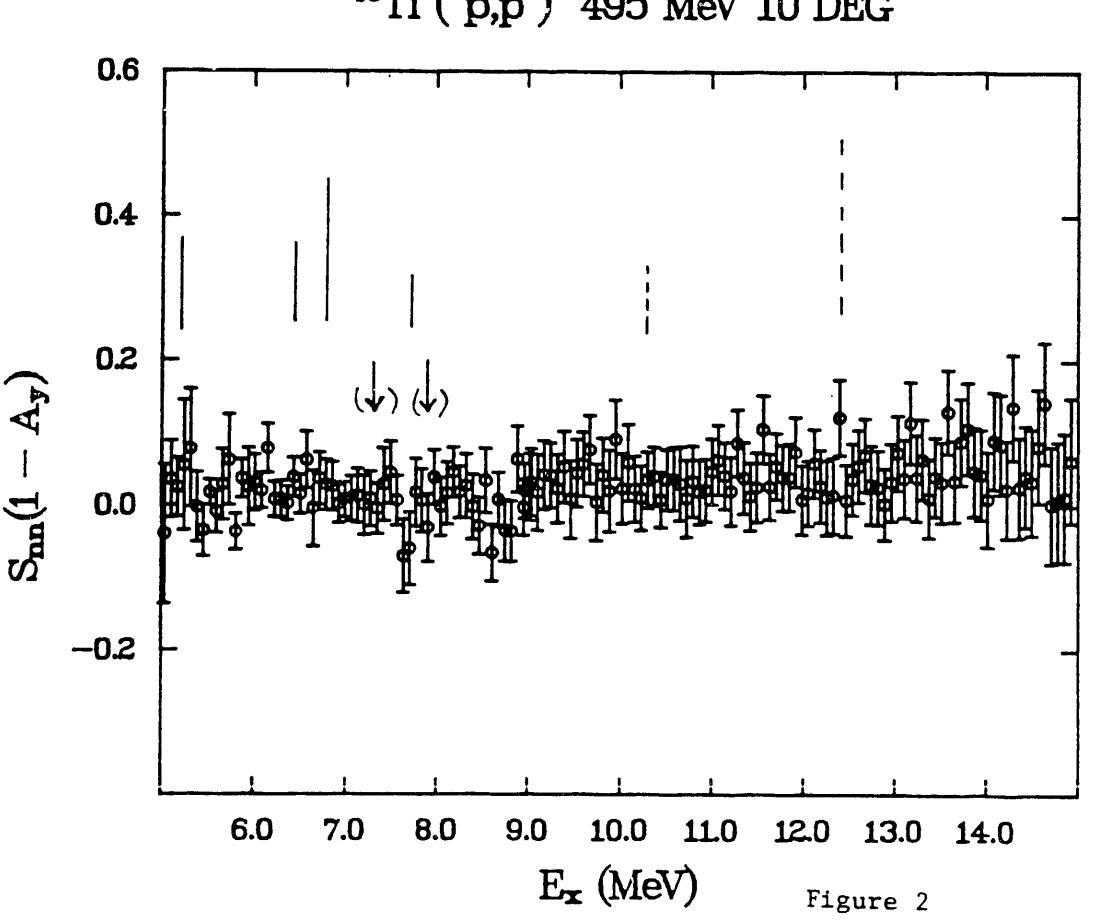

Figure 2

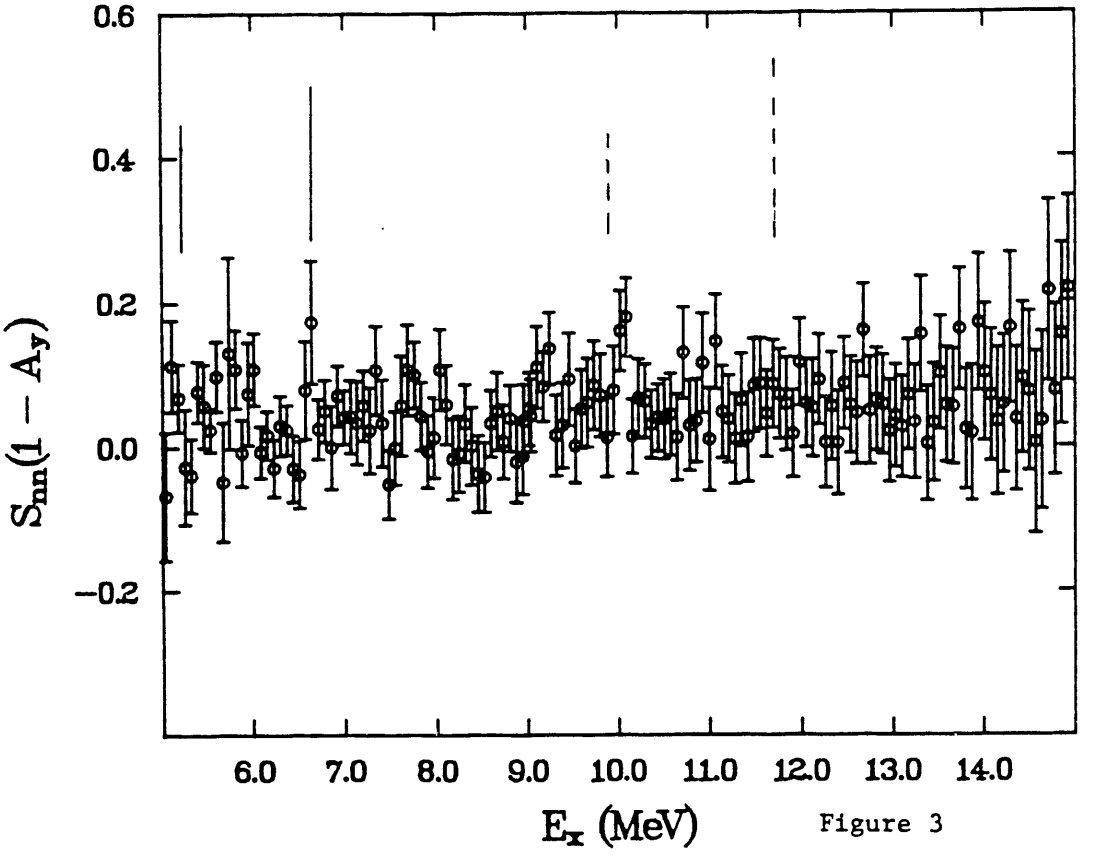

Figure 3

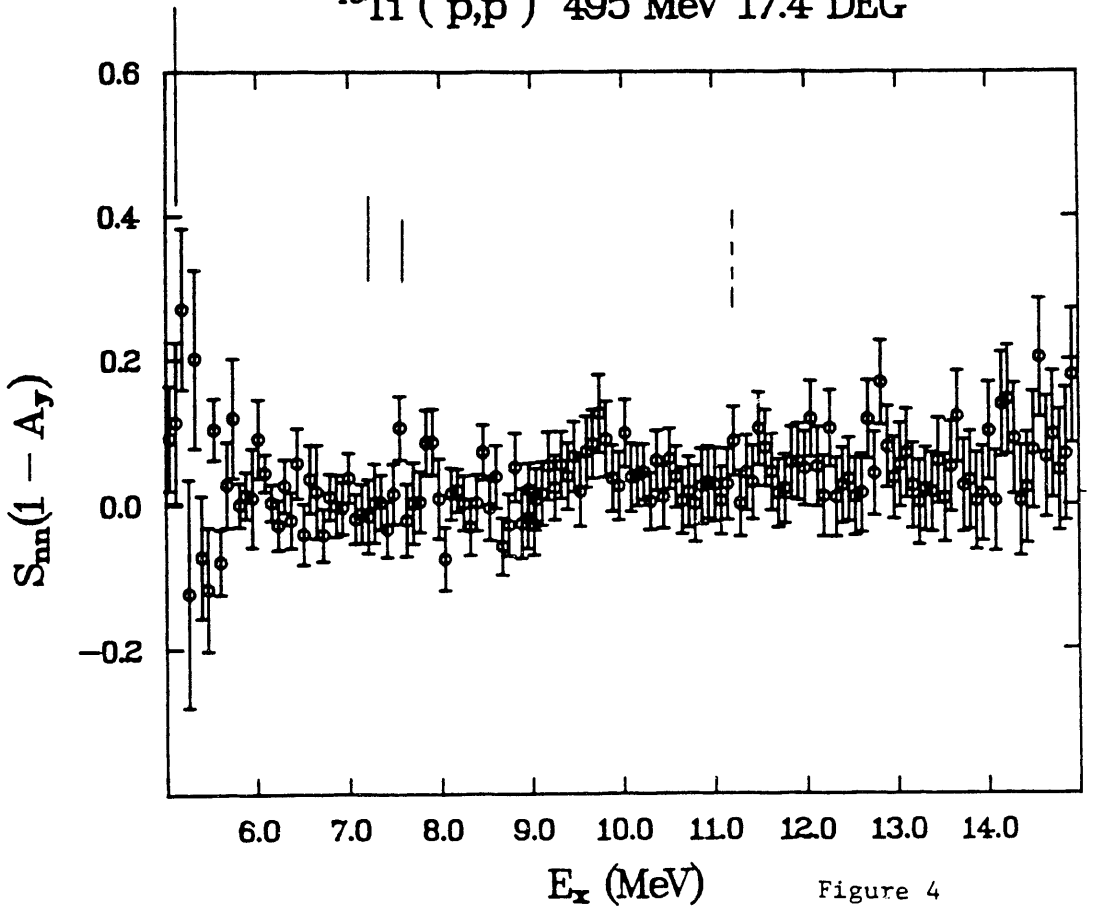

Figure 4

II.G. Proton Nucleus Scattering and the Swelling of Nucleons in Nuclei from E347, 451, 686, and 855. (with G. E. Brown, SUNY).

This work began in the summer of 1988 with the suggestion by Brown, Dover, Siegel and Weise[1] that the "swelling" of nucleons in nuclear matter due to the reduction of scalar (σ) and vector (ρ,ω) meson masses in medium (m^*) could account for the phenomenological "shrinking" of the matter density radius needed to fit $K^+ + {}^{12}C$ elastic scattering in the first order impulse approximation.[2] The decrease in the scalar meson (σ) mass is predicted by the Nambu-Jona-Lasinio model[2] and supported by chiral invariance. The situation with respect to vector meson masses is less clear but recently considerable theoretical work has been directed to calculate meson masses as a function of temperature (T)[3,4] using QCD Sum rules. For moderate T these calculations admit a scaling solution $m_v^*/m_v = m_N^*/m_N = f_\pi^*/f_\pi$ for vector meson and nucleon masses, where f_π is the pion weak decay constant. These calculations are easily extended to finite density. For the purposes of this work we have assumed all masses (meson and nucleon) scale with density (ρ) as

$$m^*/m = 1 - \frac{\lambda}{2}\,\rho/\rho_0$$

where ρ_0 is the central density in nuclei. In Ref. 1 this assumption, was found to remove the discrepancy between experiment and first order impulse approximation calculations for $K^+ + {}^{12}C$ scattering, using hadronic densities derived from electron scattering.

A more sophisticated calculation of $K^+ + {}^{12}C$ scattering has been done recently by J. Labarsouque[5] using the Brueckner reaction matrix and a K^+-nucleon potential derived from a constituent quark model. This calculation showed little improvement over the impulse approximation but good agreement with the data was obtained by swelling the quark confinement radius and reducing the quark mass, both with a $\lambda = 0.2$.

A similar discrepancy has been noted in the case of proton-nucleus scattering. First order non-relativistic impulse approximation (NRIA) calculations, using the free N-N t-matrix and densities derived from electron scattering fail to reproduce the correct phase of the diffraction structure in both elastic[6] and inelastic scattering.[7] The static (or transition) potentials, so derived, have radii slightly too large, as can be seen in Figs. 1-7.

If the scalar (σ) and vector (ω) mass scaling is introduced in the first order IA[1] the t-matrix scales <u>approximately</u> as $(m/m^*)^2 \simeq 1 + \lambda\rho/\rho_0$. For a nucleon density of the form $\rho/\rho_0(1 + e^{(r-R)/a})^{-1}$, this scaling (in the zero-range approximation) leads to a renormalization of the optical potentials by a factor $(1-\lambda)^{-1}$ and an effective 2pF density with a reduced radius parameter $R' = R - \lambda a$. The effect of the meson mass scaling has been to add a term of the form $t\rho^2$ to the usual $t\rho$ approximation in the first order IA. However, it is known that a number of corrections to the first order non-relativistic IA (correlations, non-locality, multi-step processes, etc.) can also introduce quadratic (in ρ) terms to the potential.

Our approach has been empirical; calculations were made with an effective density, $\rho' = \rho + \lambda\rho^2/\rho_0$ where ρ was obtained from electron scattering and λ was varied to fit the data. The zero range approximation,

discussed above, can be improved somewhat by treating the density dependent correction as a three-body force[8,9] ("finite range approximation") which involves folding the ρ dependent correction over a virtual pion range of $\sim h/2m_\pi c$.

In our elastic calculations, the central and spin-orbit, real and imaginary terms have been calculated with different values of λ. Arguments based on relativistic mean field theories[8] suggest that the spin-orbit term should scale as $(m/m^*)^3$. Thus we have taken λ (spin-orbit) = 3/2 λ(central). Initially we assumed λ(real) = λ(imaginary) but later simple considerations based on the Born Approximation[8] indicate that the imaginary part is not much affected by the meson mass reduction. Hence we have also made calculations with λ(imag) = 0 (for both central and spin-orbit parts). A few results for several energies, nuclei, and combinations of λ-values are shown in Figs. 8-14. It can be seen that the fits to the cross section are considerably improved with $\lambda \simeq 0.3$, corresponding to $m^*/m = 0.85$ at central density. However, despite the large increase in the spin-orbit strength for typical values of λ, the analyzing power (A_y) predictions are not much improved, showing again the failure of non-relativistic treatments to account for spin-observable data.

It should be noted that in order to properly test the consequences of density dependent scaling of meson masses one needs to calculate the t-matrix using medium modified meson propagators, rather than use, as we have, the simple scaling procedure, suggested by the Born approximation to the t-matrix. Some preliminary work along these lines has been done recently by Tjon and Wallace[10] in a relativistic framework (RIA). They find that, contrary to what we have assumed, the real parts of the optical

potential are changed only slightly ($\lesssim$ 25%) but that the imaginary parts are increased by much larger amounts. However, it is not clear that they have included all of the effective mass corrections in their calculations. The empirical situation with respect to the RIA and the need for introducing additional density dependence beyond that already contained in relativistic treatments is also not yet clear but will be explored as a result of these suggestions on meson mass reduction in medium.

A paper on this work[8], including also a discussion on the consequences of these ideas for the RIA has been submitted to Phys. Rev. C.

References

1. G. E. Brown, C. B. Dover, P. B. Siegel and W. Weise, Phys. Rev. Lett. 60, 2723 (1988).
2. V. Bernard, U.-G. Meissner and I. Zahed, Phys. Rev. Lett. 59, 966 (1987).
3. R. J. Furnstahl, T. Hatsuda and S. H. Lie, Univ. of Maryland preprint, 90-031.
4. C. Adami, T. Hatsuda and I. Zahed, State University of New York at Stony Brook Preprint, NTG-89-69.
5. J. Labarsouque, Universite de Bordeaux I preprint, 1989.
6. See for example, N. M. Hintz, et al, Univ. of Minnesota Summary Progress Report 1984-87, p. 112 (1987).
7. N. M. Hintz, et al., Phys. Rev. C30, 1976 (1984).
8. G. E. Brown, A. Sethi and N. M. Hintz, submitted to Phys. Rev. C (1989).

9. T. L. Ainsworth, G. E. Brown, M. Prakash and W. Wise, Phys. Lett. B200, 413 (1988).

10. S. Wallace, private communication, July 1990.

11. D. Cook, et al., Phys. Rev. C35, 456 (1987).

12. D. A. Hutcheon, et al., Nucl. Phys. A483, 429 (1988).

13. G. W. Hoffmann, et al., Phys. Rev. Lett. 47, 1436 (1981).

14. N. Hintz, et al., Univ. of Minnesota Summary Progress Report 1984-87, unpublished.

Figure Captions

Fig. 1: Uncorrected non-relativistic impulse approximation (NRIA) predictions for ^{208}Pb(p,p) elastic scattering cross section at T_p = 318 MeV. The nucleon densities used were derived from electron scattering and theory (for n-p difference). The data are from Ref. 11.

Fig. 2: Same as Fig. 1, but for the analyzing power at T_p = 300 MeV. The data are from Ref. 12.

Fig. 3: Same as Fig. 1 but at 498 MeV. The data are from Ref. 13.

Fig. 4: Same as Fig. 2 but at 498 MeV. The data are from Ref. 13.

Fig. 5: Same as Fig. 1 but for ^{58}Ni at 498 MeV. The data are from Ref. 14.

Fig. 6: Same as Fig. 2 but for ^{58}Ni at 498 MeV. The data are from Ref. 14.

Fig. 7: Same as Fig. 1 but for ^{40}Ca at 498 MeV. The data are from Ref. 13.

Fig. 8: Modified density, NRIA calculations with zero-range (dashed

curve) and finite-range (solid curve) approximations for ^{208}Pb elastic scattering at T_p = 498 MeV. The data are from Ref. 13. In these calculations λ (real) = λ (imag.) and $\lambda_{so} = 1.5\lambda$.

Fig. 9: Same as Fig. 8 but for the analyzing power at T_p = 498 MeV.

Fig. 10: Same as Fig. 8 but for ^{58}Ni at T_p = 498 MeV.

Fig. 11: Same as Fig. 9 but for ^{58}Ni at T_p = 498 MeV.

Fig. 12: Same as Fig. 8 but for ^{40}Ca at T_p = 498 MeV.

Fig. 13: Modified density, NRIA calculation with finite range approximation and $\lambda_{imag.} = 0$ (for both central and spin orbit potentials) for ^{208}Pb elastic scattering at T_p = 498 MeV. For real potentials, $\lambda_{central} = 0.4$ and $\lambda_{so} = 0.6$ were used.

Fig. 14: Same as Fig. 13, but for ^{40}Ca at T_p = 498 MeV.

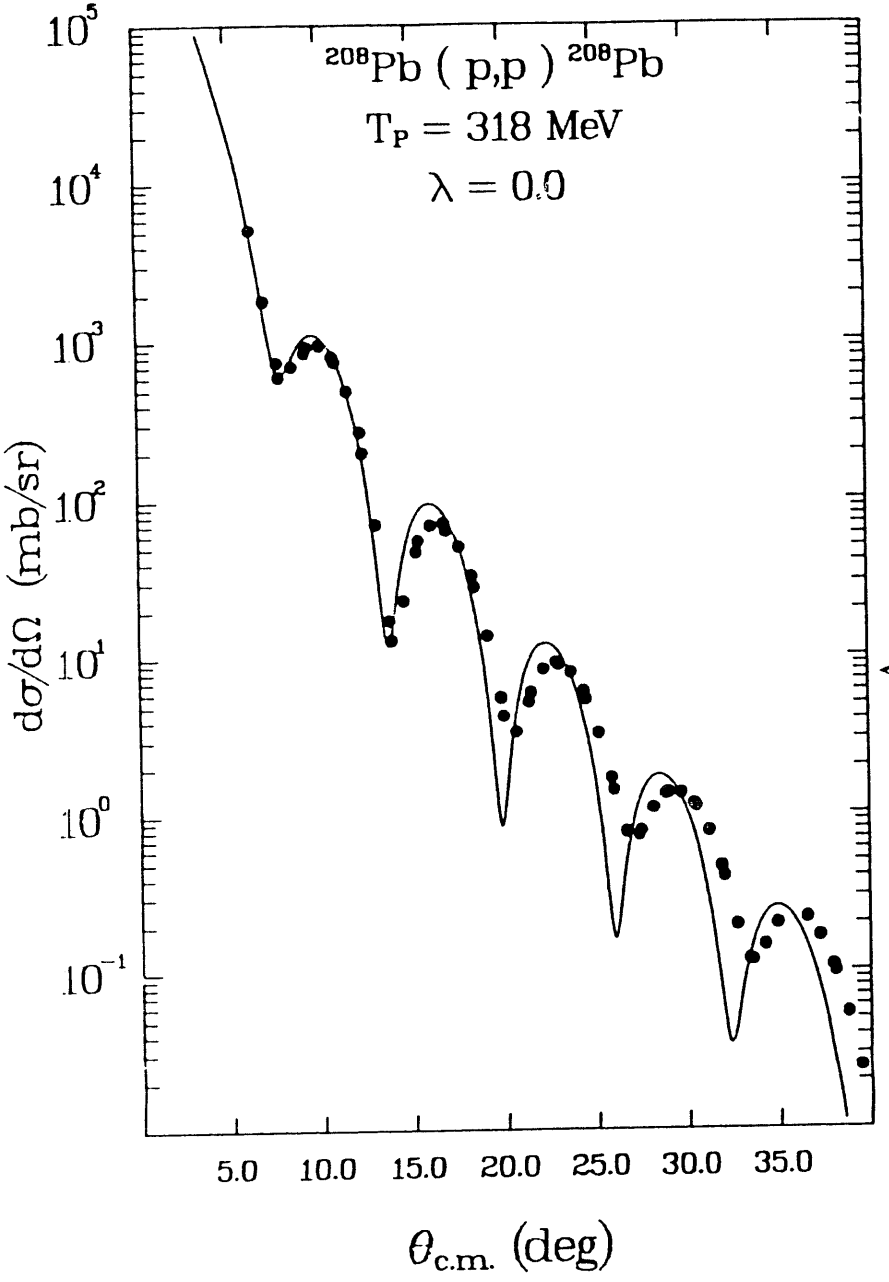

Figure 1

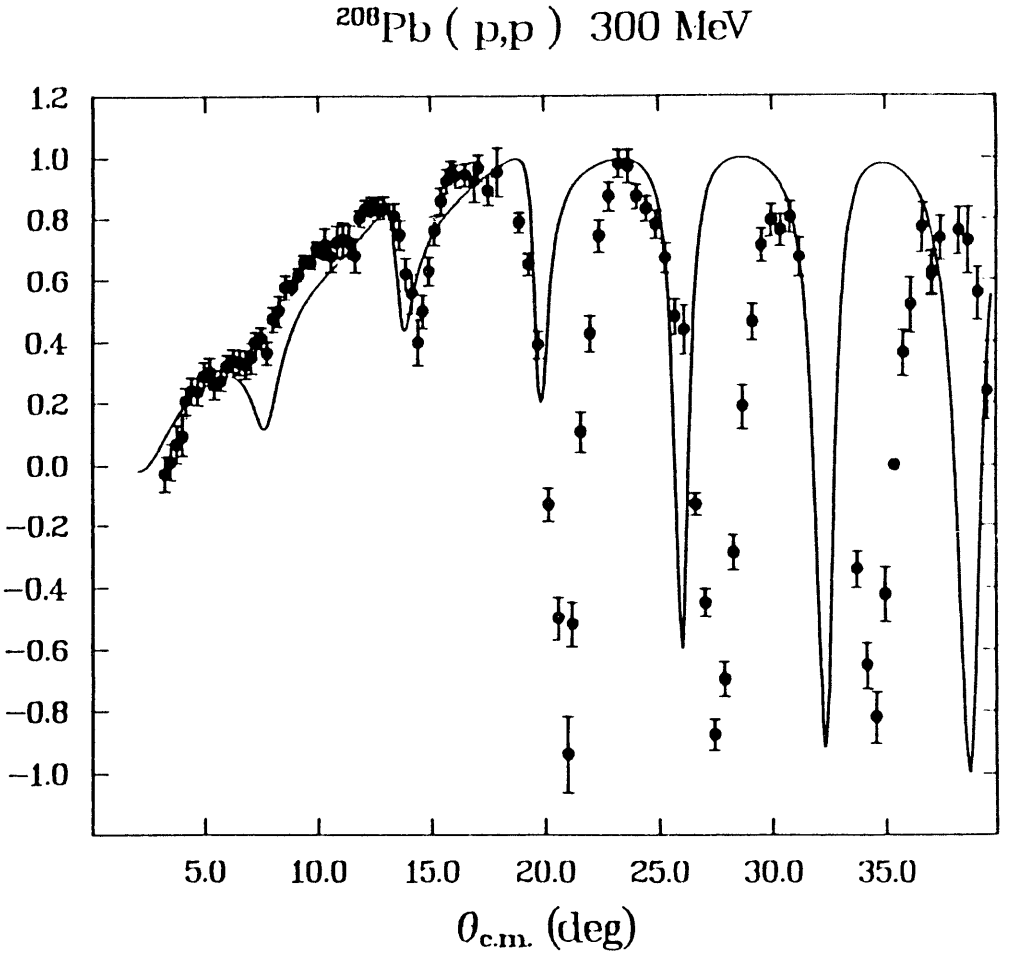

Figure 2

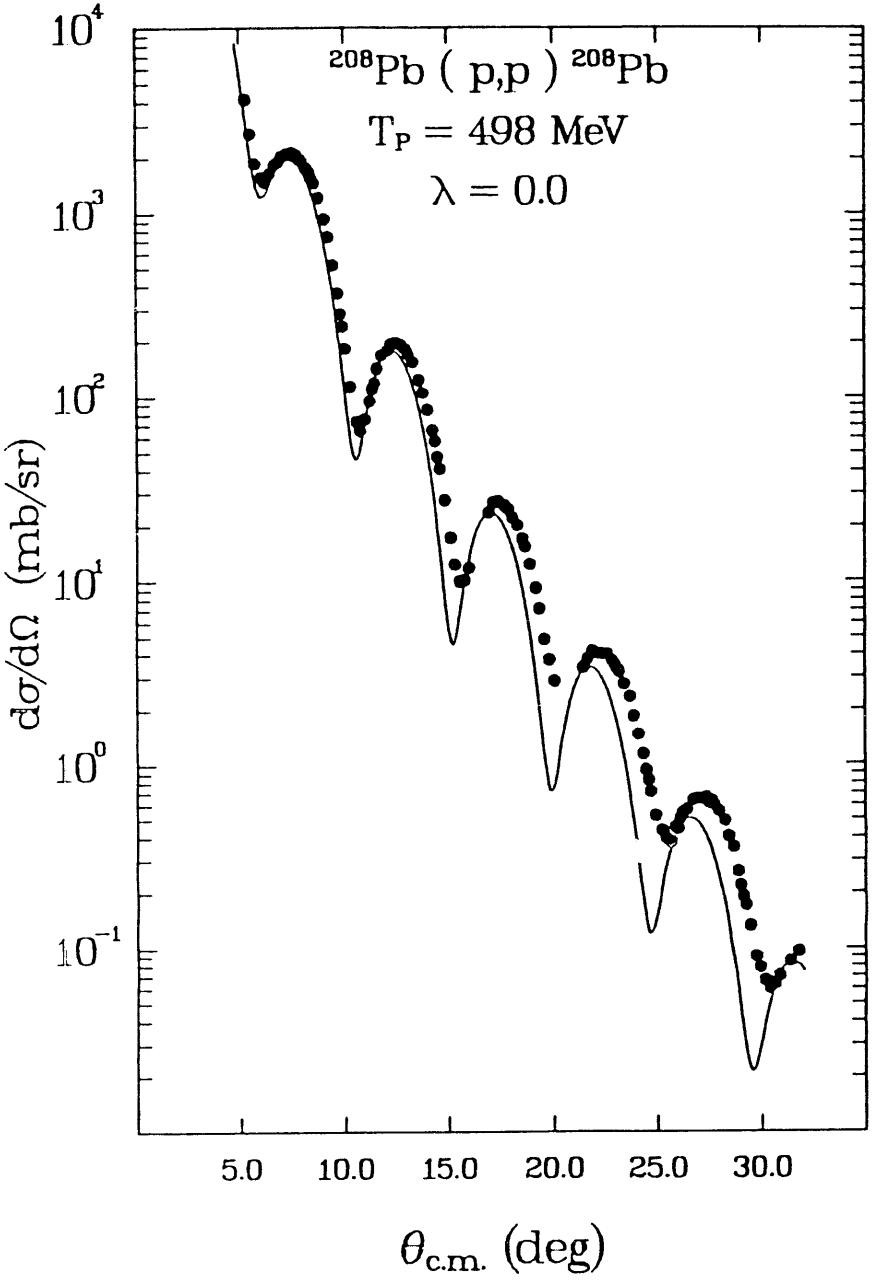

Figure 3

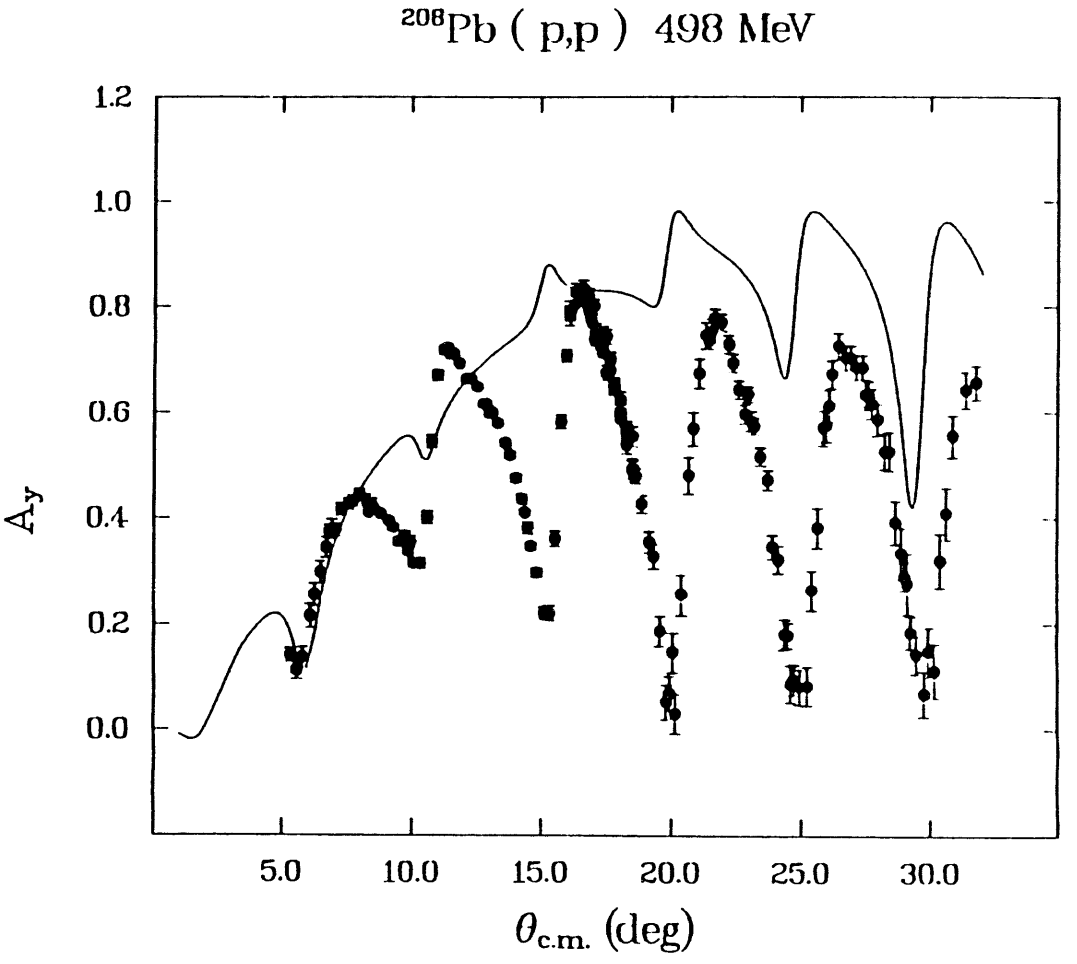

Figure 4

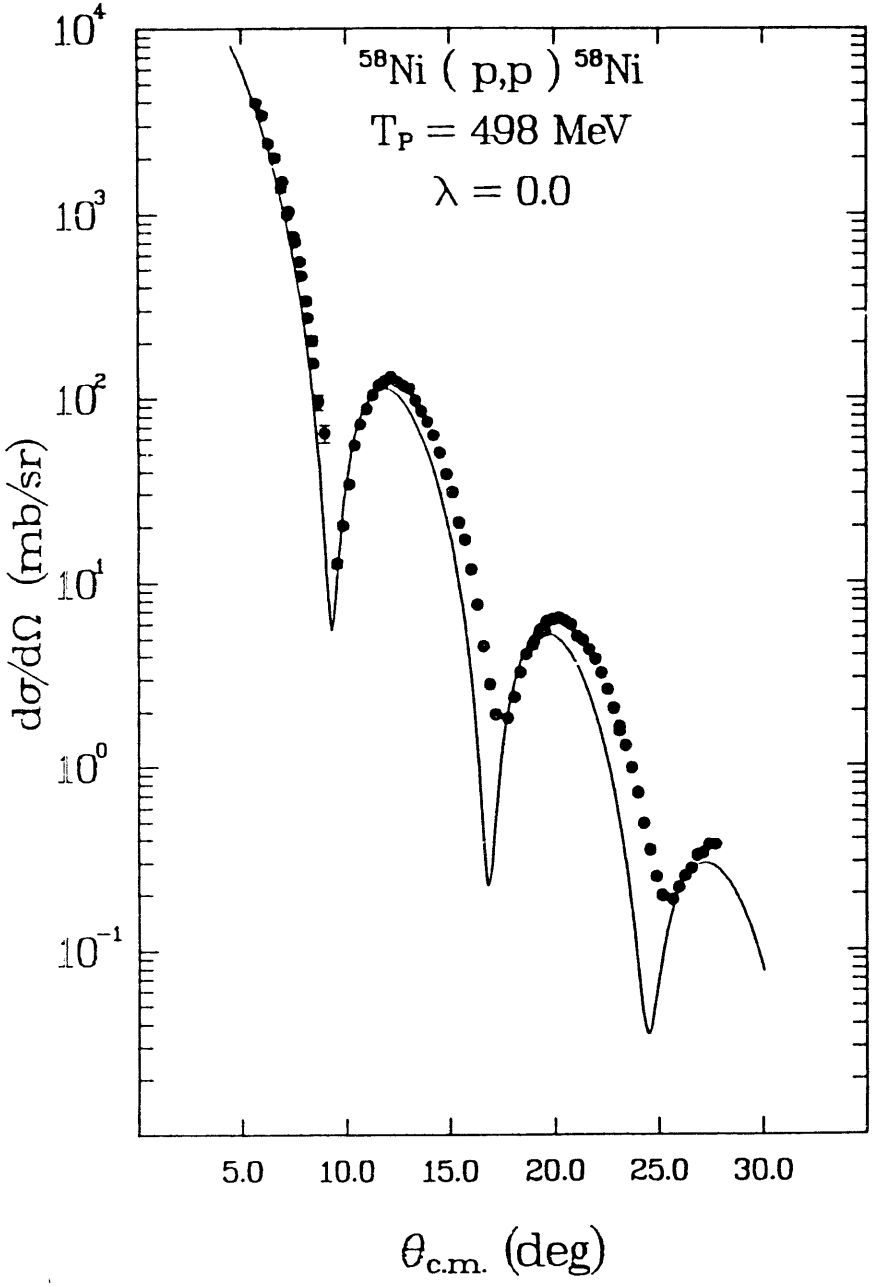

Figure 5

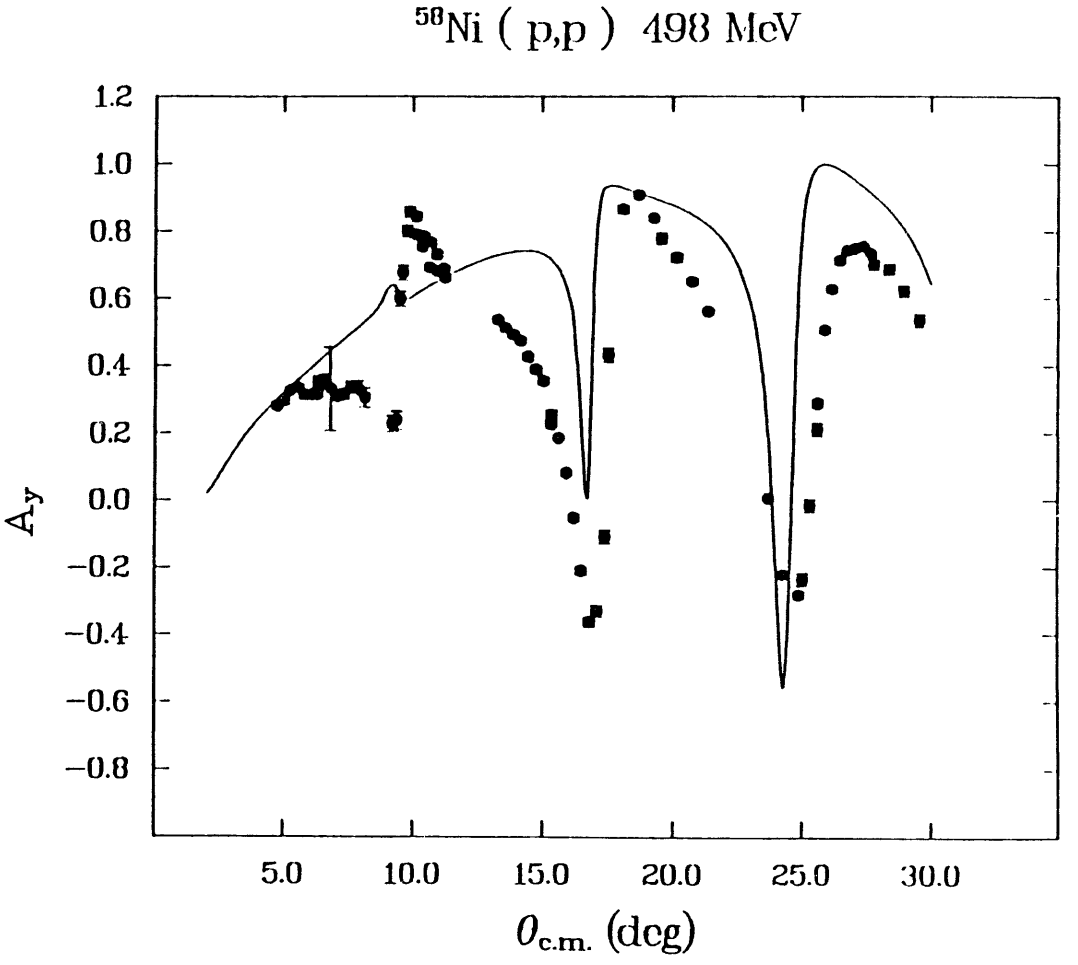

Figure 6

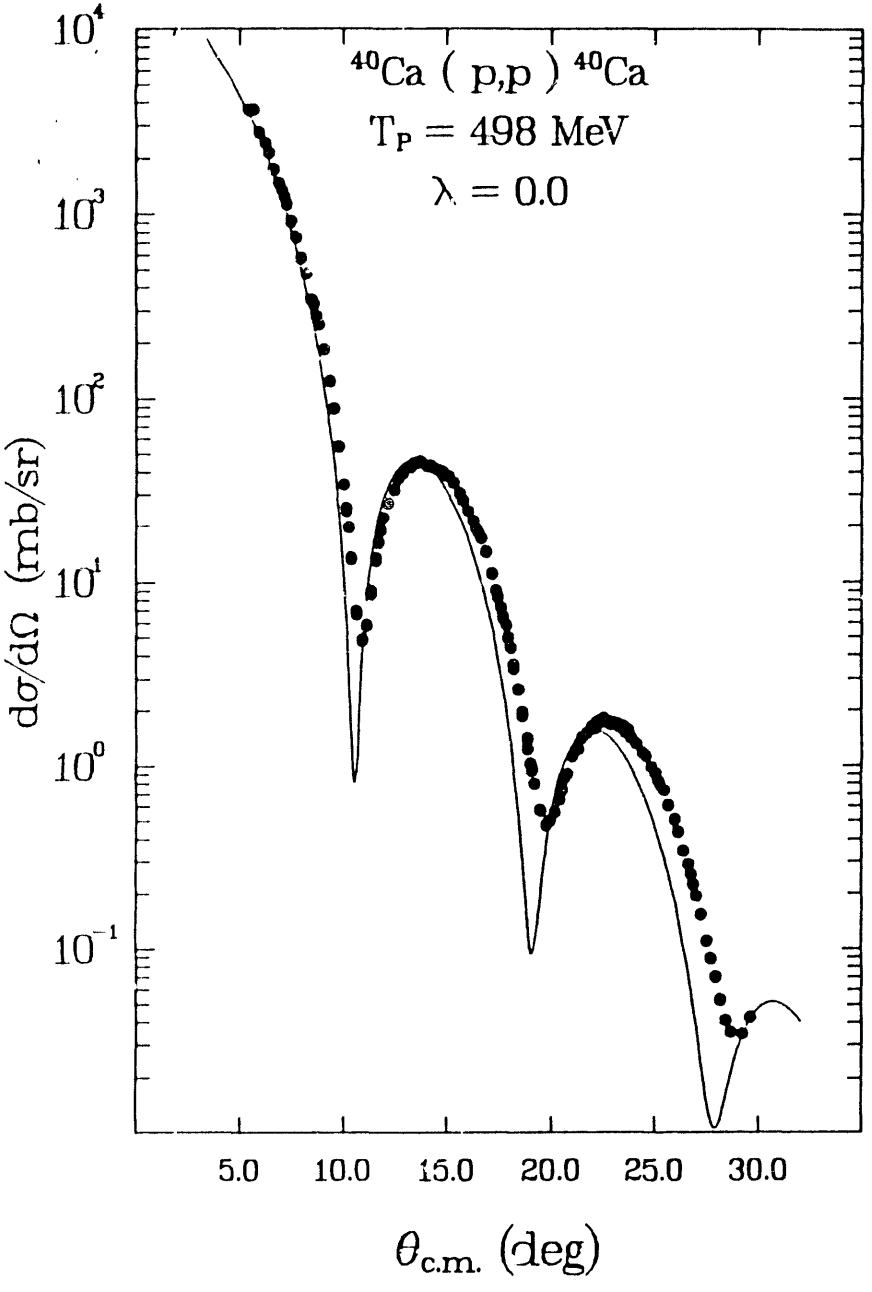

Figure 7

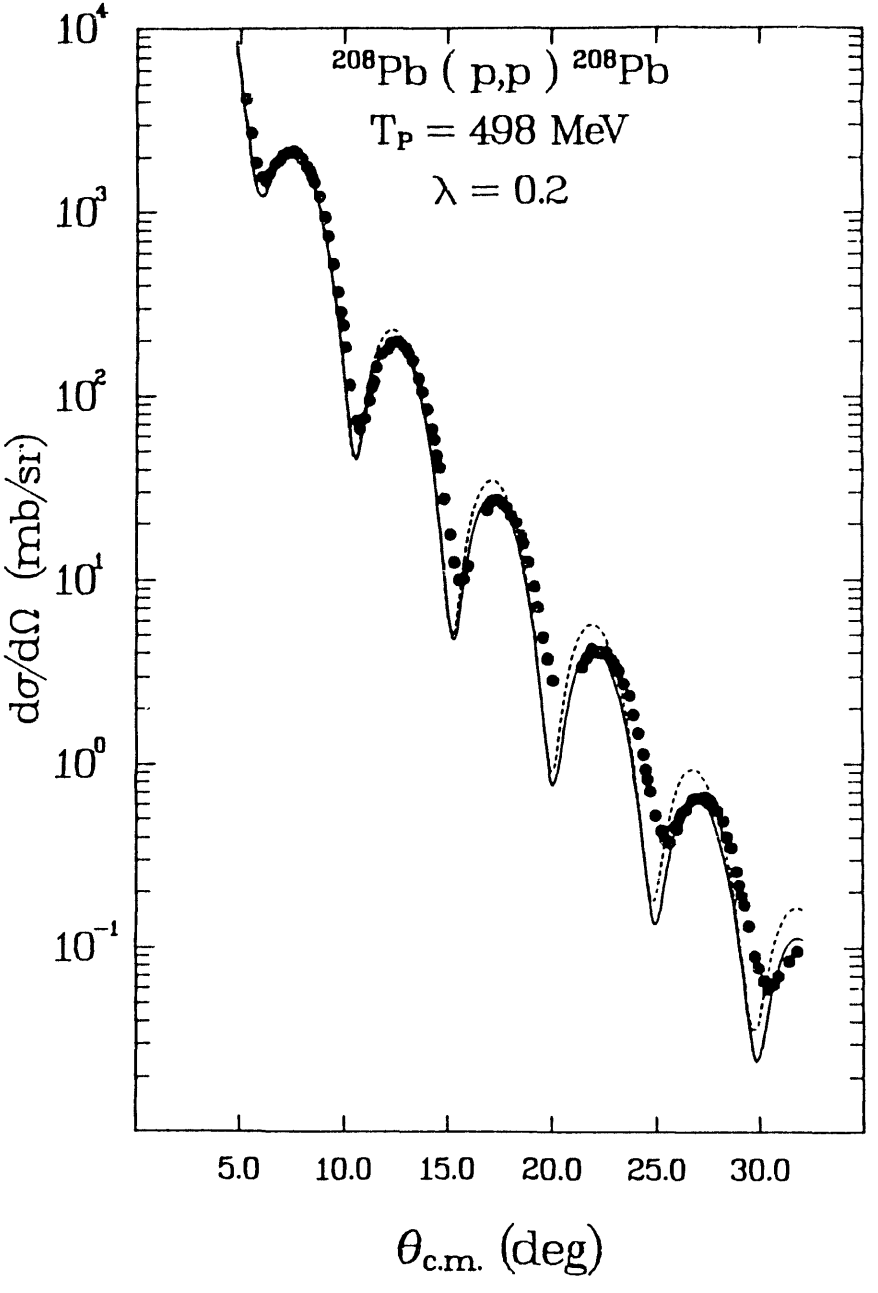

Figure 8

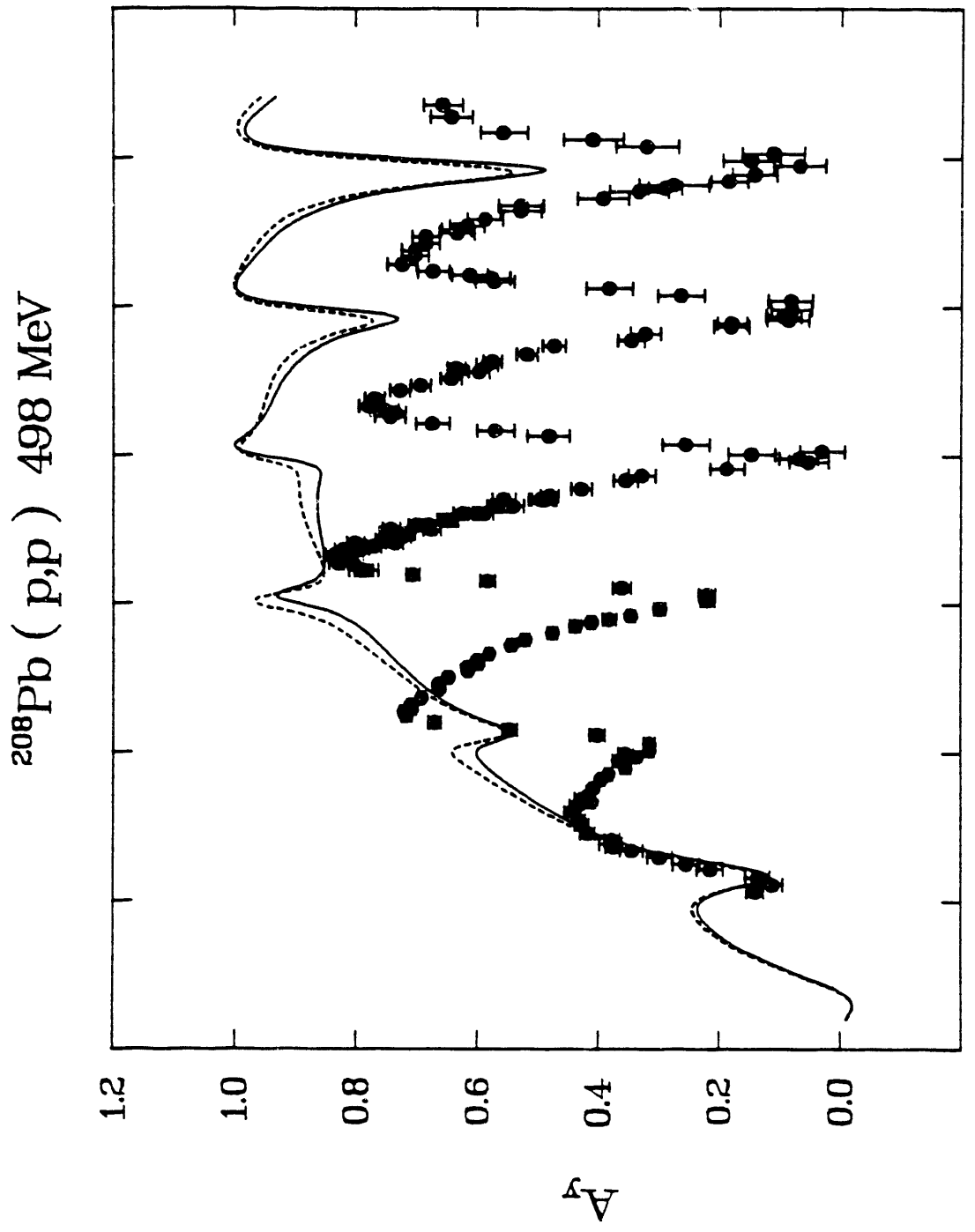
^{208}Pb (p,p) 498 MeV
A_y
1.2
1.0
0.8
0.6
0.4
0.2
0.0
5.0
10.0
15.0
20.0
25.0
30.0
$\theta_{c.m.}$ (deg)

Figure 9

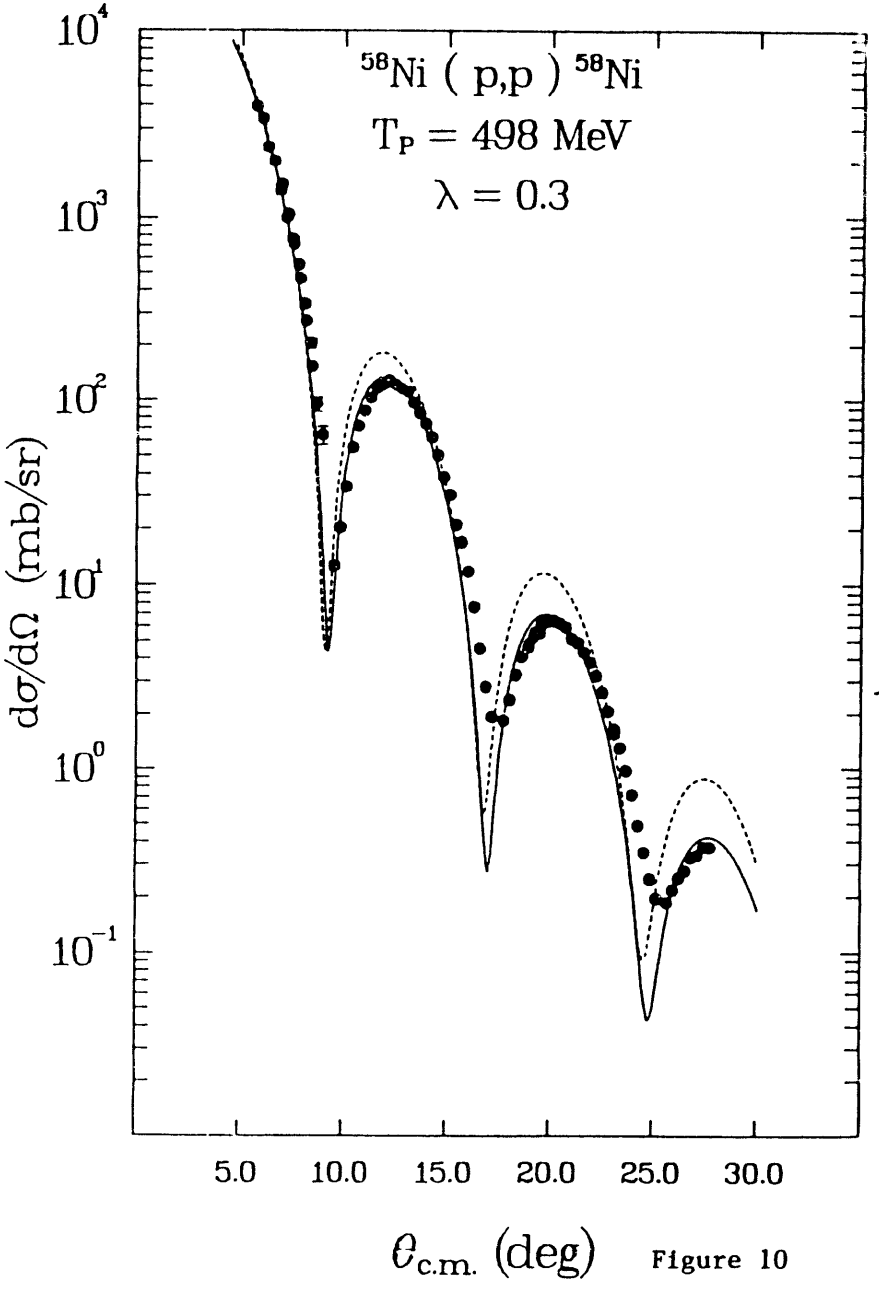

Figure 10

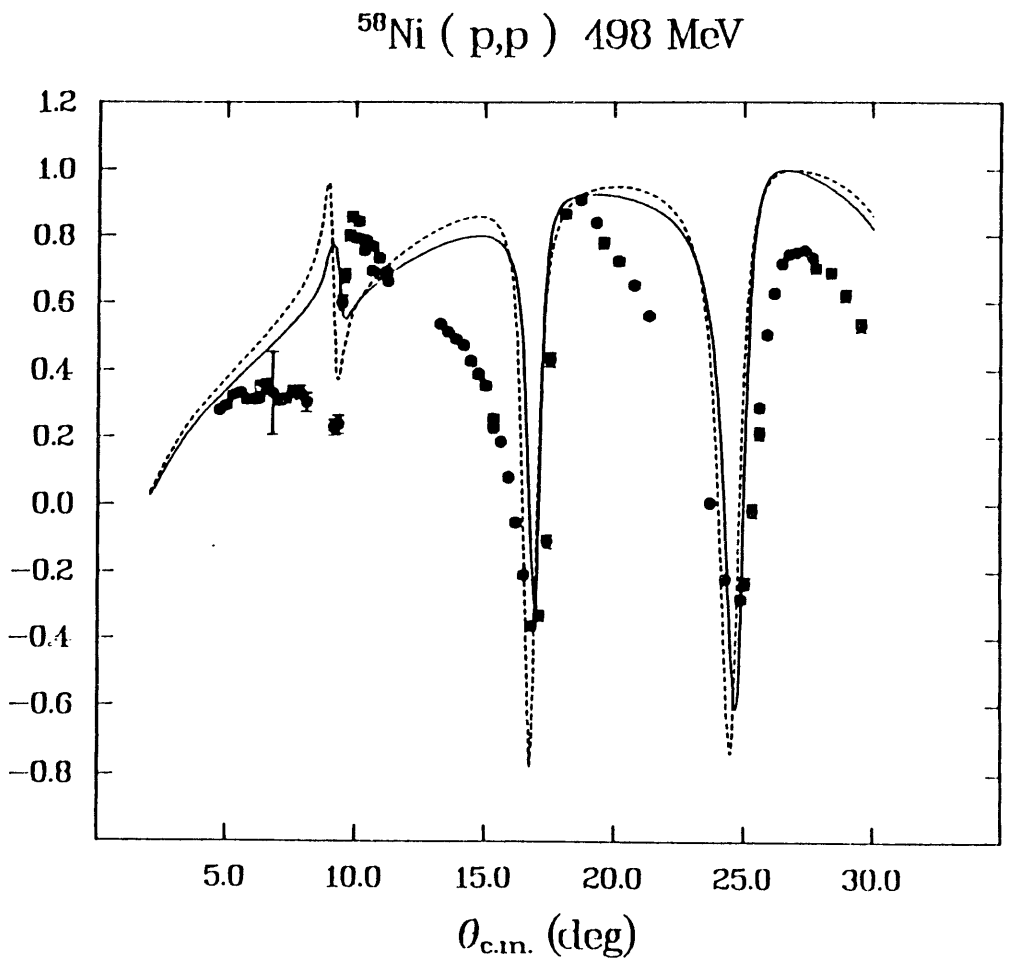

Figure 11

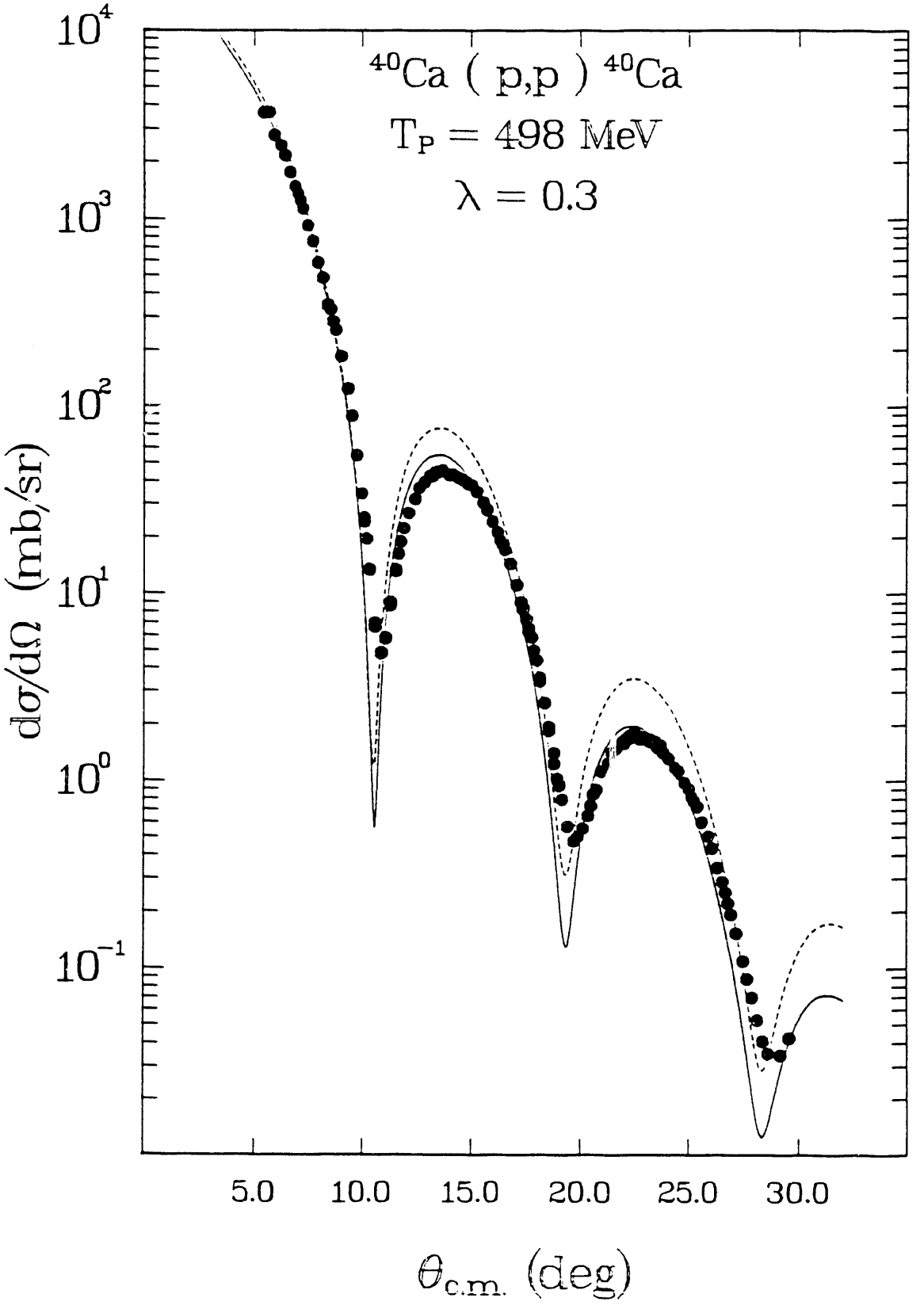
^{40}Ca (p,p) ^{40}Ca
$T_P = 498$ MeV
$\lambda = 0.3$
10^4
10^3
10^2
10^1
10^0
10^{-1}
dσ/dΩ (mb/sr)
5.0
10.0
15.0
20.0
25.0
30.0
$\theta_{c.m.}$ (deg)

Figure 12

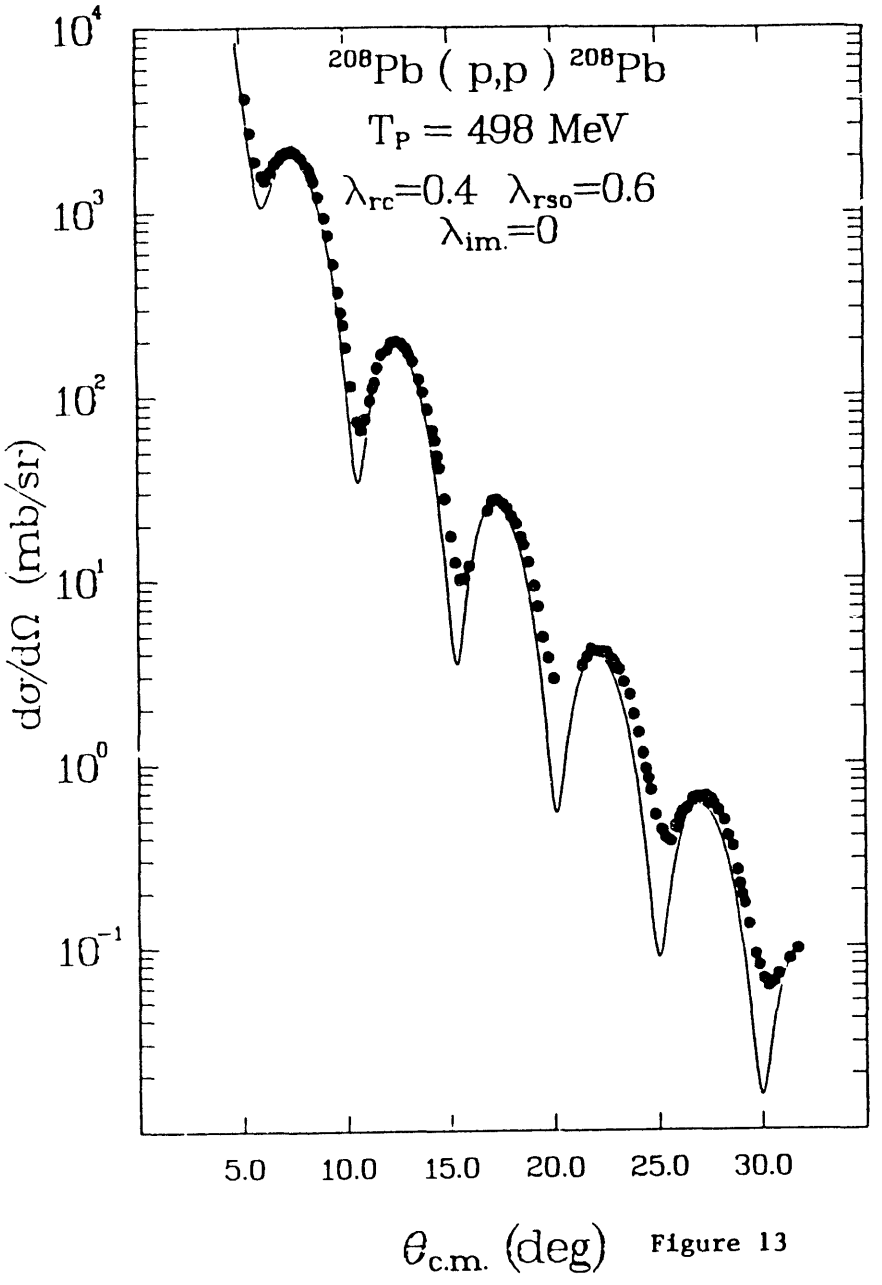

Figure 13

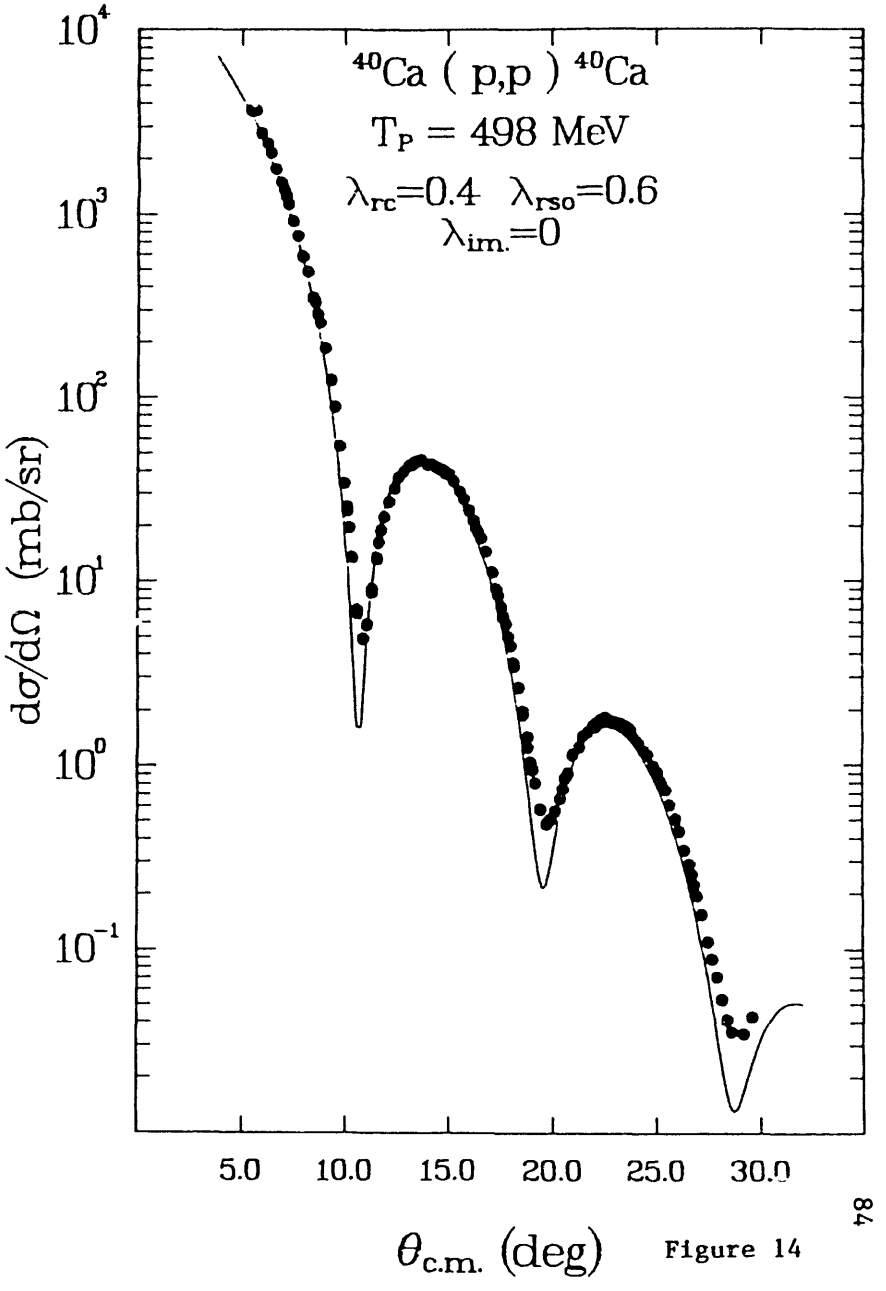

Figure 14

II.H. Measurement of Spin Observables in the ^{28}Si(p,p') Reaction at 500 MeV and Comparison with the Distorted Wave Impulse Approximation (Analysis of E623 and E451; with C. Glashausser, et al., Rutgers University).

Measurements of spin observables in intermediate energy proton scattering have been rich sources of information on nuclear structure and reaction mechanisms in recent years. Interest in application of the Dirac equation to nuclear scattering problems has grown enormously after its success, in contrast to non-relativistic approaches, in describing analyzing power (A_y) and spin rotation (Q) parameters for elastic scattering. Complete data on the spin transfer parameters, D_{ij} for normal (N), longitudinal (L) and sidewise (S) polarized beams have permitted the separation of the spin-longitudinal and transverse components of continuum excitations. Combinations of the D_{ij} (the D_K) can be formed to isolate individual components of the proton-nucleus interaction.

E623 is the first experiment to measure a complete set of proton inelastic spin observables for natural and unnatural parity states at high q, above 200 MeV. A main purpose of this work is to compare predictions of the Dirac relativistic impulse approximation (RIA) with those of the non-relativistic IA (NRIA). McClelland, et al.[1] took such data for the 1^+ states in ^{12}C at low momentum transfer and it was found that the NRIA gave good agreement with the data. A second focus of this work is to test whether the free NN amplitudes (when used in the IA) are capable of accounting for the D_{ij}, in a case where the nuclear structure is simple.

Here we report data in the 5^-(9.70 MeV) collective state and the 6^-, T = 0 and 1 stretched states (11.58 and 14.35 MeV) in ^{28}Si at T_p =

500 MeV. The data reduction for E623 was done by the Rutgers group and the theoretical analysis by our group. Cross section data[2] from Minnesota E451 was included in the analysis. The results for σ, Ay and the D_{ij} are shown in Figs. 1-28 together with the RIA and NRIA predictions discussed below.

Microscopic calculations were carried out using the RIA program DRIA[3] and the NRIA programs ALLWORLD[4] and DWBA70[5]. In both the RIA and NRIA the distorting optical potentials were calculated consistently (folded optical potential or FOP) using ground state densities derived from electron scattering and a N-N interaction obtained from free N-N amplitudes, which in the NRIA are of the form

$$M(q) = A + B\,\sigma_{1n}\sigma_{2n} + C\,(\sigma_{1n} + \sigma_{2n}) + E\,(\sigma_{1q}\sigma_{2q}) + F\,(\sigma_{1p}\sigma_{2p})$$

where $\sigma_{1n} = \vec{\sigma}_1 \cdot \hat{n}$, etc., $\vec{n} = \vec{k} \times \vec{k}'$, $\vec{q} = \vec{k}' - \vec{k}$ and $\hat{p} = \hat{q} \times \hat{n}$. (1)

and A, B, C, etc. have both an isospin dependent and an isospin independent part.

In the NRIA, calculations were also made using a phenomenological optical potential (POP) which gave a better fit to the elastic σ and A_y than the FOP. The parameters are shown in Table I.

Both the RIA and NRIA programs make use of the free NN amplitudes of Arndt and Roper[6]. In the RIA the NN amplitudes are expanded in terms of local relativistic covariants. In the NRIA the Franey-Love[7] t-matrix was used.

For the 5^- state the RPA amplitudes of Yen, et al.[8] were used to construct the transition density. For the 6^- states, a single stretched

configuration ($d_{5/2}^{-1}$, $f_{7/2}$) was used. Inelastic electron scattering form factors[9] were used as a guide in determining the parameters of the bound state potentials (2pF shape), although small changes in radii, relative to those giving the best (e,e') fit, were necessary to obtain the best (p,p') cross section fits. The electron scattering calculations were made with the programs ELECTL, ELECTE, ELECTM[10] (relativistic plane wave Born approximation, RPWBA) and ALLWORLD[4] (NRPWBA). The electron scattering form factors are shown in Figs. 29-31. In Table II we list the single particle energies and in Table III the radii of the bound state potentials (2pF). In Table III we show also the normalization factors $N^2 = \sigma_{exp}/\sigma_{theo}$. It is seen, in Table III, that the relativistic (e,e') calculations require a bound state radius, r_0, ~ 10% smaller than the non-relativistic calculations for the best fit, but give similar values of N^2. It is also noted that in both relativistic and non-relativistic calculations, a smaller r_0 is needed to fit the (p,p') data than is best for (e,e') form factors (except for the 6^-, T = 1 state in the relativistic calculations). This need for an effective "shrinking" of the densities (static or transition) has been seen previously for both elastic and inelastic proton IA calculations. (See Sect. II.G above). One effect which can produce this shrinking is a density dependent modification of the N-N t-matrix due to a decrease of nuclear and meson masses in nuclei as discussed in Sect. II.G., above.

The predictions of the RIA and NRIA (FOP and POP) are shown with the data in Figs. 1-28 for σ, A_y and the D_{ij}.

Bleszynski[11], et al., and Moss[12] have shown that certain combinations (D_K) of the D_{ij} are sensitive primarily to the individual terms in the NN interaction. The D_K in terms of the D_{ij} are as follows

$$D_0 = \frac{1}{4}\,[1 + (D_{SS} + D_{LL})\cos\theta_L + D_{NN} - (D_{LS} - D_{SL})\,\sin\theta_L]$$

$$D_x = \frac{1}{4}\,[1 + (D_{SS} - D_{LL} - D_{NN})$$

$$D_y = \frac{1}{4}\,[1 - (D_{SS} + D_{LL})\cos\theta_L + D_{NN} + (D_{LS} - D_{SL})\,\sin\theta_L]$$

$$D_z = \frac{1}{4}\,[1 - D_{SS} - D_{NN} + D_{LL}]$$

and $D_0 + D_x + D_y + D_z = 1,\ 0 \le D_K \le 1$ (2)

In the plane wave impulse approximation, these quantities are, for unnatural parity states,

$$D_0 = \frac{|X^T|^2|C|^2}{I}$$

$$D_x = \frac{|X^L|^2|E|^2}{I}$$

$$D_y = \frac{|X^T|^2|B|^2}{I}$$

$$D_x = \frac{|X^T|^2|F|^2}{I}$$

where

$$I = |X^T|^2\,[|C|^2 + |B|^2 + |F|^2] + 2|X^L|^2|E|^2 \qquad (3)$$

is the unpolarized cross section and X^T and X^L are nuclear form factors defined in Ref. 13.

For natural parity states the separation is not as complete (see Ref. 11). When distortions are included, the D_K are still sensitive primarily to the same terms. The D_K values were calculated at 22^o and are shown in Table IV along with the RIA and NRIA predictions.

The following observations can be made in comparing theory with experiment for each state:

1. Elastic σ and A_y.

a. The RIA fit to the cross section is somewhat better than the NRIA (FOP) but neither is satisfactory, both showing the phase problem discussed in Sect. II.G.

b. The RIA gives a much better account of A_y than the NRIA (FOP) but the phase problem persists.

2. 5^-(9.70 MeV) collective state.

a. The RIA fit to A_y is fairly good, and superior to both the FOP and POP NRIA.

b. Likewise, the RIA shows better agreement with the D_{ij} than the NRIA.

c. The D_{ij} (both exp. and theory) are close to the values expected in the PWBA for collective natural parity states, which are the same as for elastic scattering, namely $D_{NN} \sim 1$, $D_{LL} \sim D_{SS}$ and $D_{SL} \sim -D_{LS}$.

d. Since the 5^- state is populated mainly by the (isoscalar) A and C terms of the N-N interaction we expect $D_x \simeq D_z \simeq 0$ and the ratio $D_y/D_0 = |B|^2/|C|^2$. The data (and theory) exhibit this.

3. 6^-, T = 0 (11.58 MeV) state.

a. A_y is reproduced poorly by both the RIA and NRIA (wrong sign).

b. In the PWBA, the 6^-, T = 0 state, whose excitation is dominated by the spin-orbit term (C),[2] all three diagonal D_{ij} should be roughly equal, large and positive as is observed. Also, D_0 should be large and the other D_K small, as seen.

4. 6^-, T = 1 (14.35 MeV) state.

a. Both the RIA and the NRIA fits to A_y are reasonably good.

b. In the NRIA calculations[2], the excitation of the 6^-, T = 1 state is dominated by the isovector tensor term (~ 84%); thus in the PWBA, we expect $D_{NN} \simeq D_{LL}$ (as is observed), but to be large and negative, in contrast to both experiment and calculation. For this state only D_{SS} is within one standard derivation of the RIA and NRIA predictions.

c. The tensor dominance (in the theory) implies also that D_x, D_y and D_z should be large compared to D_0. The data, in contrast shows $D_0 \simeq D_y$ and D_x much smaller than predicted.

These discrepancies may indicate a need for a reduction of the isovector tensor force and an enhancement of the isovector spin-orbit force in the nucleus as is suggested by theoretical predictions based on the reduction of vector meson-masses in medium (see Sects. II.G and II.I and Ref. 15).

In conclusion, comparison of theory and experiment shows no clear preferences for either the RIA or NRIA except for the A_y data in the elastic and 5^-, T = 0 channels. The agreement with the D_{ij} and D_K data for either the RIA or NRIA is fairly good in the T = 0 channels but several significant

discrepancies are seen in the T = 1 channel, perhaps indicating a need for modification, in nuclei, of the spin-orbit and tensor interactions.

Table I

Phenomenological optical potential[a)]

(POP) parameters for p + ^{28}Si at

T_p = 500 MeV (lengths in fm, energies in MeV)

r_c	V	r_v	a_v	W	r_w	a_w
1.05	-0.557	1.573	0.397	-24.5	1.203	0.550

V_{LS}	W_{LS}	r_{LS}	a_{LS}
-1.65	4.18	0.981	0.641

a) the potential is of the form:

$$U = Vf(r;r_v,a_v) + iWf(r;r_w,a_w)$$

$$- (V_{LS} + iW_{LS})\left(\frac{h}{m_\pi c}\right)^2 \frac{2}{r}\frac{d}{dr} f(r;r_{LS},a_{LS})\vec{\ell}\cdot\vec{\sigma} + V_c$$

where V_c is the coulomb potential of a uniformly charged sphere of radius $R_c = r_c A^{1/3}$, $f(r;r_x,a_x) = [1 + \exp(r-R_x)/a_x]^{-1}$, and $R_x = r_x A^{1/3}$.

Table II

Single particle energies used for bound state wave functions (Mev)

State	5^-	6^-0	6^-1
$1d_{5/2}$	-17.2	-17.2	-17.2
$1d_{3/2}$	-5	-	-
$1f_{7/2}$	-4	-2[a)]	-2
$1f_{5/2}$	-3	-	-

a) No significant difference was found between -2 and -4 MeV for the $1f_{7/2}$ energy.

Table III

Bound state potential reduced radii (r_0) and normalization factors, $N^2 = \sigma_{exp}/\sigma_{theo}$ for states J^π, T.

	STATE					
	$5^-,0$		$6^-,0$		$6^-,1$	
Calculation	r_0	N^2	r_0	N^2	r_0	N^2
(e,e')						
RPWBA[a]	1.375	1.06	-	-	1.15	0.31
NRPWBA[b]	1.50	1.11	-	-	1.275	0.33
(p.p')						
RIA[c]	1.31	1.23	1.375	0.12	1.15	0.25
NRIA-FOP[d]	1.32	1.25	1.375	0.17	1.20	0.33
NRIA-POP[e]	1.375	0.83	1.375	0.13	1.25	0.26

a) Relativistic plane wave Born approximation (ELECT).

b) Non relativistic plane wave Born approximation (ALLWORLD)

c) Relativistic impulse approximation (DRIA).

d) Non relativistic impulse approximation (ALLWORLD and DWBA-70), folded (consistent) optical potential.

e) Non relativistic impulse approximation, phenomenological optical potential (RELOM, DWBA-70).

Table IV

D_K parameters at $\theta_L = 22^o$ for ^{28}Si (p,p') at $T_p = 500$ MeV

State J^π,T		D_0	D_x	D_y	D_z	$\delta D_K^{(a)}$
5^-	EXP	0.72	0.02	0.24	0.023	±0.03
	RIA	0.69	0.005	0.30	0.005	
	NRIA-FOP	0.56	0.006	0.42	0.016	
	NRIA-POP	0.62	0.085	0.27	0.02	
6^-,0	EXP	0.70	0.045	0.24	0.01	±0.08
	RIA	0.89	0.018	0.082	0.008	
	NRIA-FOP	0.82	0.015	0.11	0.05	
	NRIA-POP	0.73	0.15	0.083	0.035	
6^-,1	EXP	0.33	0.12	0.38	0.16	±0.08
	RIA	0.050	0.49	0.42	0.046	
	NRIA-FOP	0.049	0.47	0.41	0.064	
	NRIA-POP	0.132	0.48	0.30	0.092	

a) Statistical errors in D_K.

References

1. J. B. McClelland, J. M. Moss, B. Aas, A. Azizi, E. Bleszynski, M. Bleszynski, J. Geaga, G. Igo, A. Rahbar, J. B. Wagner, G. S. Weston, C. Whitten, Jr., K. Jones, S. Nanda, M. Gazzaly, and N. Hintz, Phys. Rev. Lett. 52, 98 (1984) and Errata, ibid., 52, 954 (1984).
2. N. Hintz, M. A. Franey, M. M. Gazzaly, D. Cook, G. S. Kyle, D. Dehnhard, S. J. Seestrom-Morris, G. W. Hoffmann, M. Barlett, G. S. Blanpied, J. A. McGill, J. B. McClelland, R. L. Boudrie, F. Irom, and G. Pauletta, Phys. Rev. C30, 1976 (1984) and M. Gazzaly, private communication.
3. J. Shepard, E. Rost, and J. Piekarewicz, Phys. Rev. C30, 1604 (1984).
4. J. Carr, F. Petrovich, and J. Kelly, Computer program ALLWORLD (unpublished).
5. R. Schaeffer and J. Raynal, computer program DWBA70 (modified); J. Raynal Nucl. Phys. A97, 572 (1967).
6. R. A. Arndt and D. Roper, VPI and SU Scattering Analysis Interactive Dialin Program and Data Base.
7. M. A. Franey and W. G. Love, Phys. Rev. C31, 488 (1985).
8. S. Yen, R. J. Sobie, T. E. Drake, A. D. Bacher, G. T. Emery, W. P. Jones, D. W. Miller, C. Olmer, and P. Schwandt, Phys. Lett. 105B, 421 (1981).
9. S. Yen, R. Sobie, H. Zarek, B. O. Pich, T. E. Drake, C. F. Williamson, S. Kowalski and C. P. Sargent, Phys. Lett. 93B, 250 (1980) and S. Yen, R. Sobie, T. E. Drake, H. Zarek, C. F. Williamson, S. Kowalski, and C. P. Sargent, Phys. Rev. C27, 1939 (1983), and private communication,

S. Yen.

10. J. R. Shepard, E. Rost, and J. A. McNeil, Phys. Rev. C33, 634 (1986). See also J. R. Shepard, E. Rost, E. R. Siciliano and J. A. McNeil, Phys. Rev. C29, 2243 (1984).

11. M. Bleszynski, E. Bleszynski, and C. A. Whitten, Jr., Phys. Rev. C26, 2063 (1982).

12. J. M. Moss, Phys. Rev. C26, 727 (1982).

13. T. W. Donnelly and W. C. Haxton, Atomic Data and Nuclear Data Tables, 23, 103 (1979).

14. W. G. Love and A. Klein, Proc. Sixth Int. Conf. on Polarization Phenomena in Nucl. Phys., Journ. Phys. Soc. Japan Suppl. 55, 78 (1986).

15. G. E. Brown and M. Rho, Phys. Lett. B237, 3 (1990).

Figure Captions

Fig. 1: Differential cross section for p + ^{28}Si elastic scattering at T_p = 498 MeV. The curve is the prediction of the relativistic impulse approximation (RIA). The data are from Ref. 2.

Fig. 2: Same as Fig. 1 but the curves are predictions of the nonrelativistic impulse approximation (NRIA) with a folded ("consistent") optical potential (FOP, solid line) and a phenomenological optical potential (POP, dashed line).

Fig. 3: Elastic analyzing power for p + ^{28}Si at T_p = 500 MeV. The curve is the RIA prediction.

Fig. 4: Same as Fig. 3 but the curves are the NRIA-FOP (solid line) and NRIA-POP (dashed line).

Fig. 5: Inelastic cross section for ^{28}Si(p,p') to the 5^- (9.70 MeV), T = 0 state at T_p = 498 MeV. The curve is the RIA prediction. The data are from Ref. 2.

Fig. 6: Same as Fig. 5 except the curves are the NRIA-FOP (solid) and NRIA-POP (dashed) predictions.

Fig. 7: Analyzing power for the 5^-(9.70 MeV) state in ^{28}Si(p,p') at T_p = 500 MeV. The curve is the RIA prediction.

Fig. 8: Same as Fig. 7 but the curves are the NRIA-FOP (solid) and NRIA-POP (dashed) predictions.

Fig. 9: Spin observables, D_{NN}, D_{SS} and D_{LL} for ^{28}Si(p,p') to the 5^-(9.70) MeV) state at T_p = 500 MeV. The curves are the RIA predictions.

Fig. 10: Same as Fig. 9 but the curves are the NRIA-FOP (solid) and NRIA-POP (dashed) predictions.

Fig. 11: Same as Fig. 9 but for the D_{SL} and D_{LS}.

Fig. 12: Same as Fig. 10 but for the D_{SL} and D_{LS}.

Fig. 13: Inelastic cross section for $^{28}Si(p,p')$ to the 6^-(11.58 MeV), T = 0 state at T_p = 498 MeV. The curve is the RIA prediction. The data are from Ref. 2.

Fig. 14: Same as Fig. 13 but the curves are the NRIA-FOP (solid) and NRIA-POP (dashed) predictions.

Fig. 15: Analyzing power for the 6^-(11.58 MeV), T = 0 state in $^{28}Si(p,p')$ at T_p = 500 MeV. The curve is the RIA prediction.

Fig. 16: Same as Fig. 15 but the curves are the NRIA-FOP (solid) and NRIA-POP (dashed) predictions.

Fig. 17: Spin observables, D_{NN}, D_{SS} and D_{LL} for $^{28}Si(p,p')$ to the 6^-(11.58 MeV) T = 0 state at T_p = 500 MeV. The curves are the RIA predictions.

Fig. 18: Same as Fig. 17 but the curves are the NRIA-FOP (solid) and NRIA-POP (dashed) predictions.

Fig. 19: Same as Fig. 17 but for the D_{SL} and D_{LS}.

Fig. 20: Same as Fig. 18 but for the D_{SL} and D_{LS}.

Fig. 21: Inelastic cross section for $^{28}Si(p,p')$ to the 6^-(14.35 MeV), T = 1 state at T_p = 498 MeV. The curve is the RIA prediction. The data are from Ref. 2.

Fig. 22: Same as Fig. 21 but the curves are the NRIA-FOP (solid) and NRIA-POP (dashed) predictions.

Fig. 23: Analyzing power for the 6^-(14.35 MeV), T = 1 state in $^{28}Si(p,p')$ at T_p = 500 MeV. The curve is the RIA prediction.

Fig. 24: Same as Fig. 23 but the curves are the NRIA-FOP (solid) and NRIA-

POP (dashed) predictions.

Fig. 25: Spin observables, D_{NN}, D_{SS} and D_{SL} for $^{28}Si(p,p')$ to the 6^- (14.35 MeV) T = 1 state at T_p = 500 MeV. The curves are the RIA predictions.

Fig. 26: Same as Fig. 25 but the curves are the NRIA-FOP (solid) and NRIA-POP (dashed) predictions.

Fig. 27: Same as Fig. 25 but for the D_{SL} and D_{LS}.

Fig. 28: Same as Fig. 26 but for the D_{SL} and D_{LS}.

Fig. 29: Total form factor squared for $^{28}Si(e,e')$ to the 5^-(9.70) MeV), T = 0 state at $\theta = 90^o$ (crosses, dashed line) and $\theta = 160^o$ (solid circles, solid line) vs. q_{eff}. Curves are predictions of the relativistic plane wave Born approximation. The data are from Refs. 8. and 9.

Fig. 30: Same as Fig. 29 but the curves are predictions of the nonrelativistic plane wave Born approximation.

Fig. 31: Transverse form factor squared for $^{28}Si(e,e')$ to the 6^- (14.35 MeV), T = 1 state. The solid curve is the prediciton of the relativistic and the dashed curve the nonrelativistic plane wave Born approximation. The data are from Refs. 8 and 9.

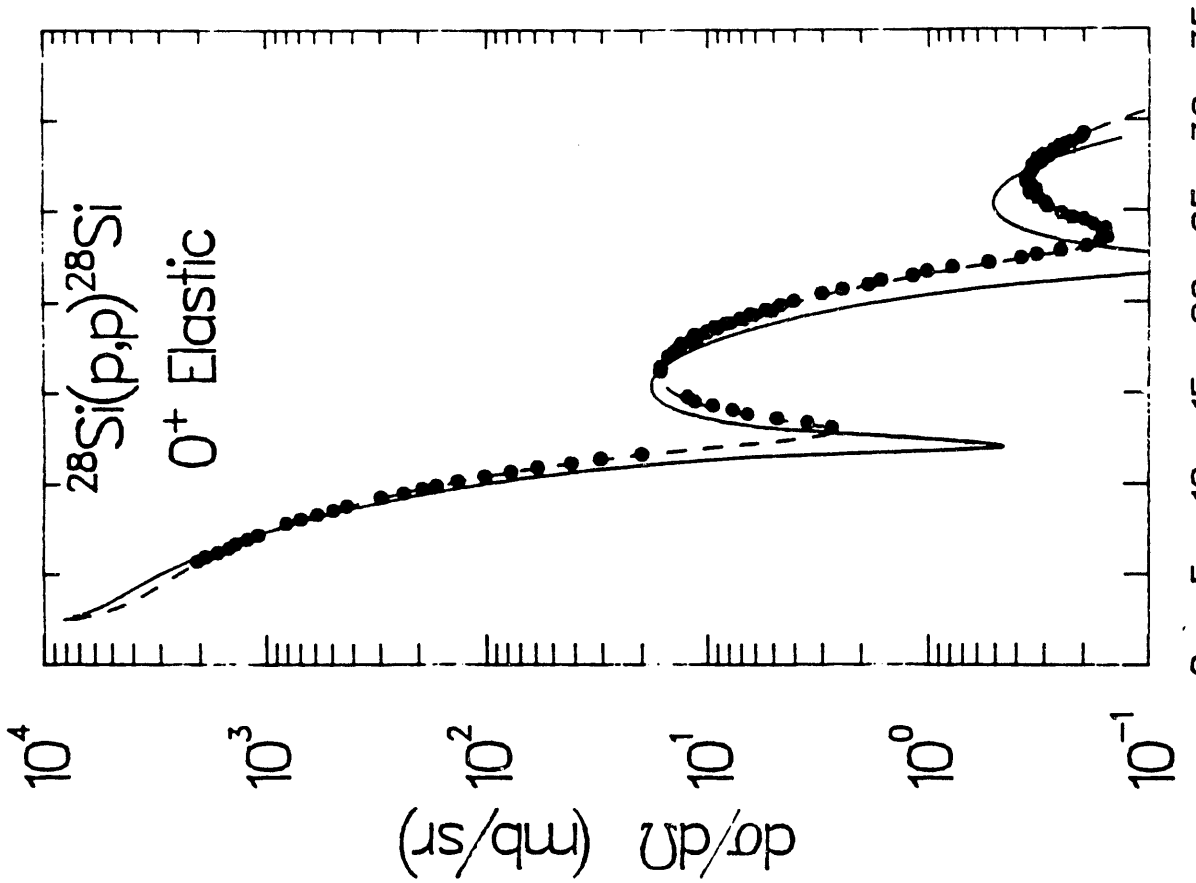

Figure 2

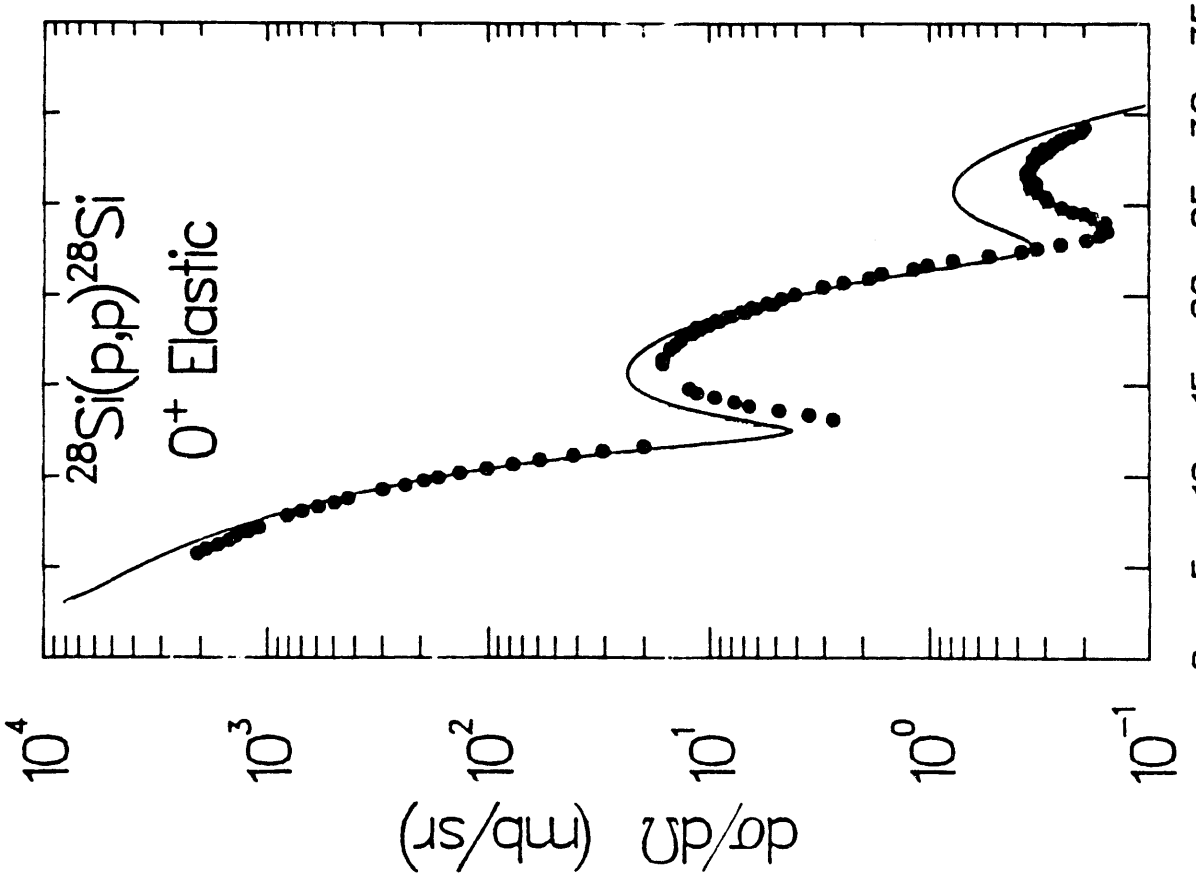

Figure 1

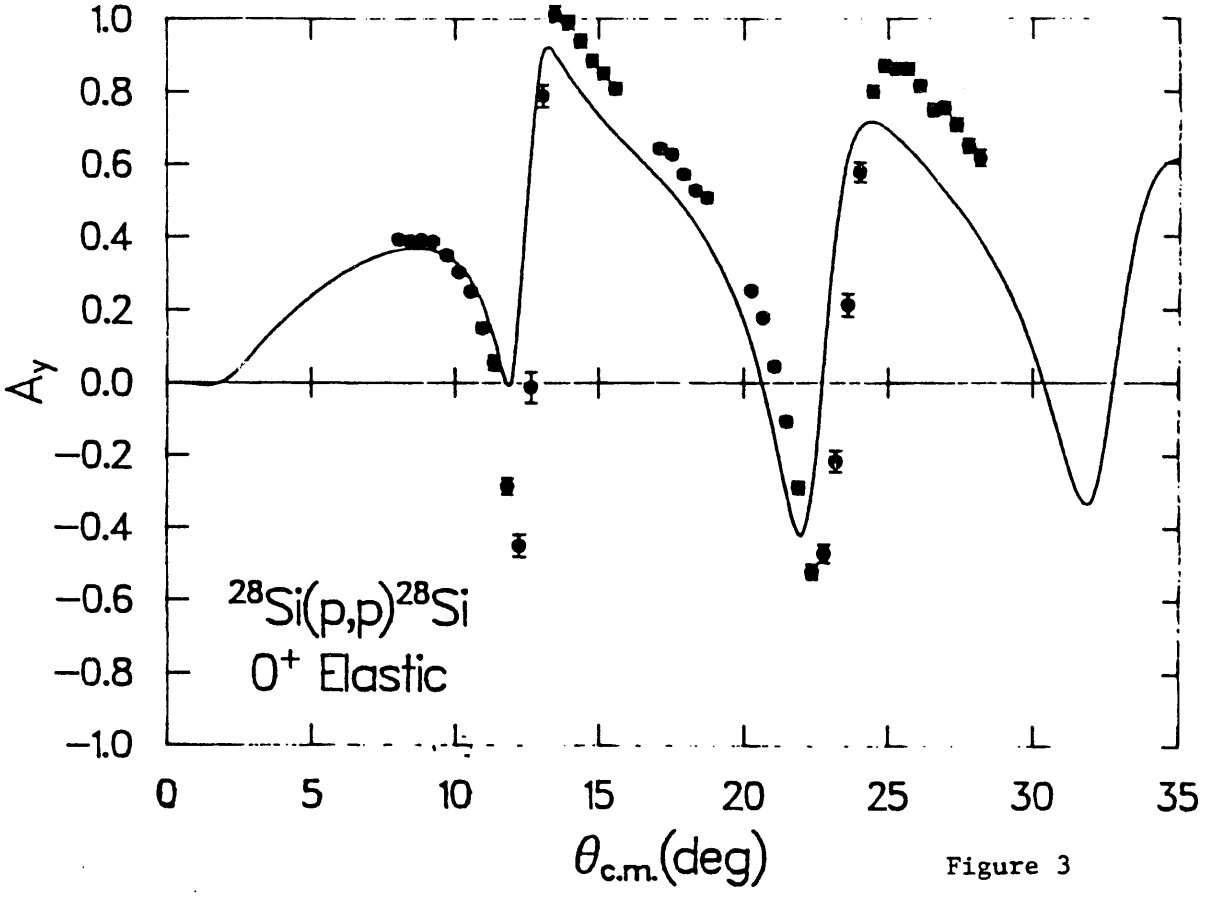

Figure 3

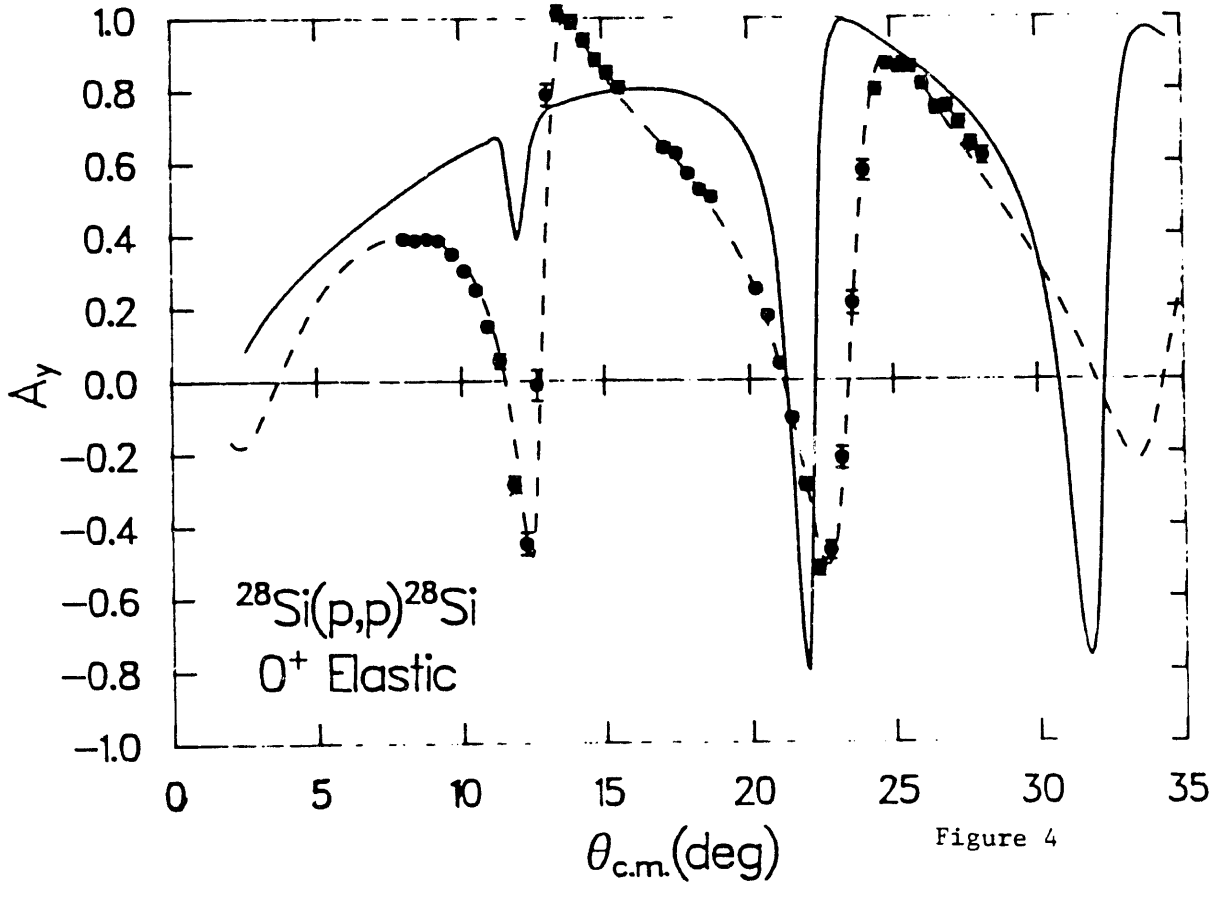

Figure 4

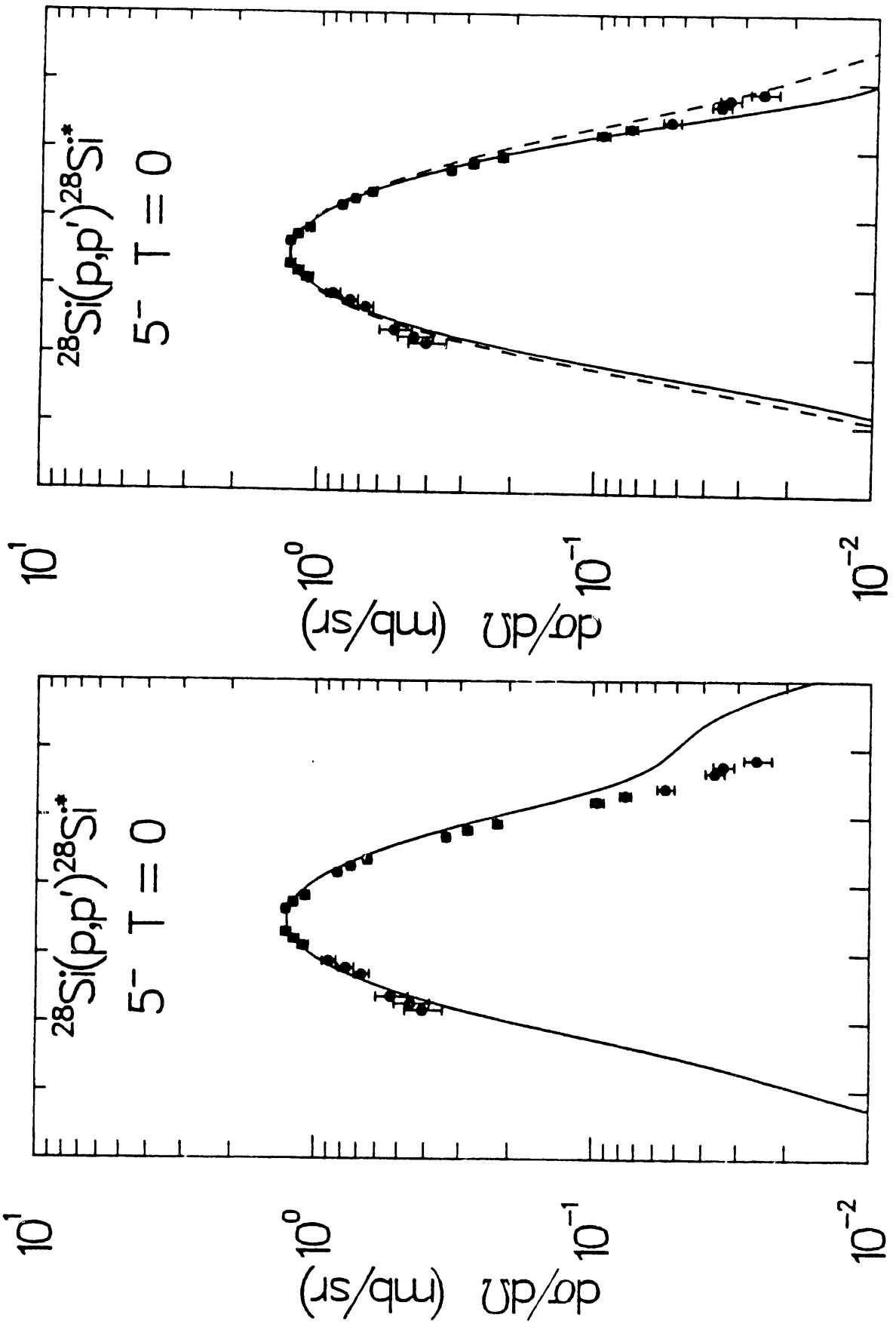

Figure 6

Figure 5

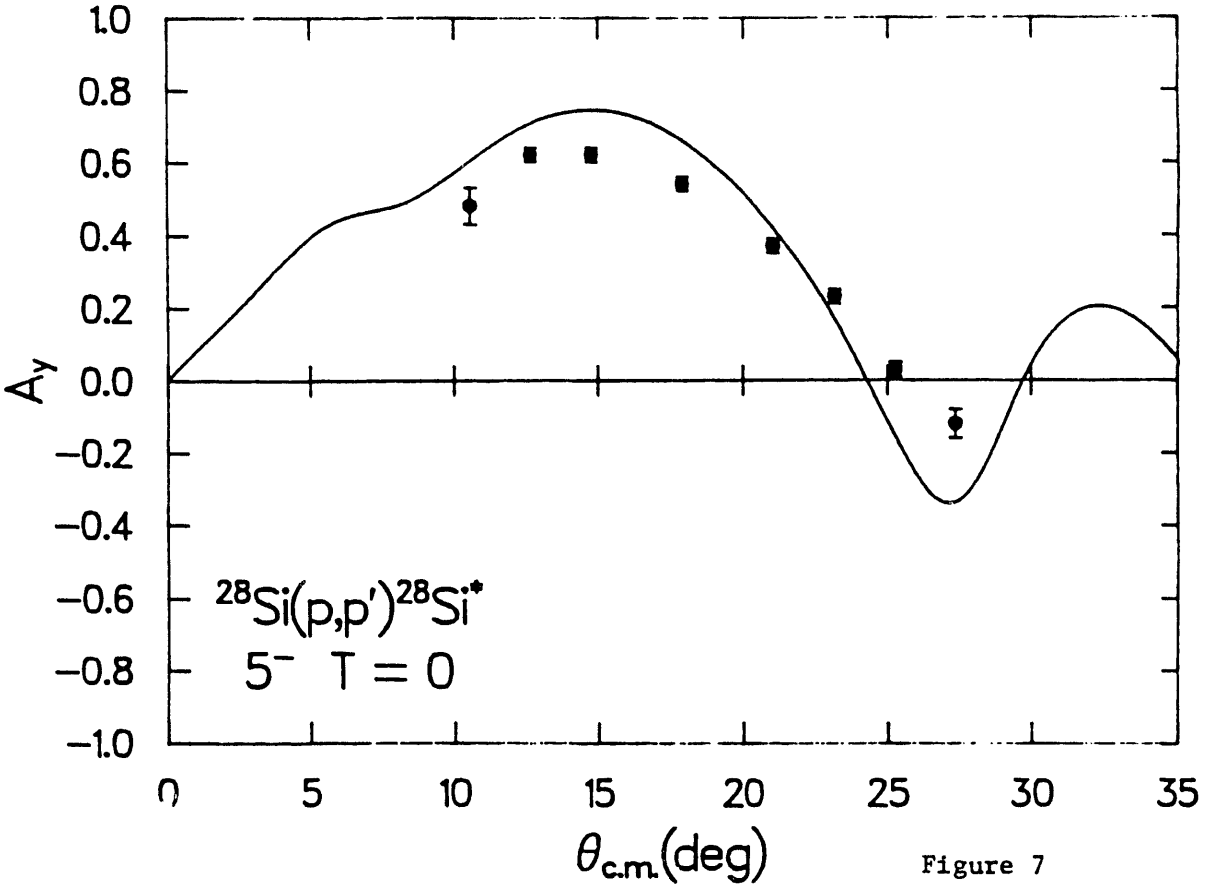

Figure 7

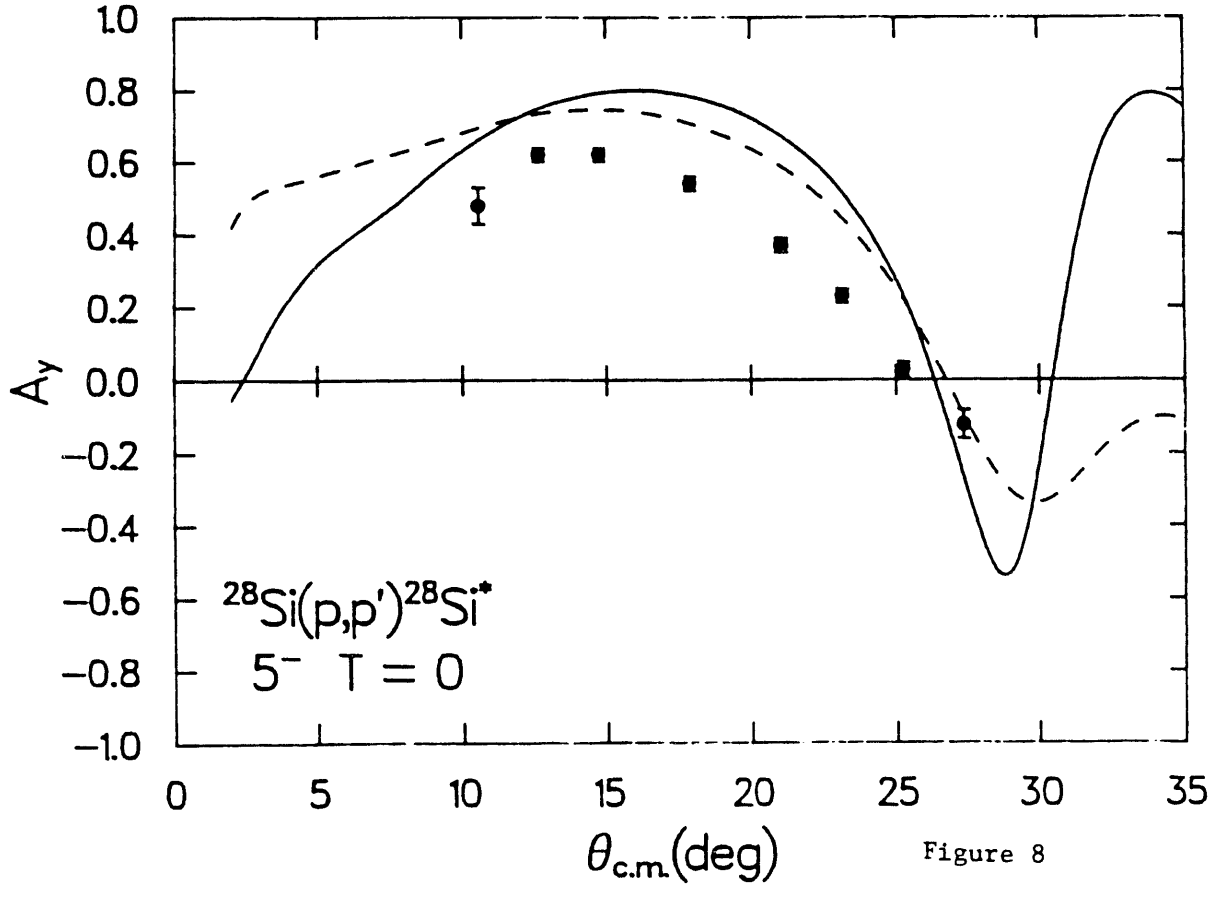

Figure 8

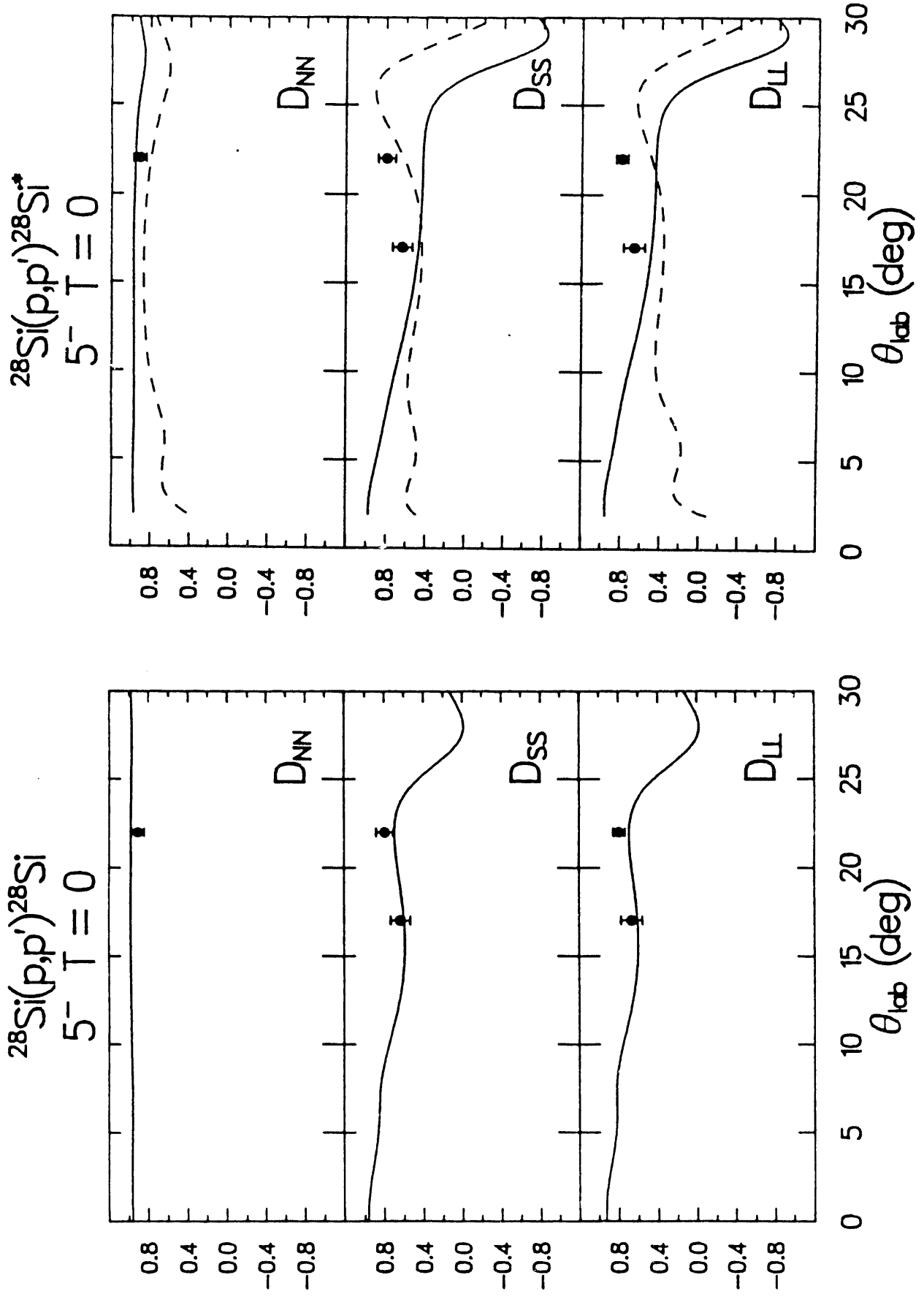

Figure 9

Figure 10

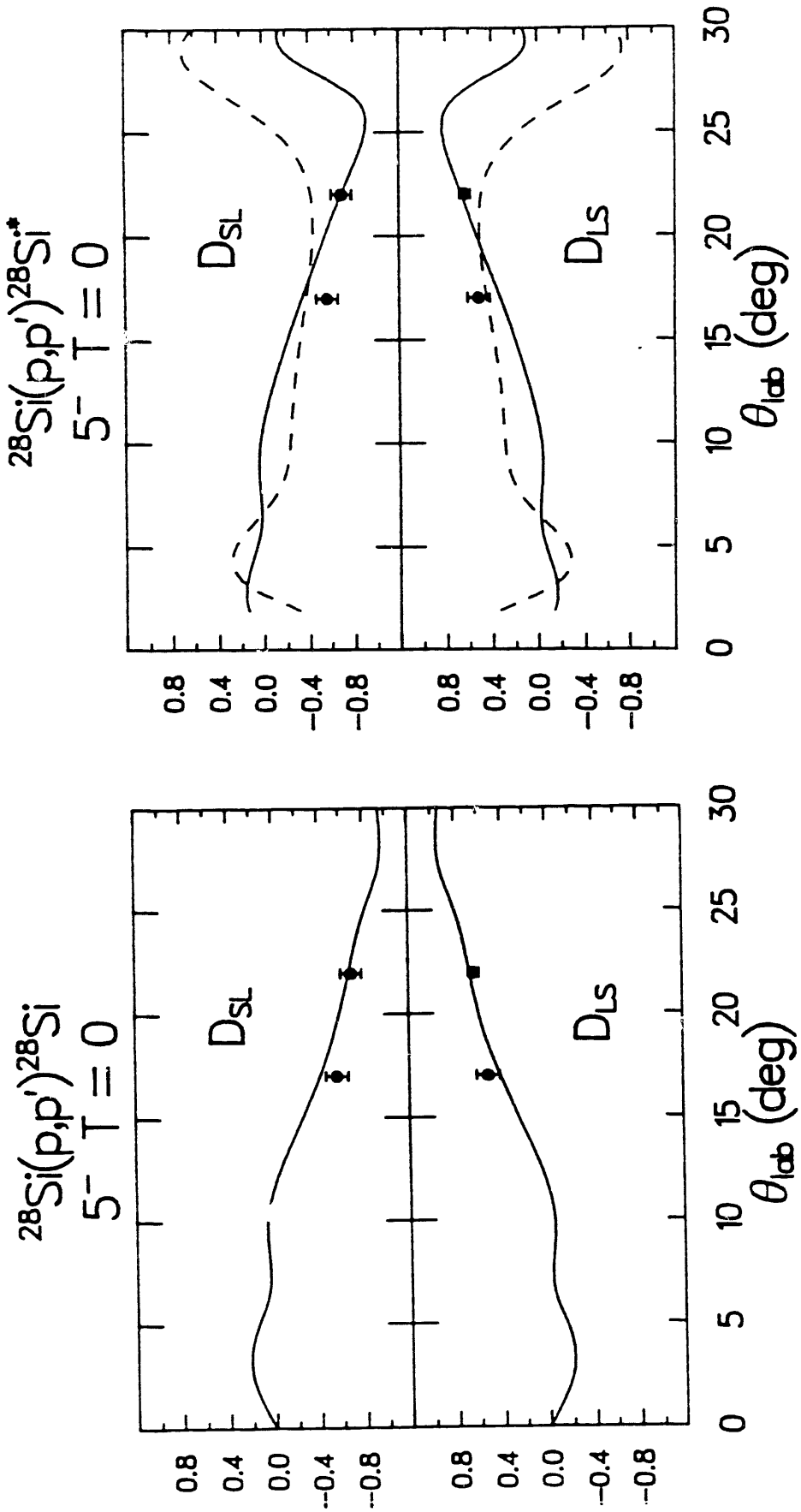

Figure 12

Figure 11

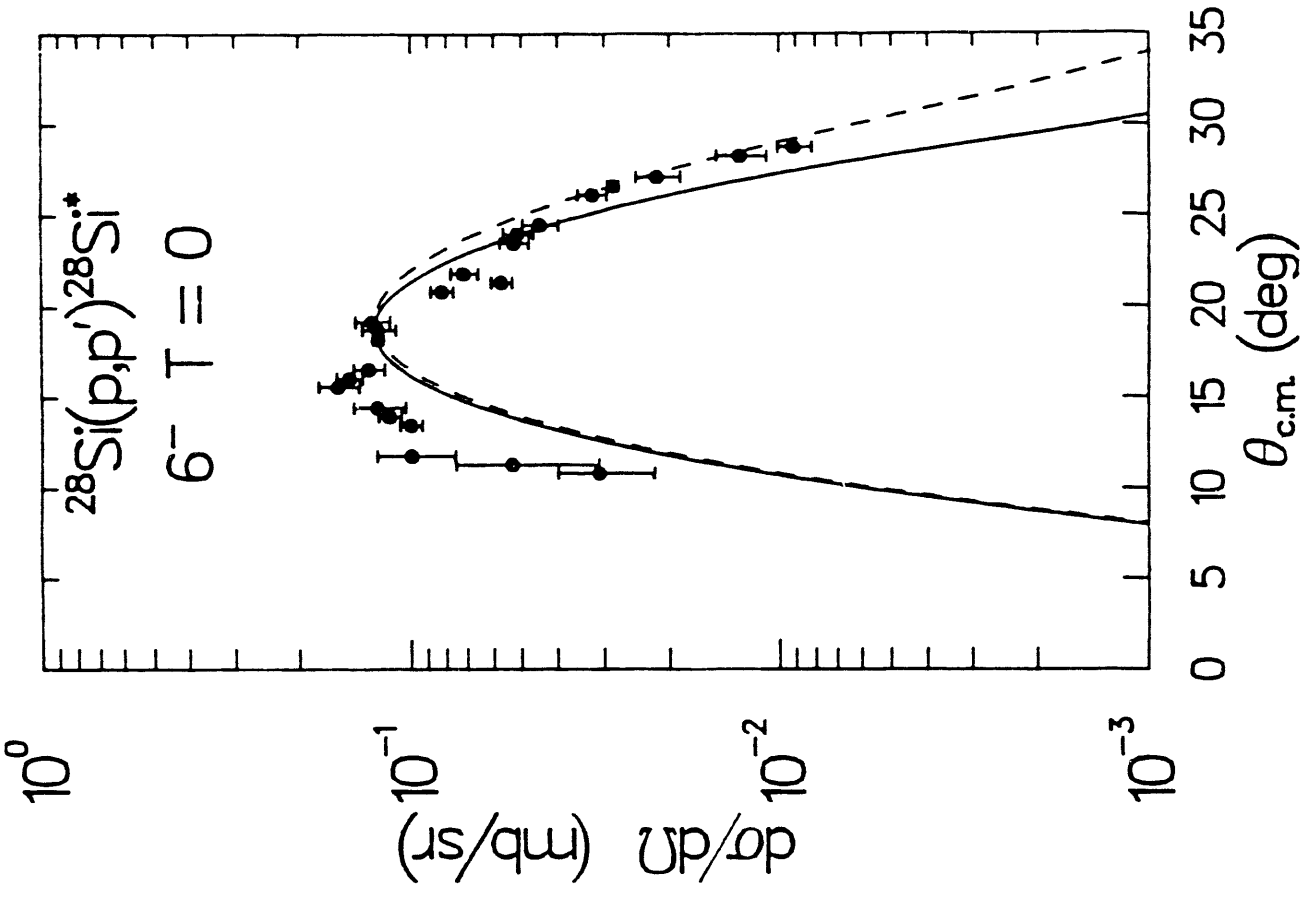

Figure 14

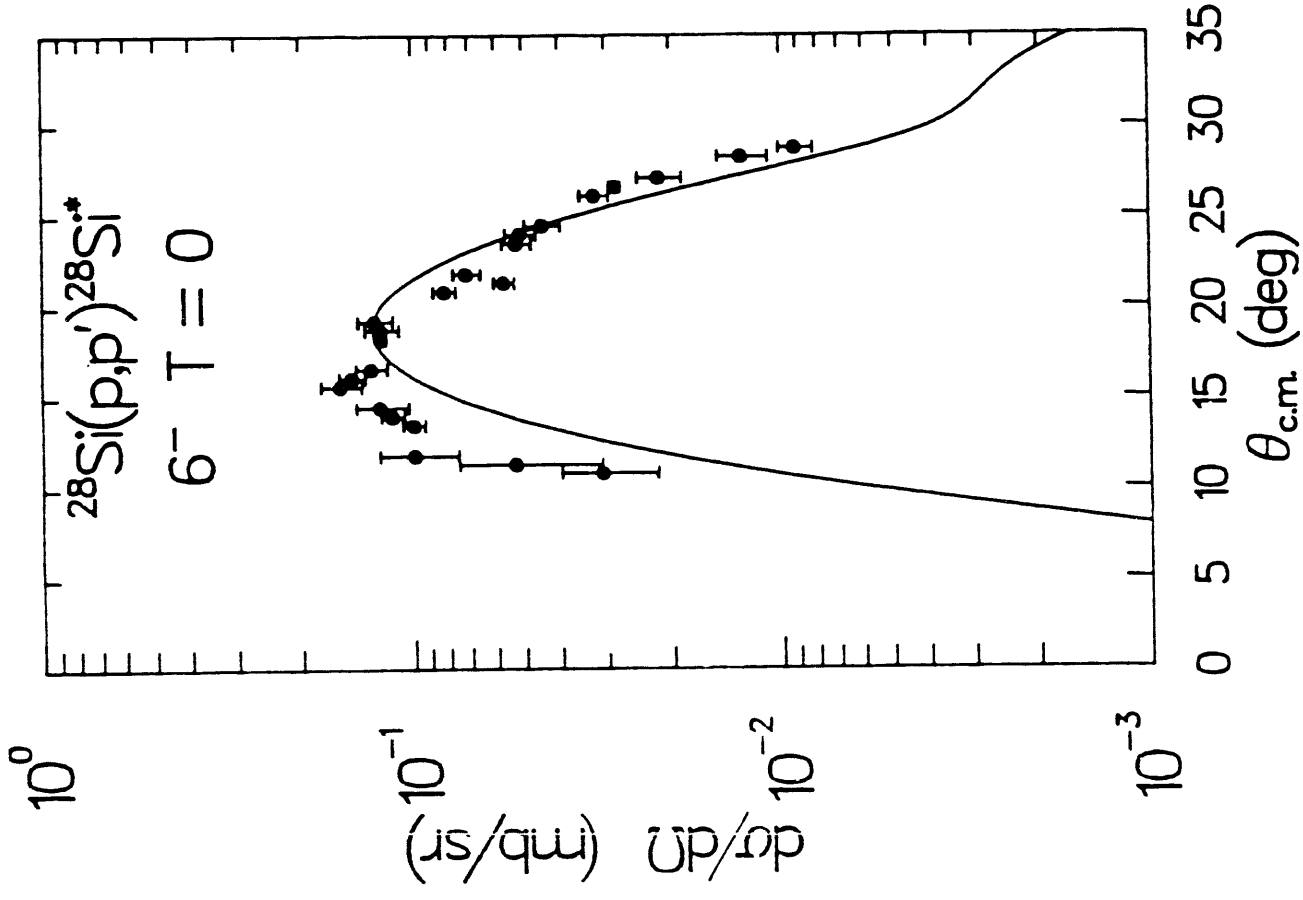

Figure 13

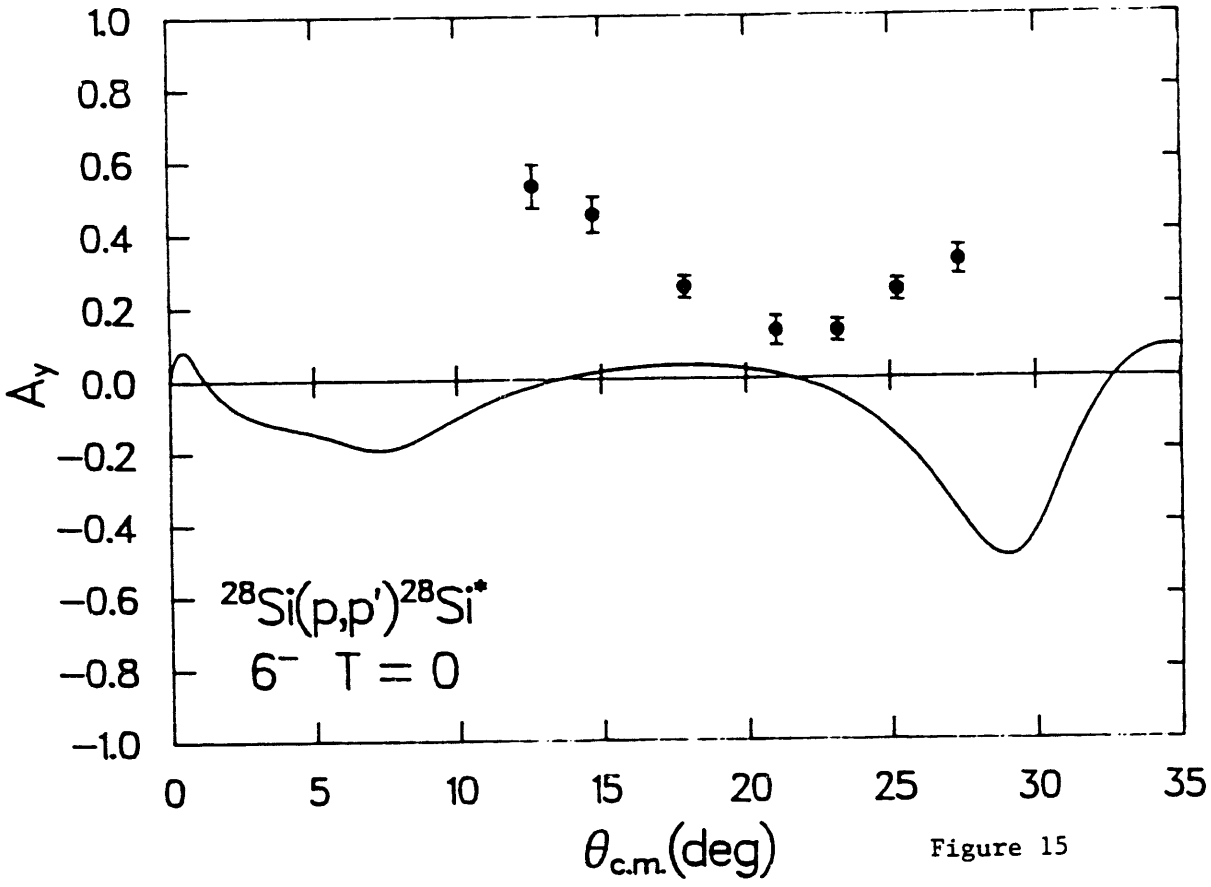

Figure 15

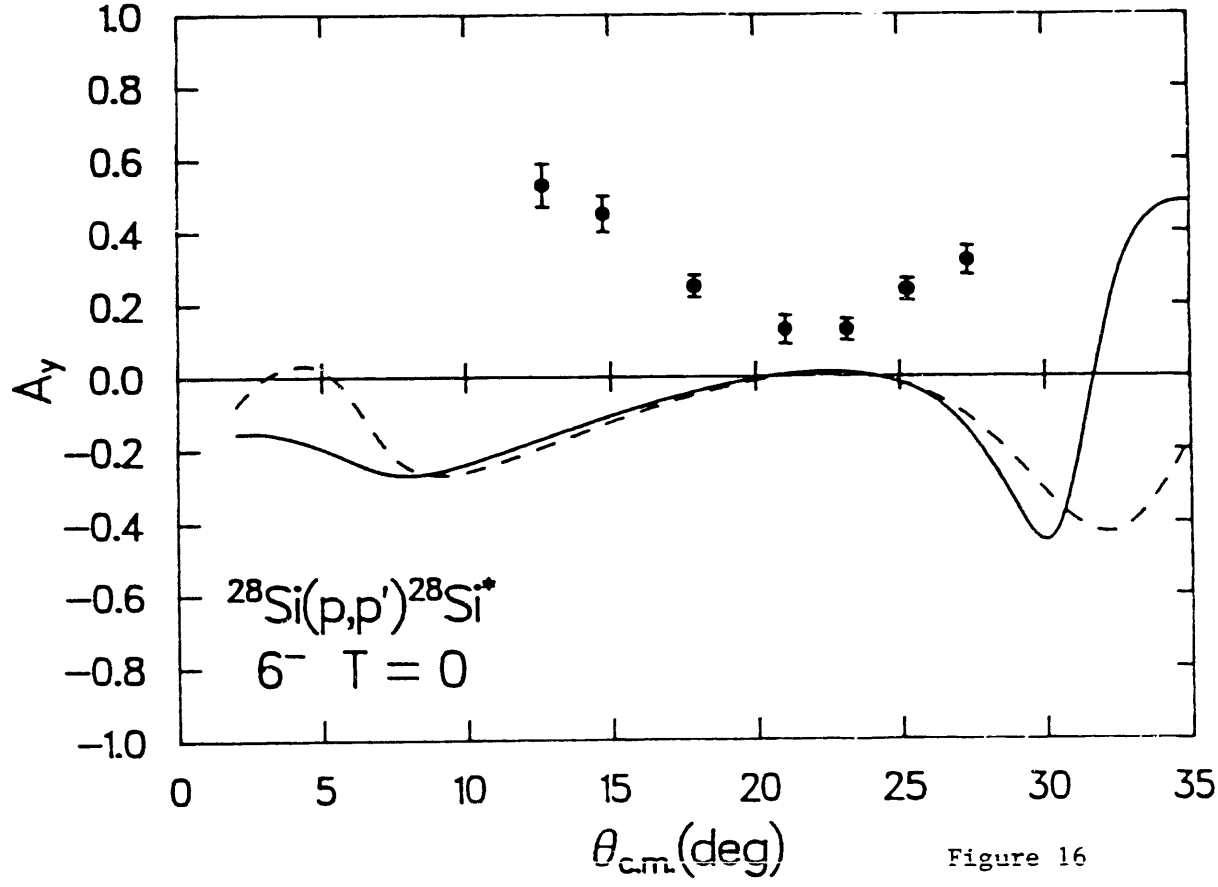

Figure 16

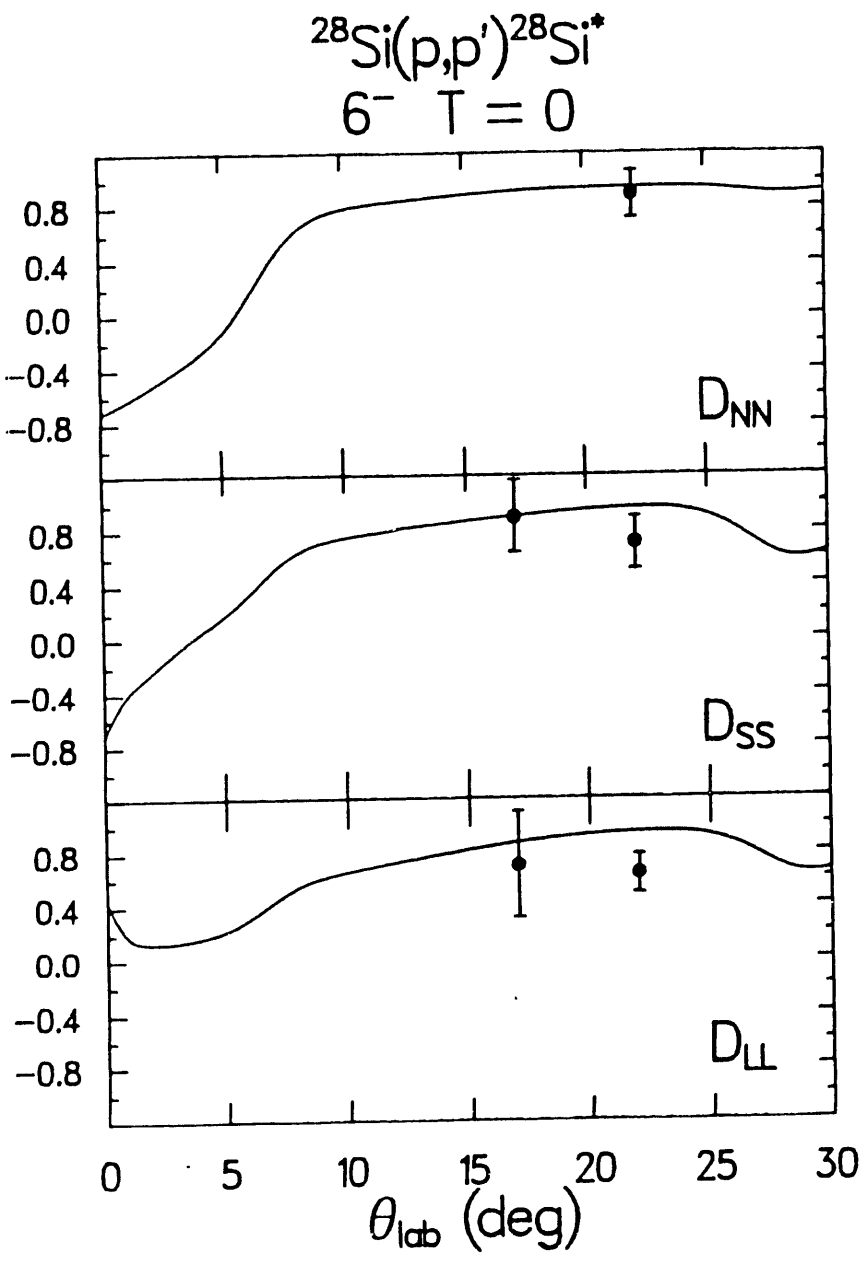

Figure 17

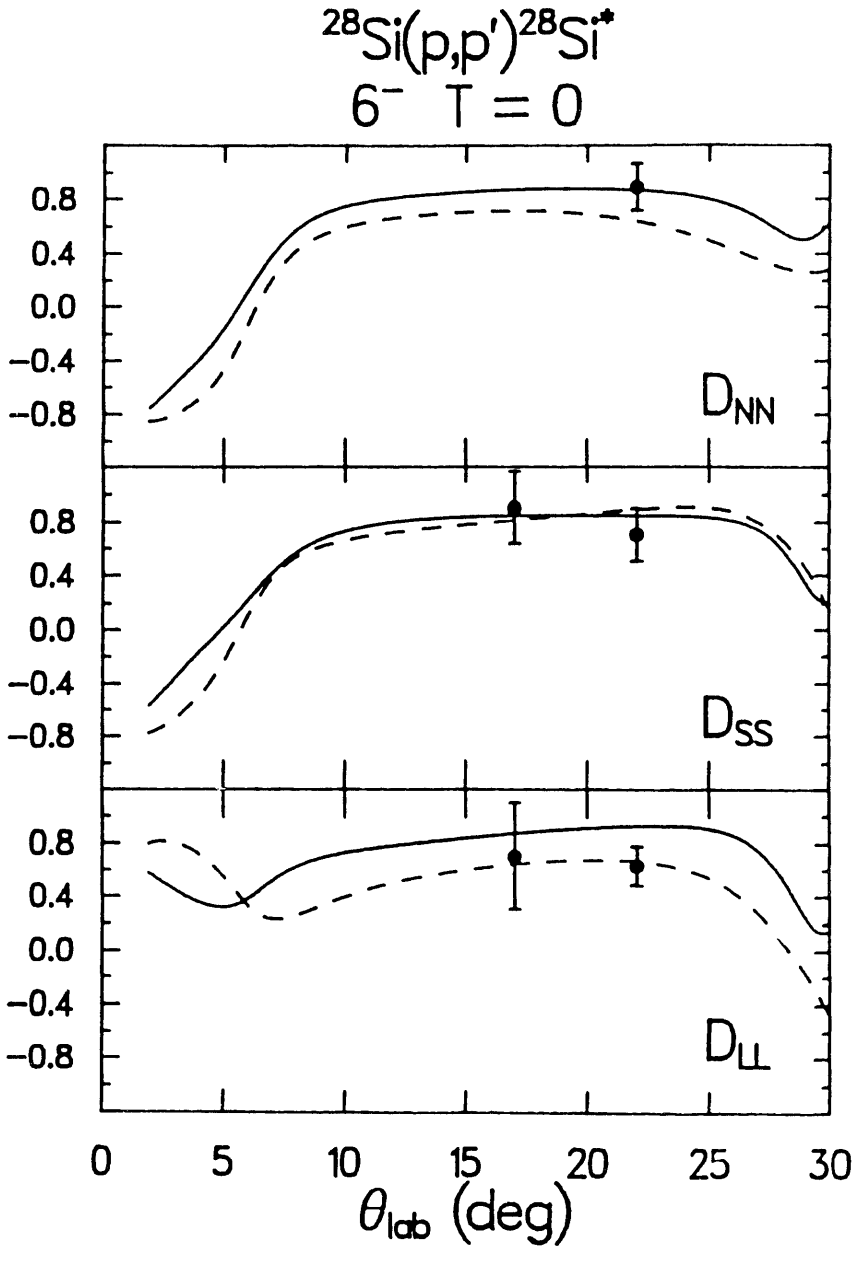

Figure 18

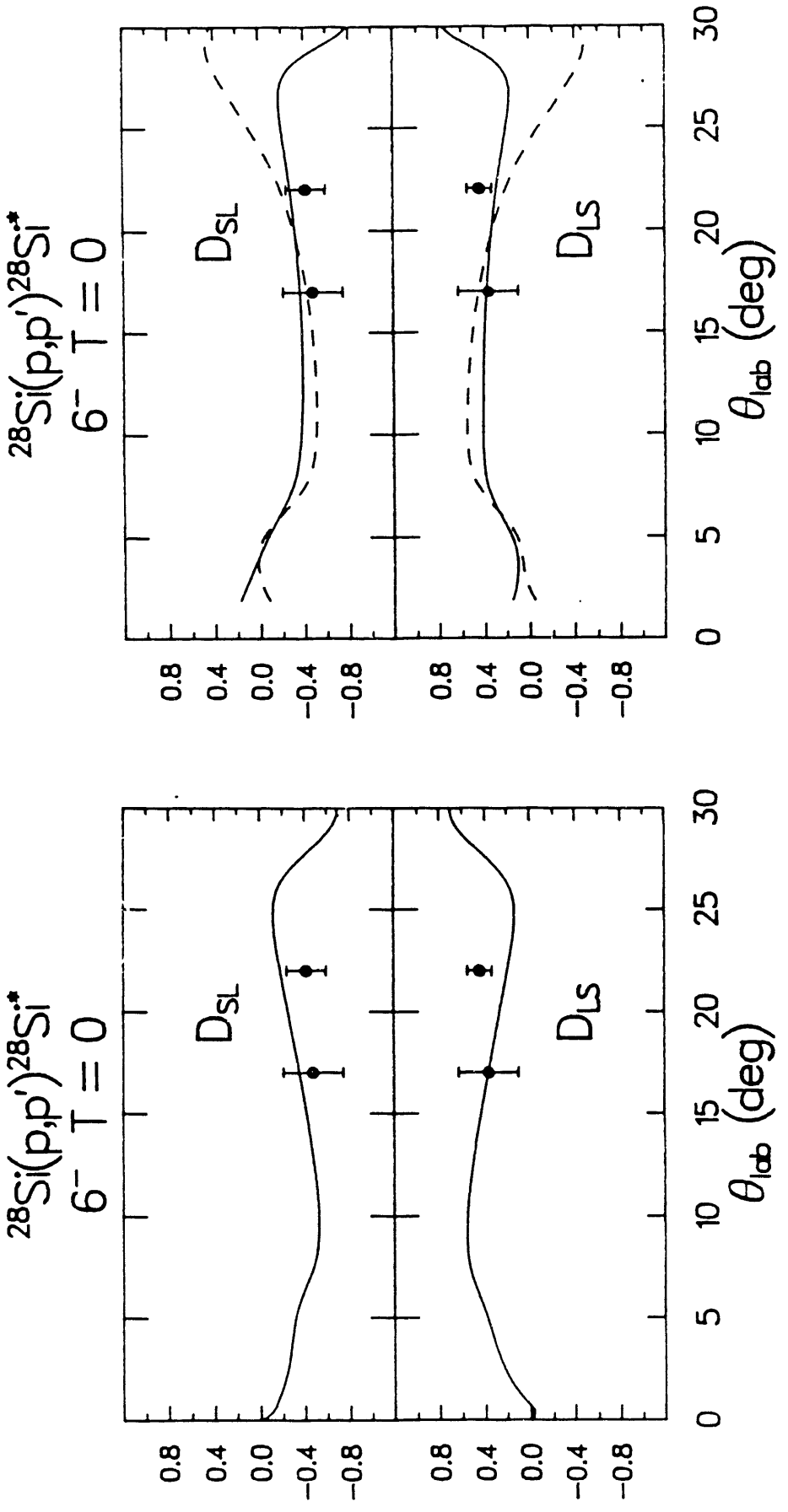

Figure 19

Figure 20

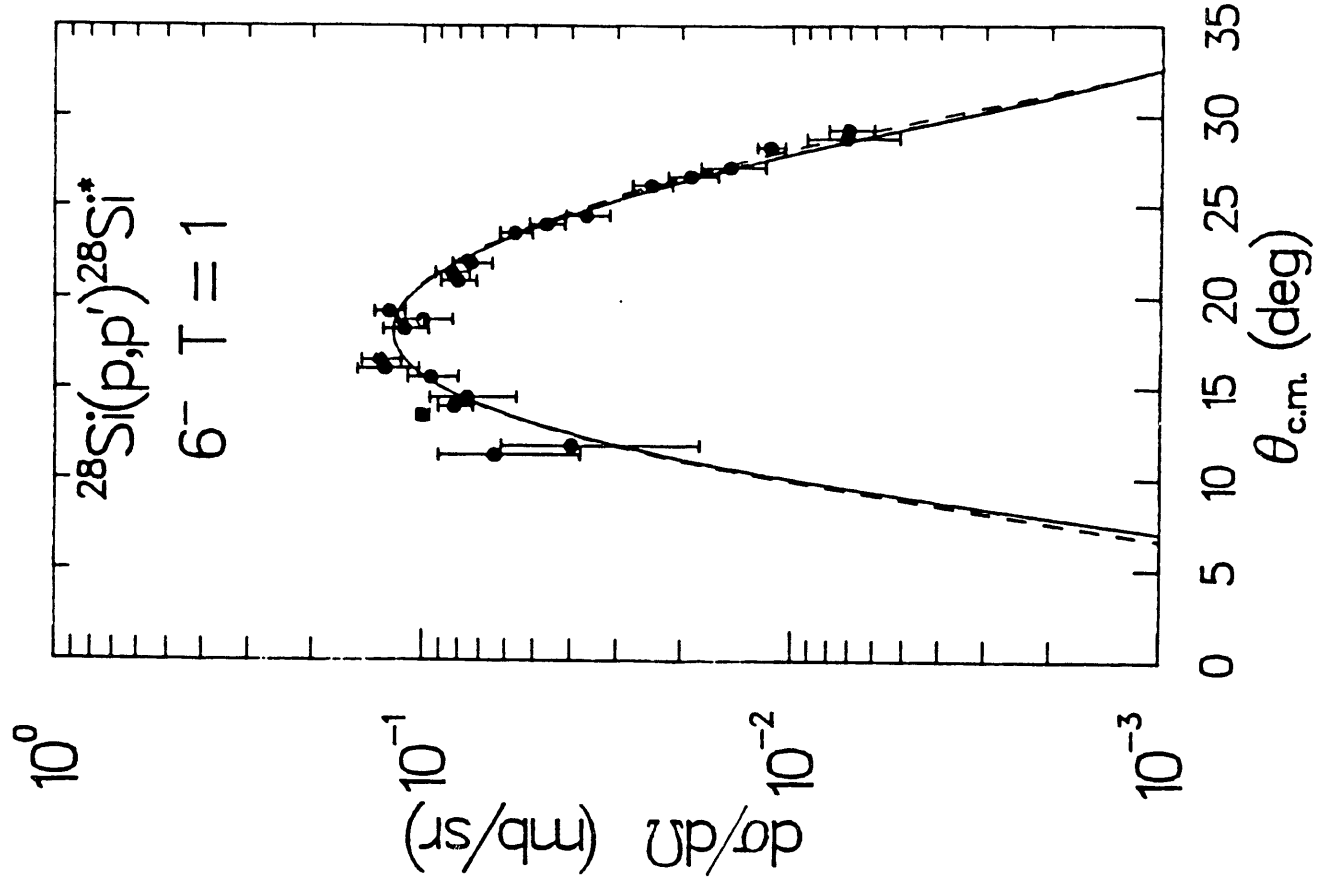

Figure 22

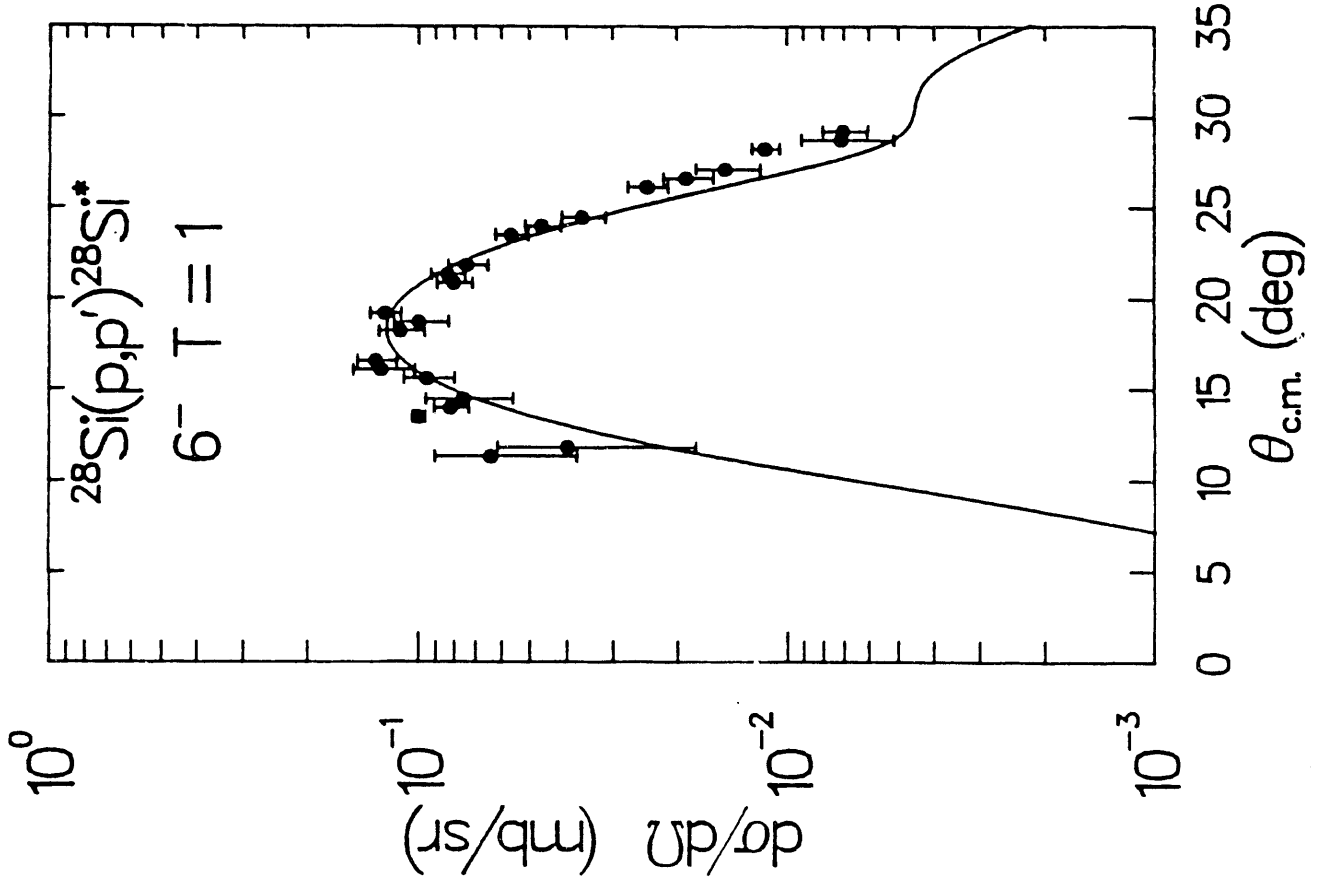

Figure 21

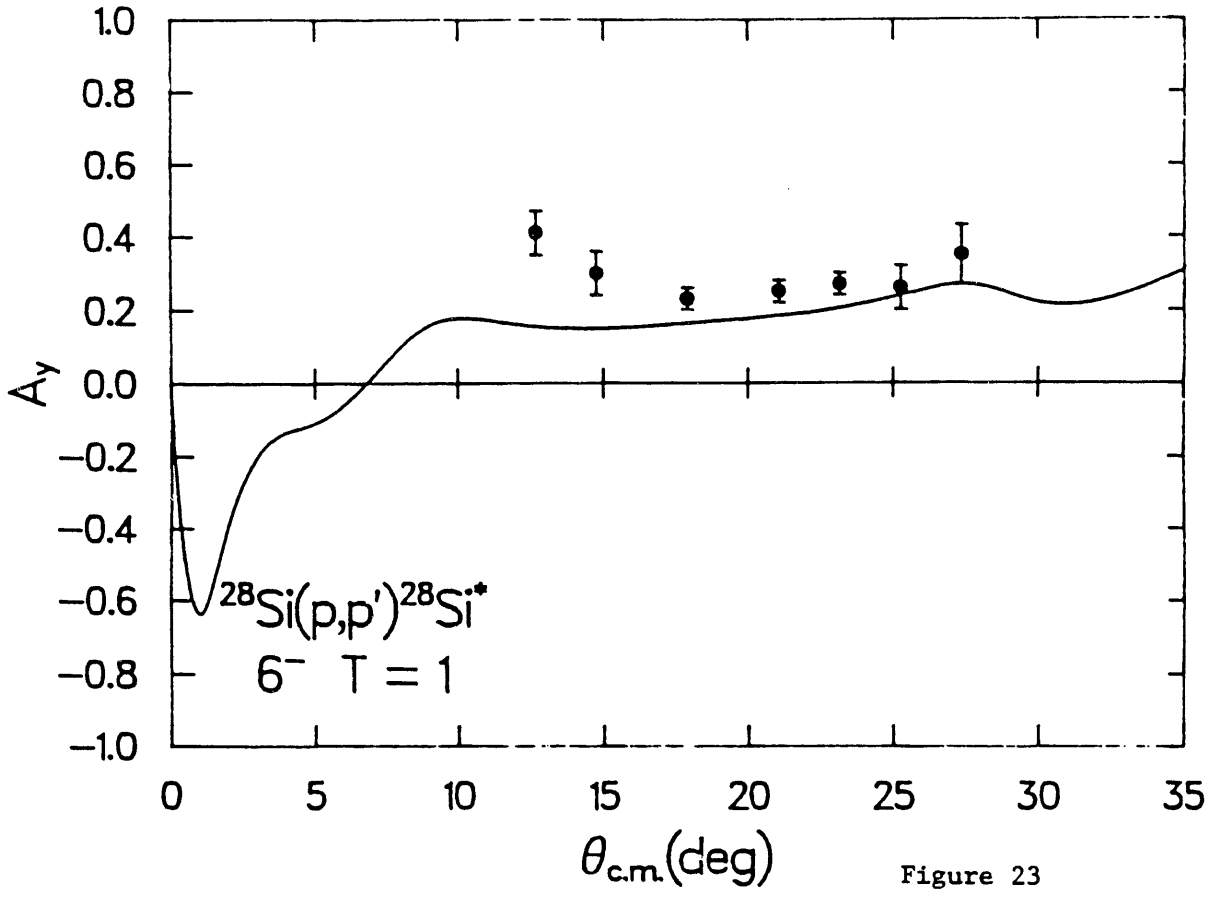

Figure 23

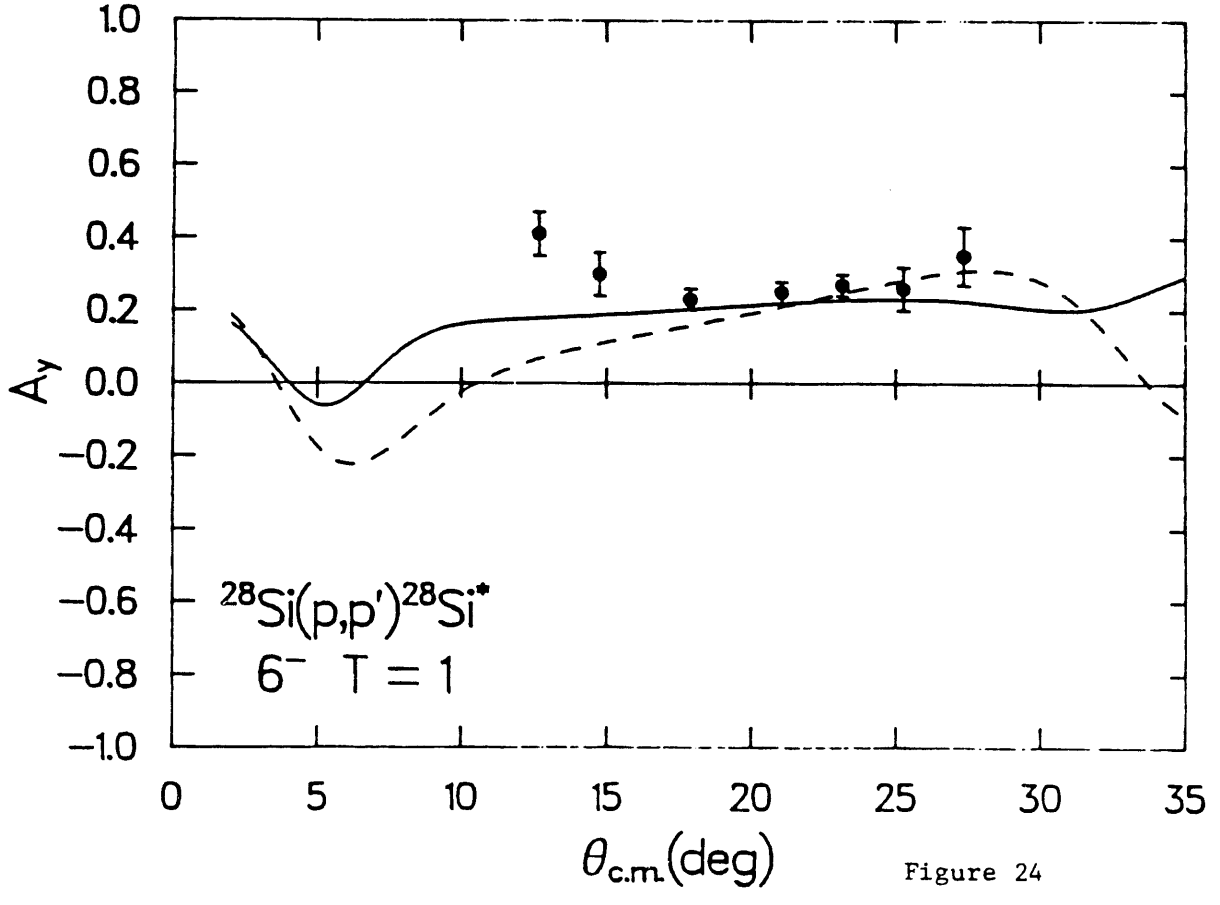

Figure 24

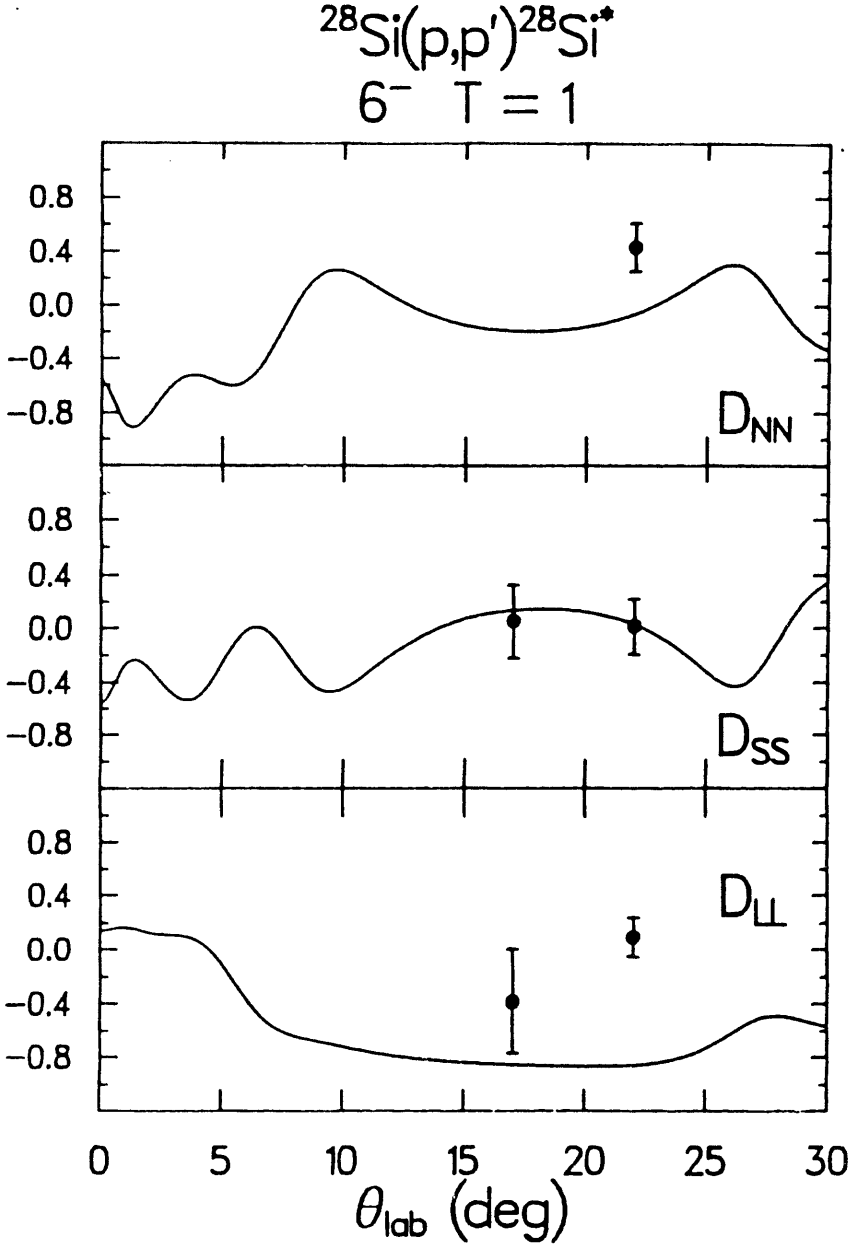

Figure 25

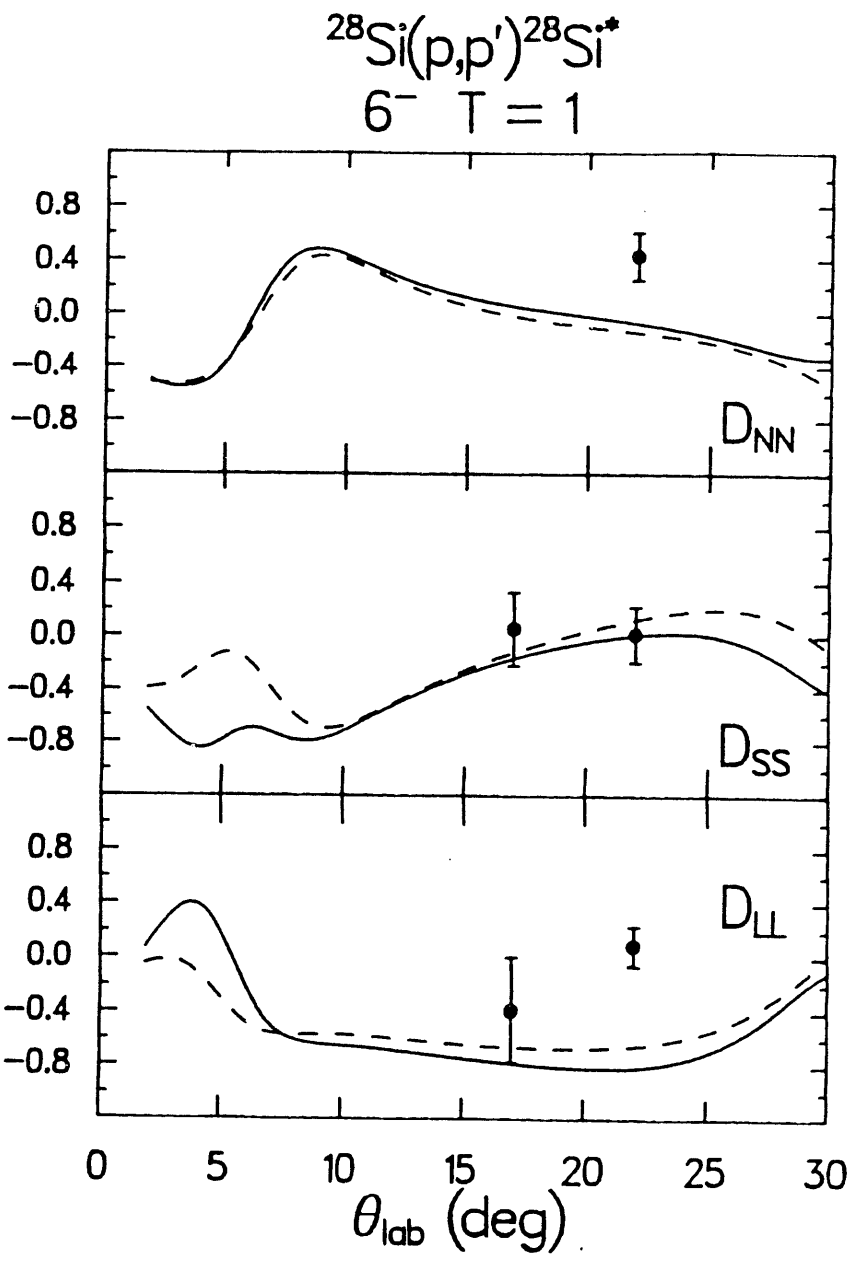

Figure 26

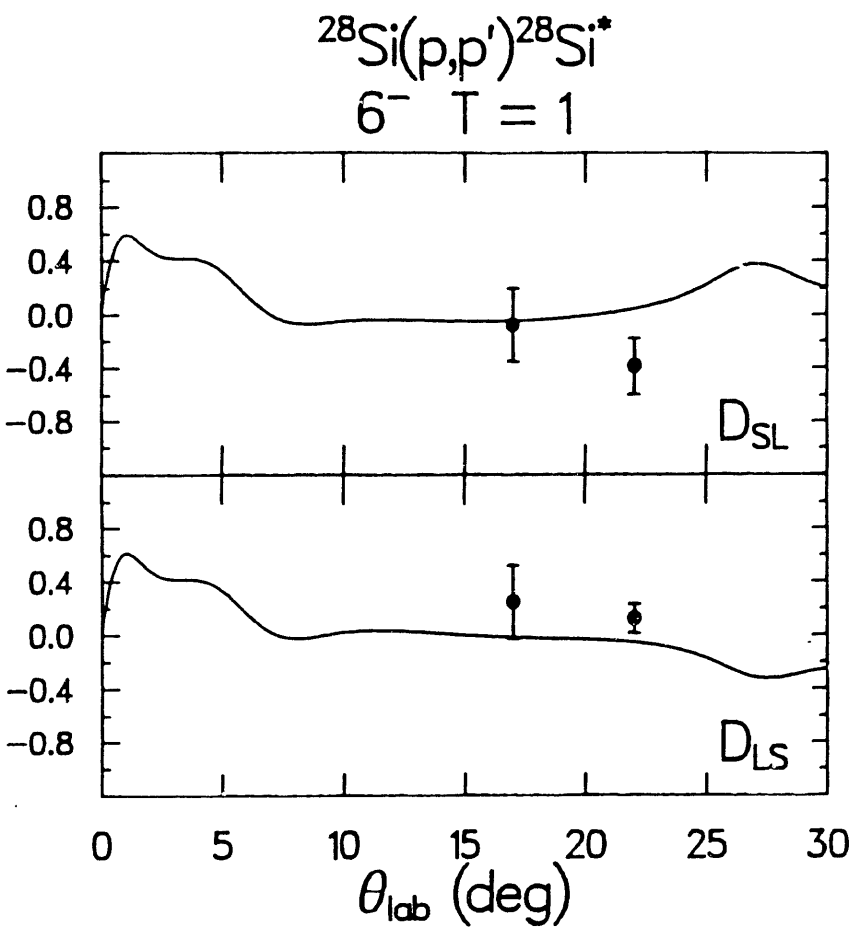

Figure 27

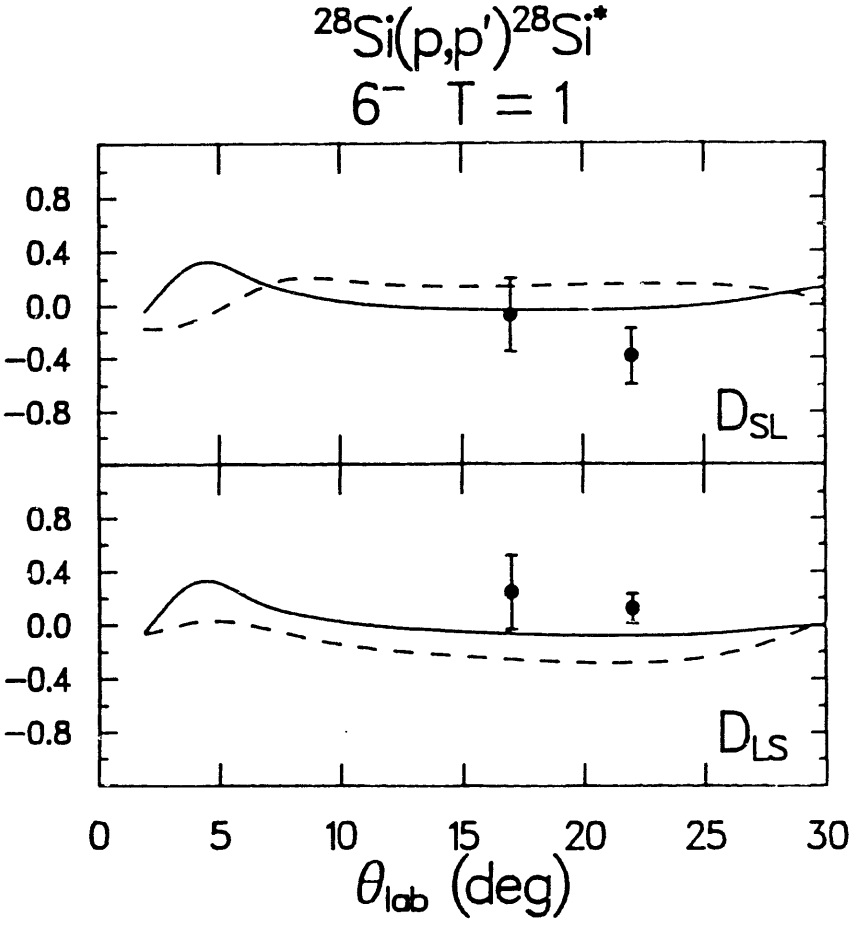

Figure 28

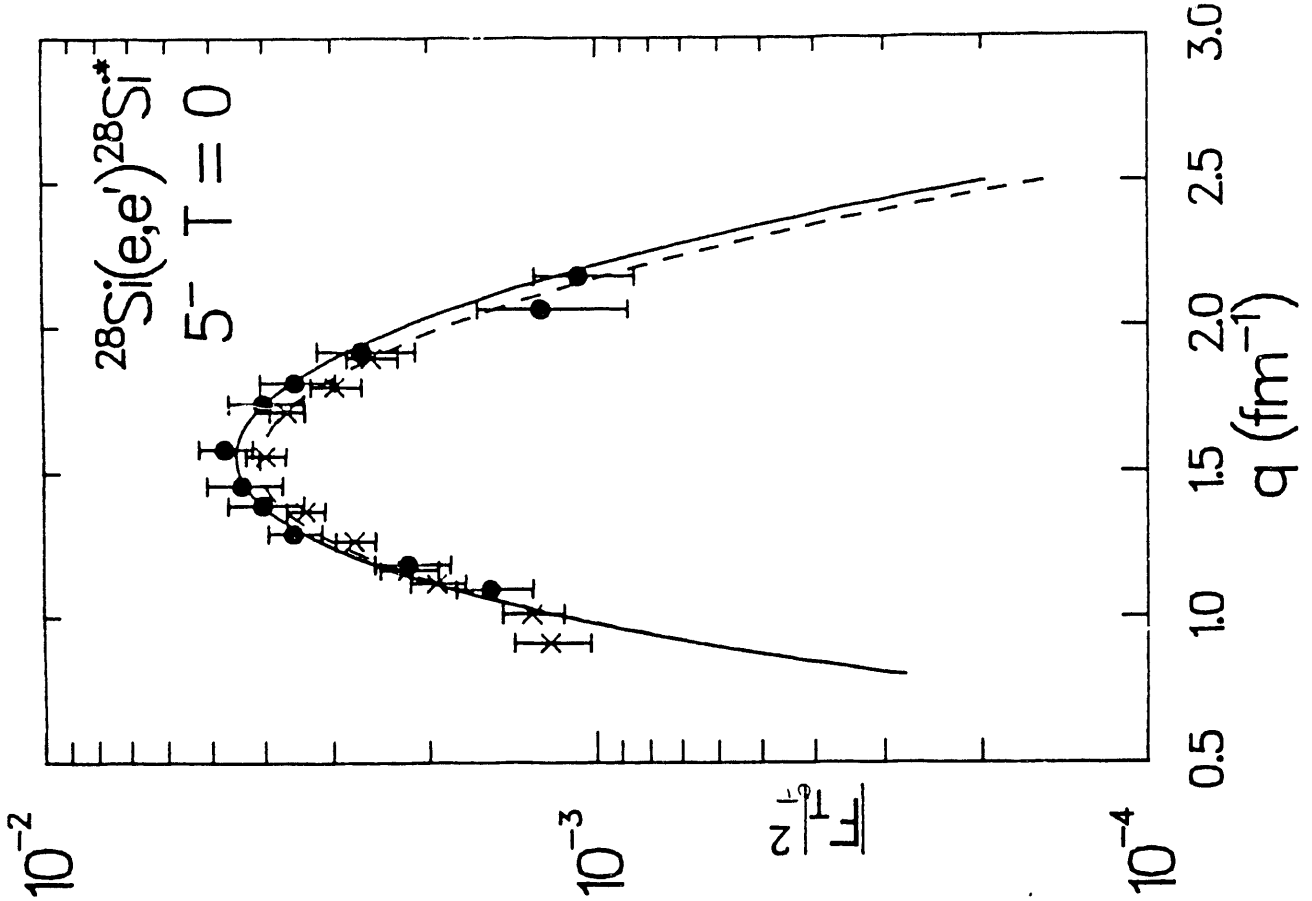

Figure 30

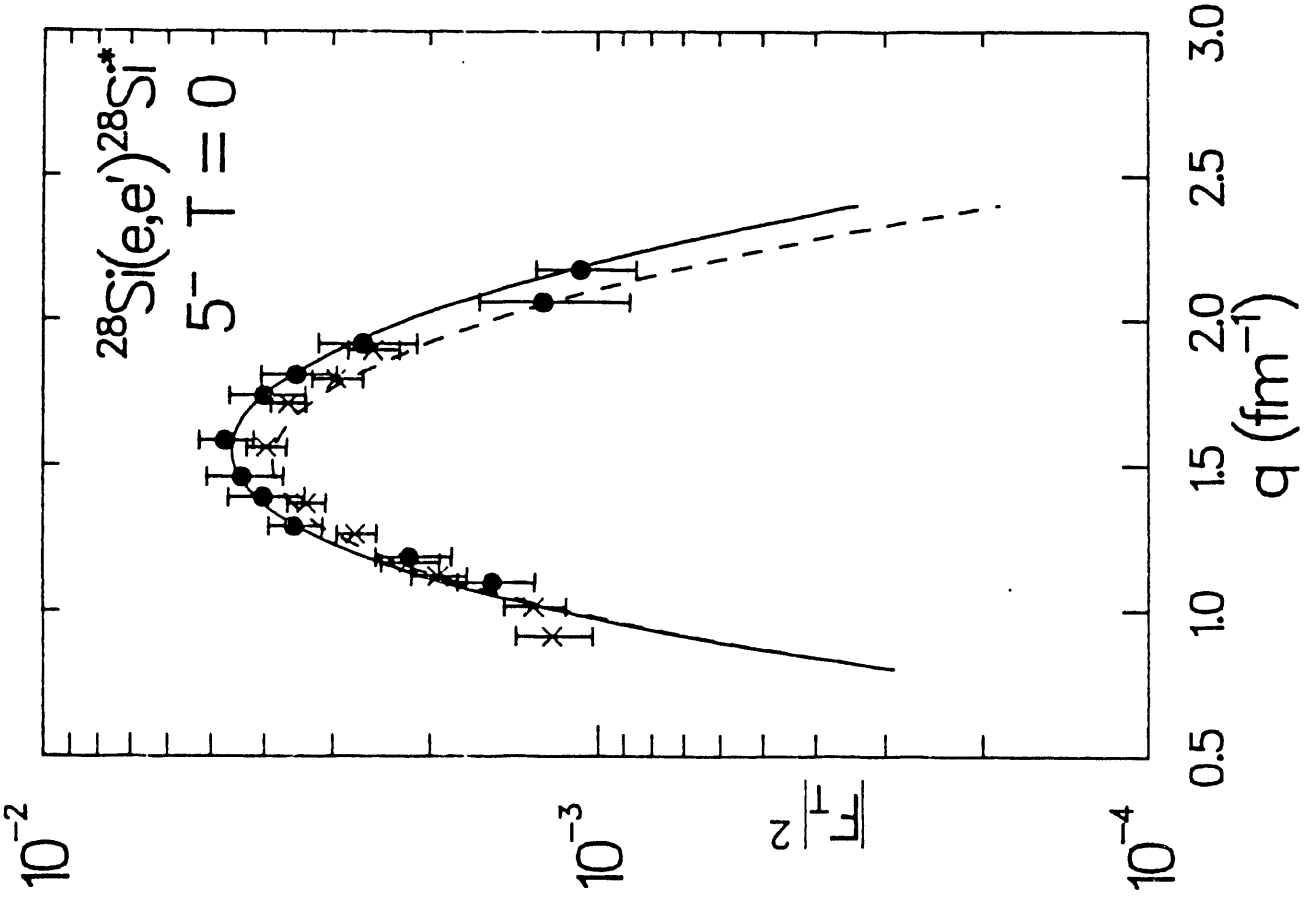

Figure 29

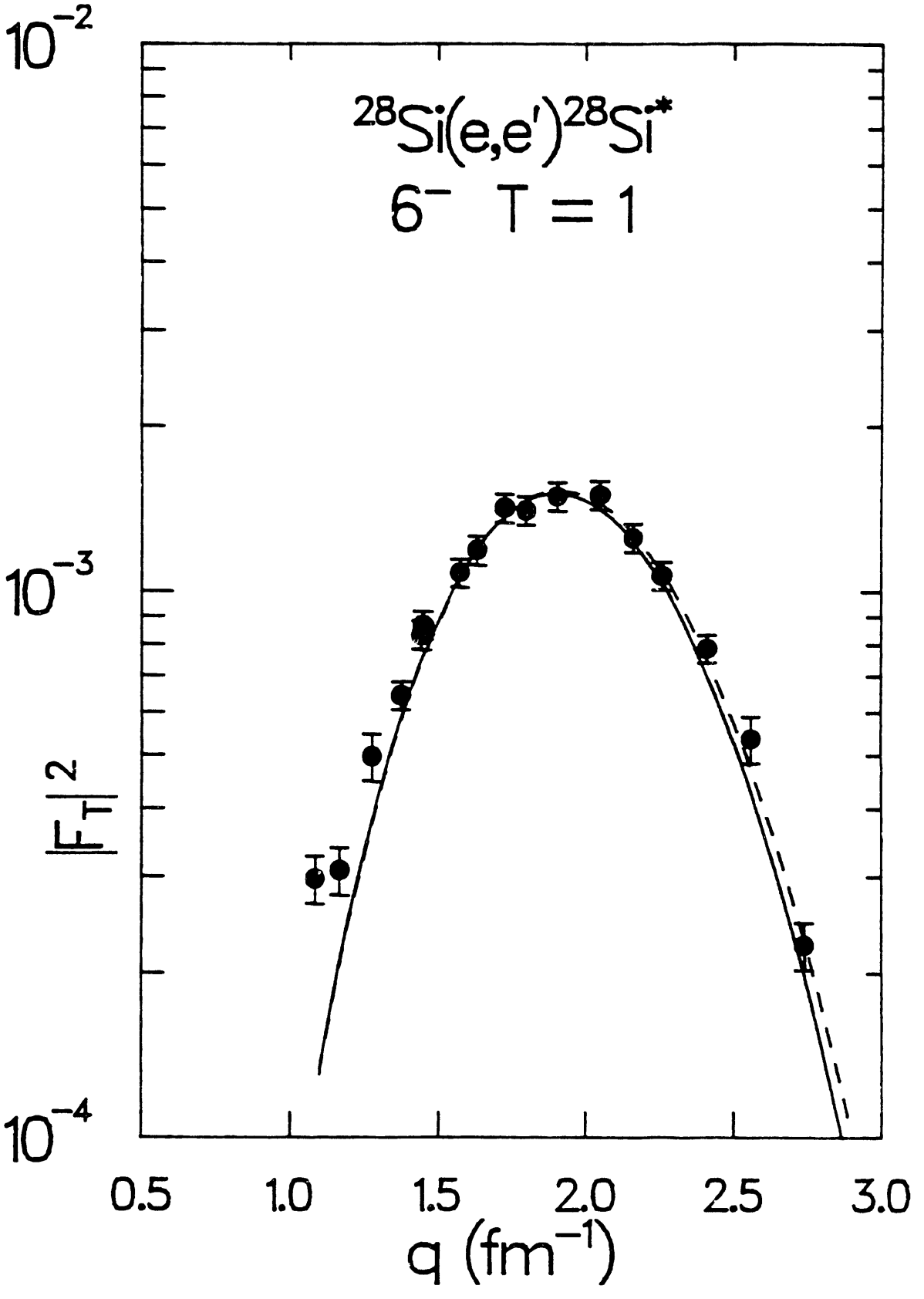

Figure 31

II.I. Strength of Tensor Force in Nuclei and Mixing of High Spin Stretched States in ^{208}Pb (with A. M. Lallena, Univ. of Granada, and G. E. Brown, SUNY, Analysis of data from E686).

It has been known for some time (empirically) that the residual tensor interaction, V_T, in the nuclear medium, needs to be reduced considerably from that given by $\pi + \rho$ meson exchange models.[1,2] There is also evidence that the isovector tensor force used in the impulse approximation for proton-nucleus inelastic scattering needs also to be reduced from the free N-N interaction (Refs. 3,4 and Sect. II.H. above). The long range attractive part of V_T comes from one π exchange, and the short range repulsive part mainly from one ρ exchange.

Recently A. M. Lallena[5] has explored the role of the $\pi + \rho$ exchange part of the residual particle-hole force in configuration mixing in the high spin unnatural parity states of ^{208}Pb. The states of interest here are the 12^-_1 (6.43 MeV) "neutron state" and the 12^-_2 (7.06 MeV) "proton" state. In the original analysis of electron scattering data[6] single neutron (12^-_1): $\nu(j_{15/2}, i^{-1}_{13/2})$ or. proton (12^-_2): $\pi(i_{13/2}, h^{-1}_{11/2})$, particle-hole configurations were assumed for each state. However, subsequent analysis of (p,p') data[7,8] using the same pure configurations, gave quenching factors, $Q = \sigma_{exp}/\sigma_{theo}$ in disagreement with those found for (e,e'), and thus incompatible with the pure configuration assumption. A solution was found,[8] using mixed configurations for the 12^- states, which was compatible with all of the data, giving similar quenching factors for (e,e') and (p,p') for each state but with different quenching factors for the 12^-_1 ($Q \simeq 0.76$) and the 12^-_2($Q \simeq 0.43$) states.

The original calculations of Lallena were done using the RPA with the Landau-Migdal zero range interaction (δ force) alone or with the δ plus the full $\pi + \rho$ force. In Lallena's original large basis RPA calculations[5] the dominant configurations contributing to the 12^- states are $\nu(j_{15/2}, i^{-1}_{13/2})$ and $\pi(i_{13/2}, i^{-1}_{11/2})$, with other configurations having X and Y amplitudes $\lesssim 0.04$. For the pure δ-force, Lallena finds for the 12^-_1 state, $X_\nu = 0.97$ and $X_\pi = 0.26$, and for the 12^-_2 state, $X_\nu = -0.26$ and $X_\pi = 0.96$ for the dominant neutron (ν) and proton (π) configurations. (The Y amplitudes are small). For the δ-force plus the full $\pi + \rho$ exchange force he finds for the 12^-_1, $X_\nu = -0.98$ and $X_\pi = 0.22$; and for the 12^-_2, $X_\nu = 0.22$ and $X_\pi = 0.97$.

We had previously analyzed both the (e,e') data and the (p,p') cross sections at $T_p = 318$ MeV (from our E686) for the two 12^- states in terms of a simple two state model:

$$|12^-_1> = (1-a^2)^{1/2} |\nu(j_{15/2}, i^{-1}_{13/2})> + a\ |\pi(i_{13/2}, h^{-1}_{11/2})>$$

$$|12^-_2> = -\ a\ |\nu(j_{15/2}, i^{-1}_{13/2})> + (1-a^2)^{1/2}\ |\pi(i_{13/2}, h^{-1}_{11/2})> \qquad (1)$$

Our conclusion was that a simultaneous fit to the (p,p') and (e,e') could be obtained with $a \simeq 0.07$ with similar quenching factors ($Q = \sigma_{exp}/\sigma_{theo}$) for electrons and protons ($Q_1 \simeq 0.76$, $Q_2 \simeq 0.43$ for the 12^-_1 and 12^-_2 states) as shown in Fig. 1. In the two state model, the mixing parameter, a, is roughly equivalent to $X_\pi(12^-_1)$ or $-X_\nu\ (12^-_2)$ of the full RPA calculation. From the X values above it is seen that there is too much mixing in the δ-force only calculation, and similar mixing but with the wrong sign for the full $\delta + \pi + \rho$ force. Thus a solution consistent with

experiment might be found for some intermediate case with partial quenching of the $\pi + \rho$ force. Considerations based on the reduction of effective nucleon and meson masses in medium[4] indicate that the (attractive) π exchange part of the force is only slightly reduced, but that the (repulsive) ρ force should be enhanced by a factor of ~ 1.5-2, giving a reduction of the net tensor force for $r \gtrsim 0.8$ fm, the region most relevant for nuclear structure.

In collaboration with Lallena we are now exploring empirically the effect of a modification of the residual tensor interaction on the structure of the 12^- states and the consequences for electron and proton inelastic scattering. The residual interaction used by Lallena is:

$$V_R = V_M + V_\pi + V_\rho$$

$$= V_M + V_\pi^{\sigma\tau} + V_\pi^T + V_\rho^{\sigma\tau} + V_\rho^T \qquad (2)$$

where

$$V_M = C_0 \left[f_0 + f_0' \vec{\tau}_1 \cdot \vec{\tau}_2 + g_0 \vec{\sigma}_1 \cdot \vec{\sigma}_2 + g_0' (\sigma_1 \cdot \sigma_2)(\tau_1 \cdot \tau_2)\right] \delta(\vec{r}_1 - \vec{r}_2) \qquad (3)$$

is the Migdal force, and

$$V_\pi^{\sigma\tau} = \frac{1}{3} f_\pi^2 m_\pi \frac{e^{-m_\pi r}}{m_\pi r} (\vec{\sigma}_1 \cdot \vec{\sigma}_2) (\vec{\tau}_1 \cdot \vec{\tau}_2)$$

$$V_\pi^T = \frac{1}{3} f_\pi^2 m_\pi \left(1 + \frac{3}{m_\pi r} + \frac{3}{(m_\pi r)^2}\right) \frac{e^{-m_\pi r}}{m_\pi r} \vec{\tau}_1 \cdot \vec{\tau}_2 S_{12}$$

$$V_\rho^{\sigma\tau} = \frac{2}{3} f_\rho^2 m_\rho \frac{e^{-m_\rho r}}{m_\rho r} (\vec{\sigma}_1 \cdot \vec{\sigma}_2) (\vec{\tau}_1 \cdot \vec{\tau}_2)$$

$$V_\rho^T = -\frac{1}{3} f_\rho^2 m_\rho \left(1 + \frac{3}{m_\pi r} + \frac{3}{(m_\pi r)^2}\right) \frac{e^{-m_\pi r}}{m_\pi r} \vec{\tau}_1 \cdot \vec{\tau}_2 S_{12}$$

$$S_{12} = 3(\vec{\sigma}_1 \cdot r)(\vec{\sigma}_2 \cdot r) - \vec{\sigma}_1 \cdot \vec{\sigma}_2 \qquad (4)$$

where

$$C_0 = \frac{\hbar^2 \pi^2}{m_N k_F} = 302 \text{ MeV fm}^3 \text{ (density of states)}$$

Three prescriptions were then tried for modifying the π and ρ parts of V_R by introducing parameters α, β and ϵ:

a) $V_R = V_M + \alpha(V_\pi^{\sigma\tau} + V_\pi^T + V_\rho^{\sigma\tau} + V_\rho^T)$

b) $V_R = V_M + V_\pi^{\sigma\tau} + V_\rho^{\sigma\tau} + \beta\ (V_\pi^T + V_\rho^T)$

c) $V_R = V_M + V_\pi^{\sigma\tau} + V_\pi^T + \epsilon\ (V_\rho^{\sigma\tau} + V_\rho^T)$ (5)

The last, c) being the prescription suggested by Brown and Rho[4].

An approximate picture of the effects of varying the π and ρ strength parameters α, β and ϵ can be obtained by plotting the overall RPA amplitudes, $A = X + (-1)^J Y$ for the two dominant configurations, as in Figs. 2-4. In these calculations, as the strength parameters (α,β,ϵ) are varied, both g_0 and g_0' of the Migdal force were adjusted to reproduce the energies of the 1^+ states (E_x = 5.85, 7.30 MeV). From the figures it can be seen that possible solutions ($A_\pi \simeq a \sim 0.05 - 0.1$, $A_\nu \sim 1$ for the 12_1^-) exist for $\alpha \sim 0.5 - 0.6$, or $\beta \sim 0.0 - 0.5$ but no solutions are found for ϵ in the range suggested by Brown and Rho[5] ($\epsilon \sim 1.5 - 2$).

However, the estimates of mixing from a comparison of (e,e') and (p,p') data were obtained from the two-component model (Eq. 1). For more quantitive results we need to reanalyze the (e,e') and (p,p') data using the full theoretical RPA wave functions (~ 75 -100 components). These calculations are now in progress. Preliminary indications are that the inclusion of the smaller RPA components will not qualitatively change the conclusions from the two-component model.

References

1. See for example: K. Nakayama, Phys. Lett. 165B, 239 (1985); S. Drozdz, J. L. Tain and J. Wambach, Phys. Rev. C34, 345 (1986); J. L. Tain, et al., Phys. Rev. C35, 1288 (1987); A. Abbas, J. Phys. G: Nucl. Part. Phys. 15, 793 (1989); G. E. Brown and M. Rho, Ref. 4 below.
2. S. Drożdż, et al., and J. L. Tain, et al., references above.
3. L. B. Rees, et al., Phys. Rev. C34, 627 (1986).
4. G. E. Brown and M. Rho, Phys. Lett. B237, 3 (1990).

5. A. M. Lallena, Nucl. Phys. A489, 70 (1988) and private communication.

6. J. Lichtenstadt, et al., Phys. Rev. Lett. 40, 1127 (1978); Phys. Rev. C20, 497 (1979); Phys. Rev. Lett. 44, 858 (1980) and J. Lichtenstadt, Ph.D. thesis, M.I.T., 1980 (unpublished).

7. A. D. Bacher, et al., Phys. Lett. 97B, 58 (1980); G. S. Adams, et al., ibid, 91B, 23 (1980).

8. D. Cook, et al., Phys. Rev. C35, 456 (1987).

Figure Captions

Fig. 1: Proton and electron quenching factors (Q) vs mixing parameter, a, in the empirical two-component model (Eq. 1) for the 12^- states of ^{208}Pb (Ref. 8). The dashed curves show estimates of modification of Q_e if meson exchange contributions were to be included in σ_{theo}.

Fig. 2: Overall RPA Amplitudes $A = X + (-1)^J Y$ for the dominant admixed configurations: A_π for the 12^-_1 with $A_\nu > 0$ (dots), and $-A_\nu$ for the 12^-_2, with $A_\pi > 0$ (crosses). vs the reduction parameter α for the full $\pi + \rho$ interaction (See Eq. 5). These A are approximately equivalent to the mixing parameter, a, for the two-state model defined by Eq. 1 of the text. The shaded area indicates the approximate range of values compatible with the (e,e') and (p,p') cross section data (see Ref. 8).

Fig. 3: Same as Fig. 1 but for the reduction parameter, β, applied to the tensor part only of the $\pi + \rho$ interaction.

Fig. 4: Same as Fig. 1 but for the enhancement parameter, ϵ for the full ρ interaction only.

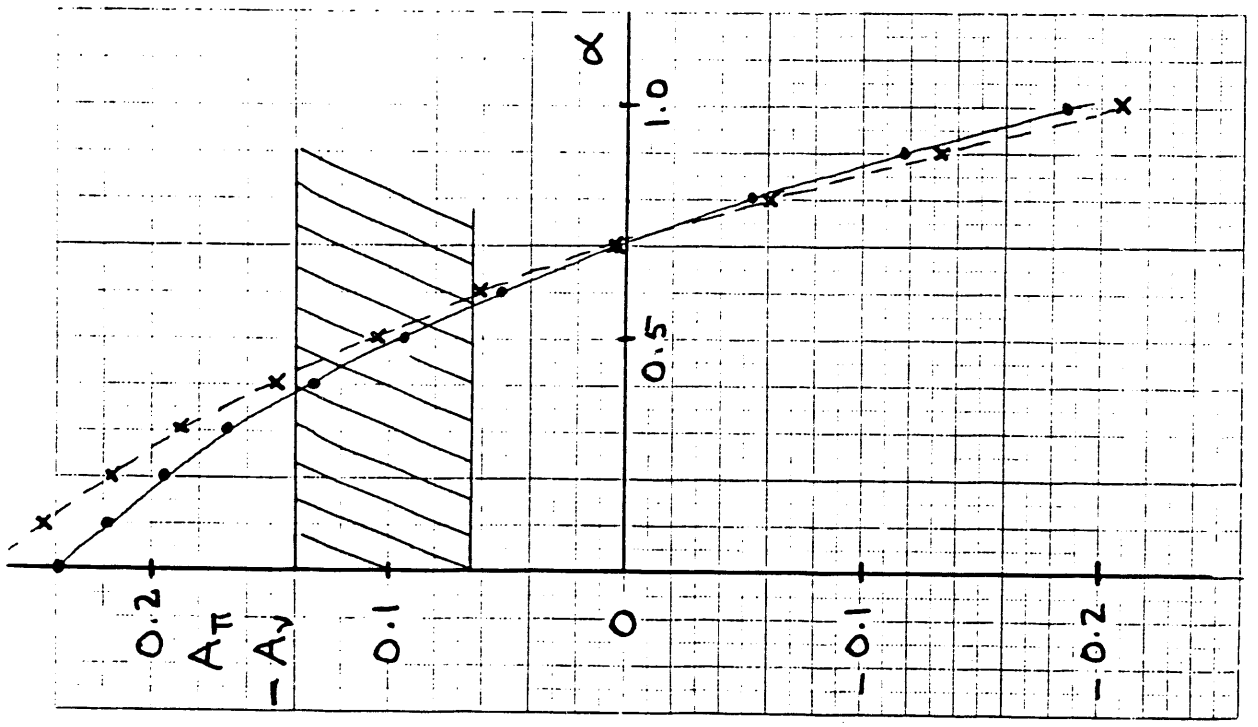

Figure 2

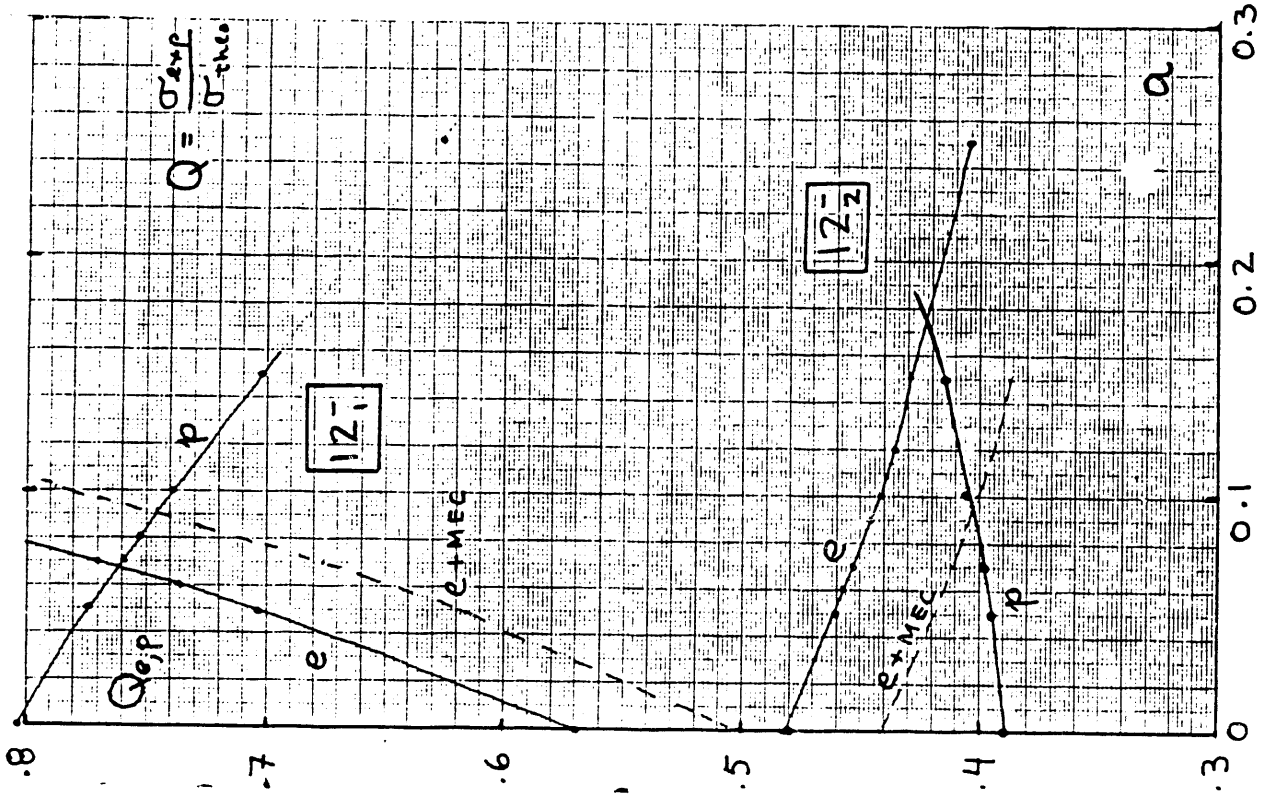

Figure 1

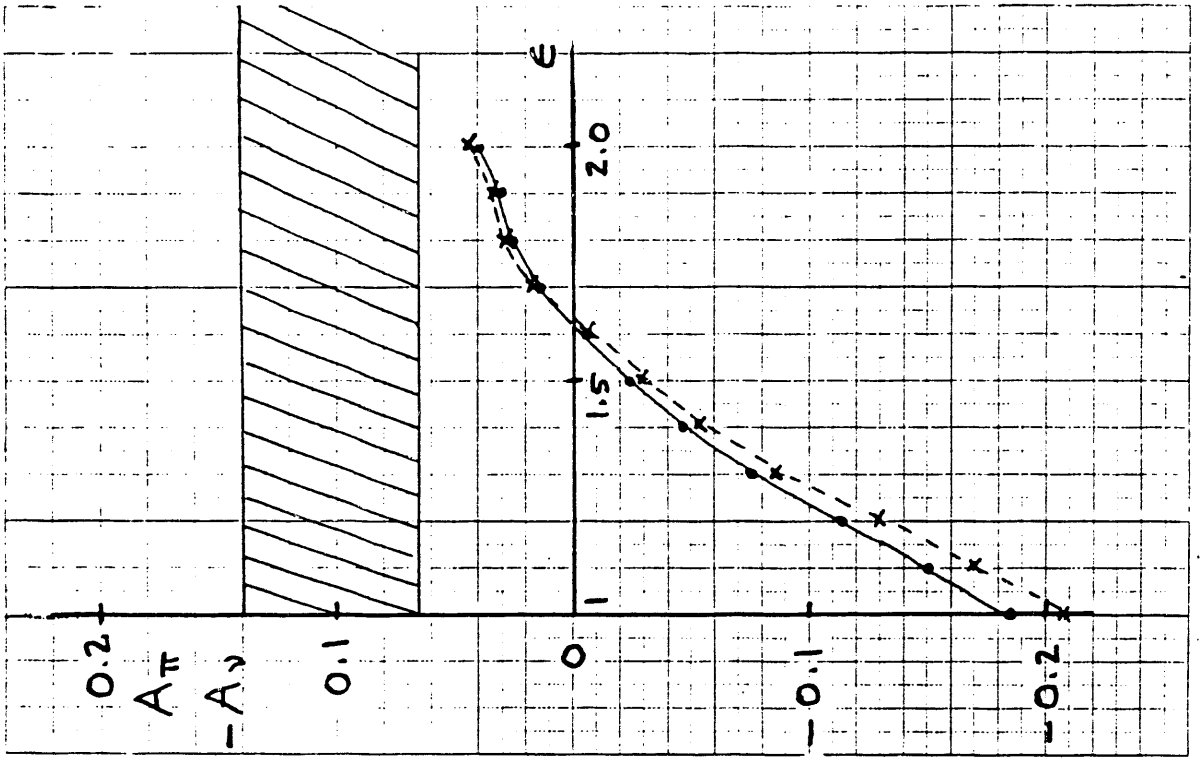

Figure 4

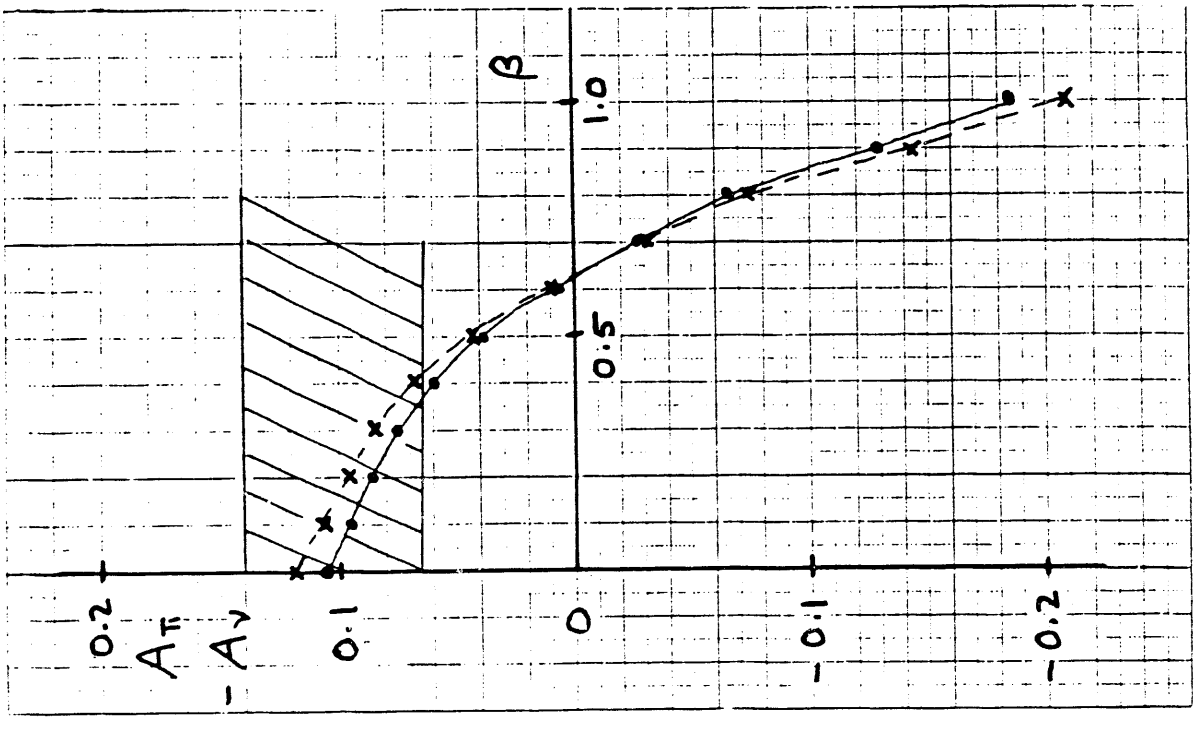

Figure 3

II.J. Global Analysis of (p,p') Reactions to High Spin States in ^{28}Si and ^{58}Ni (135-800 MeV), and Density Dependent Modifications of the IA.

The inelastic transition amplitudes for high spin stretched states are usually dominated by a single particle-hole configuration. For this reason they are good for testing direct reaction models. Data on (p,p') now exist for the 5^- (9.70 MeV), 6^-, T = 0 (11.58 MeV), 6^-, T = 1 (14.36) states of ^{28}Si at 135 (σ, A_y), 333 (σ), 500 (σ,A_y,D_{ij}) and 800 (σ) MeV and for the 6^+ (5.13 MeV) state of ^{58}Ni at 178 (σ), 333 (σ), 500 (σ,A_y,D_{ij}) and 800 (σ) MeV. These states have also been studied in (e,e'). With the recent availability of programs which calculate (p,p') observables in a relativistic impulse approximation (RIA) it is useful to do a global analysis, comparing predictions of the RIA with those of the non-relativistic impulse approximation (NRIA). In particular, we are interested in comparing (p,p') observables with RIA and NRIA predictions, at various energies, using static and transition densities derived from electron scattering, and with distorting (optical) potentials calculated "consistently" with the same N-N interaction in both the elastic and inelastic channels. In earlier NRIA analyses,[1] mostly phenomenological optical potentials were employed for the distorted waves.

Some preliminary work using data from E178, 451, 896 (Minnesota) and E686 (Rutgers) has been reported in our 1984-87 Summary Progress Report[2], in this report (Sect. II.H.), and in a paper to be submitted to Phys. Rev. C[3]. Some of the conclusions to date are:

1) Neither the RIA nor the NRIA give satisfactory fits to the elastic observables with static densities derived from electron scattering, the main

problem being a shift (towards smaller angles) of the diffraction structure, relative to the data. One way to fix this phase problem is to introduce a density dependence in the N-N interaction, believed to arise, at least in part, from a reduction of meson and nucleon masses in medium as described in Sect. II.G. Despite this problem, the RIA gives significantly better fits to the elastic spin observables than does the NRIA.

2) When transition densities derived from (e,e') are used in the inelastic (p,p') programs (RIA or NRIA), a similar shift (to smaller angles) is seen relative to the data. In the earlier analysis we fixed this phase problem by arbitrarily "shrinking" the bound state radii by ~ 5-10%.

3) The (p,p') normalization factors, $N_p^2 = \sigma_{exp}/\sigma_{theo}$ for the natural parity states show an energy dependence, with N_p^2 in agreement with the (e,e') value (N_e^2) at 800 MeV, but increasing with decreasing proton energy if "consistent" (FOP, folded optical potential) distorting potentials were used or decreasing if phenomenological optical potentials (POP) were employed.

4) The (p,p') normalization factors for the unnatural parity states show no systematic energy dependence but scatter somewhat in magnitude around the (e,e') values. It is noted that the (p,p') excitation of natural parity states is dominated by the central spin-independent and projectile spin flip (spin-orbit) parts of the N-N interaction, whereas the unnatural parity states are excited mainly by the target spin-flip (spin-orbit) and tensor components of the force.

5) No clear preference for the RIA over the NRIA is seen in comparing theory with the inelastic spin rotation parameters (D_{ij}), but the RIA is clearly superior in describing the inelastic analyzing powers, A_y.

Because of the elastic and inelastic phase problems (items 1 and 2 above), we are now studying the effect of density dependent modifications (See Sect. II.G.) of the N-N interaction on both elastic and inelastic proton scattering at various energies. In the first calculations, shown here, the elastic and inelastic interactions were modified using the simple "zero range" prescription described in Sect. II.G., in which approximation a density dependent modification of the N-N t-matrix is equivalent to a corresponding modification of the densities. For the elastic waves, the point densities were contracted by the fraction, $\Delta r/r = \lambda a/R$, and multiplied by $1/1-\lambda$. The inelastic densities were modified by a factor, $f(r) = [1-\lambda\ \rho(r)/\rho_0]^{-1}$, where $\rho(r)$ is the ground state (ρ_0:central) density. In keeping with the ideas discussed in Sect.II.G. we have taken λ(central) = 0.4 and λ(spin-orbit) = 0.6, corresponding to $m^*/m = 0.8$ at $\rho = \rho_0$. Only the <u>real</u> parts of the potentials were modified, and the tensor force was left unchanged.

The results for the (p,p') cross sections, calculated in the NRIA, for the 5^- (9.70 MeV) state of ^{28}Si and the 6^+ (5.13 MeV) state of ^{58}Ni at T_p = 500 MeV are shown in Figs. 1 and 2, along with the unmodified calculations. The transition densities for the (p,p') calculations <u>are now those which fit the (e,e') data</u>. The main effects of the density dependent modifications are a centroid shift (tc larger angle), a broadening and an increase in magnitude of the cross section peak. For both ^{28}Si and ^{58}Ni the (p,p') N_p^2 are now in good agreement with the N_e^2 from (e,e'). The theoretical shape for the 5^- in ^{28}Si is nearly perfect but the 6^+ (^{58}Ni) is slightly too braod. These preliminary calculations are fairly crude but may indicate the effects expected in better ("finite range") approximations. We are now

exploring the effects of density dependent modifications of separate parts of the N-N interaction as suggested by the cross section and spin observable (D_{ij}) data on ^{28}Si and ^{208}Pb (Sects. II. H. and I.) and by meson and nucleon effective mass considerations[4,5].

References

1. N. M. Hintz, et al., Phys. Rev. C30, 1976 (1984) and reference therein.
2. Univ. of Minnesota Summary Progress Report, 1984-1987, p. 51; unpublished.
3. E. Donoghue, C. Glashausser, N. Hintz, A. Sethi, J. Shepard, R. Fergerson, M. Franey, M. Gazzaly, K. Jones, J. McClelland, S. Nanda and M. Plum, preprint (1990); to be submitted, Phys. Rev. C.
4. See G. E. Brown and M. Rho, Phys. Lett. B 237, 3 (1990) for a discussion of tensor force modification in medium, submitted to Phys. Rev. C.
5. G. E. Brown, A. Sethi, N. Hintz, preprint (1989) on the effects of meson and nucleon mass reduction in medium, submitted to Phys. Rev. C.

Figure Captions

Fig. 1: Inelastic cross sections for $^{28}Si(p,p')$ to the 5^- (9.70) MeV collective state at T_p = 500 MeV. The solid curve shows the unmodified NRIA prediction (N_p^2 = 1.15) and the dashed curve shows the modified prediction (N_p^2 = 1.0) with λ_C = 0.4, λ_{so} = 0.6 (real parts only). The data is from Ref. 1.

Fig. 2: Same as Fig. 1 but for the 6^+ (5.13 MeV) state of ^{58}Ni and with normalization factors N_p^2 = 1.47 (unmodified) and N_p^2 = 1.07 (modified).

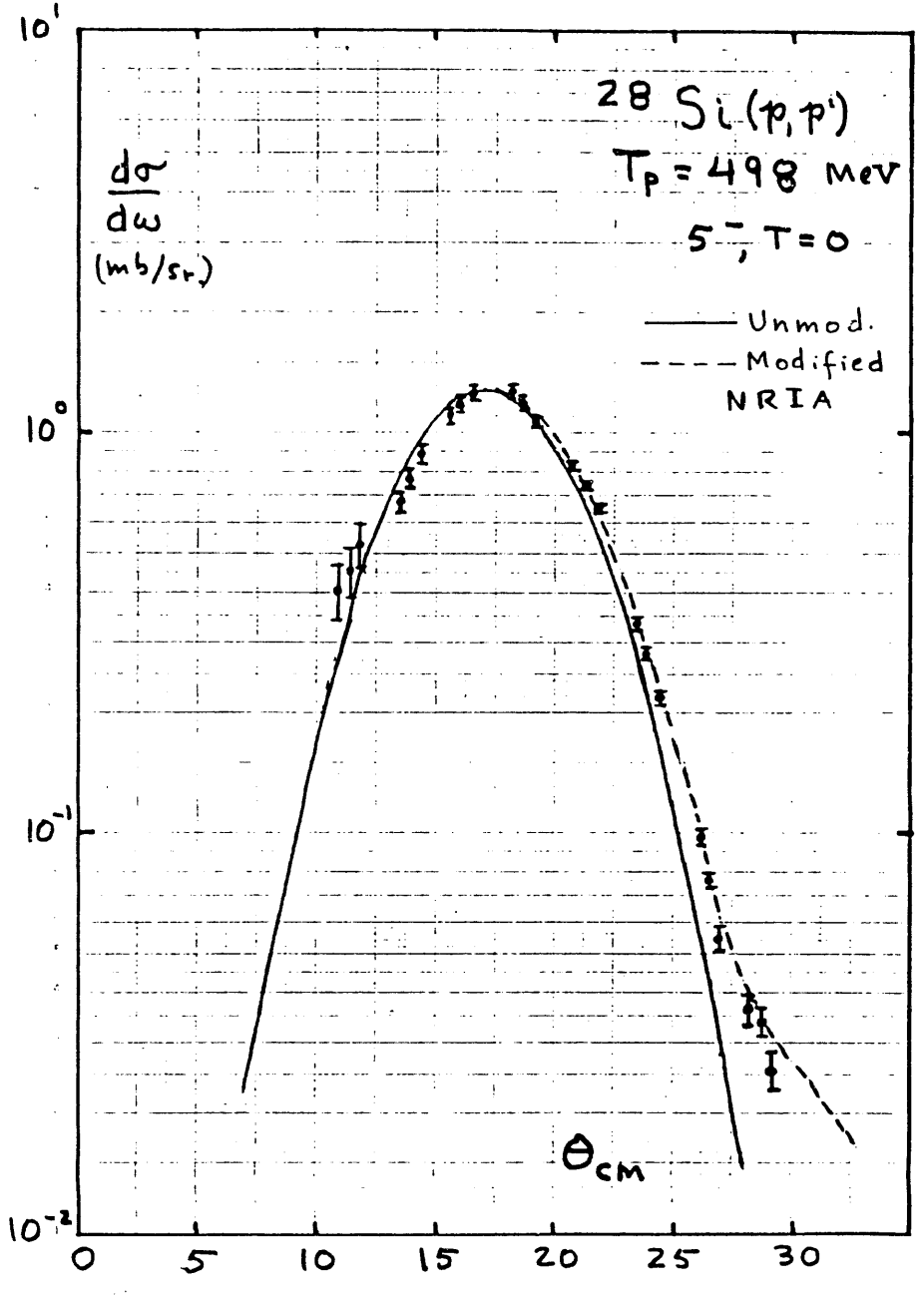

Figure 1

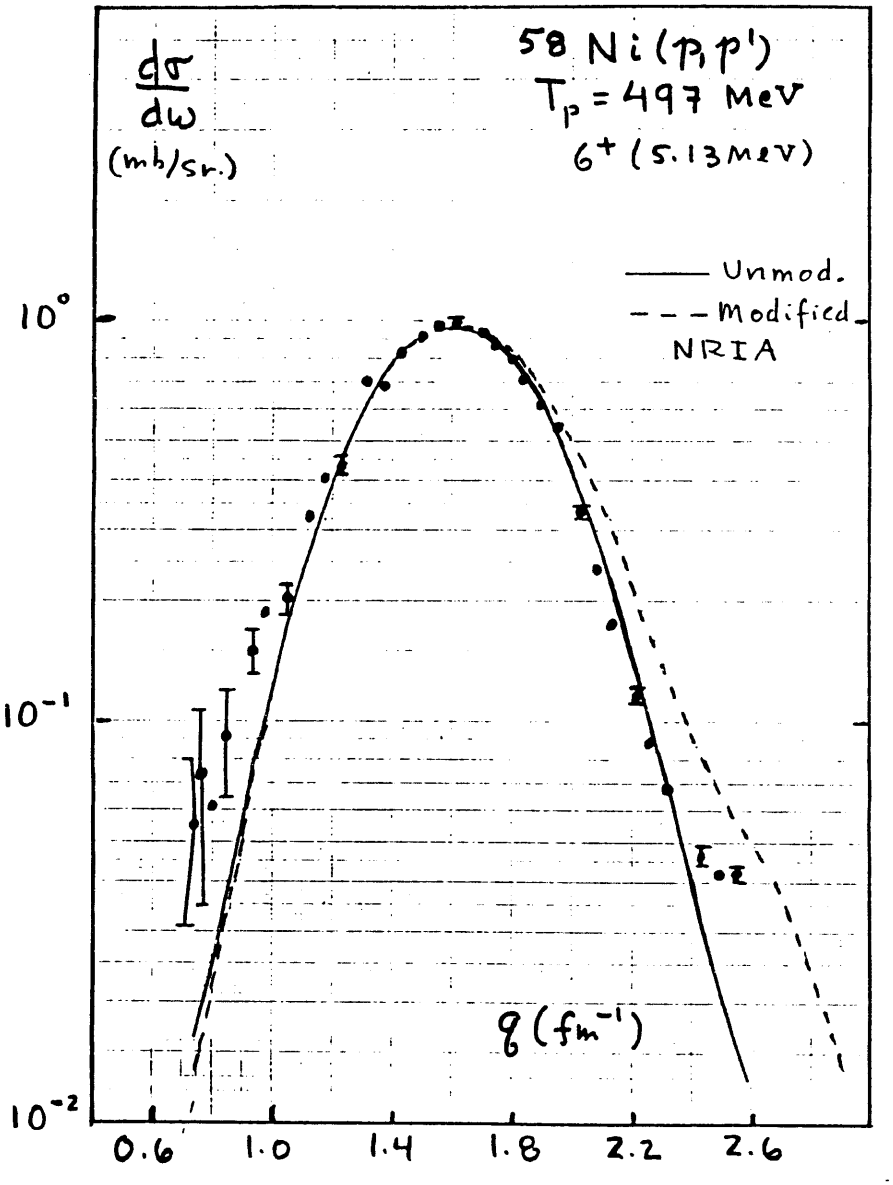

Figure 2

II.K. MRS Set-Up and Development.

During the last two beam cycles (cy54 and cy55) at LAMPF, of the calendar year 1989, and the first run cycle (cy56) of 1990 the Medium Resolution Spectrometer (MRS)[1] was run in a development mode.

Our group (D.M. and A.S.) in collaboration with LAMPF, U of Texas, U of Rutgers, U of Colorado and other institutions, actively participated in the set-up, tune-up and data replay of the MRS spectrometer. The task of our group was:

(1) To install the Focal Plane Polarimeter (FPP)[2] "box" which consists of four wire chambers, four scintillators and a carbon block, the so called Carbon Analyzer (CA), in the arrangement shown in Fig. 1. The MRS FPP is similar in principle to the High Resolution Spectrometer (HRS) FPP that has been used very successfully at LAMPF for several years. The main difference is in the design of the carbon analyzer. Due to the large momentum acceptance of the MRS, the analyzer is designed with a triangular shape; a thickness of 28 cm at the bottom edge and 3 cm at the top. The MRS is dispersion matched to a momentum dispersed proton beam. Momentum loss in the target is determined from particle coordinates measured in the focal plane. Since this device (FPP) uses asymmetries from the second scattering in the CA to measure polarizations of particles in the focal plane, two sets of angle measurements have to be made for each particle.

(2) To work on the electronics which transfer event and time signals from the experimental dome to the counting house. For this we did the necessary instrumentation and cabling with the guidance of MP-10 staff.

(3) To assemble and test the scintillators for the spectrometer and the beam polarimeter. We prepared the FPP scintillators and tested them for "good" signals using a radioactive source, and later with the proton beam, also checked their efficiency ("plateauing" of the scintillators). In addition, we assembled and tested the small scintillators used for the beam line polarimeter, which measures the polarization of the incident beam on the target.

(4) To prepare the targets and mount them on the target wheel in the scattering chamber. The targets were thin and thick ^{12}C, ^{56}Fe, vertical and horizontal rods, and some ^{12}C and ^{9}Be plates. The vertical and horizontal targets were used for angle (θ and ϕ) calibration as will be described briefly below.

(5) To participate in the MRS tune-up (calibration) runs. There were two such runs, the first in August and September of 1989 and the second more recently in May and June of 1990. The beam energy during these runs was 500 and 800 MeV. Data collected during these development runs were replayed and the results obtained from the recent runs (1990) for angle (θ,ϕ) and energy ($\Delta\Gamma$) calibration were very satisfactory (Figs. 2-6) i.e., close to the design resolution

We briefly report some of the calibrations[3] we made for the MRS spectrometer. Given the large angular acceptance angle, ($\pm$ 60 mrad horizontal and $\pm$ 40 mrad vertical) and large momentum acceptance ($\pm$ 20% $\frac{\Delta p}{p}$) of MRS, the knowledge of the target angles ϕ-target, θ-target and the target positions X-target and Y-target is essential for accurate missing-mass (Figure 2) measurements. At the target the same coordinate system is used as at the focal plane. Z is the direction of the central ray (beam

direction being positive Z), X is perpendicular to Z and points downwards forming a right-hand system (X,Y,Z). It is important at this point, to mention that all quantities measured at the focal plane can be converted through the optics of the spectrometer into information at the target.

Another important calibration was the δ-calibration[3]. The optical focal plane, where different rays with the same momentum loss converge, is tilted by about 68^{o} with respect to the Z axis. Due to hardware limitations the actual detector is mounted perpendicular to the Z axis. The second of the front two wire chambers was placed at the intersection of the Z-axis with the optical focal plane. The task of δ-calibration was to account for the remaining rotation between the optical focal plane and the wire chamber plane and to take care of any alignment errors and second order correlations in θ-focal plane in order to guarantee a good energy resolution independent of the particle location on the detector plane. A typical δ-calibration histogram is shown in Figure 3. The relationship between $\frac{\Delta p}{p}$ and $\frac{\Delta T}{T}$ (energy resolution) is:

$$\frac{\Delta p}{p} = \left(\frac{m+T}{2m+T} \right) \frac{\Delta T}{T} \qquad (1)$$

where, m is mass of the proton, p and T denote beam momentum and kinetic energy respectively.

In Figure 3, $\frac{\Delta p}{p} \sim .1\%$ which gives $\Delta T = 1.23$ MeV at 800 MeV. This is close to the design value of 1.0 MeV (FWHM), at $T_p = 800$ MeV.

References

1. R. L. Boudrie, "Planning Experiments With MRS" LAMPF April 1989 (unpublished).

2. C. L. Morris, Nucl. Inst. and Meth. 196, 263 (1982).

3. K. M. Koch, "MRS performance" MP-10 LAMPF December 1989 (unpublished).

Figure Captions

Fig. 1: Conceptual layout of MRS magnets, frame, scattering chamber, and detectors.

Fig. 2: Missing Mass histogram for ^{12}C (p,p') at T_p = 500 MeV at $\theta_{MRS} = 20^{o}$. The broken line is a peak fit (Gaussian) with background included.

Fig. 3: "Full acceptance", δ-calibration histogram at T_p = 800 MeV on a ^{12}C target at $\theta_{MRS} = 17^{o}$. Here $\frac{\Delta p}{p} = 0.1$ (FWHM) and the energy resolution is $\Delta T = 1.23$ MeV (θ-focal and ϕ-focal cuts are included).

Fig. 4: δ-calibration histogram without ϕ-focal cuts and with the same parameters as in Fig. 3.

Fig. 5: θ-focal plane as a function of x-focal plane at the same energy, angle and target as in Fig. 3. The three dark bands on the right are the ground and the first two excited states of ^{12}C.

Fig. 6: A projection on x of a slice of the histogram shown in Fig 5. The ground and the first two excited states of ^{12}C are easy to see.

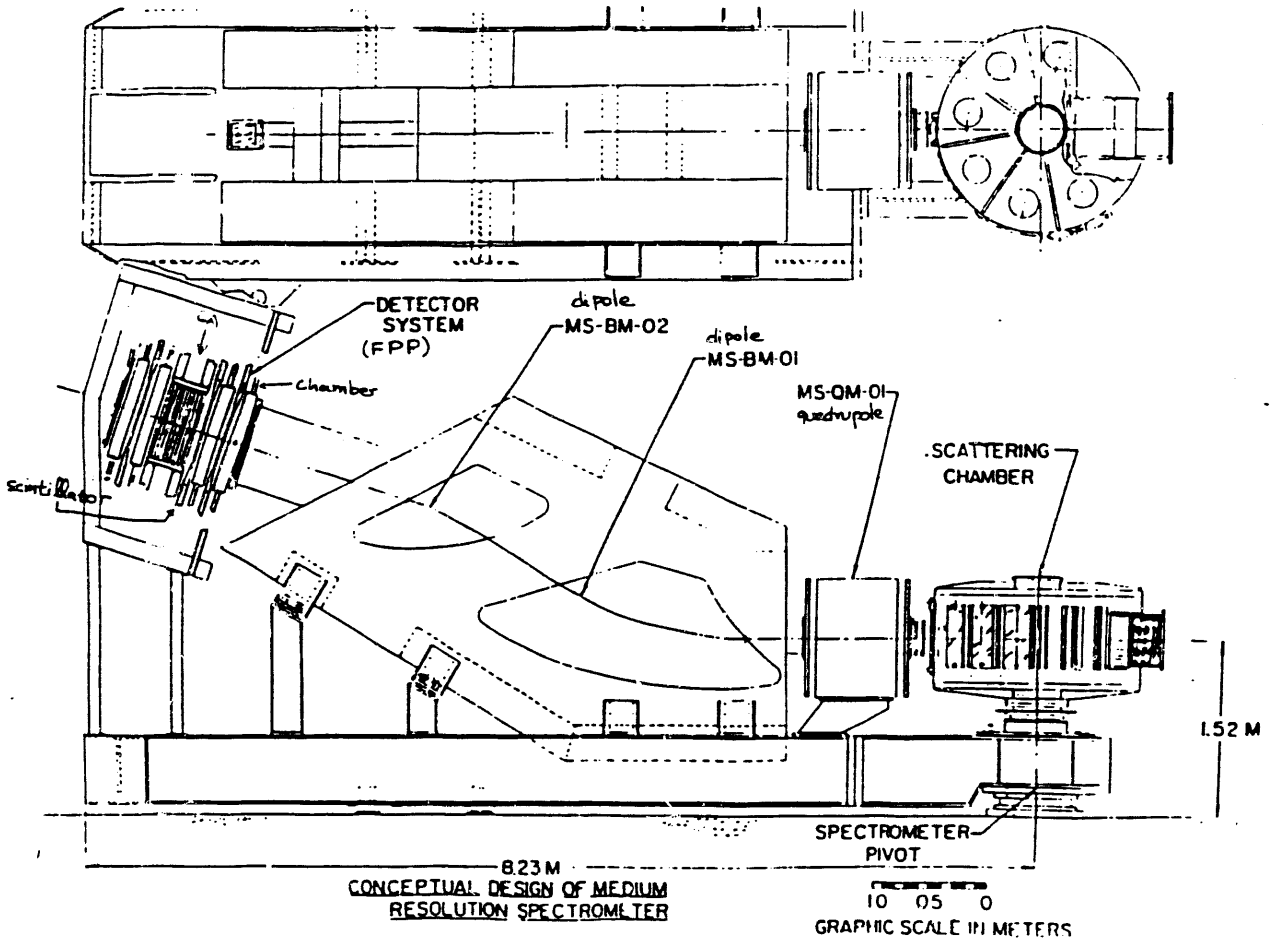

Figure 1

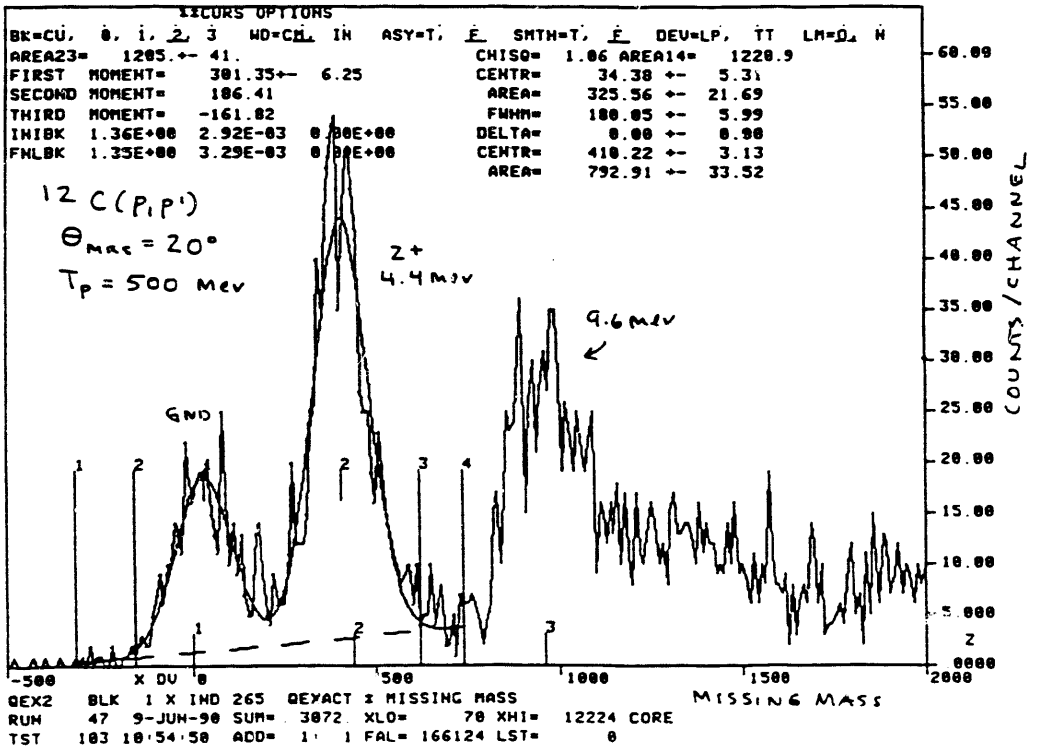

Figure 2

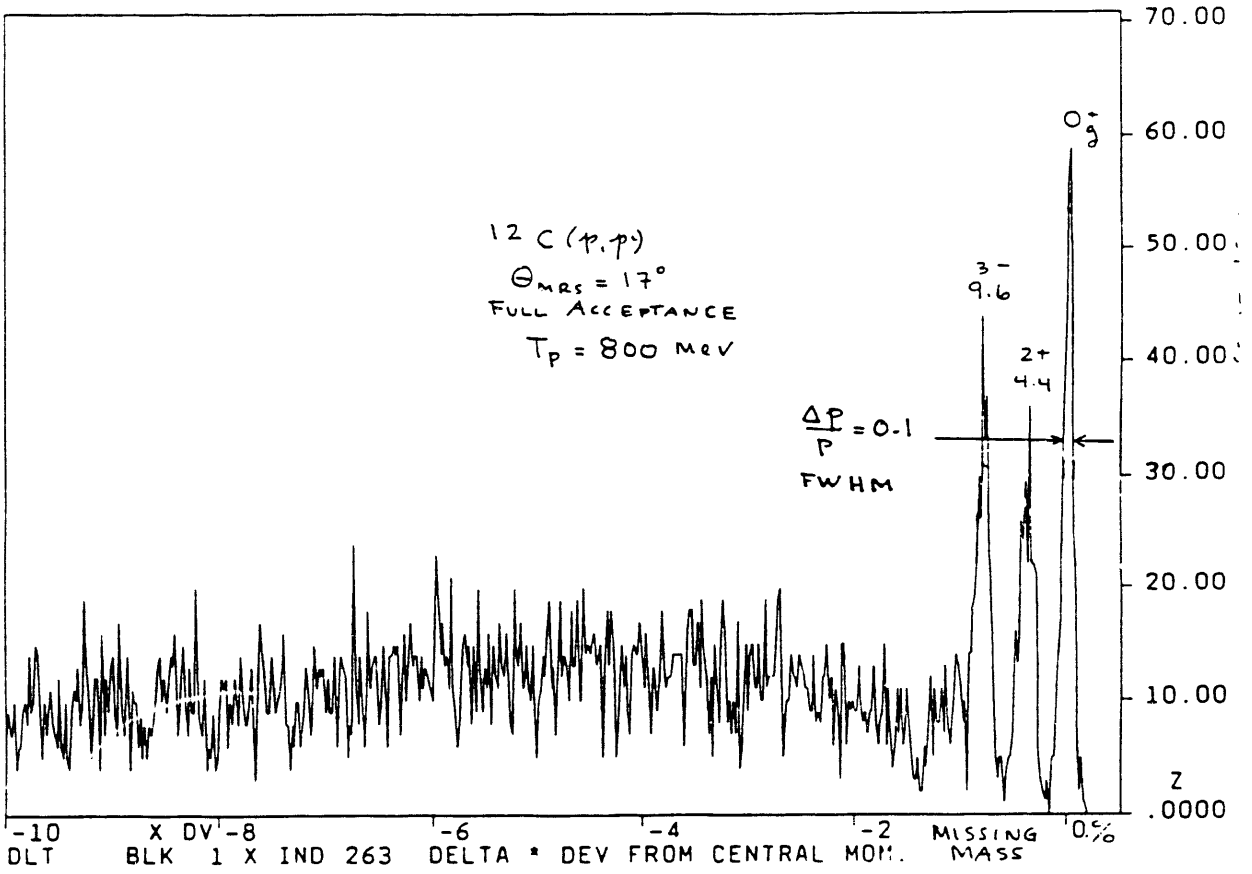

Figure 3

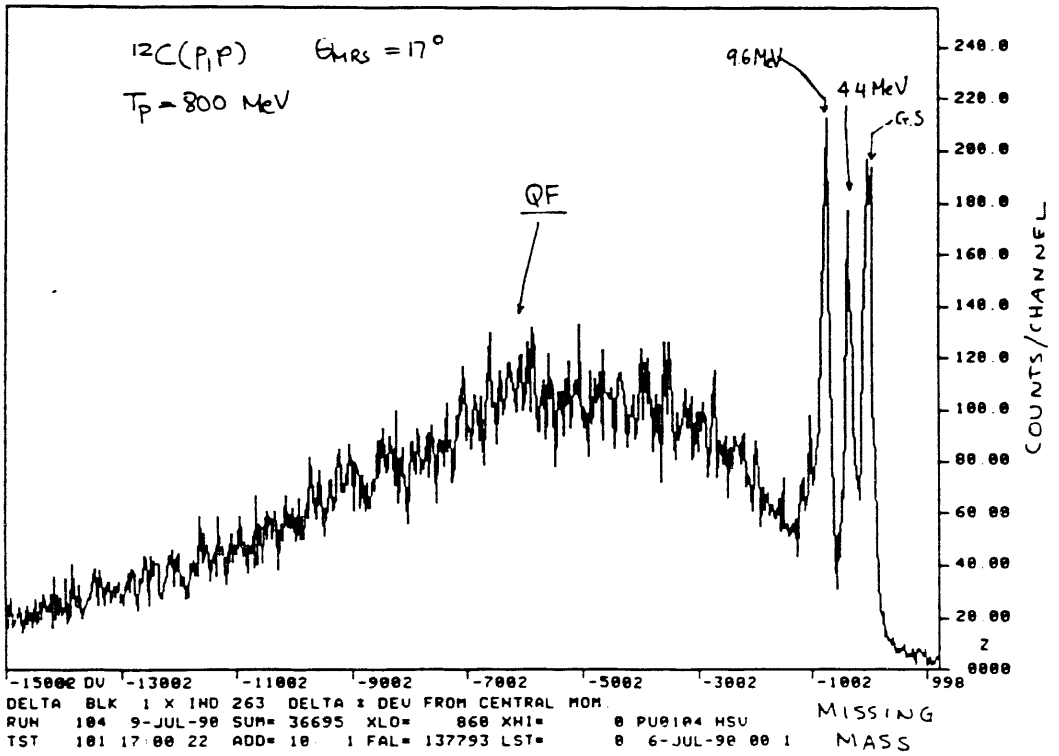

Figure 4

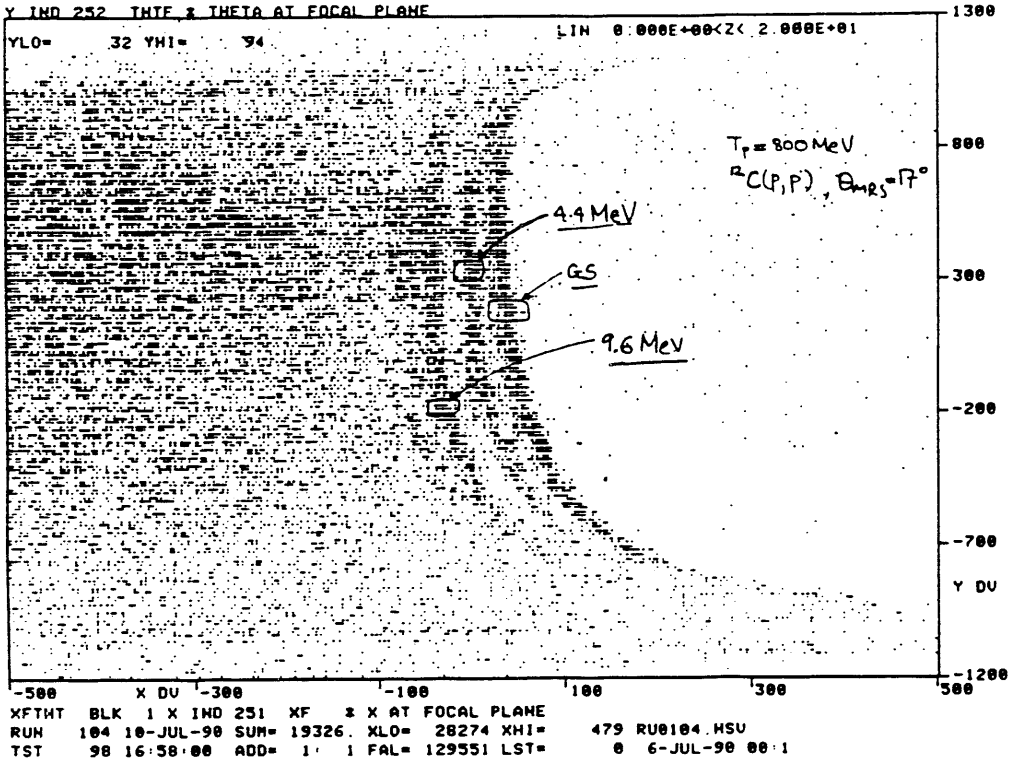

Figure 5

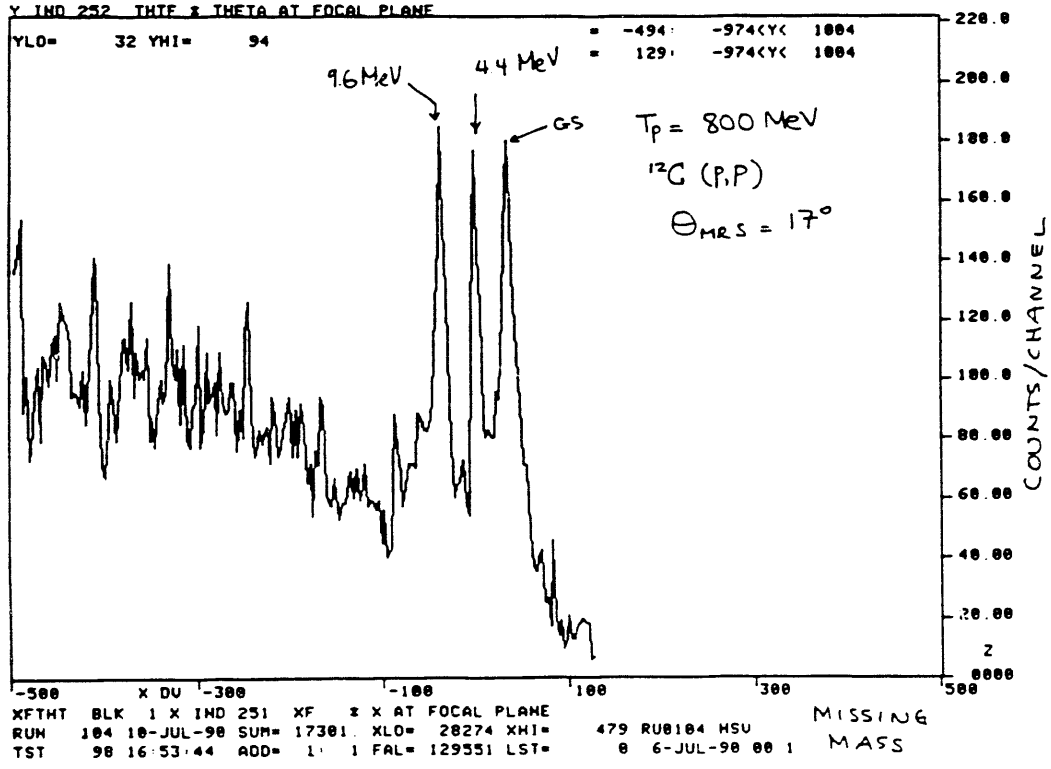

Figure 6

II.L. Development of Coincidence Studies with MRS (E1201, Minnesota spokesman and participants, LANL, Rutgers participants).

The MRS being a completely new spectrometer, needs to be studied carefully and to do this several experiments must run to explore its abilities. One such experiment (exploratory) is E1131 with spokesmen from U of Rutgers, U of Texas (Austin) and LANL. Our group (D.M., A.S.) being part of the development team of MRS is participating in this experiment which has the title "Measurements of Polarization Transfer for 800 MeV Inclusive Proton Scattering at MRS".

Inclusive reactions are not the only ones possible to explore the MRS. Polarized target and coincidence experiments will be proposed in the very near future by many experimenters.

Our group has had approved the first MRS coincidence experiment, E1201, (December 1989) with the title, "Coincidence Study of Quasielastic Proton Scattering". E1201 will be an exploratory experiment to perfect coincidence techniques with the MRS, which shhould also be useful for other experiments. The MRS, because of its large momentum acceptance and medium resolution, is an ideal spectrometer for reactions over the continuum region such as those exploring Giant Resonances (GR), Quasifree (QF) and Delta Resonance (DR) scattering. Our coincidence experiment (E1201) will focus on the QF region with a $(\vec{p},2p)$ reaction at an incident energy T_p = 650-800 MeV, depending on beam availability. Most studies to date of the quasi-elastic region have been single arm inclusive experiments, and their results are not entirely consistent with theory. E1201 will allow us to test assumptions about the background (due, for example, to multiple scattering) under the inclusive

quasi-elastic peaks, and to explore the full kinematic domain of the two outgoing protons.

Development time for E1201 has been scheduled during the beginning of the last run cycle (cy58) of 1990. The development time will be between 1-1/2 and 2 weeks. We shall use this time to test the secondary proton arm, prepare the electronics for the coincidence and develop the software for experiments which use a second arm in addition to the spectrometer. During the development runs of MRS (Sec. II.K) we (D.M. and A.S.) have worked on the assembly and testing of detectors for the second proton arm, and at the same time included the coincidence in the main spectrometer (MRS) software with the guidance and help of Dr. K. M. Koch (MP-10 Research associate), who is the staff member responsible for the MRS and who has maintained all the electronics and computer software for the spectrometer. During the last phase of the development runs we had the opportunity to look for singles rates in a NaI detector installed outside the scattering chamber at an angle suggested by the QF (p,2p) kinematics. We hope to do further coincidence tests during part of E1131 (cycle57) development.

In E1201, the conjugate proton detectors will be four 3"x3"x12" CsI crystals stacked in a 6"x6"x12" array placed horizontally (Fig. 1) to detect the recoil (conjugate) proton from the QF p-p scattering events, the forward proton being detected in the MRS. The solid angle of the conjugate proton detector will be approximately 180msr. Currently we are preparing CsI detectors, attaching photomultiplier tubes at each end of the array to be able to collect total energy (250 MeV protons are stopped by 6" of CsI), timing and position ($\Delta x \sim \pm 1"$, $\Delta\theta \sim \pm 3^{o}$) information. Work is also underway on testing the CsI crystals for energy and time resolution using

multichannel analyzers (MCA) and time to analog converters (TAC). Theoretical calculations for (p,2p) reactions using the program THREEDEE[1] are also being performed. Our present task is to continue the technical development for E1201 in preparation for the development run in September 1990.

Reference

1. N. S. Chant, program THREEDEE, Univ. of Maryland (unpublished).

Figure Caption

Fig. 1: Schematic layout of (p,2p) coincidence experiment, E1201.

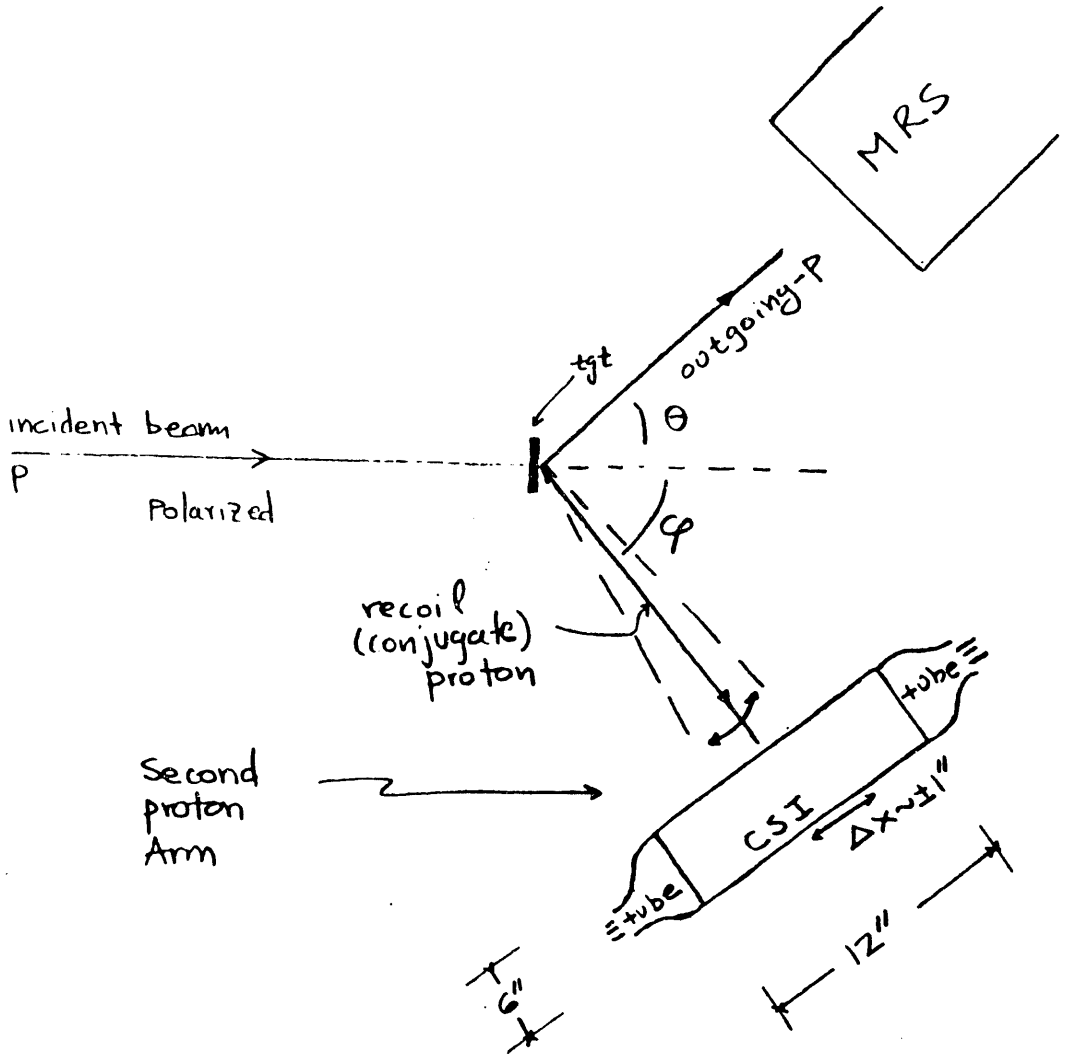

Figure 1

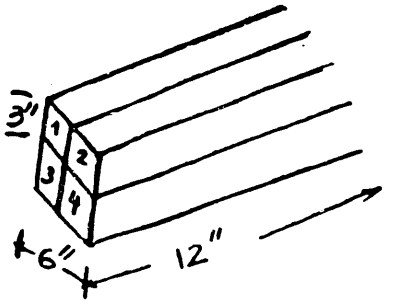

SIDE VIEW OF
THE DETECTOR ARRAY
FOR THE SECOND PROTON
ARM

II.M. Other experiments, Minnesota Participation.

During the period of this report, one or more members of the Minnesota group participated in the following experiments at LAMPF (unless otherwise noted) during data taking and/or in the subsequent analysis:

1) E955, "Search for Experimental Proof of the Existence of Lower Components in the Nuclear Wavefunction" (Texas, LANL spokesmen; Minnesota, LANL, ANL, New Mexico State U., Ohio State U., IBM, Rutgers participation). The experiment consisted of measuring cross sections and spin observables for $\vec{p} + {}^{13}\vec{C}$ (polarized target) scattering at T_p = 500 Mev.

2) Fermilab E581, Coulomb-Nuclear Polarimeter.

3) Fermilab E704, p + p and $\bar{p}$ + p Spin Parameters.

4) IPN (Orsay) experiments at Saclay (Saturne) on p + ^{28}Si inelastic scattering to low lying T = 0 and 1, 1^+ states vs. energy from T_p = 200 - 800 MeV. Participation was in experimental runs and data analysis.

5) E1027 "Measurement of Spin Averaged Slope Parameter for pp Elastic Scattering between 1.1 and 1.5 GeV/c."

6) E1080 "The Longitudinal/Transverse Decomposition of the Enhanced Nuclear spin Response in ^{40}Ca at T_p = 500 MeV" (Rutgers, LANL spokesmen; Minnesota and other groups participation - at HRS).

7) E1131, "Measurements of Polarization Transfer for 800 MeV Inclusive Proton Scattering at the MRS" (Univ. of Rutgers spokesman; Minnesota and other groups participation running July 90 at MRS).

II.N. Computer Program Library Development

We have continued the updating of our computer library by adding new programs and modifying old programs. The main programs used in our data analysis are:

1) Proton Scattering

a) Non-relativistic

DWBA70	Nucleon nucleus scattering program
ALLWORLD	Folds static and transition nuclear densities with NN interaction
RELOM	Elastic scattering optical potential search program
ECIS	Coupled channels proton-nucleus scattering

b) Relativistic

DREX	Elastic and inelastic proton-nucleus scattering (explicit exchange)
DRIA	Elastic and inelastic proton nucleus scattering (implicit exchange)
MNPOTSYM	Folds NN interaction with scalar, vector and tensor densities (elastic scattering)
MNDIRAC	Solves the Dirac equation (elastic scattering)
GLOBAL	Calculates scalar and vector optical potentials

2) Electron Scattering (Relativistic, plane wave programs)

ELECTE	Calculates transverse electric form factor
ELECTL	Calculates longitudinal (Coulomb) form factor
ELECTM	Calculates transverse (magnetic) form factor

3) Pion Scattering

DWPI	Coordinate space elastic and inelastic pion-nucleus scattering
PIPIT	Momentum space elastic pion-nucleus scattering
HL	Momentum space inelastic pion-nucleus scattering

4) Interacting Boson Model (IBM-1)

PHINT	Diagonalizes sdg IBM hamiltonian
FBEM	Computes transition matrix elements

These programs and their application in data analysis are summarized below.

1. Non-relativistic proton-nucleus scattering

There are two main programs used in the non-relativistic analysis of the proton-nucleus scattering data: ALLWORLD and DWBA70. The former was written by J. Carr and F. Petrovich and the latter by J. Raynal and R. Schaeffer. Program ALLWORLD performs folding of NN interaction with the nuclear transition densities to calculate scattering potentials. These potentials are then used by DWBA70 to compute the scattering observables (σ, A_y, D_{ij}, etc.). To study the effect of density dependent meson masses in nuclei on proton-nucleus scattering we have modified ALLWORLD to include an option to do modified density calculations as described in Sect. II.G. Similarly an option now exists in DWBA70 to study this effect on the inelastic transitions.

2. Relativistic proton-nucleus and electron-nucleus scattering

Dirac relativistic programs are being used in the analysis of high spin stretched states in ^{28}Si (see Sect. II.H) and ^{58}Ni. One of the objectives was to make a critical comparison of the relativistic and non-relativistic treatments of proton-nucleus scattering using equivalent ground state and transition densities derived from electron scattering. The programs DREX and DRIA (obtained from E. Rost and J. Shepard, U. of Colorado) were used in the analysis. The main difference between the two programs is that DREX uses explicit exchange whereas the exchange is included implicitly in DRIA. Also the NN interaction used in DREX is available at only four energies between 135 MeV and 400 MeV whereas DRIA uses NN interaction available at all energies between 0.1 - 1 GeV.

The programs use standard 2 or 3pF shape option for the input density. They have now been modified to accept external point densities. This is useful in comparing scattering calculations using densities obtained directly from electron scattering. In addition, an option to selectively study the real and imaginary parts of the S (scalar) and V (vector) optical potentials has also been added to the programs. We have also enlarged DREX to accept up to 75 partial waves, which is quite useful in analysis of 333 - 800 MeV proton scattering data.

Another version of the Dirac relativistic impulse approximation program (MNPOTSYM and MNDIRAC) for elastic scattering has been obtained from S. Wallace at U. of Maryland. The program can perform both IA1 and IA2 calculations and has the advantage of using a more complete (and more accurate) IA2 treatment using pseudo-vector coupling. The programs generate potentials from input files of NN amplitudes and nuclear densities. Scalar, vector and tensor nuclear densities are used and these are generated by the

program LIMORA due to C. Horowitz (NP A368, 503 (1981) and Phys. Rev. C35, 280 (1987)).

The global Dirac optical potential program for proton-nucleus elastic scattering (S. Hama, B. Clark et al.) has also been installed at the University of Minnesota. It calculates scalar (S) and vector (V) optical potentials for proton nucleus scattering in the energy range T_p = 65 - 1040 MeV from any target (^{40}Ca-^{208}Pb).

We have also recently obtained relativistic electron scattering programs (J. Shepard and E. Rost, U. of Colorado), namely ELECTE, ELECTL and ELECTM, which respectively calculate the electric transverse, longitudinal (Coulomb) and transverse (magnetic) form factors. These are quite useful in a "consistent" analysis of the electron and proton scattering data as described in Sect. II.H.

3. Pion Nucleus Scattering

The elastic and inelastic pion scattering codes in momentum space, PIPIT and HL, have been modified to run on a CRAY computer and were installed on the University of Minnesota CRAY-2. These codes are used in the analysis of 180 MeV pion scattering data from ^{208}Pb as described in Sect. II.B. We have also obtained the original version of ARPIN from Argonne National Laboratory (T.-S. H. Lee). Some modifications have been made to run it on a CRAY computer and the code was installed on the University of Minnesota CRAY-2.

4. IBM Calculations

The IBM codes PHINT and FBEM were used to analyze the low lying states of transitional nuclei as described in Sec. II.D. The usual IBM-1 sd

version of the programs was modified by P. van Isacker (Ghant, Belgium) to include also a single g-boson. PHINT calculates the eigenfunctions of a given IBM hamiltonian by matrix diagonalization. These eigenfunctions are then used by FBEM to calculate the transition matrix elements to be compared with the experimental data. Another version used for IBM-2 (proton-neutron) calculations, NPBOS has also been acquired from O. Scholten. When operative on the CRAY, this should provide a powerful package to compare IBM-1/IBM-2 results for the transition region.

The above programs, admitting of L = even (s,d,g) bosons, cannot describe transitions to the negative parity states. We are in the process of acquiring a "spdf" version of IBM-1 from MSU in collaboration with D. Kusnezov. A collaboration to study the negative parity states in transition nuclei is being pursued with F. Iachello at Yale.

III. Bibliography -July 1987 - July 1990 (Minnesota authors are underlined)

A. Published Papers.

1. "Isovector Couplings for Nucleon Charge-Exchange Reactions at Intermediate Energies", W. G. Love, K. Nakayma and M. A. Franey, Phys. Rev. Lett. 59, 1401 (1987).

2. "Nucleon charge-exchange reactions at intermediate energies", W. G. Love, Amir Klein, M. A. Franey and K. Nakayama, Can. J. Phys. 65, 536 (1987).

3. "Medium energy proton scattering from ^{154}Gd and the interacting boson model of nuclei", J. N. Ginocchio, G. Wenes, R. D. Amado, D. C. Cook, N. M. Hintz and M. M. Gazzaly, Phys. Rev. C36, 2436 (1987).

4. "Energy dependence of neutron-proton matrix element ratios derived from 25-800 MeV energy proton scattering", N. M. Hintz, D. C. Cook, M. M. Gazzaly, M. A. Franey, M. L. Barlett, G. W. Hoffmann, R. Fergerson, J. McGill, G. Pauletta, R. L. Boudrie, J. B. McClelland and K. W. Jones, Phys. Rev. C37, 692 (1988).

5. "Large angle $\vec{p}$ + ^{40}Ca elastic scattering at 497.5 MeV", G. W. Hoffmann, M. L. Barlett, G. Pauletta, L. Ray, J. F. Amann, K. Jones, J. B. McClelland, R. W. Fergerson, M. M. Gazzaly, B. C. Clark and R. L. Mercer, Phys. Rev. C37, 1307 (1988).

6. "Spin dependence of pp inelasticities at intermediate energies", N. Tanaka, M. M. Gazzaly, G. Pauletta, B. Aas, D. Adams, H. Fujisawa, S. Greene, H. Hasai, G. Igo, S. Isagawa, S. Ishimoto, K. Iwatani, K. Jones, D. Lopiano, A. Masaike, F. Nishiyama, Y. Ohashi, A. Okihana, S. Okumi, F. Sperisen, G. Weston and C. Whitten, Phys. Rev. C37, 2071

(1988).

7. "Spin observables in Small-angle elastic $\vec{p}\vec{d} \rightarrow \vec{p}d$ with an L-type deuteron target at 800 MeV;, D. L. Adams, B. Aas, E. Bleszynski, M. Bleszynski, G. Igo, C. Newsom, Y. Ohashi, G. Pauletta, F. Sperisen, C. A. Whitten, Jr., H. Fujisawa, M. Gazzaly, S. J. Greene, K. Jones, J. B. McClelland, N. Tanaka, H. Hasai, K. Iwatani, S. Ishimoto, S. Isagawa, A. Masaike, A. Okihana and S. Okumi, Nucl. Phys. A480, 530 (1988).

8. "Evidence for Narrow Structure in the Analyzing Power of the $^3He(\vec{p},d)X$ Reactions", L. Santi, M. Barlett, D. Ciskowski, R. Garfagnini, M. M. Gazzaly, G. W. Hoffmann, K. W. Jones, M. A. Naser, G. Pauletta, C. Smith, N. Tanaka, and R. Whitney, Phys. Rev. C38, 2466 (1988).

9. "A_{LL} At Small Momentum Transfer for the First Complete Determination of the Forward pp Scattering Amplitudes", G. Pauletta, M. Gazzaly, N. Tanaka, B. Aas, D. Adams, S. Green, H. Hasai, G. Igo, S. Ishimoto, K. Jones, D. Lopiano, A. Masaike, K. Iwatani, Y. Ohashi, S. Okumi, L. Santi, F. Sperisen and C. Whitten, Phys. Lett. B211, 19 (1988).

10. "Spin Observables in Small-angle elastic $\vec{p}\vec{d} \rightarrow \vec{p}d$ with an N-type deuteron target at 800 MeV", G. Igo, A. Masaike, D. L. Adams, B. Aas, E. Bleszynski, M. Bleszynski, M. Gazzaly, S. J. Greene, H. Hasai, S. Ishimoto, S. Isagawa, K. Jones, D. Lopiano, J. B. McClelland, F. Nishiyama, Y. Ohashi, A. Okihana, G. Pauletta, F. Sperisen, Tsu-Hsun Sun, N. Tanaka, G. S. Weston and C. A. Whitten, Jr., Phys. Rev. C38, 2777 (1988).

11. "$^{192}Os(\vec{p},p')$ Reaction at 135 MeV", F. Todd Baker, A. Sethi, V. Penumetcha, G. T. Emery, W. P. Jones, M. A. Grimm and M. L. Whiten, Nucl. Phys. A501, 546 (1989).

12. "Analyzing powers for $\vec{p}$ + ^{208}Pb at large momentum transfers", M. G. Moshi, C. A. Whitten, Jr., B. Aas, G. Igo, and D. Lopiano, L. Ray, K. Jones, and M. Gazzaly, Phys. Rev. C41, 1279 (1990).

13. "Cross sections, analyzing powers, and spin-rotation-depolarization observables for 500 MeV proton elastic scattering from ^{12}C and ^{13}C" G. W. Hoffmann, M. L. Barlett, D. Ciskowski, G. Pauletta, M. Purcell, and L. Ray, J. F. Amann, J. J. Jarmer, K. W. Jones, S. Penttilä, and N. Tanaka, M. M. Gazzaly, J. R. Comfort, B. C. Clark and S. Hama, Phys. Rev. C41, 1651 (1990).

14. "Density dependent interaction applied to low-multipole (p,p') and (p,n) transitions in light nuclei", K. Ieki, J. Iimura, M. Iwase, H. Ohnuma, H. Shimizu, and H. Toyokawa, K. Furukawa, H. Kabasawa, T. Nakagawa, and T. Tohei, H. Orihara, S. I. Hayakawa, T. Hasegawa, K. Nisimura, M. Yasue, K. Miura, T. Suehiro, and M. A. Franey, Phys. Rev. C42, 457 (1990).

15. "Nuclear Physics Computer Networking", Report of the Nuclear Physics Panel on Computer Networking, C. Bemis, J. Erskine, M. Franey, D. Greiner, M. Hoehn, M. Kaletka, M. LeVine, R. Roberson, L. Welch, U.S. Department of Energy Report DOE/ER-0458T, May 1990.

16. "Analyzing-Power Measurements of Coulomb-Nuclear Interference with the Polarized-Proton and -Antiproton Beam at 185 GeV/c", FNAL, E-581 Collaboration, 49 authors, including M. M. Gazzaly (see copy of title page, Sec. III.F), Phys. Lett. B229, 299 (1989).

17. "The Design and Performance of the FNAL High-Energy Polarized Beam Facility", FNAL-E-581/704 Collaboration, 62 authors including

M. M. Gazzaly (see copy of title page, Sec. III.F), Nucl. Inst. and Meth. A290, 1268 (1990).

18. "Solitons and Lorentz Covariance at a Quantum Level", Xin-hua Yang and J. Parmentola, Mod. Phys. Lett. A26, 2509 (1989).

B. Articles in Press or (to be submitted)

1. "Proton-nucleus Scattering and the Swelling of Nucleons in Nuclei", G. E. Brown, A. Sethi and N. M. Hintz, submitted to Phys. Rev. C.

2. "$^{194,198}Pt(\vec{p},p')$ Reaction aand the IBA Model", A. Sethi, F. Todd Baker, G. T. Emery, W. P. Jones and M. A. Grimm, Nuclear Physics A, to be published.

3. "Dressed Quarks and the Proton's Spin", Xin-hua Yang, Chun Wa Wong and Keh-cheng Chu, to be submitted to International Journal of Modern Physics A.

4. "Quantum Soliton for All Momenta", J. A. Parmentola, I. Zahed and Xin-hua Yang, to be submitted to Phys. Rev. D.

5. "The $^{16}O(\vec{p},p')$ Reaction at 35 MeV", H. Ohnuma, N. Hoshino, K. Ieki, M. Iwase, H. Shimizu, H. Toyokawa, T. Hasegawa, K. Nisimura, M. Yasue, H. Kabasawa, T. Nakagawa, T. Tohei, H. Orihara, S. I. Hayakawa, K. Miura, T. Suehiro, S. K. Nanda, D. Dehnhard, and M. A. Franey, submitted to Phys. Rev. C.

6. "Measurement of Spin Observables of the $^{28}Si(p,p')$ reaction at 500 MeV and Comparison with the Distorted Wave Impulse Approximation", C. Glashausser, N. Hintz, A. Sethi, J. Shepard, E. Donoghue, R. Fergerson, M. Franey, M. Gazzaly, K. Jones, J. McClelland, S. Nanda, M. Plum, Phys. Rev. C, to be submitted.

7. "Platinum isotopes and the Interacting Boson Model", A. Sethi, N. Hintz, A. Mack, D. Mihailidis, M. Franey, M. Gazzaly, F. T. Baker, K. Jones, D. Ciskowski, G. Pauletta, L. Santi, D. Goutte, Phys. Rev. C, to be submitted.
8. "Polarized Proton Elastic Scattering from Polarized ^{13}C", G. W. Hoffmann, M. L. Barlett, W. Kielhorn, G. Pauletta, M. Purcell, L. Ray, J. F. Amann, J. J. Jarmer, K. W. Jones, S. Penttilä, N. Tanaka, G. Burleson, J. Faucett, M. Gilani, G. Kyle, L. Stevens, A. Mack, D. Mihailidis, D. Dehnhard, T. Averett, J. Comfort, J. Gorgen, J. Tinsley, B. C. Clark, S. Hama, and R. L. Mercer, Phys. Rev. Lett., to be submitted (Aug. 1990).

C. Contributed Papers

1. "The Nuclear Spin Response of ^{12}C in Proton Inelastic Scattering at 318 MeV", A. Green, F. T. Baker, V. Cupps, C. Djalali, L. Bimbot, H. Esbensen, R. Fergerson, G. Graw, K. W. Jones, M. Gazzaly, C. Glashausser, M. Morlet, S. K. Nanda, A. Sethi, R. D. Smith, and A. Willis, BAPS 32, 1559 (1987).
2. "The Nuclear Spin Response of ^{48}Ca in Proton Inelastic Scattering at 318 MeV", K. W. Jones, F. T. Baker, L. Bimbot, V. Cupps, C. Djalali, R. Fergerson, M. Gazzaly, C. Glashausser, A. Green, M. Morlet, S. K. Nanda, A. Willis, BAPS 32, 1559 (1987).
3. "Swelling of Nucleons in Nuclei and Proton-Nucleus Scattering", A. Sethi, N. Hintz, G. Brown, T. Mack, J. Amann, B. Andrews, M. Barlett, D. Ciskowski, D. Cook, M. Franey, G. Pauletta and M. Purcell, Substitution for paper DE14, BAPS, 33, 1957 (1988) (Santa Fe Meeting,

October 1988).

4. "Density Dependent Interaction Applied for Low-Multipole (p,p') and (p,n) Transitions in Light Nuclei", K. Ieki, J. Iimura, M. Iwase, H. Ohnuma, H. Shimizu, H. Toyokawa, K. Furukawa, H. Kabasawa, T. Nakagawa, T. Tohei, H. Orihara, S. Hayakawa, T. Hasegawa, M. Yasue, K. Nisimura, K. Miura, T. Suehiro and M. A. Franey, International Conference on Nuclear Reaction Mechanisms, Jan. 3-9, 1989, Calcutta, India.

5. "500 MeV Elastic $\vec{p}$ + $^{13}\vec{C}$ Analyzing Power Measurements", G. Hoffmann, M. Barlett, W. Kielhorn, G. Pauletta, M. Purcell, L. Ray, J. Amann, J. Jarmer, K. Jones, S. Penttila, N. Tanaka, G. Burleson, J. Faucett, M. Gilaini, G. Kyle, L. Stevens, T. Mack, D. Mihailidis, T. Avereti, J. Comfort, J. Georgen, J. Tinsley, B. Clark, S. Hama and R. Mercer, BAPS 34, 1829 (1989).

6. "500 MeV Elastic $\vec{p}$ + $^{13}\vec{C}$ Analyzing Power Measurements", G. Hoffmann, M. Barlett, W. Kielhorn, G. Pauletta, M. Purcell, L. Ray, J. Amann, J. Jarmer, K. Jones, S. Penttilä, N. Tanaka, G. Burleson, J. Faucett, M. Gilaini, G. Kyle, L. Stevens, T. Mack, D. Mihailidis, T. Avereti, J. Comfort, J. Georgen, J. Tinsley, B. Clark, S. Hama and R. Mercer, BAPS 35, 1038 (1990).

7. "^{194,6}PT(p,p') and the IBM with g-Bosons", A. Sethi, M. Franey, M. Gazzaly, N. Hintz, A. Mack, D. N. Mihailidis, K. Jones, D. Ciskowski, G. Pauletta, L. Santi, and D. Goutte, Symposium in Honor of Akito Arima, Santa Fe, May 1990.

8. "Proton Elastic Scattering from Polarized $^{13}\vec{C}$ at 500 MeV", G. Hoffmann, M. Barlett, W. Kielhorn, G. Pauletta, M. Purcell, L. Ray, J. Amann,

J. Jarmer, K. Jones, S. Penttilä, N. Tanaka, G. Burleson, J. Faucett, M. Gilani, G. Kyle, L. Stevens, T. Mack, D. Mihailidis, D. Dehnhard, T. Avereti, J. Comfort, J. Georgen, J. Tinsley, B. Clark and S. Hama, PANIC XII, MIT, June 1990.

9. "Dressed Quarks and the Proton's Spin", Xin-hua Yang, Chun Wa Wong and Keh-cheng Chu, PANIC XII, MIT, June 1990.

D. Invited talks and Seminars

Norton M. Hintz

1. "Successes and Failures of the Impulse Approximation at Intermediate Energies", Seminar, Univ. of Maryland, March 1988.
2. "Effect of Swelling of Nucleons in Nuclei on Proton Scattering at Intermediate Energy", Seminar, IPN, Orsay, France, 6 February 1989.
3. "Effect of Swelling of Nucleons in Nuclei on Proton Scattering at Intermediate Energy", Seminar, GANIL, Caen, France, 23 March 1989.
4. "Effect of Swelling of Nucleons in Nuclei on Proton Scattering at Intermediate Energy", Invited talk, 10^{e} Session D'Etudes Biennale De Physique Nucleaire, Aussois, France, 6-10 March 1989.
5. "Proton-Nucleus Scattering and the Swelling of Nucleons in Nuclei", Seminar, University of Granada, Spain, 25 April 1989.
6. "Proton-Nucleus Scattering and the Swelling of Nucleons in Nuclei", Seminar, University of Munich, Germany, 26 May 1989.

Magdy Gazzaly

1. "Proton-proton scattering at small angles", Bates Laboratory, (MIT), October 1987.

2. "The Q data acquisition system at LAMPF", ARTTA 2nd workshop held at University of Jordan, Amman, Jordan, November 1987.
3. "Intermediate energy physics research at LAMPF" and "Resonances in the dibaryon system", University of Jordan, Amman, Jordan, November 1987.
4. "Nucleon-nucleon physics at intermediate energies" and "Recent advances in nuclear Physics", Kuwait University, City of Kuwait, Kuwait, December 1987.
5. "Intermediate energy physics research at LAMPF", United Arab Emerates University, El-EIN, December 1987.
6. "Proton-proton spin physics at small momentum transfer", California State University, Long Beach, January 1988.
7. "Evidence for Narrow Structure in the Analyzing Power of the $^{3}\vec{He}(\vec{p},d)X$ Reaction at 0.8 GeV".
8. (Also "Tests of a Coulomb-Nuclear Intereference Polarimeter" talk given by G. Pauletta included M. Gazzaly), 8th International Symposium on High Energy Spin Physics, University of Minnesota, Sept. 12-17, 1988.

E. Thesis Titles

1. Proton Inelastic Scattering to the 2^{+} State of ^{208}Pb at 650 MeV. Abboud Bali, M. A., Oct. 1976, Univ. of Minnesota.
2. Neutron Proton Decomposition of Transition Matrix Elements in $^{206,208}Pb$. A. M. Mack, M. A., June 1990, Univ. of Minnesota.

Reprints & Preprints removed

END

DATE
FILMED
01/24/92